

**AGGREGATE MORPHOLOGY AND NETWORK
PROPERTIES OF OVALBUMIN**

Promotor: Prof. dr. M.A. Cohen Stuart,
Hoogleraar fysische chemie, met bijzondere aandacht voor de
kolloïdchemie, Wageningen Universiteit

Copromotoren: Dr. R.W. Visschers
projectleider Wageningen Centre for Food Sciences
werkgroep leider, NIZO food research

Dr. ir. P.A. Barneveld
Universitair docent bij de leerstoelgroep Fysische Chemie en
Kolloïdkunde, Wageningen Universiteit

Promotiecommissie: Dr. T. Nicolai (Université du Maine, France)
Prof. dr. W. Norde (Rijksuniversiteit Groningen)
Prof. dr. E. van der Linden (Wageningen Universiteit)
Dr. R. Vreeker (Unilever Research Vlaardingen)

Dit onderzoek is uitgevoerd binnen de onderzoeksschool VLAG

AGGREGATE MORPHOLOGY AND NETWORK PROPERTIES OF OVALBUMIN

MIREILLE WEIJERS

PROEFSCHRIFT

ter verkrijging van de graad van doctor
op gezag van de rector magnificus
van Wageningen Universiteit,
prof. dr. ir. L. Speelman,
in het openbaar te verdedigen
op vrijdag 14 januari 2005
des namiddags te vier uur in de Aula

ISBN: 90-8504-115-5

M. WEIJERS (2005)

AGGREGATE MORPHOLOGY AND NETWORK PROPERTIES OF OVALBUMIN.

PhD thesis, Wageningen University, The Netherlands

KEYWORDS: ovalbumin, hen egg white proteins, β -lactoglobulin, whey protein isolate, purification, irreversible transitions, scan-rate dependence, protein denaturation, aggregation, mesoscopic structures, fibril formation, ordered structures, ionic strength, heat-induced gelation, acid-induced gelation, scanning calorimetry, chromatography, spectroscopy, electrophoresis, light scattering, SAXS, cryo-TEM, CSLM, rheology.

ABSTRACT

The objective of the research described in this thesis was to investigate the heat-induced denaturation, fibril formation and network properties of food proteins, with the main focus on engineering and understanding (fibrillar) protein structures at neutral pH. Identifying the parameters that are of relevance to the structure development and subsequent network formation allows us to understand and control these mechanisms for globular food proteins in general. Additionally, we aimed to link the mesoscopic properties of protein aggregates to the macroscopic properties of food gels (heat-induced as well as acid-induced), in order to obtain a relevant fundamental understanding and to use this knowledge in controlling texture in food applications.

The heat-induced denaturation kinetics of ovalbumin at pH 7 was found to be independent of protein concentration and salt concentration, but was strongly dependent on temperature. For pure ovalbumin, the decrease in non-denatured native protein showed first-order dependence. A kinetic model that correctly predicts the temperature-induced denaturation and aggregation of ovalbumin is presented.

Experimental results on aggregate morphology showed that protein concentration and ionic strength have important consequences for the structure formation of (ovalbumin) aggregates. Various scattering techniques and microscopy showed that at low ionic strength linear flexible chains are formed with little branching, while at high ionic strength denser branched aggregates are formed with a fractal dimension close to that found for other globular protein aggregates. The structure of these ovalbumin fibrils is compatible with that of semi-flexible strings of monomers that are more flexible and increasingly branched with increasing ionic strength. The persistence length increased with decreasing

ionic strength, which was quantitatively determined using a model of semi-flexible chains, the so-called Kratky-Porod chains. Also the importance of electrostatic repulsion on fibril formation was demonstrated and incorporated in a general aggregation model. The results showed that the charge density on the surface of (denatured) protein molecules plays a major role in the formation of fibrillar structures and therefore in the formation of transparent gels. By controlling the charge density on the protein molecules, by chemical engineering, the amount of electrostatic repulsion can be changed, which allows us to control fibril formation and therefore the turbidity and rheological properties of ovalbumin networks as presented in gelled foods.

Knowledge acquired from doing research on purified systems was extended to aggregate and network formation of industrial relevant proteins under cold-setting conditions. Since purified ovalbumin is not commonly used in food applications, industrial egg white protein was used with the aim to produce fine-stranded acid-induced gels. Several obstacles had to be overcome before fine stranded networks of egg white proteins could be formed. Various aspects such as fibril formation, transparency of the acid-induced gels, disulphide bonding in these gels and their fracture properties were studied and compared with that ovalbumin and whey protein isolate.

This work provides a general overview on the denaturation mechanism, structure morphology and network properties of ovalbumin as well as a translation of fundamental knowledge into industrial applications.

SUMMARY OF CONTENTS

CHAPTER 1	INTRODUCTION	1
PART I	DENATURATION, AGGREGATION, AND GELATION UNDER HEAT-SETTING CONDITIONS	
CHAPTER 2	HEAT-INDUCED DENATURATION AND AGGREGATION OF OVALBUMIN AT NEUTRAL PH DESCRIBED BY IRREVERSIBLE FIRST-ORDER KINETICS	17
CHAPTER 3	LIGHT SCATTERING STUDY OF HEAT-INDUCED AGGREGATION OF OVALBUMIN AT DIFFERENT IONIC STRENGTH	39
CHAPTER 4	X-RAY AND LIGHT SCATTERING STUDY OF THE STRUCTURE OF LARGE PROTEIN AGGREGATES AT DIFFERENT IONIC STRENGTH	65
CHAPTER 5	HEAT-INDUCED FORMATION OF “ORDERED” STRUCTURES OF OVALBUMIN AT LOW IONIC STRENGTH STUDIED BY X-RAY SCATTERING	81
CHAPTER 6	INFLUENCE OF THE IONIC STRENGTH ON THE STRUCTURE OF HEAT-SET GELS OF OVALBUMIN	101
CHAPTER 7	ELECTROSTATICS CONTROLS FIBRIL FORMATION PART II: ELUCIDATION OF THE MOLECULAR MECHANISM OF AGGREGATION	117
PART II	NETWORK FORMATION UNDER COLD-SETTING CONDITIONS	
CHAPTER 8	ACID-INDUCED COLD GELATION OF GLOBULAR PROTEINS: EFFECTS OF PROTEIN AGGREGATE CHARACTERISTICS AND DISULFIDE BONDING ON RHEOLOGICAL PROPERTIES	141
CHAPTER 9	STRUCTURE AND RHEOLOGICAL PROPERTIES OF ACID-INDUCED EGG WHITE PROTEIN GELS	167
	SUMMARY	193
	SAMENVATTING	199
	DANKWOORD	205
	LIST OF PUBLICATIONS	208
	CURRICULUM VITAE	211

CONTENTS

CHAPTER 1	INTRODUCTION	1
1.1	STRUCTURE FORMATION IN FOODS	2
1.2	HISTORY OF POLYMERS	3
1.3	PROTEIN AGGREGATION AND NETWORK FORMATION	4
1.4	NETWORK FORMATION AT ROOM TEMPERATURE	6
1.5	GLOBULAR FOOD PROTEINS	8
1.5.1	EGG WHITE PROTEIN	8
1.5.2	OVALEBUMIN	8
1.5.3	WHEY PROTEIN ISOLATE	9
1.5.4	β -LACTOGLOBULIN	9
1.6	MOTIVATION AND RESEARCH OBJECTIVE	10
1.7	THESIS OUTLINE	10
	REFERENCES	12

PART I DENATURATION, AGGREGATION, AND GELATION UNDER HEAT-SETTING CONDITIONS

CHAPTER 2	HEAT-INDUCED DENATURATION AND AGGREGATION OF OVALEBUMIN AT NEUTRAL PH DESCRIBED BY IRREVERSIBLE FIRST-ORDER KINETICS	17
2.1	INTRODUCTION	19
2.2	MATERIALS AND METHODS	21
2.2.1	MATERIALS	21
2.2.2	METHODS	22
2.3	RESULTS	24
2.3.1	CONVERSION OF MONOMERS INTO AGGREGATES INUCED BY HEATING	24
2.3.2	COMPARISON OF THE ACIDIFYING AND NON-ACIDIFYING METHOD	26
2.3.3	DEPENDENCE OF TEMPERATURE AND PROTEIN CONCENTRATION ON THE DENATURATION RATE	26
2.3.4	DIFFERENTIAL SCANNING CALORIMETRY OF OVALEBUMIN UNDER IRREVERSIBLE CONDITIONS	29
2.3.5	ACTIVATION ENERGY OF OVALEBUMIN	32
2.3.6	FITTING THERMOGRAMS OF OVALEBUMIN WITH IRREVERSIBLE FIRST-ORDER KINETICS	33
2.3.7	EXPERIMENTAL DATA DESCRIBED WITH TWO FIRST-ORDER RATE CONSTANTS	34
2.4	DISCUSSION	35
2.5	CONCLUSIONS	37
	REFERENCES	37

CHAPTER 3	LIGHT SCATTERING STUDY OF HEAT-INDUCED AGGREGATION OF OVALEBUMIN AT DIFFERENT IONIC STRENGTH	39
3.1	INTRODUCTION	41
3.2	MATERIALS AND METHODS	42
3.2.1	MATERIALS	42
3.2.2	METHODS	42
3.2.3	DATA ANALYSIS	43
3.3	RESULTS AND DISCUSSION	45
3.3.1	NATIVE OVALEBUMIN	45
3.3.2	DILUTE OVALEBUMIN AGGREGATES	47
3.3.3	UNDILUTED OVALEBUMIN SOLUTIONS	53
3.3.4	PROGRESSIVE DILUTION OF AN OVALEBUMIN SOLUTION CLOSE TO THE GEL POINT	59

3.4	CONCLUSIONS	61
	ACKNOWLEDGEMENT	62
	REFERENCES	62
CHAPTER 4	X-RAY AND LIGHT SCATTERING STUDY OF THE STRUCTURE OF LARGE PROTEIN AGGREGATES AT DIFFERENT IONIC STRENGTH	65
4.1	INTRODUCTION	67
4.2	MATERIALS AND METHODS	68
	4.2.1 SAMPLE PREPARATION	68
	4.2.2 SCATTERING EXPERIMENTS	69
	4.2.3 CRYO-TRANSMISSION ELECTRON MICROSCOPY	70
4.3	RESULTS AND DISCUSSION	70
4.4	CONCLUSIONS	75
	ACKNOWLEDGEMENTS	78
	REFERENCES	78
CHAPTER 5	HEAT-INDUCED FORMATION OF “ORDERED” STRUCTURES OF OVALBUMIN AT LOW IONIC STRENGTH STUDIED BY SMALL ANGLE X-RAY SCATTERING	81
5.1	INTRODUCTION	83
5.2	MATERIALS AND METHODS	84
	5.2.1 MATERIALS	84
	5.2.2 METHODS	85
5.3	RESULTS	85
	5.3.1 NATIVE OVALBUMIN IN AQUEOUS SOLUTION	85
	5.3.1.1 SIZE OF NATIVE OVALBUMIN MOLECULES	85
	5.3.1.2 SCALING BEHAVIOR OF NATIVE OVALBUMIN IN AQUEOUS SOLUTIONS	87
	5.3.1.3 FITTING EXPERIMENTAL INTERACTION PEAK OF OVALBUMIN MONOMERS IN AQUEOUS SOLUTION	91
	5.3.2 LONG FIBRILLAR AGGREGATES IN AQUEOUS SOLUTION	
	5.3.2.1 SCALING BEHAVIOR OF FIBRILLAR AGGREGATES UPON DILUTION IN AQUEOUS SOLUTIONS	91
	5.3.2.2 CROSS-SECTION OF LONG OVALBUMIN AGGREGATES	92
	5.3.3 SCALING BEHAVIOR OF OVALBUMIN AGGREGATES HEATED AT DIFFERENT PROTEIN CONCENTRATIONS	94
	5.3.4 CRYO-TRANSMISSION ELECTRON MICROSCOPY	95
5.4	DISCUSSION	96
5.5	CONCLUSIONS	97
	ACKNOWLEDGEMENTS	98
	REFERENCES	98
CHAPTER 6	INFLUENCE OF THE IONIC STRENGTH ON THE STRUCTURE OF HEAT-SET GELS OF OVALBUMIN	101
6.1	INTRODUCTION	103
6.2	MATERIALS AND METHODS	104
	6.2.1 MATERIALS	104
	6.2.2 METHODS	104
6.3	RESULTS	105
	6.3.1 DILUTED OVALBUMIN AGGREGATES	105
	6.3.2 UNDILUTED OVALBUMIN SYSTEMS	106
6.4	DISCUSSION AND CONCLUSIONS	111
	ACKNOWLEDGEMENTS	115
	REFERENCES	115

CHAPTER 7	ELECTROSTATICS CONTROLS FIBRIL FORMATION. PART II: ELUCIDATION OF THE MOLECULAR MECHANISM OF AGGREGATION	117
7.1	INTRODUCTION	119
7.2	MATERIALS AND METHODS	120
7.3	RESULTS	122
7.3.1	DENATURATION AND AGGREGATION KINETICS	122
7.3.1.1	CONVERSION OF MONOMERS INTO AGGREGATES INDUCED BY HEATING	123
7.3.1.2	FITTING DSC THERMOGRAMS OF OVALBUMIN VARIANTS WITH IRREVERSIBLE FIRST-ORDER KINETICS	124
7.3.2	CHARACTERIZATION OF THE PHYSICOCHEMICAL PROPERTIES OF PROTEIN AGGREGATES	126
7.3.2.1	SDS-PAGE AND AGAROSE ELECTROPHORESIS	126
7.3.2.2	SEC-MALLS	128
7.3.2.3	CRYO-TEM	130
7.3.2.4	CRITICAL GELATION CONCENTRATION	130
7.3.3	FUNCTIONAL PROPERTIES OF HEAT-INDUCED OVALBUMIN GELS	132
7.4	DISCUSSION	133
7.5	CONCLUSIONS	137
	ACKNOWLEDGEMENTS	137
	REFERENCES	137
 PART II	 NETWORK FORMATION UNDER COLD-SETTING CONDITIONS	
 CHAPTER 8	 ACID-INDUCED COLD GELATION OF GLOBULAR PROTEINS: EFFECTS OF PROTEIN AGGREGATE CHARACTERISTICS AND DISULFIDE BONDING ON RHEOLOGICAL PROPERTIES	 141
8.1	INTRODUCTION	143
8.2	MATERIALS AND METHODS	144
8.2.1	MATERIALS	144
8.2.2	METHODS	145
8.3	RESULTS AND DISCUSSION	148
8.3.1	PREPARATION OF DISULFIDE CROSS-LINKED OVALBUMIN AGGREGATES	148
8.3.2	CHARACTERIZATION OF PROTEIN AGGREGATES	150
8.3.2.1	SIZE	150
8.3.2.2	SHAPE	150
8.3.2.3	NUMBER OF EXPOSED THIOL GROUPS	152
8.3.3	ACID-INDUCED COLD GELATION	152
8.3.4	APPEARANCE OF COLD-SET GELS	153
8.3.5	LARGE DEFORMATION PROPERTIES	153
8.3.6	STRUCTURAL PROPERTIES	155
8.3.7	SMALL DEFORMATION AND SCATTERING PROPERTIES	156
8.3.8	TEM OF ACID-INDUCED PROTEIN GELS	159
8.3.9	DETERMINATION OF DISULPHIDE CROSS-LINKING IN ACID-INDUCED GELS	160
8.4	CONCLUSIONS	162
	ACKNOWLEDGEMENTS	163
	REFERENCES	163

CHAPTER 9	STRUCTURE AND RHEOLOGICAL PROPERTIES OF ACID-INDUCED EGG WHITE PROTEIN GELS	167
9.1	INTRODUCTION	169
9.2	MATERIALS AND METHODS	171
	9.2.1 REAGENTS AND CHEMICALS	171
	9.2.2 SAMPLE PREPARATION	171
	9.2.3 PREPARATION OF EWP AND EWP _{PREHEAT}	174
	9.2.4 PREPARATION OF AGGREGATES	173
	9.2.5 DIFFERENTIAL SCANNING CALORIMETRY	173
	9.2.6 REVERSED PHASE CHROMATOGRAPHY	173
	9.2.7 DYNAMIC LIGHT SCATTERING	174
	9.2.8 CRYO-TRANSMISSION ELECTRON MICROSCOPY	174
	9.2.9 DETERMINATION OF REACTIVE THIOL GROUPS	174
	9.2.10 SDS-AGAROSE ELECTROPHORESIS	174
	9.2.11 GDL-INDUCED GELATION	175
	9.2.12 TURBIDITY MEASUREMENTS	175
	9.2.13 LARGE DEFORMATION RHEOLOGY	175
9.3	RESULTS	176
	9.3.1 PREPARATION OF PREHEATED EGG WHITE PROTEIN	176
	9.3.2 AGGREGATES FORMATION	178
	9.3.3 CHARACTERIZATION OF PROTEIN AGGREGATES	179
	9.3.3.1 HYDRODYNAMIC RADIUS	179
	9.3.3.2 CRYO-TRANSMISSION ELECTRON MICROSCOPY	181
	9.3.3.3 ELECTROPHORETIC MOBILITY	182
9.3.4	ACID-INDUCED GELATION	183
	9.3.4.1 TURBIDITY OF COLD-SET GELS	183
	9.3.4.2 FRACTURE PROPERTIES OF ACID-INDUCED GELS	184
	9.3.4.3 DISULPHIDE CROSS-LINKING	185
9.4	DISCUSSION	186
9.5	CONCLUSIONS	190
	ACKNOWLEDGEMENTS	191
	REFERENCES	191
SUMMARY		193
SAMENVATTING		199
DANKWOORD		205
LIST OF PUBLICATIONS		208
CURRICULUM VITAE		211

CHAPTER 1

INTRODUCTION

1.1 STRUCTURE FORMATION IN FOODS

Functional properties of foods such as texture, perception, appearance, shelf-life, quality, flavor release, stability are important to consumers and manufacturers. These functionalities reveal itself on a macroscopic level. The macroscopic properties depend on the structure, interactions, chemical reactivity, organization of the polymers etc., which can be explained by the microscopic properties of the polymers. Based on their size polymeric structures can be divided in three categories: microscopic, mesoscopic, and macroscopic structures (Figure 1.1). Figure 1.1 also presents different types of particles, which are classified to their size.

The area between molecular chemistry and macroscopic properties is generally entitled as “The Colloidal Domain” or the “mesoscopic” region, since it is typically intermediate, combining properties of the molecular world (dominance of thermal motion) with those of the macroscopic world (dominance of external forces). This thesis focuses on the mesoscopic properties of food biopolymer dispersions and gels, exploring structure formation of globular proteins and its interaction as the centre of interest. Our idea is that starting at a mesoscopic level enables us to better understand and explain mechanisms, properties and functionalities that occur on a macroscopic level.

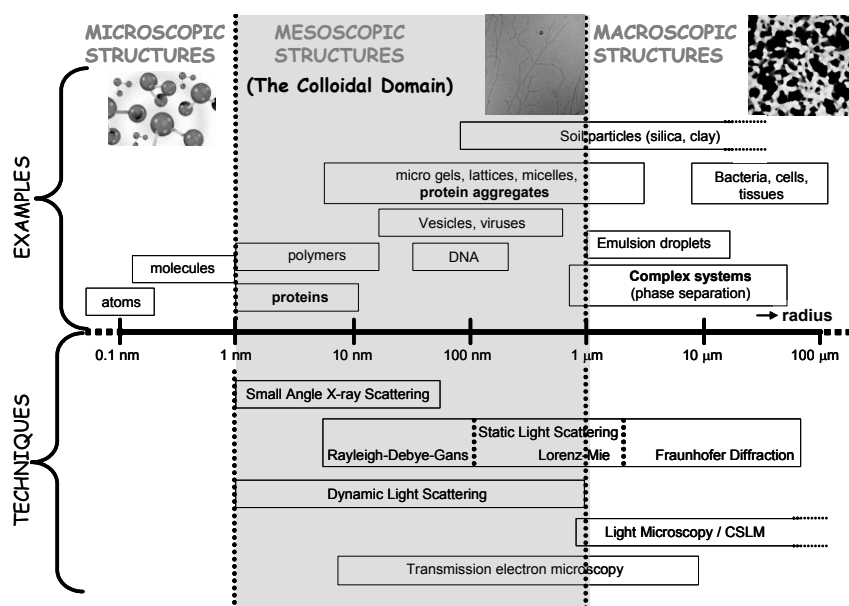


Figure 1.1. Structural length scales of polymers. The upper panel gives an overview of different classifications of structures dependent on length scale. The lower panel indicates techniques which were used in this thesis for measuring the size of proteins, protein aggregates and complex systems.

The gels we consider in this thesis originate from aggregation processes, which we can simply imagine as colloidal particles sticking together and forming a three-dimensional network of aggregated colloidal particles that fills the entire volume of the system. The particles we used in this thesis are globular proteins. These proteins are also macromolecules; we therefore insert a scientific investigation of the history of polymers.

1.2 HISTORY OF POLYMER SCIENCE

In general, polymers are very large molecules consisting of simple building blocks that occur either in nature (proteins, polysaccharides, DNA, natural rubber, silk, cotton, wool) or can be synthesized in laboratories (plastics, synthetic fibers, synthetic rubber). Today, the polymer industry has grown to be larger than the aluminum, copper and steel industries together. Polymers have a wide range of applications, for example in agriculture and agribusiness, medicine, consumer products, industry, and sports.¹

The use of cellulose-based fibres (linen, wood, cotton, papyrus) and proteinaceous substances (silk, wool) as material for clothing, and construction is very old. In Europe, a new polymer was introduced in the 16th century, when rubber samples were first brought to Europe from South America. Priestly discovered that this emulsion which oozed from trees could rub out lead pencil marks; it was therefore called “rubber”. Rubber had limited commercial applications because it melted in summer and froze in winter. Goodyear accidentally mixed sulphur and rubber on a hot stove, and found that the rubber obtained did not melt. Goodyear patented the process, which he entitled “vulcanization”, after Vulcan, the roman god of fire.² Vulcanized rubber is a polymeric substance that is much more durable than natural rubber, and is used today in automobile tires.

Since experiments on polymers showed that the molecular weight of these substances was so large that scientists initially did not believe that this could be due to a single molecule. This changed when the chemical structure of cellulose was discovered in 1917 by Polanyi, where he used X-ray crystallography for analyzing crystal structures. This established the fact that polymers are built up of long chain molecules rather than small molecular species somehow stuck together in a colloidal aggregate. The first scientist who discussed that polymers were made of single chain-molecules was Staudinger (1920). He argued that these molecules consisted of repeating units and that their atoms (units) were held together by covalent bonds. For his groundbreaking work on polymers, he is generally

credited as being the father of modern polymer chemistry. There was a decade of controversy before these ideas began to experience widespread acceptance. Staudinger was awarded the Nobel Prize in 1953 for his work with polymers. Flory obtained the Nobel Prize in 1976 for his famous book on the principles of polymer chemistry (1953).

By the 1930s, Carothers began synthesizing polymers using well-established reactions of organic chemicals, such as esterification and amidation. One well known polymeric product developed in that period is nylon. Nylon is a common material used today for applications such as ropes and clothes. Later, Kuhn, Guth and Mark applied statistics and crystallography in order to describe the variability in shape of polymer structures, and to explain several properties observed in experiments.³ Because the delivery of natural rubber was failed during the second World War, the synthetic rubber industry development very fast, especially on the production of purified monomers on a large scale. This have caused that the polymer industry has continued to grow and has evolved into one of the fastest growing industries in the world.

Since 1960, the knowledge obtained from synthetic polymers is also applied to biopolymers; food structure has systematically been studied since the seventies. Scientific and technological interest in relationships between structure and functionality at that time led academic food science/technology and industrial research laboratories to purchase microscopes. In that time new methods, which were developed in biology and medicine started to find applications in food science. Sir Alexander Robertus Todd (1907-1997) has clearly expressed the importance of polymers in the following phrase:

“I am inclined to think that the development of polymerization is perhaps the biggest thing chemistry has done, were it has had the biggest impact on everyday life”.

1.3 PROTEIN AGGREGATION AND NETWORK FORMATION

The globular proteins which we used to study the formation of aggregate structures under different conditions were: ovalbumin, egg white protein (EWP), β -lactoglobulin (β -lg), and whey protein isolate (WPI). EWP and WPI are both industrial preparations containing mixtures of various proteins.^{4,5,6,7} Ovalbumin and β -lg are the most predominant proteins present in EWP and WPI, respectively. To study the effect of electrostatic interaction on the self-assembly into fibrillar structures and networks in more detail, ovalbumin was studied. Because fibrillar structures may lead to improved or new

properties, a comparison was made with β -lactoglobulin which is known to form more fractal aggregates at neutral pH. In this section we focus on aggregation and network formation under heat-setting conditions.

In general, the formation of heat-induced network structures of proteins occurs in three stages: unfolding (and denaturation) of individual molecules, aggregation, and network formation. In their native state, the attractive forces between the protein molecules in solution, mainly van der Waals and hydrophobic, are not sufficiently strong enough to overcome the repulsive forces (mainly electrostatic, hydration, entropic). Therefore molecules tend to exist as monomers or small aggregates.⁸ Reactive groups, such as hydrophobic and cysteine residues, are located in the interior of the native protein, but can be exposed by a heating step that causes to unfold and denature the protein. The exposure of hydrophobic groups and of cysteine residues plays an important role in the subsequent aggregation process.^{9,10} After the proteins have been heated to a temperature where they unfold, they can form various types of aggregate structures depending on the balance between attractive and repulsive interactions^{11,12}.

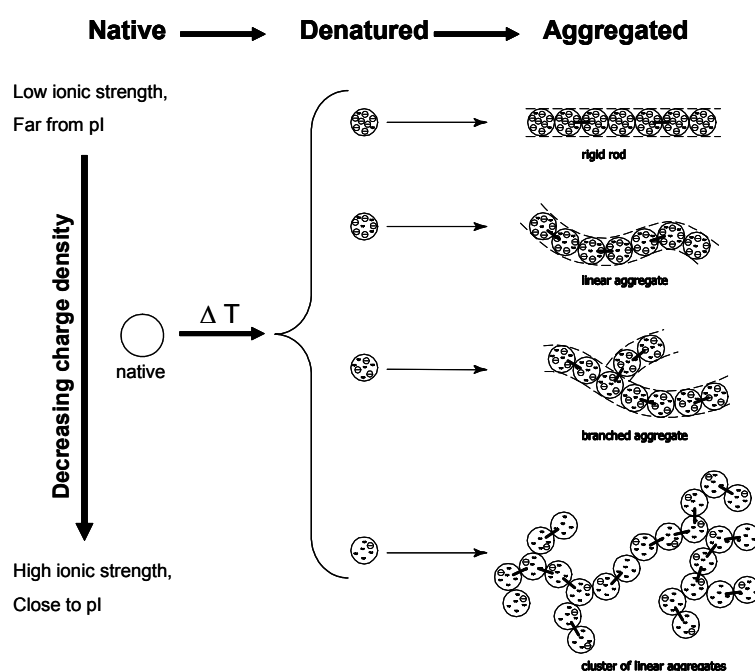


Figure 1.2. A proposed model for the thermal denaturation and aggregate formation of ovalbumin with various charge densities on the surface of the protein molecule. Shadows (◐) indicate hydrophobic areas exposed by thermal denaturation, minus signs (Θ) and dashed symbols (–) indicate the calculated net charge at pH 7 and disulphide bonding respectively.

In terms of experimental conditions, this means that the formation of aggregate structures depends on the following factors: pH, which controls the net charge on the protein molecule; the ionic strength, which controls the screening of electrostatic interactions, and on protein concentration, which in many systems controls the rate of the reaction. Figure 1.2 shows a general hypothetical scheme for the formation of various fibrillar and non-fibrillar aggregate as a function of the net charge on a denatured protein molecule.

At pH values far from the iso-electric point and at low ionic strength, the charge density on the surface of the protein molecule is rather high. Due to the strong electrostatic repulsion under these conditions it is energetically more favorable to form linear aggregates than random aggregates. At pH values close to the iso-electric point and at high ionic strength, the charge density on the protein molecule is rather low or screened, this consequently results in the formation of clusters of aggregates.¹³⁻¹⁶ Dependent on pH, ionic strength or charge density at pH 7 (induced by chemical modification), various intermediate aggregate structures can be formed as presented in Figure 1.2.¹⁷

A heat-induced gel is formed when the protein concentration exceeds some critical gelation concentration or percolation threshold, C^* , because the protein aggregates form a three-dimensional network of cross-linked or entangled molecules that fills the entire volume of the system.¹⁵

1.4 NETWORK FORMATION AT ROOM TEMPERATURE

In the heat-induced gelation process as mentioned in section 1.2.2, protein solutions are heated at relatively high temperatures ($>60^\circ\text{C}$) at concentrations above C^* . Heating above C^* results in the formation of gelled systems. The application of heat-induced gelation has limitations or is not always desired.¹⁸ Therefore, new techniques were developed in the late 90's for whey protein applications. These whey proteins were able to thicken solutions and forming gels at room temperatures and at refrigerating temperatures. Gels obtained with this method are entitled cold-set gels (Figure 1.3)^{11,18-34}. Relatively few papers have been published on cold-gelation of ovalbumin^{35,36} and soy-protein.^{37,38} The unique feature of the cold-gelation process, compared to heat-induced gelation, is that the aggregation step is decoupled from the subsequent gelation step. An industrial advantage is the formation of gels at low protein concentrations ($<2\%$) as compared to heat-induced gelation. Another

advantage might be that heat-labile or volatile compounds can be added (in the gelation step) without any losses or off-flavor occurring.

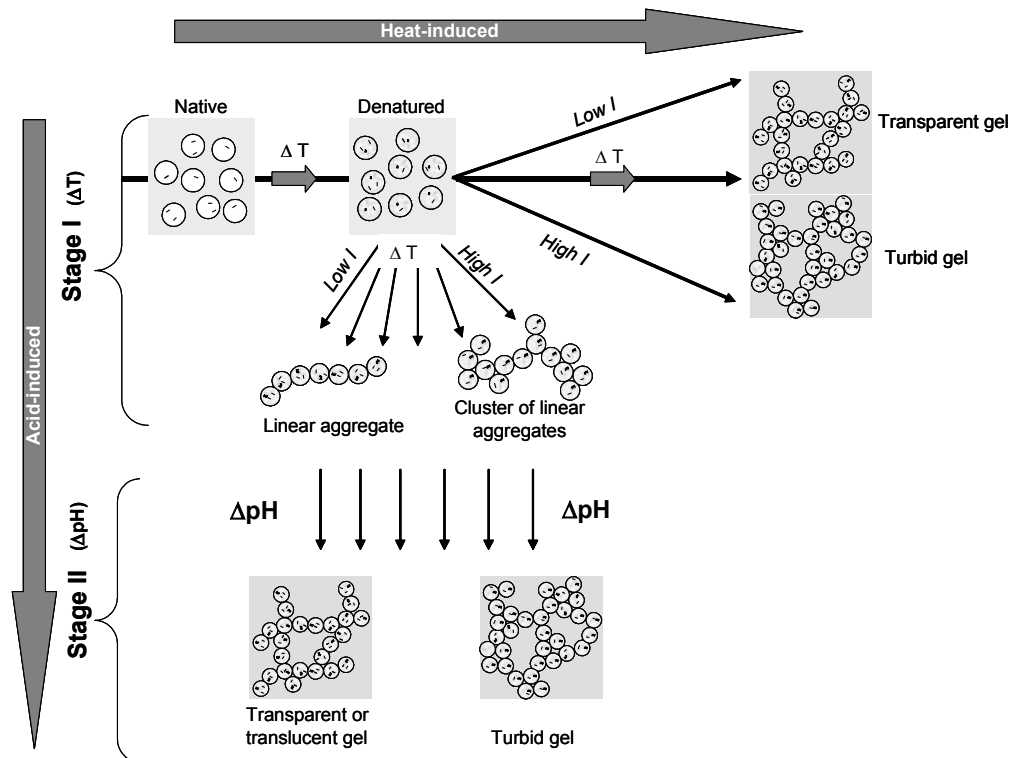


Figure 1.3. Conversion from monomers into a protein network according to the heat-induced or cold-set gelation process. In the heat-induced process, denaturation, aggregation and network formation are intertwined, whereas in the cold gelation process, the formation of aggregates and the formation of a protein network are clearly separated. Shadows indicate hydrophobic areas exposed by thermal denaturation; minus signs indicate the presence of negative charges on the surface of the protein.

The formation of acid-induced cold-set gels involves two stages. In the first stage, the preparation of a solution of aggregates of heat-denatured protein occurs, usually at pH 7 and low ionic strength. In the second step, carried out at ambient temperature, gelation is induced by changing the pH towards the iso-electric point of the protein, or by addition of mono- or polyvalent cations. Both processes reduce the electrostatic repulsion between the aggregates and therefore promote the formation of a percolation network. Dependent on the type of aggregates produced in the first stage, and the ability to form disulphide bonds in the second stage, different gel network structures, rheological and mechanical properties can be obtained (Figure 1.3).

1.5 GLOBULAR FOOD PROTEINS

Typical proteins of interest as food ingredients include proteins from milk, soy, fish and egg, and they are used in a number of foods including beverages, confectionary, desserts, dairy products and meat and fish products. These proteins provide structures, which contribute to the increased preferences of consumers for more tasty, natural, healthy, and convenient food products. The protein preparations used in this thesis were ovalbumin, industrial spray-dried egg white protein (EWP), commercial whey protein isolate (WPI), and β -lactoglobulin (β -lg).

1.5.1 EGG WHITE PROTEIN

Egg white proteins have been the subject of investigation by many researchers from diverse disciplines, including food science, animal science, biochemistry, microbiology and medicine.⁵ Egg white protein is a relevant industrial ingredient, therefore it is important to study the composition of the egg white preparation because this determines the functional properties of the final product. The composition of the major proteins present in egg white and some of their characteristics are summarized in table 1.1. A remarkable aspect of the composition is that egg white protein is predominantly composed of ovalbumin. Several other smaller proteins are present, each having a number of disulfide bridges, but only ovalbumin contains free thiol groups. It is relatively easy to isolate and crystallize several proteins from egg white in gram quantities.³⁹

1.5.2 OVALBUMIN

Ovalbumin is the major protein in avian egg white. It is a glycoprotein with a molecular mass of 45 kDa with 386 amino acids present, a pI of about 4.7, and a radius of about 2.8 nm³⁹. The sequence includes four free thiol groups with a single internal disulfide bond between Cys 74 and Cys 121. The molecule has two potential phosphorylation sites at serine 69 and 345. Different degrees of phosphorylation may occur: zero, one or two phosphate groups per ovalbumin molecule.⁴⁵ Ovalbumin belongs to the serine protease inhibitor (serpin) superfamily, although it does not exhibit any protease-inhibitory activity due to failure of insertion of the cleaved reactive loop into a beta sheet.⁴⁶ After heating of ovalbumin, hydrophobic areas that were buried become exposed and the four thiol groups which do not react with DTT before heat treatment do so after heat induced denaturation.

Table 1.1. Overview of egg white protein composition and properties

<i>Protein</i>	<i>% (w/w)</i>	<i>pI</i>	<i>M_w (kDa)</i>	<i>T_d (°C)</i>	<i>Cysteines</i>	<i>-SH</i>	<i>S-S</i>
<i>Ovalbumin</i> ^{4,42-45}	54	4.5-4.9	45	75-84	6	4	1
<i>Ovotransferrin</i> ^{4,41-44} (conalbumin)	12-13	6.0-6.1	77.7	61-65 (76,5, Al ³⁺)	30	-	15
<i>Ovomucoid</i> ^{4,40-42}	11	4.1	28	77	18	-	9
<i>Ovomucin</i> ^{4,40-42}	1.5-3.5	4.5-5.0	110, 5500-8300, 220-270000		(2)	-	
<i>Lysozyme</i> ^{4,40-43}	3.4-3.5	10.7	14.3-14.6	69-77	6		4
<i>G2 ovoglobulin</i> ^{4,41,42}	1.0	4.9-5.5	47-49				
<i>G3 ovoglobulin</i> ^{4,41,42}	1.0	4.8, 5.8	49-50				
<i>Ovoflavoprotein</i> ⁴⁰⁻⁴²	0.8	4.0	32-35, 80		5		2
<i>Ovostatin</i> ⁴⁰⁻⁴²	0.5	4.5-4.7	760-900				
<i>Cystatin</i> ^{41,42}	0.05	5.1	12				
<i>Avidin</i> ^{4,40-42}	0.05	10.0	55-68.3		2		1

Ovalbumin can undergo a conformational change to the more stable “S” form in time. The “S” form differs from the native form in its greater stability, compactness and hydrophobicity and increased peak temperature which changes from 78 °C up to approximately 86 °C.⁴⁷

1.5.3 WHEY PROTEIN ISOLATE

WPI was formerly obtained as a waste product of the cheese making process, but nowadays it is a source of high-quality proteins used in many applications.^{48,49} Analogously to egg white proteins, whey proteins mainly consists of β -lactoglobulin (>60%) and α -lactalbumin (~22%), and a number of minor proteins like bovine serum albumin (~5.5%) and immunoglobulins (~9.1%).¹¹ α -Lactalbumin contains four disulfide bonds and no free thiol groups and bovine serum albumin contains seventeen disulfide bonds and one free thiol group. Comparable effects on the functional properties as for EWP can be mentioned.

1.5.4 β -LACTOGLOBULIN

β -Lg is the major whey protein in bovine milk. The amino acid sequence this globular protein consists of 162 amino acid residues resulting in a molecular mass of 18.3 kDa, a pI

of 5.2, and a radius about 2 nm. In aqueous solution, a reversible dimerization occurs of which the extent depends on the genetic variant, pH, concentration, temperature, and degree of screening or the electrostatic repulsions.^{48,52} The sequence includes one free thiol group (Cys121) and two disulphide bonds. One of the two disulphide bonds (Cys106-119) is buried at the sheet-helix interface. The other disulphide bridge (Cys66-160) is found in one of the external loops of β -lg.^{50,51} β -Lg belongs to the lipocalin family of proteins, which structure is formed by nine strands of anti-parallel β -sheets, which are wrapped round to form a flattened cone. The nine β -sheets and the two disulphide bonds give the compact structure of the molecule. The biological function of this large group of proteins is to bind fatty-acid like molecules and transport them. In β -lg, a cone shaped structure functions as binding site for these molecules.

1.6 MOTIVATION AND RESEARCH OBJECTIVE

Globular food proteins are widely used in food industries because these proteins provide structures, which contribute to the increased preferences of consumers for more tasty, natural, healthy and convenient food products. This study was part of a project that was aimed to achieve a better control of the structural properties and stability that results from aggregation, gelation and gelation arrested phase separation of food biopolymers, in such a way that the obtained knowledge is relevant for the Dutch food industry.

The objective of the research described in this thesis was to investigate the heat-induced denaturation, fibril formation and network formation of food proteins, with the main focus on engineering (fibrillar) protein structures at neutral pH. Identifying the parameters that are of relevance to the structure development and subsequent network formation allows us to understand and control these mechanisms for globular food proteins in general. Additionally, we aimed to link the mesoscopic properties of protein aggregates to the macroscopic properties of food gels (heat-induced as well as acid-induced), in order to obtain a relevant fundamental understanding and to use this knowledge in applications.

1.7 THESIS OUTLINE

This thesis is divided into two parts. The first part (Chapters 2 – 7) deals with the heat-induced denaturation, aggregation and gelation of ovalbumin under heat-setting conditions. The properties of ovalbumin and its aggregation mechanisms are compared with β -

lactoglobulin to draw more general conclusions. In the second part the focus is on the network formation of industrially relevant proteins under cold-setting conditions (Chapters 8 and 9).

In Chapter 2, we studied the denaturation kinetics of ovalbumin using differential scanning calorimetry and chromatography. A kinetic model for the temperature-induced denaturation and aggregation of ovalbumin is presented that describes the experimental data. Chapter 3 presents the results of the effect of protein concentration on the size of the ovalbumin aggregates and the influence of ionic strength on fibril formation and inter-fibrillar interaction. In Chapter 4, we take an in-depth look at the structure of large aggregates of ovalbumin and β -lactoglobulin as a function of ionic strength; attempts are made to describe ovalbumin fibrils in terms of semi-flexible strings of monomers. A detailed study is presented in Chapter 5 on the interactions in concentrated systems of charged monomers and aggregates. To explain the experimental findings, a theoretical model is applied that describes the distribution of spaces in a random network of straight fibers. In Chapter 6 we elaborate on the effect of the ionic strength, but now we focus on the structure and the turbidity of ovalbumin gels using cross-correlation dynamic light scattering technique, in which we are able to perform light scattering experiments on turbid systems. Here, we consider that the structure of heated globular protein solutions and gels is generally determined by the interplay between the growth of the aggregates and the electrostatic interaction between the aggregates. In Chapter 7 we study the structure formation of protein fibrils. Special attention is paid to the influence of net charge on the surface of the protein molecule (electrostatic repulsion) on the denaturation kinetics, fibril formation and gelation properties. This resulted in a general aggregation model, which we developed to explain the formation of different structures and their resulting networks.

In the second part of this thesis, we focus more on network formation of industrial relevant proteins under cold-setting conditions. The aggregate properties studied in Part I are used in Chapter 8 to generate and study acid-induced gels of ovalbumin and WPI, which are formed at significantly lower protein concentration compared to gels obtained under heat-setting conditions. Protein specific and more general mechanisms in this cold gelation process are examined. Since purified ovalbumin is not commonly used in food applications, industrial egg white protein was used in Chapter 9 to describe how to produce fine-stranded acid-induced gels. Several obstacles had to be overcome before fine stranded networks of egg white proteins could be formed. Various aspects such as fibril formation,

transparency of the acid-induced gels, disulphide bridge formation in these gels and their fracture properties are studied and compared with that ovalbumin and whey protein isolate.

REFERENCES

1. <http://matse1.mse.uiuc.edu/~tw/polymers/ware.html>.
2. <http://mooni.fccj.org/~ethall/polymer/polymer.htm>.
3. Hiemenz, P.C. (1984). In *Polymer Chemistry, the basic concepts* (eds. M. Dekker), pp 1. New York.
4. Mine, Y. (1995). *Trends Food Sci. Technol.*, 6, 225.
5. Li-Chan, E., and Nakai, S. (1989). *CRC Crit. Rev. Poultry Biol.*, 2, 21.
6. Powrie, W.D. and Nakai, S. (1986). In *Egg Science and Technology*, 3rd ed. (eds. W.J. Stadelman and O.J. Cotterill), p97-139. Westport, Connecticut.
7. Alting, A.C., Jongh de, H.H.J, Visschers, R.W., and Simons, J-W.F.A. J. (2002). *Agric. Food Chem.*, 50, 4682.
8. Kinsella, J.E., and Whitehead, D.M. (1989). *Adv. Food Nutr. Res.* 33, 343-438.
9. Ma, C.-Y., and Holme, J. (1982). *J. Food Sci.*, 47,1454.
10. Boye, J.I., Alli, I., and Ismail, A.A. (1996). *J. Agric. Food Chem.*, 44, 996.
11. Bryant, C.M. and McClements, D.J. (1998). *Trends Food Sci. Technol.*, 9, 143.
12. Nakamura, R., Sugiyama, H., and Sato, Y. 1978. *Agric. Biol. Chem.* **42**: 819.
13. Clark, A.H. (1998). In *Functional properties of food macromolecules* (eds. S.E. Hill, D.A. Ledward, and Mitchell, J.R.), p77-142. Aspen Publishers, Great Britain.
14. Koseki, T., Kitabatake, N. and Doi, E. 1989. *Food Hydrocolloids* **3**: 123.
15. Doi, E. (1993). *Trends in Food Sci. Technol.*, 4, 1.
16. Nemoto, N., Koike, A., Osaki, K., Koseki, T., and Doi, E. (1993). *Biopolymers*, 33, 551.
17. Weijers, M., Broersen, K. Barneveld, P.A., Cohen Stuart, M.A., de Jongh, Hamer, R.J. and Visschers R. W. (2004). (*Submitted*).
18. Barbut, S., and Foegeding, E.A. (1993). *J. Food Sci.*, 58, 867.
19. Alting, A.C., Hamer, R.J., de Kruif, C.G., and R.W. Visschers. (2000). *J. Agric. Food Chem.*, 48, 5001.
20. Alting, A.C., de Jongh, H.J.J., Visschers, R.W., and Simons, J.F.A. (2002). *J. Agric. Food Chem.*, 50, 4674.
21. Alting, A.C., Hamer, R.J., de Kruif C.G., Paques, M., and Visschers, R.W. (2003). *Food Hydrocolloids*, 17, 469.
22. Alting, A.C., Hamer, R.J., de Kruif, C.G., and Visschers, R.W. (2003). *J. Agric. Food Chem.*, 51, 3150.
23. Elofsson, C., Dejmek, P., Paulsson, M., and Burling, H. (1997). *Int. Dairy J.*, 7, 601.
24. Hongsprabhas, P., and Barbut, S. (1996). *Food Res. Int.*, 29, 135.
25. Hongsprabhas, P., and Barbut, S. (1997). *J. Food Sci.*, 62, 382.
26. Hongsprabhas, P., and Barbut, S. (1997). *Lebensm.-Wiss. U.-Technol.*, 30, 45.

27. Hongsprabhas, P., Barbut, S., and Marangoni A.G. (1999). *Lebensm.-Wiss. U.-Technol.*, 32, 196.
28. Ju, Z.Y., and Kilara, A. (1998) *J. Agric. Food Chem.*, 46, 1830.
29. Ju, Z.Y., and Kilara, A. (1998). *J. Agric. Food Chem.*, 46, 3604.
30. Kinekawa, Y-I., Foyuki, T., and Kitabatake, N. (1996) *J. Dairy Sci.*, 81, 1532-1544.
31. Roff, C.F., and Foegeding, E.A. (1996). *Food Hydrocolloids*, 10, 193.
32. Sato, K., Nakamura, M., Nishiya, M., Kawanari, M., and Nakajima, I. (1995). *Milchwissenschaft*, 50, 389.
33. Veerman, C., Bapist, H., Sagis, L.M.C. and van der Linden, E. (2003). *J. Agric. Food Chem.*, 51, 3880.
34. Vreeker, R., Hoekstra, L.L., den Boer, C., and Agterof, W.G.M. (1992). *Food Hydrocolloids*, 5, 423.
35. Kitabatake, N., Hatta, H., and Doi, E. (1987) *Agric. Biol. Chem.*, 51, 771.
36. Alting A.C., Weijers, M., de Hoog, E.H.A., van de Pijpekamp, A.M., Cohen Stuart, M.A., Hamer, R.J., de Kruif, C.G., and Visschers, R.W. (2004). *J. Agric. Food Chem.*, 52, 623.
37. Soeda, T. (1996). *J. Jap. Soc. Food Sci. Technol.*, 43, 130.
38. Soeda, T. (1997). *J. Jap. Soc. Food Sci. Technol.*, 44, 393.
39. Nisbet, A.D., Saundry, R.H., Moir, A.J.G., Fothergill, L.A., and Fothergill, J.E. (1981). *Eur. J. Biochem.*, 115, 335.
40. Gossett, P.W, and Rizvi, S.S.H. (1984). *Food Technol.*, 38.
41. [http://www.food-allergens.de/symposium-voll1\(1\)/data/egg-white/egg-composition.htm](http://www.food-allergens.de/symposium-voll1(1)/data/egg-white/egg-composition.htm)
42. Awadé, A.C., and Efstathiou T. (1999). *J. Chromatogr. B*, 723, 69.
43. Hammershøj, M., Larsen, L.B., Andersen, A.B., and Qvist, K.B. (2002). *Lebensm. Wiss. U.-Technol.*, 35, 62.
44. Donovan, J.W., Mapes, C.J., Davis, J.G.D., and Garibaldi, J.A., (1975). *J. Sci. Fd Agric.*, 26, 73.
45. Kitabake, M., Ishida, A., and Doi, E. (1988). *Agric. Biol. Chem.*, 52, 967.
46. Stein, P.E., Leslie, A.G.W., Finch, J.T., and Carell, R.W. (1991). *J. Mol. Biol.*, 941.
47. Nakamura, R., and Ishimaru, M. (1981). *Agric. Biol. Chem.*, 45, 2775.
48. McKenzie, H.A. (1971). In *Milk proteins: Chemistry and Molecular Biology*, Academic Press, New York, vol II, pp 255.
49. Kinsella, J.E., and Whitehead, D.M. (1989). *Adv. Food Nutr. Res.*, 33, 343.
50. Hoffmann, M.A., and Mil, van, J.J.M. (1997). *J. Agric. Food Chem.*, 45, 2942.
51. Papiz, M.Z., Sawyer, L., Eliopoulos, E.E., North, A.C.T., Findlay, J.B.C., Sivaprasadarao, R., Jones, T.A., Newcomer, M.E., and Kraulis, P.J. (1986). *Nature*, 324, 383.
52. Aymard, P., Durand, D., and Nicolai, T. (1996). *Int. J. Biol. Macromol.*, 19, 213.

PART I

DENATURATION, AGGREGATION AND GELATION UNDER HEAT-SETTING CONDITIONS

CHAPTER 2

HEAT-INDUCED DENATURATION AND AGGREGATION OF OVALBUMIN AT NEUTRAL PH DESCRIBED BY IRREVERSIBLE FIRST-ORDER KINETICS

Weijers, M., Barneveld, P.A., Cohen Stuart, M.A. and Visschers, R. W.

Protein Science 2003, 12, 2693-2703

Protein Science 2003, 12, 2693-2703

ABSTRACT

The heat-induced denaturation kinetics of two different sources of ovalbumin at pH 7 was studied by chromatography and differential scanning calorimetry. The kinetics was found to be independent of protein concentration and salt concentration, but was strongly dependent on temperature. For highly pure ovalbumin, the decrease in non-denatured native protein showed first-order dependence. The activation energy obtained with different techniques varied between 430 and 490 kJ·mol⁻¹. First-order behavior was studied in detail using differential scanning calorimetry. The calorimetric traces were irreversible and highly scan rate dependent. The shape of the thermograms as well as the scan rate dependence can be explained by assuming that the thermal denaturation takes place according to a simplified kinetic process $N \xrightarrow{k} D$, where N is the native state, D is denatured (or another final state) and k a first-order kinetic constant that changes with temperature, according to the Arrhenius equation. A kinetic model for the temperature-induced denaturation and aggregation of ovalbumin is presented. Commercially obtained ovalbumin was found to contain an intermediate-stable fraction (IS) of about 20% that was unable to form aggregates. The denaturation of this fraction did not satisfy first-order kinetics.

2.1 INTRODUCTION

Aggregation of proteins is an important process in many biological systems and industrial processes. In biological systems it is required for the assembly of structures with specific functions such as microtubules, blood-clots and viral coatings. The formation of plaques is also related to aggregation of specific proteins that have somehow been modified. The aggregation of proteins is in general triggered by a conformational change of the protein induced by heat, enzymatic cleavage or other processes that affect the folded structure. After this change of structure a series of reactions takes place that lead to the formation of aggregates. In many cases it is not clear what drives the formation of specific structures in these aggregates or the formation of fibrils.¹ Here we present a study of the heat-induced aggregation of chicken egg white ovalbumin. Ovalbumin is known to form fibrillar types of aggregates upon aggregation and, at high enough protein concentrations, a gel can be formed.² It is our aim to use ovalbumin as a model system to study how fibrillar aggregates can be formed and what conditions affect the properties of these aggregates. The results are relevant both to understanding the biological function of protein aggregation and for the industrial applications of proteins in food and non-food systems.

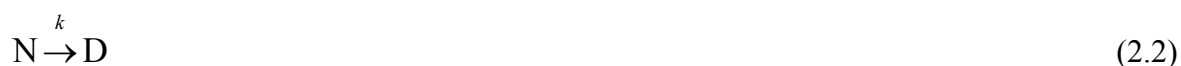
Egg white ovalbumin is a member of the serine protease inhibitor (serpin) superfamily, but shows no recognized protease-inhibitory activity.³ Egg white proteins are applied in a wide range of food products. The ability of egg white proteins to form a gel upon heating and their water-binding and emulsifying capacity are important functional properties.⁴ Typical applications are in the meat industry (emulsifier), in foams, in the confectionery industry and in bakery products.^{5,6} For most functional applications, denaturation and aggregation is required. Ovalbumin is the major protein in egg albumin and much work has been conducted on its thermal aggregation and gelation.⁷⁻¹⁴ It was found by Smith and Back¹⁵ that ovalbumin behaves as a mixture of two proteins, where the amount of S-ovalbumin depends on the storage time and pH of the eggs. In literature, different terminologies are used for ovalbumin. Native (N-) ovalbumin can be converted into Stable (S-) ovalbumin through the formation of an Intermediate (I-). All these species are able to aggregate. The ovalbumin used in this study (SIGMA) contains N-ovalbumin (N₁) and a fraction native ovalbumin (N₂) which can denature, but not aggregate. The DSC profile shows this intermediate fraction and this fraction is therefore referred as Stable Intermediate (SI-) ovalbumin.

To study the heat-induced denaturation of ovalbumin, we used the model proposed by Lumry and Eyring¹⁶ for the irreversible denaturation.



Here N, U, D and A are native, unfolded, denatured and aggregated protein forms respectively and k_1 , k_{-1} and k_2 are the rate constants for the corresponding reactions. We assume that only D can form aggregates. A commonly used method to study the transition from the native to the denatured state is differential scanning calorimetry (DSC). Equilibrium analysis (N↔U) of DSC thermograms corresponding to reversible unfolding of proteins provides information about the thermodynamics and mechanisms of the reversible unfolding.¹⁷⁻¹⁹ However, there are many proteins whose denaturation is irreversible²⁰⁻²⁴ probably due to the occurrence of “side” processes such as aggregation.²⁵ Due to denaturation, hydrophobic interaction can occur and exposed thiol groups can form disulfide bonds, which results in irreversible behavior. Unfolding in the absence of denaturation has been studied using different denaturants,²⁶ but is of less importance in this study, because no kinetic parameters (E_a) can be obtained. Here, thermodynamic parameters such as K will be obtained. Analysis of DSC data for the irreversible denaturation has been reported by several authors.²⁷⁻²⁹ In these cases, theoretical equations describing the dependence of the excess heat capacity on temperature were fitted to experimental DSC curves.

Irreversible protein denaturation, as shown in equation 2.1, involves at least two steps: reversible unfolding of the native protein, followed by the irreversible alteration of the unfolded state to a denatured state and possibly to another final state. If $k_2 \gg k_{-1}$, most of the U molecules will be converted to D (or another final state). The concentration of U will be very low and the amount of U converted into D is restricted to k_1 . This results in a simple first-order reaction, the DSC analysis of which has been worked out by Sanchez-Ruiz²¹ using a practical two-state model is represented by:



To study aggregation kinetics, DSC is not a useful technique. Gel permeation chromatography is a more suitable method. The aggregation process can be quenched by rapidly cooling the sample to room temperature. Structural properties of the aggregates

formed can then be studied. Recently, we reported a detailed study of the heat-induced aggregation and gelation of ovalbumin at low and high ionic strength at neutral pH.² As mentioned above, heat-induced aggregation of ovalbumin has been studied intensively by several workers, but none of the earlier investigations on ovalbumin clearly showed the effect of concentration or demonstrated that first-order kinetics applies. Koseki et al. found that when a 5 g/L ovalbumin solution in 20 mM potassium-phosphate buffer of pH 7 was heated, the process satisfied first order kinetics.^{30,31}

In the present study, we investigated the rate of protein conversion for many conditions by varying temperature, protein concentration and salt concentration. Samples were analyzed by gel-permeation chromatography (GPC). From these results the reaction order, energy of activation (E_a) and the overall rate constants were determined. Subsequently, the kinetic parameters determined by GPC were combined with the kinetic parameters found with DSC, and we propose a new model for the heat-induced denaturation and aggregation of ovalbumin. This model (an extension of the Lumry and Eyring model), which incorporates a heat-stable fraction, is used to describe both sets of experimental data (protein conversion upon heating and DSC data).

2.2 MATERIALS AND METHODS

2.2.1 MATERIALS

Two different sources of hen egg ovalbumin were used in this study. Ovalbumin was purified from egg white of freshly laid hens' eggs (less than 2 hours) based on the procedure of Vachier et al.³² In the text, this source of pure ovalbumin is referred to 'WCFS-ovalbumin'. Another source of hen egg ovalbumin was purchased from Sigma (grade V, >99% pure by agarose electrophoresis, crystallized and lyophilized, Lot # 19H7002). This type of ovalbumin is referred in the text as SIGMA ovalbumin. The purity of both sources was checked with Mass spectrometry and SDS PAGE. The latter showed for WCFS ovalbumin one clear spot at 45 kDa and for Sigma ovalbumin an additional very small spot was observed at about 80 kDa (data not shown). Mass spectrometry was not possible for ovalbumin because it showed many envelopes since it contains 2, 1 and 0 phosphate groups per molecule and is usually glycosylated.

For kinetic experiments, ovalbumin (both WCFS and SIGMA) was dissolved in double-distilled water with 3 mM NaN_3 added to avoid bacterial growth. Final protein concentrations were varied between 0.1 and 60 g/L and NaCl concentrations between 0 and

100 mM. The solutions were subsequently stirred for at least 2 hours at ambient temperature to allow the protein to dissolve. The pH of the solution was adjusted to 7.0 and the solution was subsequently centrifuged and filtered (0.45 μm ; Millex-SV, Millipore Corp., Bedford, MA) to remove a small fraction of insoluble material. The protein solutions were heated in screw-cap vials containing ca. 5 ml of ovalbumin solution in a temperature-controlled water bath at temperatures varying between 68.5 and 80°C. After heating, the solutions were rapidly cooled by placing the tubes in ice-water. The amount of non-denatured native proteins after heat treatment was determined with a standard assay involving acid precipitation and high-performance Size exclusion chromatography (HPSEC).³³ The total amount of monomeric protein (non-denatured as well as denatured) after heat treatment was determined with a standard assay without acidification step, employing Size exclusion chromatography in combination with multi angle laser light scattering (SECMALLS).

For differential scanning calorimetry (DSC) experiments, ovalbumin solutions (WCFS) of 1, 5, 10 and 20 g/L without added NaCl were prepared as described above. For ovalbumin solutions (SIGMA), concentrations of 20 and 35 g/L without added NaCl were used.

2.2.2 METHODS

HPSEC

For the determination of the rate of decrease in concentration of non-denatured ovalbumin upon heating, different series of screw-cap vials containing ca. 5 ml of ovalbumin solution with different initial concentrations were heated at 80, 78, 75, 72, and 68.5°C for WCFS ovalbumin, and 80, 78, 76.5, 75, 72, and 70°C for SIGMA ovalbumin. The vials were cooled in ice-water and the protein solutions were diluted to a final concentration of non-denatured protein in the range of 0.1 to 5 g/L, to be within the calibration range. Then, the pH was adjusted to 4.7 ± 0.1 with 0.1M HCl, which causes the denatured and aggregated ovalbumin to precipitate. After centrifugation at 20,000g for 5 minutes at ambient temperature, the concentration of non-denatured ovalbumin in the supernatant was determined by HPSEC (Phenomenex BioSep-SEC-S2000 column, 300 \times 7.5 mm) with UV detection at 280 nm. In this report, this technique is referred to the

‘acidification’ method and is assumed to measure the amount of non-denatured native protein left after heating.

SECMALLS

Heated ovalbumin solutions (without acid treatment) were injected after cooling into a high-performance gel chromatography system consisting of a PL-GFC 300, PL-GFC 1000 and PL-GFC 4000 column (300×7.5 mm) in series (Polymer Laboratories Ltd., UK). The specified exclusion limits of these three columns are $1 \cdot 10^5$, $2 \cdot 10^6$, $1 \cdot 10^7$ Da respectively. The eluant was a 25 mM TRIS/Tricine buffer, pH 8.0, the flow rate was 1.0 ml/min. Heated ovalbumin samples were diluted with double-distilled water to a protein concentration of approximately 10 g/L. These samples were subsequently diluted with two-fold concentrated eluant (50 mM TRIS/Tricine), after which 200 μ L aliquots were injected into the chromatographic system. This technique is referred in this report as the ‘non-acidification’ method; it determines the total amount of monomeric protein (both native and denatured).

For on-line light-scattering detection a DAWN-F MALLS photometer (Wyatt Technology, Santa Barbara, California) was used, equipped with a K5 flow cell and a linearly polarized He-Ne laser light source (5 mW) with a wavelength of 632.8 nm. The DAWN contains 18 detectors, but the four smallest scattering angles (θ) were excluded, as the signal-to-noise ratio of these detectors was too low for an accurate measurement. The concentration of the eluting material was determined with a UV spectrophotometer (Jasco CD-1595, Japan) at 280 nm and a differential refractometer (ERC-7510 ERMA Optical Works Ltd). The data were accumulated and processed using Astra for Windows, version 4.0. The molar mass M_i of the ovalbumin monomers and aggregates in each fraction i was calculated with a first-order Debye fit, using a specific refractive index increment (dn/dc) of $0.172 \text{ cm}^3/\text{g}$ for ovalbumin in TRIS/Tricine buffer.

DSC

DSC scans were carried out with a SETARAM (Caluire, France) micro DSC III with stainless steel 1 ml sample cells. Calibration was done with naphthalene. The DSC has two measuring cells: one is used for the sample and the other for the reference. Samples were prepared at ovalbumin (WCFS) concentrations of 5, 10, and 20 g/L, pH 7.0, without added

salt. For ovalbumin (SIGMA) concentrations of 20 and 35 g/L were used. The same solution without the protein was used in the reference cell. The temperature was scanned from 25 to 120°C at scanning rates of 0.05, 0.10, 0.20, 0.30, 0.50, 1.00, 1.50, 2.00, and 3.00 °C min⁻¹. In order to obtain the C_p^{eff} curves, reference-reference baselines were obtained at the same scanning rate and subtracted from the sample curves.

For DSC scans at an ovalbumin (WCFS) concentration of 1 g/L, a Microcal MC-2 calorimeter was used. Experiments with varying protein concentrations in the range of 1-10 g/L have shown that DSC transitions do not depend on protein concentration (data not shown).

The statistics of the fit are calculated using the following equation:

$$\chi^2 = \frac{1}{n^{\text{eff}} - p} \sum [y_i - f(x_i; p_1, p_2, \dots)]^2$$

where n^{eff} are the number of data points and p the number of parameters.

2.3 RESULTS

2.3.1 CONVERSION OF MONOMERS INTO AGGREGATES INUCED BY HEATING

The heat-induced conversion of ovalbumin monomers to aggregates at neutral pH was measured using two slightly different chromatographic techniques: HPSEC and SEC-MALLS. Temperature, ovalbumin concentration, NaCl concentration and protein source (WCFS and SIGMA) were varied. The heat-induced aggregates are stable under cooling and dilution and can thus be characterized at room temperature. As described in the materials and methods section, with HPSEC the samples were acidified to their isoelectric point prior to elution, the denatured and aggregated protein precipitated and the amount of non-denatured monomeric protein left after heating was determined. With SEC-MALLS the heated protein samples, which were cooled to room temperature, were injected on the column without further treatment. In this case, denatured as well as non-denatured monomers will elute at the same volume, and consequently no discrimination between denatured and non-denatured monomers can be made. Combining the results determined with both techniques allowed us to properly discriminate non-denatured, denatured monomers and the aggregated fractions.

Figure 2.1 shows a chromatogram of heated ovalbumin (WCFS) that was not acidified prior to elution. The ovalbumin solutions were heated at 72°C for different times ranging

from 0 to 5000 minutes. Ovalbumin aggregates elute at volumes between 18 and 23 ml. With increasing heating time, the relatively broad aggregate peak shifts to smaller volumes and the scattered intensity of the aggregate peak increases, this means that the size and amount of the aggregates formed increases. The inset in figure 2.1 shows the weight average molar mass of the aggregate peak as calculated from the MALLS data. The molar mass increased from $47 \cdot 10^3$ Da (M of a monomer) for the shortest heating times to $2 \cdot 10^6$ Da (corresponding to aggregates consisting of approximately 45 monomers) for a heating time of $1 \cdot 10^4$ minutes. The ovalbumin aggregates were always large enough to be clearly distinguished from native proteins. This indicates that under these conditions no or very few stable oligomers (dimers, trimers etc.) are formed. The size of the aggregates depends on the initial protein concentration and salt concentration during heating, as reported earlier.² The polydispersity (M_w/M_n) of the ovalbumin aggregates was approximately 1.5 and did not change significantly as a function of heating time.

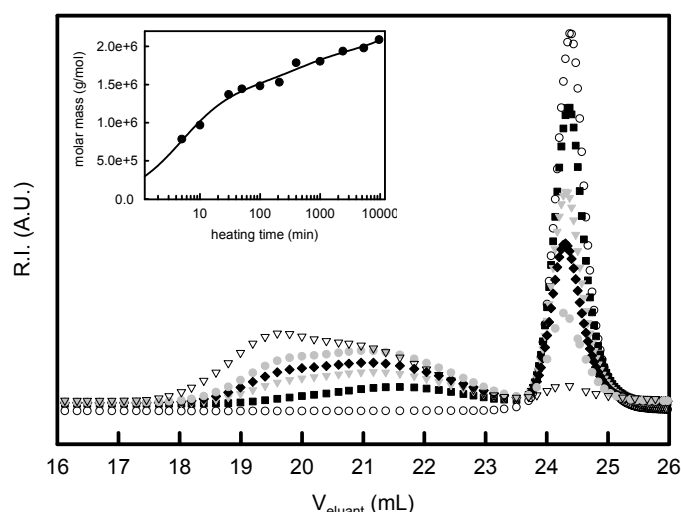


Figure 2.1. Chromatograms of ovalbumin (WCFS) solutions at pH 7, $C=27.1 \text{ g l}^{-1}$ and 200 ppm NaN_3 at different heating times at 72°C . Heating times: \circ not heated; \blacksquare 10 minutes; \blacktriangledown 30 minutes; \blacklozenge 50 minutes; \bullet 100 minutes; ∇ 5338 minutes. The inset shows the molar mass of the aggregates formed corresponding to the aggregate peaks in the chromatogram.

The narrow peak at volumes between 24 and 25 ml corresponds to non-aggregated monomers. With increasing heating time, the fraction of monomers decreases and stabilizes at about 6% monomers for heating times longer than 1000 minutes. The size distribution of this fraction was narrow; the polydispersity was about 1.0 and did not increase upon heating.

2.3.2 COMPARISON OF THE ACIDIFYING AND NON-ACIDIFYING METHOD

The fraction of monomers as a function of heating time, for the acidifying and non-acidifying methods, is shown in figure 2.2 for two protein samples (WCFS and SIGMA). Data from acidified and non-acidified heated samples gave significantly different results at long heating times. When SIGMA ovalbumin samples had been subjected to long heating times and subsequently acidified, we found precipitation of all of the monomers, whereas the same samples without acid treatment showed a stable intermediate fraction (SI-ovalbumin) of monomers of approximately 20%. The abundance of this stable fraction did not depend on temperature in the range 72°C to 85°C (data not shown). From the nature of the techniques used, we therefore conclude that this SI-fraction is due to monomers that are denatured but not aggregated. These SI-fractions do not aggregate and therefore cannot participate in the formation of a network. Consequently, this SI-fraction does not contribute to the structure and gelling functionality. Similar results were obtained for WCFS ovalbumin, but the SI-fraction was smaller, namely approximately 6%.

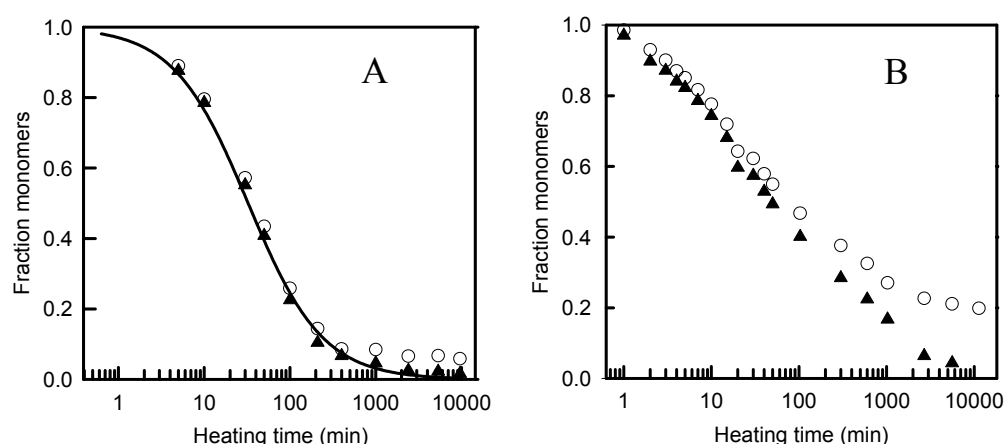


Figure 2.2. Heating time dependence of the fraction of monomers using the non-acidifying (○) and acidifying (▲) method. (A) WCFS ovalbumin (pH 7, $C=27 \text{ g l}^{-1}$, $T=72^\circ\text{C}$), (B) SIGMA ovalbumin (pH 7, $C=27 \text{ g l}^{-1}$, $T=78^\circ\text{C}$). Solid line in panel A represents a fit with reaction order 1.

2.3.3 DEPENDENCE OF TEMPERATURE AND PROTEIN CONCENTRATION ON THE DENATURATION RATE

In order to present a kinetic model for the temperature-induced denaturation and aggregation, a detailed study of the influence of temperature and protein concentration on the denaturation rate was carried out. The relative concentration of non-denatured

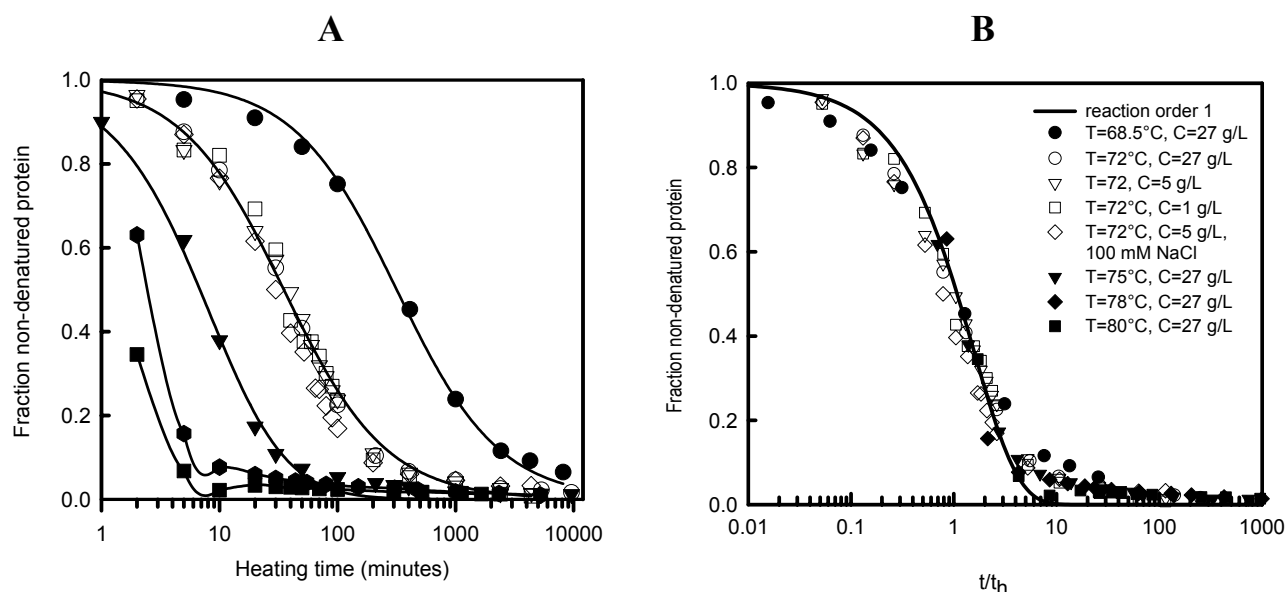


Figure 2.3. Heating time dependence of the fraction of non-denatured ovalbumin (WCFS) under different conditions. (B) Same data as in (A) plotted as a function of heating time, normalized by the time needed to denature and aggregate half of the proteins (t_h). Solid lines in panel A are guides to the eye.

ovalbumin in the supernatant as a function of heating time, at five temperatures and three initial protein concentrations, is shown in figure 2.3a. Table 2.1 gives an overview of all conditions investigated, for WCFS ovalbumin as well as for SIGMA ovalbumin, and the half time of these reactions. From figure 2.3 and table 2.1, three interesting observations can be made:

1. A strong temperature dependence on the reaction rate was observed. At 80°C half of the protein was denatured and aggregated in less than 2 minutes (half time, t_h), while at 68.5°C this took approximately 6 hours. For SIGMA ovalbumin the effect was even bigger. The rate at which the proteins denatured was strongly temperature dependent, but the shape of the conversion-time curves was the same for all conditions. This is illustrated in figure 2.3b, where the data are plotted as a function of time normalized by t_h . Clearly all data superimpose within experimental error. The data satisfy a denaturation rate with order 1 (solid curve in Fig. 2.3B). The temperature dependence of the denaturation rate is shown to satisfy Arrhenius' relation (Fig. 2.4b). An activation energy of about 480 kJ·mol⁻¹ was found. This is comparable to the activation energy found for other proteins, such as β -lactoglobulin,³⁴ actin, carboxypeptidase, creatine kinase, et cetera.²⁹ The large value of E_a might be expected, because the highly

cooperative nature of the protein implies a large Δh between the folded and denatured protein, and E_a always larger than Δh (see also Le bon et al.).³⁴

Table 2.1. Heating conditions of WCFS and SIGMA ovalbumin and the half times (t_h), in which 50% of the protein was denatured and/or aggregated.

<i>Ovalbumin (WCFS)</i>			<i>Ovalbumin (SIGMA)</i>					
Temp. (°C)	Conc. (g/L), added salt	t_h (min) ^a	Temp. (°C)	Conc. (g/L), added salt	t_h (min) ^a	Temp. (°C)	Conc. (g/L), added salt	t_h (min) ^a
80	27, 0 mM	1.2	80	27, 0 mM	1	72	27, 0 mM	126
78	27, 0 mM	2.3 (2.6)	78	27, 0 mM		72	10, 20 mM	125
75	27, 0 mM	7.2 (7.9)	76.5	27, 0 mM	6.7	72	10, 50 mM	127
72	27, 0 mM	37 (39)	76.5	10, 0 mM	5.8	72	10, 100 mM	126
72	5, 0 mM	37(35)	76.5	5, 0 mM	6.8	70	27, 0 mM	500
72	5, 100 mM	37 (37)	76.5	1, 0 mM	6.4			
72	1, 0 mM	37 (43)	74.8	27, 0 mM	48			
68.5	27, 0 mM	320 (306)	72	60, 0 mM	126			

^a t_h determined from figure 2.3, between brackets the value of t_h calculated from first order kinetics ($\ln 2/k$) as shown in figure 2.4A.

2. The half time of the reaction, as described in table 2.1, did not depend on initial protein concentration (within the experimental range of 0.1 – 60 g/L) (Fig. 2.5). Also, no dependence of the ionic strength on the half time was found (in the range of 3 – 100 mM). This is different from results found for β -lactoglobulin, here the decrease in concentration of native β -lactoglobulin during heating was fitted by a reaction order of 1.5.^{34,35} For comparison, the concentration dependence of the half time of β -lactoglobulin is also plotted in figure 2.5 (data taken from Le Bon et al.).³⁴ From the data presented in figure 2.5, they found for β -lactoglobulin a total reaction order of 1.5. From the results so far, it is clear that the decrease of non-denatured protein as a function of heating time only depends on temperature and neither on protein concentration nor on NaCl concentration, which suggests that a uni-molecular process like denaturation is the rate-limiting step in this process.
3. Finally, remarkable differences in denaturation rates were observed between the two sources of ovalbumin. SIGMA ovalbumin denatures much more slowly than WCFS ovalbumin. This may be due to the storage time of the eggs before purification or to the purification itself, and will be discussed in the general discussion section.

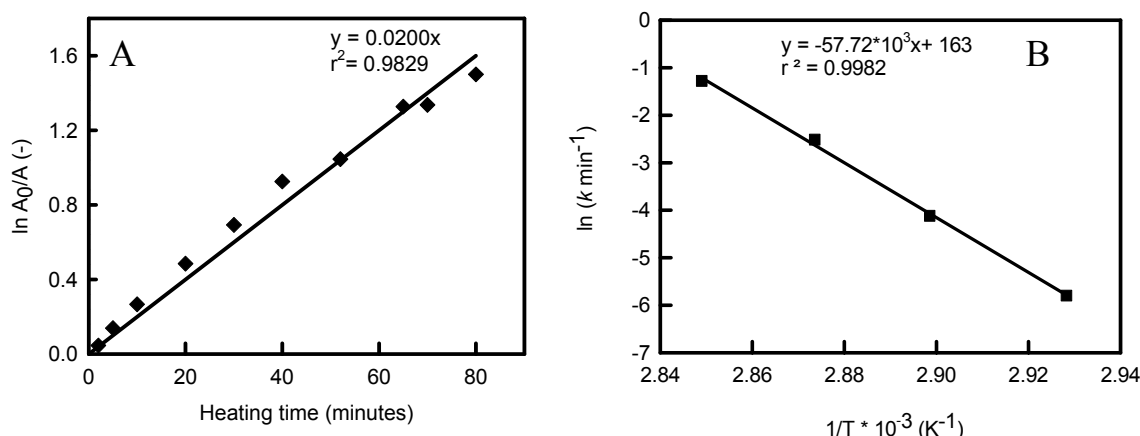


Figure 2.4. (A) The fraction of non-denatured ovalbumin (WCFS) ($A_0=5$ g/L, $[\text{NaCl}]=100$ mM, $T=72^\circ\text{C}$) as a function of heating time shows a first-order dependence. The half time (t_h) is calculated from $\ln 2/k$, where k is a temperature-dependent rate constant, obtained from the slope. (B) Arrhenius plot obtained from data from figure 2.3A, which are analysed as in figure 2.4A.

2.3.4 DIFFERENTIAL SCANNING CALORIMETRY OF OVALBUMIN UNDER IRREVERSIBLE CONDITIONS

Differences between WCFS and SIGMA ovalbumin were also observed with DSC. Figure 2.6 shows the DSC thermograms of both ovalbumin sources, at a scan rate of $0.5^\circ\text{C min}^{-1}$. For both ovalbumin sources the calorimetric transitions were apparently irreversible. After cooling from the first run, no transition could be detected in the second heating run. The ovalbumin obtained from SIGMA shows two overlapping endothermic peaks centered at 78.4°C (T_{p1}) and 82.45°C (T_{p2}) respectively. The second peak represents a stable-intermediate (SI), which is an intermediate in the conversion of native ovalbumin (N) into stable ovalbumin (S). The presence of this intermediate has been reported by others.^{36,37} The appearance of two distinct peaks in the thermogram of SIGMA ovalbumin indicates that no rapid conversion between the two native states is possible, and therefore both fractions denature independently. A fast equilibrium between the two fractions (N_1 and N_2) would imply a fixed ratio between N_1 and N_2 . Therefore, the ratio between $\frac{dD_1}{dt}$ and $\frac{dD_2}{dt}$ would also be fixed and no calorimetric distinction could be made between the two fractions. Barbut and Findlay have shown that when ovalbumin and its stable form (S-ovalbumin) are both present in a solution, they undergo denaturation independently

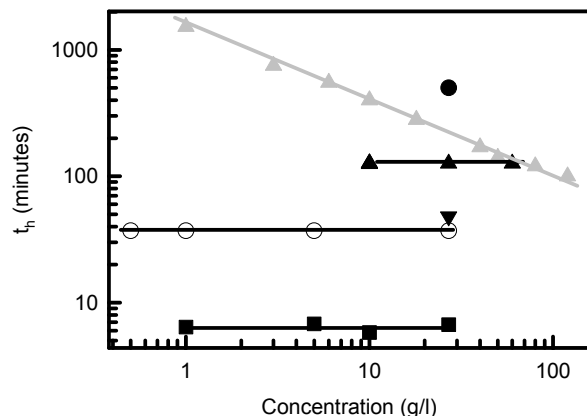


Figure 2.5. Concentration dependence of the half time for ovalbumin and β -lactoglobulin (data β -lactoglobulin taken from Le Bon et al., 1999). Black symbols represent SIGMA ovalbumin. Open symbols represent WCFS ovalbumin and grey symbols represent β -lactoglobulin. Heating conditions: ● $T=70^\circ\text{C}$; ▲ $T=72^\circ\text{C}$; ▼ $T=75^\circ\text{C}$; ■ $T=76.5^\circ\text{C}$; ○ $T=72^\circ\text{C}$; ▲ $T=67^\circ\text{C}$.

From DSC experiments (Fig. 2.6), the presence of an SI- fraction of about 20%, as observed with SEC-MALLS, is confirmed. We suggest that the decrease in denaturation rate of SIGMA ovalbumin is probably due to the interference of a 20% SI-fraction (intermediate between N-ovalbumin and S-ovalbumin), which can denature but cannot aggregate. Lumrey and Eyring¹⁶ originally proposed the two-state kinetic model. Based on our findings, we propose an irreversible two-state kinetic model for the denaturation and aggregation of ovalbumin in general.

In our model we assume two different native states in the starting material; both native states denature independently upon heating. There is no fast equilibrium between N_1 and



N_2 . Denaturation is the rate-limiting step in this process, which means that when the protein unfolds (and denatures), one of the denatured states (D_1) aggregates immediately, while the other one cannot aggregate and is therefore referred to as the stable fraction (D_2).

As we show below, our irreversible two-state kinetic model, based on a mixture of two different ovalbumin fractions, is supported by DSC measurements.

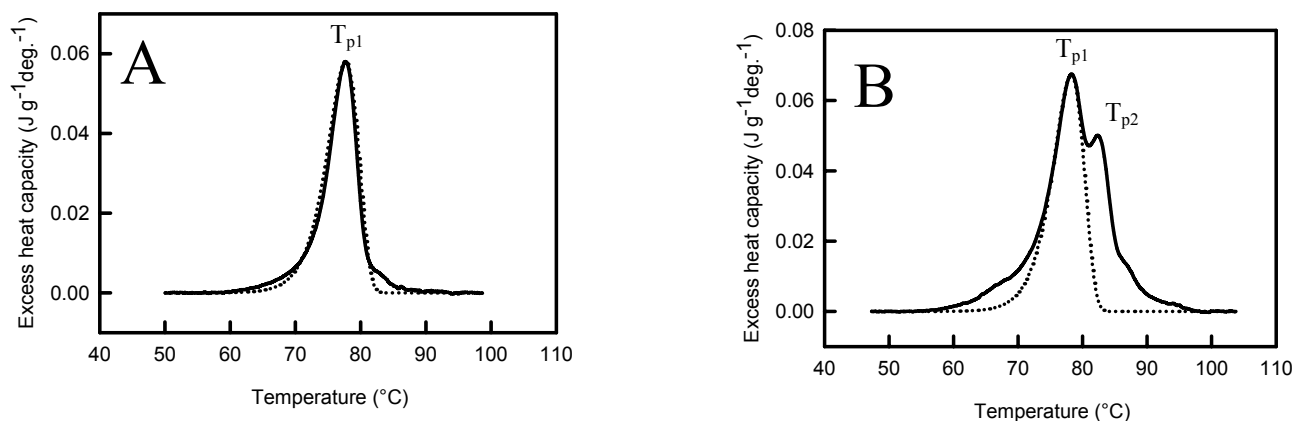


Figure 2.6. Differential scanning calorimetry thermograms and the best fit of the two-state irreversible denaturation model (χ^2 of $4 \cdot 10^{-6}$) of WCFS ovalbumin (A) and SIGMA ovalbumin (B) solutions at a scan rate of 0.5°C/min (solid lines) and pH 7.0, protein concentrations of 20 g/L and 35 g/L respectively. Dashed lines represent irreversible first-order fits.

From detailed DSC experiments we attempted to get answers to the following questions. (1) What is the activation energy of both sources of ovalbumin and are these values comparable with the values found for E_a with other techniques as described above? (2) Can we describe experimental DSC thermograms of WCFS and SIGMA ovalbumin with irreversible first-order kinetics? (3) Is it possible to describe experimental data for the conversion of non-denatured monomers into aggregates with two first-order rate constants, as we assume in our model?

Table 2.2. Effect of scan rate on peak temperatures (T_p) for WCFS ovalbumin (C=10 g/L) and SIGMA ovalbumin solutions (C=20 g/L).

Ovalbumin (WCFS)		Ovalbumin (SIGMA)		
Scanrate (°C/min)	T_{p1} (°C)	Scanrate (°C/min)	T_{p1} (°C)	T_{p2} (°C)
0.10	74.81	0.05	X	78.22
0.20	75.40	0.10	75.72	79.41
0.30	76.66	0.20	76.62	80.78
0.50	77.72	0.50	78.38	82.45
1.00	79.04	1.00	79.86	83.46
1.50	79.71	1.50	80.66	83.31
2.00	80.82	2.00	81.34	83.95

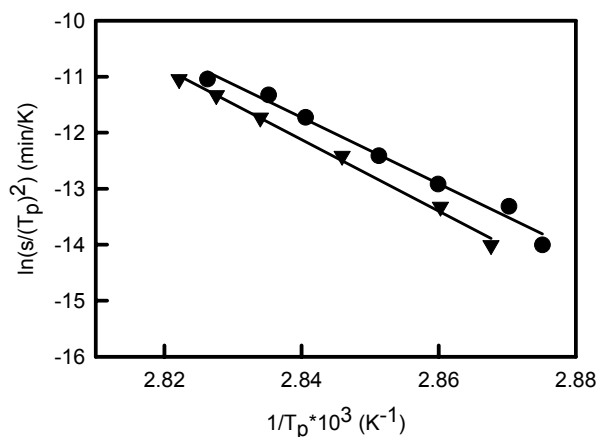


Figure 2.7. Plots of $\ln(v/T_p^2)$ versus $1/T_p$ for WCFS (●) and SIGMA (▼) ovalbumin corresponding to Equation 2.2 in the text. Each data point corresponds to a scan rate given in table 2.2.

2.3.5 ACTIVATION ENERGY OF OVALBUMIN

The activation energy for the denaturation of ovalbumin can be obtained from the scan rate dependence of the peak temperature from a DSC thermogram. Table 2.2 gives the temperatures corresponding to the maximum in heat capacity (T_p) at different scan rates for both ovalbumin sources. The results presented in table 2.2 clearly show a strong dependence on the scan rate, which indicates the absence of equilibrium between native and the denatured state, during scanning.

To check whether the results are in agreement with the proposed first-order reactions, we used the model developed by Sanchez-Ruiz et al.²¹ Briefly, the two-state model can be represented as $N \xrightarrow{k} D$, where N is the native state, D is the unfolded state or, more probably, a final state, with k being a first-order rate constant. From the following equation the energy of activation can be calculated from DSC data.

$$\frac{v}{T_p^2} = \frac{AR}{E} e^{-E_a/RT_p} \quad (2.4)$$

Where v is the scan rate, E_a the energy of activation, A the frequency factor of the Arrhenius equation and R the gas constant.

If the proposed model is correct, equation (2.4) requires a linear dependence of $\ln(v/T_p^2)$ versus $1/T_p$. Indeed a linear dependence is observed (see Fig. 2.7). The E_a calculated from the scan rate dependence was found to be $490 \text{ kJ}\cdot\text{mol}^{-1}$ for WCFS

ovalbumin, which is in very good agreement with values found with other techniques as reported in table 2.3. The energy of activation obtained from the scan rate dependence for SIGMA ovalbumin is obtained for the main fraction. The scan rate dependence of the main peak is almost identical to the WCFS one with an E_a of $530 \text{ kJ}\cdot\text{mol}^{-1}$. The E_a of the additional fraction (T_{p2}) has not been calculated, because it is doubtful from HPSEC and DSC analysis whether this fraction shows first-order behavior. Using the E_a and A obtained from experimental data of WCFS and SIGMA (T_{p1}) ovalbumin, the rate constants are calculated at different temperatures (Fig. 2.8). From figure 2.8 it is clear that the rate constants for WCFS and the main fraction of SIGMA ovalbumin are almost identical. This indicates that the main fraction of SIGMA is probably the same as the WCFS ovalbumin and that both can be described with first-order kinetics.

Table 2.3. Activation energy (E_a) and frequency factor (A) of the Arrhenius equation determined from experimental DSC and HPGPC data and the best fit (thermograms) for WCFS and SIGMA ovalbumin.

	HPGPC		DSC		DSC FIT
	$E_a \text{ (kJ}\cdot\text{mol}^{-1})$	$A \text{ (-)}$	$E_a \text{ (kJ}\cdot\text{mol}^{-1})$	$A \text{ (-)}$	$E_a \text{ (kJ}\cdot\text{mol}^{-1})$
WCFS	480	6.17×10^{70}	492	5.17×10^{72}	430
SIGMA (T_{p1})			530	1.67×10^{78}	430

2.3.6 FITTING THERMOGRAMS OF OVALBUMIN WITH IRREVERSIBLE FIRST-ORDER KINETICS

Figure 2.6 shows the best fit of the experimental DSC profile (including a baseline correction, resulting in $\Delta C_p = 0 \text{ Jg}^{-1}\text{K}^{-1}$) recorded at $0.5 \text{ }^\circ\text{C}/\text{min}$, for WCFS and SIGMA ovalbumin. It is evident that the two-state irreversible denaturation ($N \rightarrow D$) model reproduces the experimental data well in the whole temperature range for WCFS ovalbumin. The parameters obtained from the best fit are: $E_a = 430 \text{ kJ}\cdot\text{mol}^{-1}$; $T_{p1} = 77.68 \text{ }^\circ\text{C}$ using the condition that the surface area under the peak is the same: $\Delta h \approx 800 \text{ kJ}\cdot\text{mol}^{-1}$. Note that DSC measures the Δh of the overall process, while kinetics deals only with the rate determining step. This result is an additional indication of a multi-step reaction. Attempts were also made to fit the experimental data for SIGMA ovalbumin by the two-state irreversible denaturation model. The main peak is successfully generated with almost the same parameters as for WCFS ovalbumin: $E_a = 430 \text{ kJ}\cdot\text{mol}^{-1}$; $T_{p1} = 78.28 \text{ }^\circ\text{C}$ and $\Delta h \approx 800 \text{ kJ}\cdot\text{mol}^{-1}$, where the fraction participating in the main peak was 81% (SI-fraction

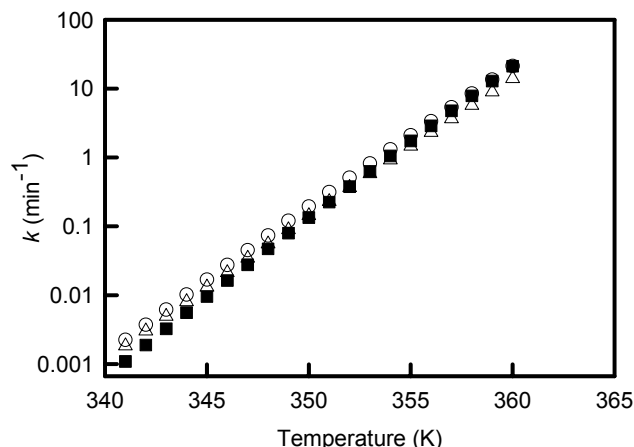


Figure 2.8. Rate constant (k) for WCFS and SIGMA ovalbumin as a function of temperature. First-order rate constant changes with temperature as described in the Arrhenius equation; frequency factor and energy of activation are obtained from table 2.3. Rate constants calculated for: ○ WCFS (DSC); Δ WCFS (HPGPC); ■ SIGMA (T_{pl}).

19%). We neglected the minor shift of the peak due to the additional fraction. However, the best fit of the additional peak was less successful. A too high E_a had to be used to fit the peak height and this resulted in a too small peak. From this result we conclude that the denaturation of the additional fraction cannot be described with irreversible first-order kinetics.

2.3.7 EXPERIMENTAL DATA DESCRIBED WITH TWO FIRST-ORDER RATE CONSTANTS

For the determination of the rate of decrease of the non-denatured ovalbumin concentration upon heating, chromatography experiments were carried out. From figure 2.4A, it is clear that experimental data for WCFS ovalbumin show first-order behavior. Experimental data of SIGMA ovalbumin could not be described with first-order dependence because this ovalbumin contained two fractions. Therefore we attempted to describe the experimental data with two first-order rate constants (equation 2.5)

$$\frac{A}{A_0} = (1 - f)e^{-k_1 t} + fe^{-k_2 t} \quad (2.5)$$

Where A/A_0 is the fraction of denatured protein, and f the fraction of denatured but not aggregated protein ($f=20\%$). Fitting the experimental data assuming two first-order rate constants was not successful, because, again, the additional fraction probably does not denature by a first-order process.

2.4 DISCUSSION

We investigated the effect of temperature, protein concentration and salt concentration on the protein consumption of ovalbumin. From the experimental results a kinetic model for the temperature-induced denaturation and aggregation of ovalbumin is presented.

We observed that t_h was not dependent on protein concentration, nor on salt concentration. For WCFS ovalbumin, first-order kinetics was observed as shown in figure 2.4A. Note that for long heating times interference of the 6% SI-ovalbumin occurs. This results at long heating times in a deviation from first-order kinetics. For SIGMA ovalbumin first-order dependence could not be obtained because of an additional fraction of 20% SI-ovalbumin. Combining the acidifying and non-acidifying techniques, we found that this additional SI-fraction is able to denature, but cannot aggregate. Two different ways to obtain heat-stable ovalbumin have been suggested (see thermograms fig. 2.6). (1) The amount of S-ovalbumin is related to the storage time and pH of the eggs. Increased storage time results in a growth of the intermediate fraction.¹⁵ We found that ovalbumin prepared from different batches of eggs resulted in different amounts of SI-ovalbumin and therefore different kinetic behavior was observed (data not shown). (2) The formation of I-ovalbumin could be induced by the incubation of purified ovalbumin at basic pH (9.9) and elevated temperature (55°). It has been demonstrated that by varying the incubation time, ovalbumin is converted in time into more heat-stable forms like I- and S-ovalbumin.³⁸ In the latter case, I- and S-ovalbumin can form aggregates, whereas we find here that it is not possible for our 20% fraction SI-ovalbumin to form aggregates. Therefore, it is most likely that the fraction SI-ovalbumin, present in the SIGMA batch, is formed in the egg as mentioned under (1).

The presence of 20% SI-ovalbumin was also confirmed by DSC, where we clearly observed that SIGMA ovalbumin behaved as a mixture of two proteins with different rates of denaturation. The thermograms for the thermal denaturation of ovalbumin can be interpreted in terms of a kinetic process $N \xrightarrow{k} D$, where k is a first-order kinetic constant that changes with temperature as described by the Arrhenius equation. This model predicts that the peak positions should be dependent on the scan rate, as is the case for ovalbumin. For SIGMA ovalbumin the scan rate dependence is used for the main peak, where we neglected the minor shift of the peak due to the additional fraction. The above-mentioned simple two-state model appears to imply that the denatured state is thermodynamically

more stable than the native one. A more realistic representation of the irreversible thermal denaturation of ovalbumin, which results in the same first-order kinetic process, is probably given by:



Where N_1 and N_2 are the native states, U_1 and U_2 the unfolded states, D_1 and D_2 the denatured states, and A a final state, which is in this case an aggregated form. If we assume that the conversions of N to U are first-order processes and $k_{3,4} \gg k_{1,2}$, most of the U molecules will be converted into A instead of returning to N through the process $U \rightarrow N$. As a result no equilibrium between N and U will be established, so that the denaturation may be considered as being an irreversible process $N \rightarrow A$, kinetically controlled by a slow conversion of $N \rightarrow U$. This is valid for WCFS ovalbumin; indeed, the DSC traces could be well described with this model resulting in a χ^2 of $4 \cdot 10^{-6}$. Calculations on the same DSC traces (given concentration, Δh and T_p) using a reversible process resulted in a χ^2 of $5 \cdot 10^{-5}$. The authors interpret the results of the fit as extra support for the proposed model.

For SIGMA ovalbumin the situation is more complex. If we assume two native fractions (as was confirmed by DSC and chromatography) and $k_{5,-5} \gg k_{1,2}$, then a fast equilibrium between N_1 and N_2 is established. This would imply a fixed ratio between N_1 and N_2 and therefore no calorimetric distinction between the two can be made. However, this is not applicable to SIGMA ovalbumin, because two peaks are observed. If $k_{5,-5} \ll k_{1,2}$, N_1 and N_2 denature independently and this will result in a calorimetric distinction between the two. The DSC traces should be consistent with two first-order reactions. For SIGMA ovalbumin it was clear that N_1 could be fitted with the same parameters as for WCFS ovalbumin, while N_2 could not be fitted with irreversible first-order kinetics at all. Therefore, we conclude that N_2 probably does not denature by a first-order process. A possibility is that $k_{5,-5} \sim k_1$ ($k_1 \sim 0.3 \text{ min}^{-1}$). For that case, and under specific conditions, numerical calculations showed that N_1 could be described with irreversible first-order kinetics, whereas N_2 could not. We must emphasize that the latter ideas are rather speculative.

2.5 CONCLUSIONS

The rate of decrease of non-denatured native WCFS ovalbumin when heating solutions of ovalbumin at pH 7 can be described with first-order kinetics, which means that denaturation is the rate-limiting step. The temperature dependence obeys Arrhenius law and is controlled by an activation energy of about $490 \text{ kJ}\cdot\text{mol}^{-1}$. From analyzing the shape of the thermograms as well as the scan rate dependence, activation energies of respectively 430 and $490 \text{ kJ}\cdot\text{mol}^{-1}$ are found. In contrast to WCFS ovalbumin, SIGMA ovalbumin showed two distinct peaks. The main peak could be successfully described with the same parameters as for WCFS ovalbumin, and assuming 81% of the protein participating in the main peak. Analyzing the scan rate dependence of the main fraction, an activation energy of $530 \text{ kJ}\cdot\text{mol}^{-1}$ was found, in good agreement with values found for WCFS ovalbumin. However, experimental results cannot be sufficiently described by implementing a second first-order process (equation 2.5) corresponding to the additional fraction in SIGMA ovalbumin. Therefore, we conclude that the denaturation of the additional fraction (SI-ovalbumin) does not behave as a first-order process.

REFERENCES

1. Thirumalai, D., Klimov, D.K. and Dima, R.I. (2003). *Curr. Opin. Struct. Biol.*, 146.
2. Weijers, M., Visschers, R.W., and Nicolai, T. (2002). *Macromolecules*, 35, 4753.
3. Stein, P.E., leslie, A.G.W., Finch, J.T. and Carrell, R.W. (1991) *J. Mol. Biol.*, 221, 941.
4. Mine, Y. (1995). *Trends Food Sci. Techn.*, 6, 225.
5. Forsythe, R.H. *Bakery technology and engineering*. 1960. In S.A. Matz, Westport, Connecticut: AVI Publishing Co Inc. pp 188-220.
6. Kiss, E., Nádudvari, V., Hoschke, Á., Biacs, P. Functional properties of food proteins. In R. Lásztity, M. Ember-Karpati, *Proc. Int Sem.*, Budapest (p.290). Budapest Technical University, Budapest.
7. Clark, A.H., Judge, F.J., Richards, J.B., Stubbs, J.M., and Suggett, A. (1981). *Int. J. Pept. Protein Res.*, 17, 380.
8. Doi, E., and Kitabatake, N. (1989). *Food Hydrocolloids*, 3, 327.
9. Harte, J.B., Zabik, M.E., Ofoli, R.Y. and Morgan, R.G. (1992). *J. Food Sci.*, 57, 1093.
10. Arntfield, S.D., Murray, E.D., and Ismond, M.A.H. (1990). *J. Agric. Food Chem.*, 38, 1335.
11. Arntfield, S.D., Murray, E.D., and Ismond, M.A.H. (1990). *J. Texture Stud.*, 21, 191.
12. Kitabatake, and N., Kinekawa, (1995). *Y. Food Chem.*, 54, 201.
13. Van der Linden, E, and Sagis, L.M.C. (2001). *Langmuir*, 17, 5821.

14. Weijers, M., Sagis, L.M.C., Veerman, C., Sperber, B., and Linden, E. v.d. (2002). *Food Hydrocolloids*, 16, 269.
15. Smith, M.B. and Back, J.F. (1962). *Nature*, 193, 878.
16. Lumry, R., and Eyring, H. (1954). *J. Phys. Chem.*, 58, 110.
17. Privalov, P.L. (1979). *Adv. Protein Chem.*, 33, 167.
18. Privalov, P.L. (1982). *Adv. Protein Chem.*, 35, 1.
19. Privalov, P.L. (1989). *Annu. rev. Biophys. Biophys. Chem.*, 18, 47.
20. Donovan, J.W., and Beardslee, R.A. (1975). *J. Biol. Chem.*, 250, 1966.
21. Sanchez-Ruiz, J.M., Lopez-Lacomba, J.L., Cortijo, M., and Mateo, P.L. (1988). *Biochemistry*, 27, 1648.
22. Davoodi, J., Wakarchuk, W.W., Surewicz, W.K., and Carey, P.R. (1998). *Protein Sci.*, 7, 1538.
23. Grinberg, V. Ya., Burova, T.V., Haertlé, T., and Tolstoguzov, V.B. (2000). *J. Biotechnol.*, 79, 269.
24. La Rosa, C., Milardi, D., Grasso, D.M., Verbeet, M.P., Canters, G.W., Sportelli, and L., Guzzi, R. (2002). *Eur. Biophys. J.*, 30, 229.
25. Klibanov, A.M., and Ahern, T.J. 1987. Thermal stability of proteins. In *Protein Engineering*. D.L. Oxender and C.F. Fox, editors. Alan R. Liss, New York, pp. 213-218.
26. Zemser, M., Friedman, M., Katzhendler, J., Greene, L.L., Minsky, A., and Gorinstein, S. (1994). *J. Protein Chem.*, 13, 261.
27. Lepock, J.R., Ritchie, K.P., Kolios, M.C., Rodahl, A.M., Heinz, K.A., and Kruuv, J. (1992). *Biochemistry*, 31, 12706.
28. Kurganov, B.I., Lyubarev, A.E., Sanchez-Ruiz, J.M., and Shnyrov, V.L. (1997). *Biophys. Chem.*, 69, 125.
29. Lyubarev, A.E., and Kurganov, B.I. (2000). *J. Therm. Anal. Cal.*, 62, 51.
30. Koseki, T., Kitabatake, N. and Doi, E. (1989). *Food Hydrocolloids*, 3, 123.
31. Koseki, T., Fukuda, T., Kitabatake, N. and Doi, E. (1989). *Food Hydrocolloids*, 3, 135.
32. Vachier, M.C., Piot M., and Awedé, A.C. (1995). *J. Chromatogr. B*, 66, 201.
33. Hoffmann, M.A.M., and Mil, P.J.J.M. v. (1997). *J. Agric. Food Chem.*, 45, 2942.
34. Le Bon, C., Nicolai, T., and Durand, D. (1999). *Macromolecules*, 32, 6120.
35. Roefs, S.P.F.M. and De Kruif K.G. (1994). *Eur. J. Biochem.*, 226, 883.
36. Huntington, J.A., Patson, P.A. and Gettins, P.G.W. (1995). *Protein Sci.*, 4, 613.
37. Hagolle, N., Relkin, P., Dalgleish, D.G., and Launay, B. (1997). *Food Hydrocolloids*, 11, 311.
38. De Groot, J. and De Jongh, H.H.J. (private communication 2003).

CHAPTER 3

LIGHT SCATTERING STUDY OF HEAT-INDUCED AGGREGATION
OF OVALBUMIN AT DIFFERENT IONIC STRENGTH

Weijers, M., Nicolai, T. and Visschers, R.W.
Macromolecules 2002, 35, 4753-4762

Macromolecules 2002, 35, 4753-4762

ABSTRACT

The effect of ionic strength on the interaction of ovalbumin, a globular egg white protein, in aqueous solution was investigated using static and dynamic light scattering. Strong repulsive interactions are observed at low ionic strength (3 mM). Aggregation of the proteins was induced by heating at low (3 mM) and high (100 mM) ionic strength as a function of the concentration. The size of the aggregates increases with increasing protein concentration and diverges close to the critical concentration for gelation which is about 60 g/L at low ionic strength and 12 g/L at high ionic strength. Static and dynamic light scattering showed that at low ionic strength linear chains are formed with little branching until close to the gel point, while at high ionic strength denser branched aggregates are formed with a fractal dimension close to that found for other globular protein aggregates. The observations were confirmed by cryo-transmission electron microscopy.

Heated systems at low ionic strength remained transparent and were studied in situ using static and dynamic light scattering. The relaxation of the concentration fluctuations occurs by cooperative diffusion except when the gel point is approached and a slow secondary relaxation process is observed. The slow mode is attributed to the selfdiffusion of the aggregates and restructuring of the system. The terminal relaxation time of the concentration fluctuations diverges in the neighborhood of the gel point because a fraction of the concentration fluctuations is progressively frozen in.

3.1 INTRODUCTION

In general, when globular proteins like ovalbumin or β -lactoglobulin are heated, the molecule unfolds partially, so that parts of the inner hydrophobic region become exposed. This denaturation process is usually followed by aggregation, and eventually a gel can be formed.¹ Partly driven by its relevance to industrial applications, heat induced aggregation of globular proteins has long been a subject of intensive investigation.

Here we investigate the heat induced aggregation of ovalbumin. Ovalbumin is the most abundant protein in avian egg whites and constitutes over half of the egg white proteins by weight. Egg white proteins possess multiple functional properties in food such as gelling, foaming, water binding and emulsifying capacity.^{2,3} Some of the functionalities relate to structure changes that occur during heat treatment.

Ovalbumin is readily purified and crystallized in gram quantities.⁴ It is a monomeric phosphoglycoprotein with a molecular weight of 45 Kg/mol and an isoelectric point of 4.5. The complete amino acid sequence, comprising 385 residues, has been determined by Nisbet et al.⁵ Purified ovalbumin contains 3 phosphorylated forms, A₁, A₂ and A₃, which contain two, one and no phosphate groups per molecule, respectively.^{6,7} The properties of ovalbumin solutions or gels formed after heat treatment depend on the pH, ionic strength and protein concentration and they can be either transparent, opaque or turbid.⁸

The structure of ovalbumin aggregates has been investigated in detail at pH 7 at low ionic strength.^{9,10,11} At these conditions heated ovalbumin solutions remain transparent. Transmission electron microscopy (TEM) has shown that linear aggregates are formed. It was concluded from static (SLS) and dynamic (DLS) light scattering, and intrinsic viscosity measurements that these linear aggregates can be described in terms of the worm-like chain model.¹¹ When salt is added to screen electrostatic interactions dense coagulates are observed with TEM.

The purpose of the present work was to study the effect of electrostatic interactions on the aggregation process of ovalbumin at pH 7 by comparing systems at low ($\mu=3$ mM) and high ($\mu=0.1$ M) ionic strength. We investigated the effect of the ionic strength on the interactions in native ovalbumin solutions by measuring the concentration dependence of the osmotic compressibility and the cooperative diffusion coefficient. We determined the structure of ovalbumin aggregates formed after extensive heat treatment using SLS and DLS. The method used to characterize the highly diluted aggregates is the same as used

earlier for aggregates of another globular protein, β -lactoglobulin.^{12,13} A similar SLS study was reported also for bovine serum albumin.¹⁴ Direct comparison of results obtained on different globular proteins is important because it may eventually lead to a general understanding of heat induced aggregation of globular proteins. The evolution of the structure and the dynamics of the ovalbumin solutions during the aggregation process was studied in-situ using SLS and DLS. Measurements on undiluted heated solutions were done only at low ionic strength, because at $\mu=0.1\text{M}$ heated solutions became turbid.

3.2 MATERIALS AND METHODS

3.2.1 MATERIALS

The ovalbumin used for this study was purchased from Sigma and used without further treatment. One batch (I: 30K7054) was used for most experiments, and another batch (II: 19H7002) was sometimes used as specified. The protein content was determined by the Kjeldahl method¹⁵, using the Kjeldahl factor of 6.12. The protein concentration was 85% for batch I and 88% for batch II. The water content was determined, using Karl Fischer titration¹⁶, and was found to be 10 % for batch I and 6 % for batch II. The ovalbumin was dissolved in Millipore water with 3 mM NaN_3 added to avoid bacterial growth. The pH was set at 7 using a NaOH solution. In some cases 0.1M NaCl was added to screen electrostatic interactions. The solutions were filtered through 0.25 μm pore size Anatop filters. Protein concentrations were measured using refractive index measurements and UV absorption at 280 nm. Consistent results were obtained using refractive index increment $\text{dn}/\text{dC}=0.181$ and extinction coefficient $\epsilon=0.698\text{ l.g}^{-1}.\text{cm}^{-1}$. These values are close to those used in the literature.

3.2.2 METHODS

Size exclusion chromatography (SEC) experiments were carried out at room temperature with TSK[®] PW 5000 + PW 6000 column set (30 cm + 60 cm) in series and a differential refractive index detector SHODEX RI 71. The columns were eluted with 0.1 M NaNO_3 at a flow rate of 1 ml/min. The injected volume was 300 μl and the injected concentration was around 1.5 g/l.

Cryo-transmission electron microscopy was done at the Unilever Research Center (Vlaardingen, the Netherlands) using a Philips CM12 transmission electron microscope

operating at 80 kV. A drop of the liquid sample was placed on a perforated carbon film, supported by a 200-mesh copper grid, and most of the liquid was removed by blotting with a filter paper. The thin liquid films formed across the holes were subsequently vitrified by plunging the grid into liquid propane at a temperature below -170°C . The specimens were stored in liquid nitrogen until they were transferred to the cry-holder. The cry-holder (Oxford) was cooled by liquid nitrogen to a temperature lower than -170°C . Images were recorded digitally by a Gatan 791 CCD camera using the Digital Micrograph software package.

Static and dynamic light scattering measurements were made using an ALV-5000 multi-bit multi-tau correlator and a Spectra Physics solid state laser operating with vertically polarized light with wave length $\lambda=532\text{ nm}$. The range of scattering wave vectors covered was $3.0 \times 10^{-3} < q < 3.5 \times 10^{-2}\text{ nm}^{-1}$ ($q=4\pi n_s \sin(\theta/2)/\lambda$, with θ the angle of observation, and n_s the refractive index of the solution). The temperature was controlled by a thermostat bath to within $\pm 0.1^{\circ}\text{C}$.

3.2.3 DATA ANALYSIS

The relative scattering intensity I_r was determined by subtracting the solvent scattering from the total scattering intensity and dividing by the scattering intensity of toluene. I_r is due to concentration fluctuations and is proportional to the osmotic compressibility $(d\pi/dC)^{-1}$ and the structure factor $(S(q))^{17,18}$:

$$I_r = KC \frac{RT}{(d\pi/dC)} S(q) \quad (3.1)$$

with R the gas constant and T the absolute temperature. $S(q)$ expresses the scattering wave vector dependence of the scattering intensity and is unity for $q \rightarrow 0$. K is a contrast factor:

$$K = \frac{4\pi^2 n_s^2}{\lambda^4 N_a} \left(\frac{\partial n}{\partial C} \right)^2 \left(\frac{n_{\text{tol}}}{n_s} \right)^2 \cdot \frac{1}{R_{\text{tol}}} \quad (3.2)$$

where N_a is Avogadro's number, $(\partial n / \partial C)$ is the refractive index increment, and R_{tol} is the Rayleigh ratio of toluene at 20°C ($R_{\text{tol}}=2.79 \times 10^{-5}\text{ cm}^{-1}$ at $\lambda=532\text{ nm}$). $(n_{\text{tol}}/n_s)^2$ corrects for

the difference in scattering volume of the solution and the toluene standard with refractive index n_{tol} .

In dilute solutions when interactions are weak, the weight average molar mass (M_w), the z-average radius of gyration ($R_{gz} = \langle R_g^2 \rangle^{0.5}$) and the second virial coefficient (A_2) can be derived using the so-called Zimm approximation:

$$\frac{KC}{I_r} = \frac{1}{M_w} \left(1 + \frac{(qR_{gz})^2}{3} \right) (1 + 2M_w A_2 C) \quad qR_{gz} < 1 \quad (3.3)$$

The intensity autocorrelation function measured with DLS ($g_2(t) = \langle I(0)I(t) \rangle / \langle I \rangle^2$) is related to the normalized electric field correlation function, $g_1(t)$, by the Siegert relation.¹⁹ $g_1(t)$ was analysed in terms of a distribution of relaxation times:

$$g_1(t) = \int A(\tau) \exp(-t / \tau) d\tau \quad (3.4)$$

using the Laplace inversion routine REPES.²⁰ This method does not assume a specific form for $A(\tau)$, but has a tendency to represent broad monomodal distributions by multiple peaks. Therefore we also used the so-called generalized exponential (GEX) distribution: $A(\log \tau) = k\tau^p \exp\left[-\left(\tau / \tau^*\right)^s\right]$. The GEX distribution contains two parameters (p, s) to describe the shape of a wide range of single peaked distributions such as the Schultz-Zimm and the Pearson distribution. τ^* is the characteristic relaxation time and k is a normalisation constant.

If the relaxation of the concentration fluctuations is due to cooperative diffusion, the cooperative diffusion coefficient (D_c) may be calculated from the average relaxation rate $\langle \Gamma \rangle = \langle 1/\tau \rangle$ as: $D_c = \langle \Gamma \rangle / q^2$.¹⁹ In dilute solutions when interactions are weak the z-average self diffusion coefficient (D_z) and the dynamic second virial coefficient (k_D) can be derived utilizing:

$$D_c = D_z(1 + k_D C) \quad qR_{gz} < 1 \quad (3.5)$$

D_z is related to the z-average hydrodynamic radius ($R_{hz} = \langle 1/R_h \rangle_z^{-1}$) via the so-called Stokes-Einstein relation:

$$D_z = kT/6\pi\eta R_{hz}, \quad (3.6)$$

with k Boltzmann's constant and η the solvent viscosity.

3.3 RESULTS

3.3.1 NATIVE OVALBUMIN

We have used SLS and DLS to characterize aqueous solutions of ovalbumin at pH 7 either with just 3 mM NaN_3 to protect against bacterial degradation or with in addition 0.1 M NaCl to screen electrostatic interactions. The scattering intensity of all solutions was independent of the scattering wave vector within the experimental error, because the radius of the particles is small compared to q^{-1} in the range covered by light scattering. In figure 3.1 the concentration dependence of KC/I_r is compared for the two ionic strengths. Extrapolation to $C=0$ gives the weight averaged molar mass of ovalbumin, which is the same at both ionic strengths: $M_w = 4.6 \times 10^4$ g/mol. The experimental value of M_w is close to that of ovalbumin monomers.

The concentration dependence of KC/I_r is much stronger at the lower ionic strength due to electrostatic interactions that are partially screened by the presence of 0.1M NaCl. From the initial linear concentration dependence we estimated the second virial coefficient: $A_2 = 2.5 \times 10^{-6}$ l.mol.g⁻² at 3 mM NaN_3 and $A_2 = 2.2 \times 10^{-7}$ l.mol.g⁻² at 0.1 M NaCl. The linear increase of KC/I_r extends to about 50 g/l at the higher ionic strength after which the contribution of ternary interactions becomes significant. At lower ionic strength the concentration dependence weakens above approximately 10 g/l. The reason is that counterions of the proteins contribute to the ionic strength so that electrostatic interaction is progressively screened with increasing protein concentration.

The intensity autocorrelation functions of ovalbumin solutions were characterized by two distinct relaxation modes. The average relaxation rate of both modes was q^2 -dependent. The slower mode decreased in amplitude after filtration and could be completely removed at lower concentrations, without significant reduction of the protein concentration. We believe that the fast mode is due to cooperative diffusion of ovalbumin

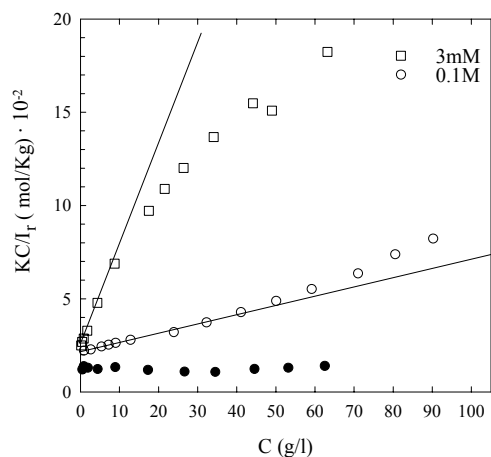


Figure 3.1. Concentration dependence of KC/I_r of native ovalbumin at pH 7 and two ionic strengths (open symbols). The filled symbols represent the results for ovalbumin solutions at $\mu=3$ mM heated at 78°C for 20 hours.

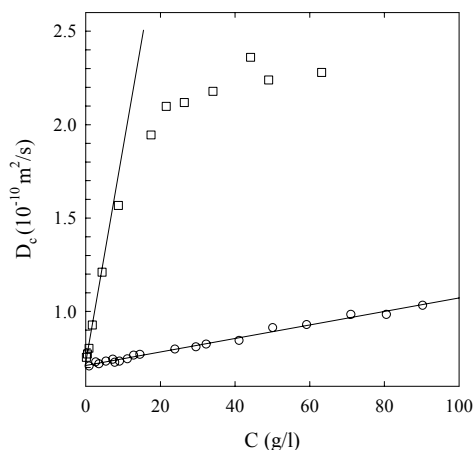


Figure 3.2. Concentration dependence of the cooperative diffusion coefficient of native ovalbumin at pH 7 and two ionic strengths. The symbols are as in figure 3.1.

monomers and that the slow mode is due to self diffusion of a very small weight fraction of large protein aggregates. At higher concentrations a slow mode with relatively weak amplitude remained even after careful filtration. Therefore we have corrected I_r for the scattering by these large aggregates.

In figure 3.2 the concentration dependence of D_c at the two ionic strengths is compared. Extrapolation to $C=0$ gives $D_c=7.1 \times 10^{-11}$ m²/s at both ionic strengths. The hydrodynamic radius calculated utilizing eq. 3.6 is 2.9 nm in agreement with the value reported by Nemoto et al.⁹ The concentration dependence of D_c is again much stronger at lower ionic strength due to electrostatic interactions. From the initial concentration dependence we estimated the dynamic second virial coefficient: $k_D=0.1$ l/g at 3 mM NaN₃ and $k_D=5.1 \times 10^{-3}$ l/g at 0.1 M NaCl. The concentration dependence of D_c is determined both by thermodynamic interactions and friction. The former cause D_c to increase with increasing concentration whereas the latter causes it to decrease. The results obtained here for ovalbumin resemble those obtained for β -lactoglobulin which was studied in detail at the same pH and ionic strengths.²¹

3.3.2 DILUTE OVALBUMIN AGGREGATES

We have characterized ovalbumin aggregates formed after heating solutions with different protein concentrations at 78°C for 20 hours. The aggregates were highly diluted so that the effect of interactions and multiple scattering could be neglected and were studied at 20°C using SEC, SLS, DLS and cryo-tem. Ovalbumin solutions at 3 mM NaN_3 remain transparent when heated, whereas at 0.1 M NaCl they become turbid. At the lower ionic strength the solutions gel if $C > 60$ g/l and an insoluble gel fraction is visible after dilution, whereas at 0.1 M NaCl the solutions gel if $C > 12$ g/l.

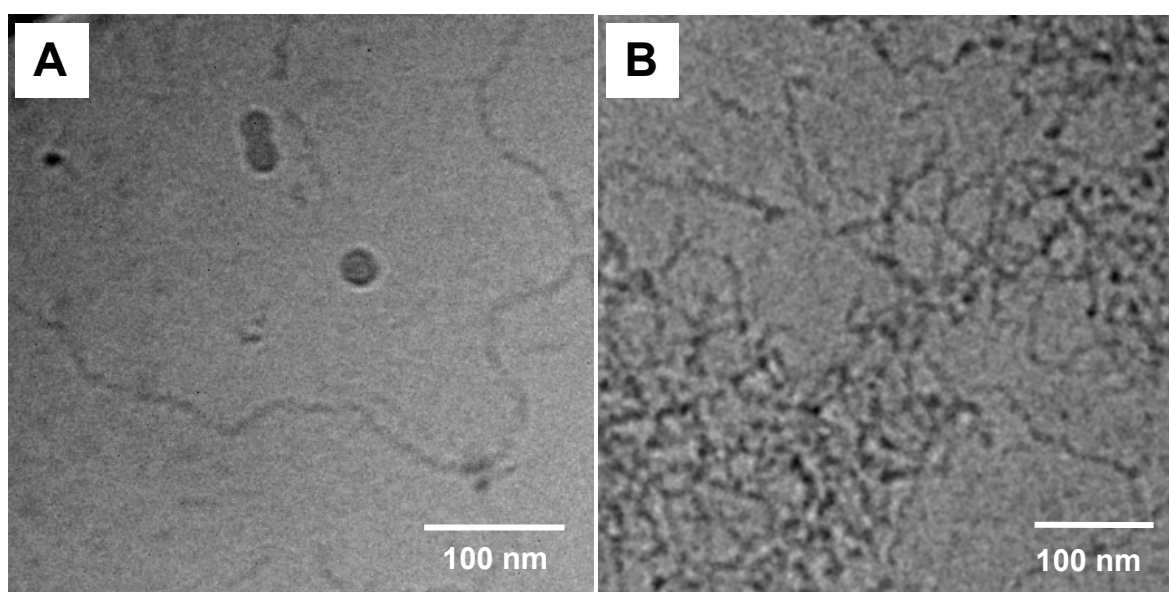


Figure 3.3. Cryo-tem micrographs of ovalbumin aggregates formed after heat treatment in 3 mM NaN_3 (a) or in 0.1 M NaCl (b). The samples were heated for 22 hours at 78°C with $C = 54$ g/l in 3 mM NaN_3 and $C = 5.4$ g/l at 0.1 M NaCl. Micrographs were obtained for diluted samples with a final concentration of $C = 1$ g/l.

Figure 3.3 shows cryo-tem micrographs of large ovalbumin aggregates formed after heat treatment in 3 mM NaN_3 or in 0.1 M NaCl. The samples were heated for 22 hours at 78°C at concentrations (54 g/l at 3 mM NaN_3 and 5.4 g/l at 0.1 M NaCl) that were chosen such that aggregates are formed with R_{gz} about 300 nm at both ionic strengths. At low ionic strength long flexible aggregates are formed with very few branch points. The diameter of the aggregates is 6 ± 1 nm, in agreement with the results at low ionic strength obtained by Koseki et al.¹¹ using transmission electron microscopy. These results suggest a simple linear aggregation of monomeric ovalbumin and not the aggregation of dimers suggested by Nemoto et al.⁹ on the basis of light scattering results. In the presence of 0.1 M NaCl

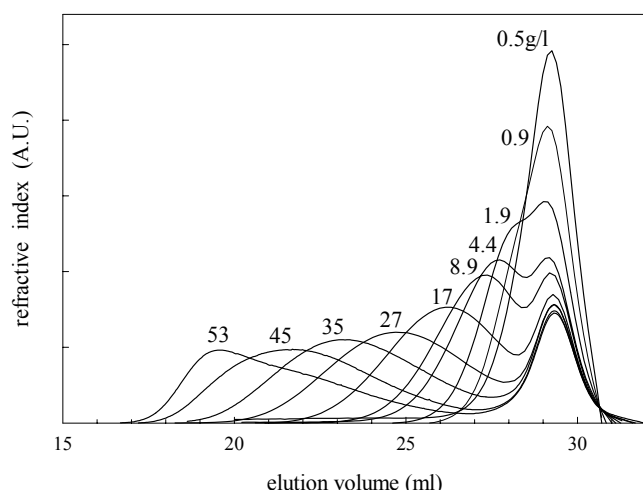


Figure 3.4. Chromatograms of ovalbumin solutions at pH 7 and $\mu=3$ mM heated at 78°C for 20 hours.

more densely branched clusters are observed, but the elementary structure of clusters is again monomeric ovalbumin. It appears that the aggregation of ovalbumin at pH 7 is essentially the same at different ionic strengths, but that branching is inhibited by electrostatic repulsion.

Figure 3.4 shows chromatograms of heated ovalbumin solutions with a range of protein concentrations at 3 mM NaN_3 . At the lowest concentrations one observes a broadening of the size distribution towards smaller elution volumes, i.e. larger sizes, compared to native ovalbumin, but for $C > 2$ g/l two distributions can be distinguished. The narrow peak at an elution volume of about 29 ml corresponds to unaggregated protein while the second peak broadens and shifts to smaller elution volumes with increasing concentration. Similar results are obtained in the presence of 0.1 M NaCl except that the increase of the average aggregate size occurs at lower protein concentrations. The fraction of unaggregated protein can be deduced from the surface area of the corresponding peak in the chromatograms if it is well resolved. This fraction is about 27 % independent of the protein concentration for $C > 5$ g/l. At lower concentrations the fraction of unaggregated ovalbumin is difficult to establish and increases with decreasing concentration. At 0.1 M NaCl we also found a fraction of about 27% unaggregated ovalbumin at all concentrations investigated.

It has been reported that ovalbumin may transform into a thermally more stable conformation²² and that the fraction of this so-called S-ovalbumin depends on the history of the batch.²³ For one solution (9.5 g/L, 0.1M) we determined the fraction of unaggregated ovalbumin as a function of heating time at 78°C . We found that this fraction decreases at

first rapidly to an apparent plateau at about 30 % after which it continues to decrease very slowly.

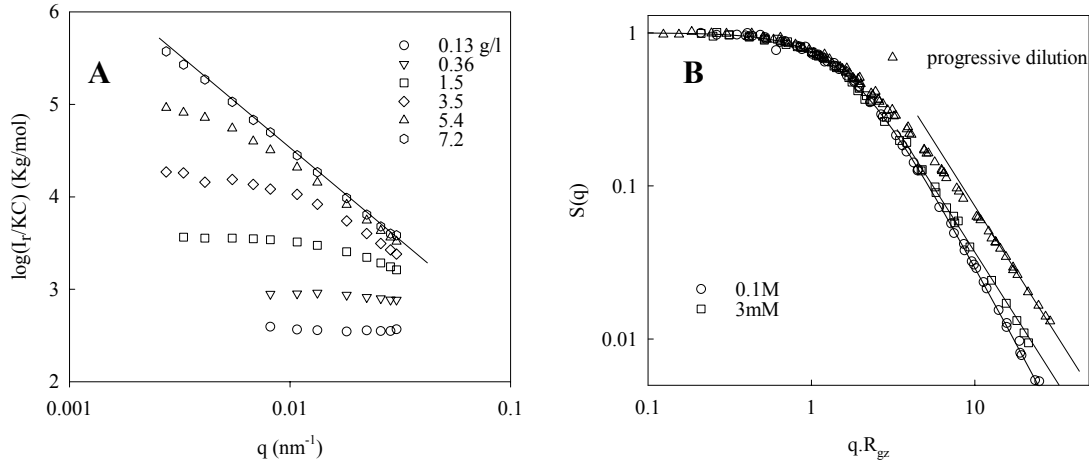


Figure 3.5. (A) Double logarithmic representation of the q -dependence of I_r/KC for ovalbumin solutions at pH 7 and $\mu=0.1$ M heated at 78°C for 20 hours. The line has slope -2.0 . (B) Structure factor of highly diluted ovalbumin aggregates formed at pH 7 and two ionic strengths. The triangles represent the structure factor of interpenetrated ovalbumin aggregates obtained by progressive dilution of a solution containing very large ovalbumin aggregates ($>1\mu\text{m}$) formed at low ionic strength. The solid line through the circles represents $S(qR_{gz})=(1+(qR_{gz})^2/3)^{-1}$. The straight lines through the squares and triangles have slope -1.7 .

This result together with the SEC results indicates that the batch used in these experiments contains about 27% thermally stable ovalbumin.

For each highly diluted sample we measured the q -dependence of the scattering intensity and the correlation function. At 0.1M NaCl the contribution of unaggregated ovalbumin to I_r is negligible for all systems investigated whereas without NaCl this is the case for $C>5$ g/l. Figure 3.5a shows the q -dependence of I_r/KC for heated ovalbumin solutions at 0.1M NaCl. With increasing concentration larger aggregates are formed which leads to an increase of I_r/KC at $q\rightarrow 0$, i.e. M_w for highly diluted samples, and a stronger q -dependence. Just below the concentration where a gel is formed I_r has a power law dependence on q , which means that we probe the internal, self-similar structure of the aggregates. The aggregates are characterized by a fractal dimension d_f that relates the molar mass to the radius of gyration: $M\propto R_g^{d_f}$. The fractal dimension can also be determined from the q -dependence of I_r : $I_r\propto q^{-d_f}$ for $qR_g\gg 1$.²⁴ The solid line in figure 3.1 has slope -2.0 from which we deduce $d_f=2.0$.

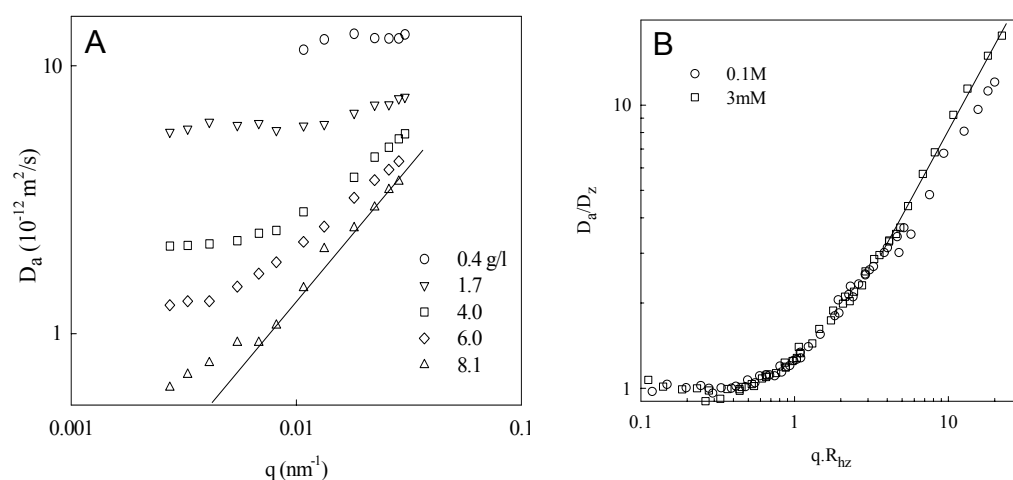


Figure 3.6. (A) Double logarithmic representation of the q -dependence of the apparent diffusion coefficient for ovalbumin solutions at pH 7 and $\mu=0.1$ M heated at 78°C for 20 hours. The solid line has slope one. (B) Normalized representation of the data shown in figure 3.6a plus the results obtained at $\mu=3$ mM. The solid line has slope one.

Often the structure factor of aggregates formed by a random aggregation process is a unique function of $q.R_{gz}$. This means that if $(I_r/KC)/M_w$, i.e. $S(q)$, is plotted as a function of $q.R_{gz}$ all data collapse on to a single master curve. Such master curves have been reported earlier for aggregates formed after heat denaturation for two other globular proteins: β -lactoglobulin¹² and BSA¹⁴. For ovalbumin we also obtain master curves, at both ionic strengths, see figure 3.5b, which shows that the structure factor of the aggregates is a unique function of $q.R_{gz}$. However, the functional form of $S(q.R_{gz})$ depends on the ionic strength. At 0.1M NaCl the structure factor is well-described by the following equation: $S(q.R_{gz})=(1+(q.R_{gz})^2/3)^{-1}$. The same function described $S(q.R_{gz})$ for β -lactoglobulin aggregates formed at the same conditions.²⁵ The structure factor of aggregates formed at low ionic strength deviates from this function at large values of $q.R_{gz}$. Even though the structure factor depends on the ionic strength at which the aggregates are formed, it is the same whether the aggregates are diluted in 3 mM NaN_3 or in 0.1 M NaCl. This implies that dilution in salt only decreases electrostatic repulsion and does not change the structure factor of aggregates.

The correlograms could in all cases be well described by a monomodal q^2 -dependent relaxation time distribution and the apparent diffusion coefficient was calculated as $D_a=\langle\Gamma\rangle/q^2$. The q -dependence of D_a is shown in figure 3.6a for aggregates formed at

different ovalbumin concentrations at 0.1M NaN_3 . At low concentrations $qR_{gz} < 1$ over the whole q -range so that D_a is independent of q and equal to D_z . At higher concentrations larger aggregates are formed and one observes the influence of internal dynamics. Master curves can be formed at both ionic strengths by plotting D_a/D_z as a function of qR_{hz} , see figure 3.6b. Notice that since $D_z \propto 1/R_{hz}$ we only use one independent parameter in the construction of the master curves. For $qR_{hz} > 5$ we find $D_a \propto q$ which is expected for flexible particles.²⁶ At $\mu = 3$ mM the limiting linear dependence of D_{app} on q is reached at lower values of qR_{gz} than at $\mu = 0.1$ M, which could mean that the aggregates formed at higher ionic strength are slightly less flexible.

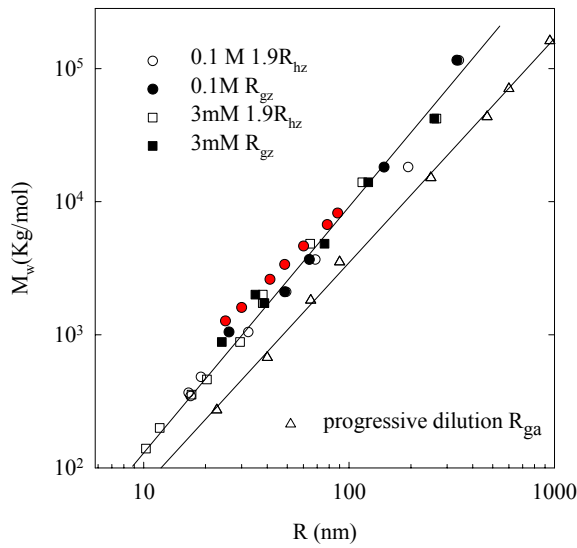


Figure 3.7. Dependence of R_{gz} and R_{hz} on M_w for ovalbumin aggregates formed at pH 7 and two ionic strengths. The line through the data has slope -1.8. The values of $1.9R_{hz}$ are shown to demonstrate that $R_{gz} \approx 1.9R_{hz}$. The triangles show the dependence of M_a on R_{ga} for progressive dilutions of a solution containing very large ovalbumin aggregates ($>1\mu\text{m}$) formed at low ionic strength. The line through the data has slope -1.65.

The construction of the master curves allows one to determine M_w , R_{gz} , and R_{hz} even if eqs 3.3 and 3.5 are no longer valid. For all systems we observed that $R_{gz} \approx 1.9R_{hz}$ within the experimental error. Notice that since $R_{gz} = \langle R_g^2 \rangle^{0.5}$ and $R_{hz} = \langle 1/R_h \rangle_z^{-1}$, polydispersity increases the ratio R_{gz}/R_{hz} . Figure 3.7 shows that M_w has a power law dependence on R_{gz} and R_{hz} , which is within the experimental error the same for the two ionic strengths. Koseki et al.¹¹ reported values of M_w and R_{gz} over a narrower range for ovalbumin aggregates formed in 20 mM salt at pH 7. Their results are close to the present results after

correction for the slightly different refractive index increment used to calculate M_w . As mentioned above the fractal dimension of the aggregates can be obtained either by utilizing $S(qR_{gz}) \propto q^{-d_f}$ at $qR_{gz} \gg 1$ or by utilizing $M_w \propto R_{gz}^{d_f}$. The first method gives $d_f=2.0$ at $\mu=0.1$ M and $d_f=1.7$ at $\mu=3$ mM. The dependence of the molar mass on the radius of the aggregates gives a single intermediate value ($d_f=1.8$), but is nevertheless consistent in view of the considerable scatter of the data.

The size of the aggregates increases with increasing ovalbumin concentration and diverges at a given concentration C_{gel} , see figure 3.8. In 3 mM NaN_3 the size of the aggregates increases monotonically from a value close to that of native ovalbumin, whereas in 0.1M NaCl the size of the aggregates is already several times larger than that of native ovalbumin even at the lowest concentration at which reliable measurements could be done.

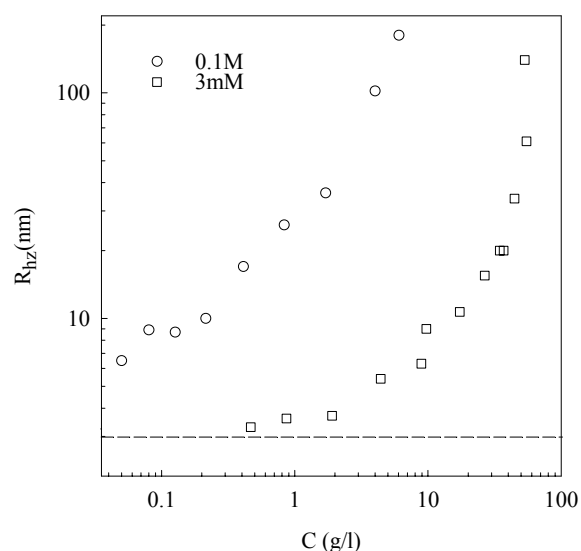


Figure 3.8. Concentration dependence of the hydrodynamic radius of ovalbumin aggregates formed after heating at 78°C for 20 hours at pH 7 and two ionic strengths. The dashed line indicates the hydrodynamic radius of native ovalbumin.

It should be remembered, however, that the data were obtained at a given heating time and temperature. After this heat treatment all active ovalbumin has aggregated, but only a small fraction of inactive ovalbumin has aggregated. In order to calculate the molar mass of the aggregates one needs to use the concentration and scattering intensity of just the aggregates in eq.3.3 and not the total protein concentration. As mentioned above, the contribution of unaggregated proteins to the scattered light is in most cases negligible.

However, the aggregate concentration is about 27% smaller than the total protein concentration except at very low concentrations where it is even smaller. This means that M_w of just the aggregates is about 27% larger than that of the total system. The values of R_{gz} and R_{hz} are not influenced by the presence of unaggregated proteins, because the concentration does not enter in the calculation of these parameters.

Microscopy showed that at low ionic strength essentially semi-flexible linear aggregates are formed. The fractal dimension of linear chains in good solvents is about 1.7²⁶ at length scales larger than the persistence length, which is consistent with the present experimental results. Linear aggregates were also observed for β -lactoglobulin at pH 2, but not at pH 7²⁷. At pH 7 and low ionic strength heat denatured β -lactoglobulin forms small well-defined so-called primary aggregates for $C < 40$ g/l. Above this concentration the aggregate size increases with increasing concentration and β -lactoglobulin solutions gel for C larger than about 75 g/l. Cryo-TEM shows that the small primary aggregates have an elongated shape. If electrostatic interactions are screened by the presence of 0.1 M salt the primary aggregates randomly associate to form larger self-similar aggregates and eventually a gel for $C > 7$ g/l. Similar association also occurs without added salt at higher protein concentrations because counterions progressively screen electrostatic interactions. A study of the structure of the larger β -lactoglobulin aggregates formed at low ionic strength is currently being pursued.

The results described so far were obtained using batch I. A number of experiments were repeated using batch II. The results were the same except that the fraction of heat stable ovalbumin is somewhat smaller in this batch (about 20%).

3.3.3 UNDILUTED OVALBUMIN SOLUTIONS

We have studied undiluted heated ovalbumin solutions at 3 mM NaN_3 using SLS and DLS. At 0.1 M NaCl heated ovalbumin solutions become turbid and special equipment is needed in order to correct for multiple scattering. With increasing concentration the heated systems are increasingly viscous and for $C > 60$ g/l they no longer flow when tilted. The q -dependence of the scattering intensity of the heated solutions is negligible which shows that the correlation length of the concentration fluctuations is less than 15 nm. KC/I_r is remarkably independent of the protein concentration, see figure 3.1, implying that at these

heating conditions the variation in aggregate size compensates for the variation in the interactions.

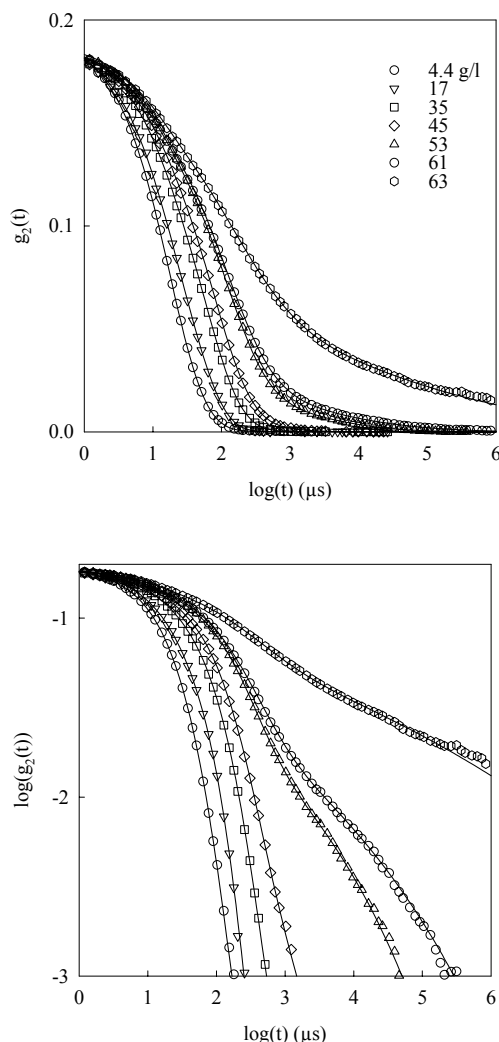


Figure 3.9. Semi (top) and double (bottom) logarithmic representation of the normalized autocorrelation functions of ovalbumin solutions at different concentrations that were heated at 78°C for 20 hours and subsequently cooled to 20°C (pH 7 and $\mu=3$ mM). The solid lines represent non-linear least squares fits described in the text.

For comparison we also show D_c of the solutions before heating. The relative amplitude of the fastest relaxation mode (1) is about 10% independent of the concentration and its diffusion coefficient, D_1 , is close to D_c . We believe that mode 1 is caused by the cooperative diffusion of the fraction of unaggregated ovalbumin and that the slower diffusional mode

On the other hand, the correlograms obtained with DLS have a clear concentration dependence, see figure 3.9. The left panel of figure 3.10 shows the corresponding relaxation time distributions. Below 10 g/l we observe a single relaxation process whereas above this concentration we can distinguish two modes. At even higher concentrations we observe a third slow relaxation mode, which is better seen in the double logarithmic representation of the correlation functions. The terminal relaxation time of this process increases strongly over a small concentration range and is outside the window of observation for $C > 61$ g/l. The correlation functions could be very well described by a sum of two log normal relaxation time distributions and one generalized exponential distribution, see solid lines in figures 3.9. Details of this fit procedure can be found in ref. 28.

The relaxation times of the first two modes are q^{-2} -dependent and the diffusion coefficients are plotted as a function of the concentration in figure 3.11. For

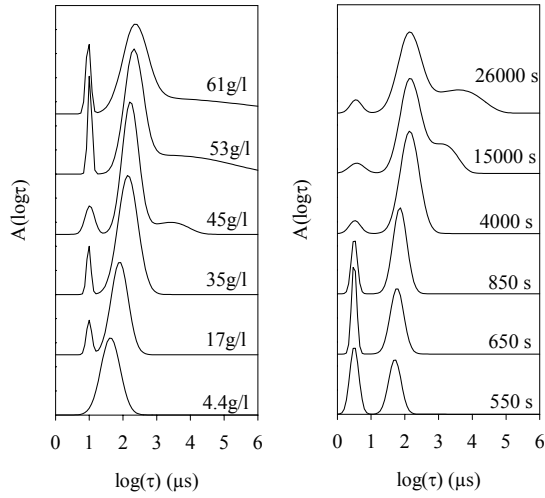


Figure 3.10. Relaxation time distributions corresponding to the correlation functions shown in figure 3.9 (upper panel) and figure 3.13a (right panel). The results shown in the left panel were obtained for ovalbumin solutions at different concentrations that were heated at 78°C for 20 hours and subsequently cooled to 20°C (pH 7 and $\mu=3$ mM). The results shown in the right panel were obtained in situ for an ovalbumin solution at $C=70$ g/l at different heating times at 74°C.

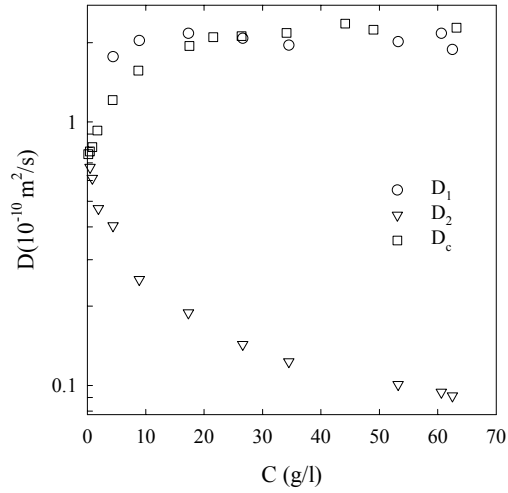


Figure 3.11. Cooperative diffusion coefficient of unaggregated ovalbumin (D_1) and aggregated ovalbumin (D_2) as a function of the concentration at which the solutions were heated at 78°C for 20 hours (pH 7 and 3 mM). For comparison the concentration dependence of the cooperative diffusion coefficient of native ovalbumin (D_c) is shown at the same pH and ionic strength.

(2) is caused by the cooperative diffusion of aggregated ovalbumin. We have seen with SEC, see figure 3.4, that at very low concentrations only small aggregates are formed so that their diffusion process cannot be well distinguished from that of native ovalbumin. With increasing concentration larger aggregates are formed resulting in a decrease of D_2 and a better separation of the two relaxation modes. At higher protein concentrations interaction between the protein aggregates compensates the growth of the aggregates resulting in a weaker concentration dependence. The average relaxation time of the third mode has a very strong q -dependence (about $\tau \propto q^{-4}$) and increases rapidly with the protein concentration close to C_{gel} . The relative amplitude of the third mode is about 15 % at 45 g/l and 40 % at 53 g/l and 61 g/l.

We have measured the scattering intensity during the heating process at 77.5°C for three protein concentrations, see figure 3.12.; a relatively low concentration (17 g/l) where rather small aggregates are formed after 20 hours ($R_{gz}=20$ nm); a concentration (61 g/l) where very large aggregates are formed ($R_{gz}>1$ μ m); and a concentration (70 g/l) where the system

gels. After placing the solutions in the apparatus it takes about 500 seconds to reach the set heating temperature. Thus at short times we measure the scattering intensity of unaggregated ovalbumin. As discussed above, I_r/C for native ovalbumin is larger at 17 g/l than at the two higher concentrations caused by strong repulsive electrostatic interactions. When the temperature of the solutions increases the intensity increases because the proteins aggregate. At the lowest concentration I_r increases first rapidly after which the increase slows down. At long times the increase is approximately logarithmic and appears to stagnate in a lin-lin representation, see inset of figure 3.12. The initial rise of I_r is caused by aggregation of the active ovalbumin fraction whereas the logarithmic growth at longer times is probably caused by slow aggregation of thermally more stable ovalbumin.

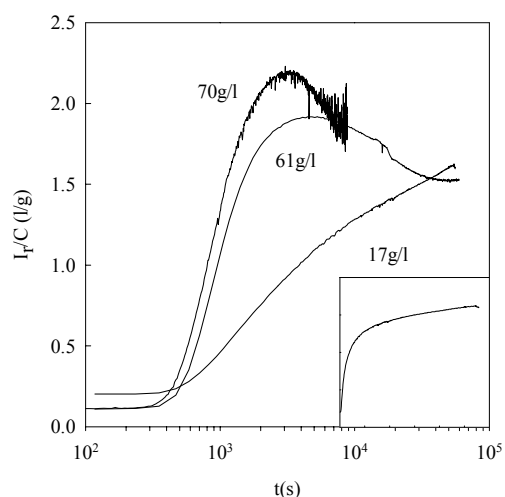


Figure 3.12. Dependence on heating time at 77.5°C of I_r/C for ovalbumin solutions at three concentrations (pH 7 and 3 mM). The inset shows the result for $C=17\text{g/l}$ with a linear time axis.

At higher protein concentrations I_r rises rapidly to a maximum after which it slowly decreases. The initial increase of I_r is caused by the increase of the number and size of the linear aggregates. Once the size and concentration of the linear aggregates is such that they start to overlap I_r reaches a maximum. Above this overlap concentration (C^*) I_r decreases weakly with increasing concentration, but is independent of further growth of the aggregates as is expected for semi dilute solutions of linear chains.²⁶ Notice that I_r/C after 20 h heating is approximately independent of the concentration. For the highest concentration I_r shows fluctuations around the average value that increase in amplitude with heating time, the origin of which will be discussed below. A similar observation has been reported for β -lactoglobulin²⁸.

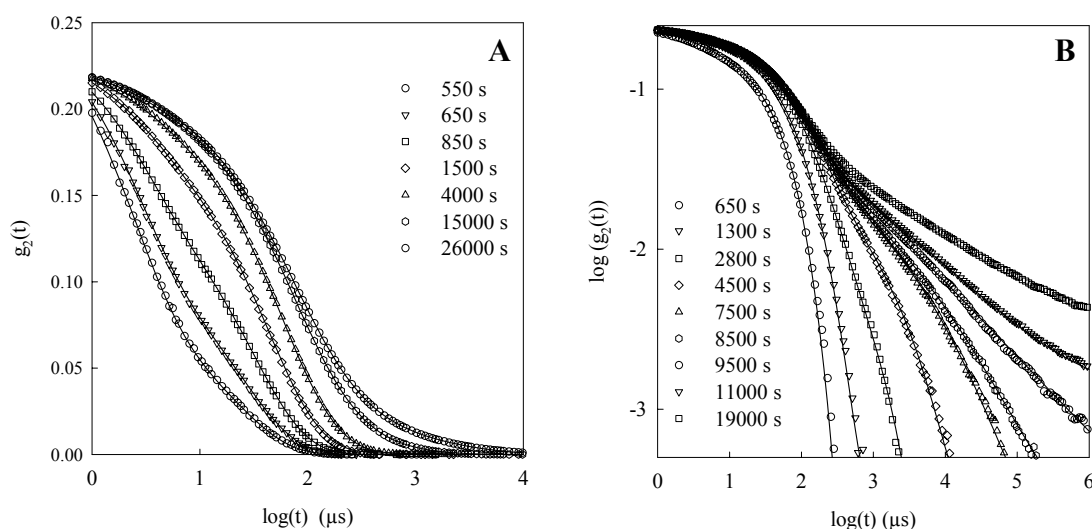


Figure 3.13. (A) Semi logarithmic representation of autocorrelation functions of ovalbumin solutions at $C=70$ g/l at different heating times at 74°C (pH 7 and 3 mM). The solid lines represent non-linear least squares fits. (B) Double logarithmic representation of autocorrelation functions of ovalbumin solutions at $C=70$ g/l at different heating times at 77°C (pH 7 and 3 mM). The solid lines represent non-linear least squares fits.

We measured the correlation functions at different times during the aggregation process for $C=70$ g/L at 74°C and at 77°C. The evolution of I_r/C is the similar at the two temperatures but the process is about 4 times slower at 74°C than at 77°C. Results obtained at 74°C are plotted on a semi logarithmic scale in figure 3.13a, while results obtained at 77°C are plotted on a double logarithmic scale in figure 3.13b. The right panel of figure 3.10 shows the relaxation time distributions corresponding to the correlation functions in figure 3.13a. Even at the earliest stages of the aggregation process we observed two distinct relaxation modes. The faster mode is due to the diffusion of unaggregated proteins and the slower mode is due the diffusion of aggregates. The relative amplitude of the fast mode decreases rapidly and stabilizes at about 6% at both temperatures. Chromatographs obtained from SEC at different heating times also showed that even when the large majority of the proteins have not yet aggregated the aggregate peak is well separated. This feature which was reported earlier by Koseki et al.¹¹, has also been observed for β -lactoglobulin.¹²

At longer heating times when I_r approaches the maximum, a third very slow mode appears which is more clearly seen in a double logarithmic representation, see figure 3.13b. With increasing heating time the terminal relaxation time of mode 3 increases and becomes longer than the time over which I_r is averaged (about 10s). This is the reason why I_r

fluctuates strongly around the average value in figure 3.12 at long heating times. The relative amplitude of mode 3 increases with heating time and is about 35% close to the gel point. Preliminary measurements of the evolution of the shear modulus showed that the appearance of very slow intensity fluctuations is correlated with a sharp rise of the storage shear modulus.

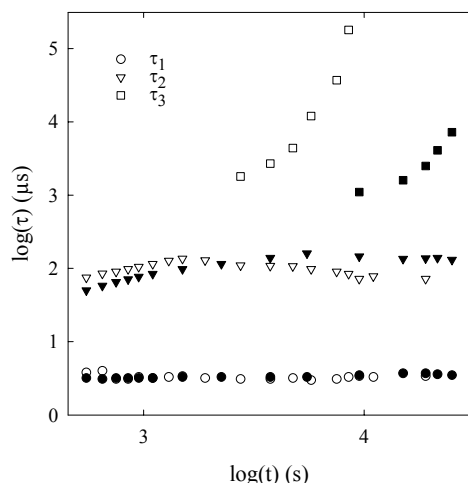


Figure 3.14. Average relaxation times of the three relaxation modes of ovalbumin solution at $C=70$ g/l as a function of heating time at 74°C (filled symbols) and 77°C (open symbols).

Figure 3.14 shows the dependence on heating time of the average relaxation time of the three modes. The average relaxation time of mode 1 (τ_1) is independent of heating time and the corresponding diffusion coefficient is close to that of unheated ovalbumin. The average relaxation time of mode 2 (τ_2) increases first with heating time and then stabilizes or even decreases very weakly. The third mode can be first detected after τ_2 has reached its maximum. Its average relaxation time (τ_3) increases rapidly and diverges at the heating time where the large fluctuations of I_r appear. Varying the temperature only varies the rate at which the system develops. At lower ovalbumin concentrations the evolution of the system is similar but the aggregation process stagnates at an earlier stage.

Results similar to those shown in figures 3.12 and 3.13 have been reported earlier for other gel forming systems. Especially, many features observed here show a remarkable resemblance with those observed during the co-polymerisation of methylmethacrylate (MMA) with a small fraction of ethylene glycol dimethacrylate (EGDMA) in solution.^{27,29} This co-polymerisation process leads to the formation of linear polymethacrylate (PMMA). The EGDMA units incorporated in the linear PMMA chains form crosslinks as the system approaches the overlap concentration. Similarly we interpret the present results at low

ionic strength as follows. Initially the fraction of active ovalbumin forms mainly linear aggregates. This aggregation process stagnates when all active ovalbumin has aggregated. The larger is the concentration of active ovalbumin the larger are the linear aggregates. Above a given ovalbumin concentration the linear aggregates reach the overlap concentration and have a small probability to form junctions. The very slow relaxation process may be interpreted in terms of self-diffusion of branched aggregates. A very strong q -dependence of the relaxation time points to anomalous diffusion, i.e. the effective friction coefficient increases if the aggregates diffuse over a larger distance. Above C_{gel} the branched aggregates percolate and form a gel.

3.3.4 PROGRESSIVE DILUTION OF AN OVALBUMIN SOLUTION CLOSE TO THE GEL POINT

An ovalbumin solution with $C=60$ g/l at 3 mM NaN_3 was heated for 22 hours at $78^\circ C$. After cooling to $20^\circ C$ the solution was progressively diluted with 0.1 M NaCl and SLS and DLS measurements were done at each dilution. As mentioned above, the q -dependence of I_r is negligible for undiluted solutions. After dilution, I_r increases and the q -dependence becomes stronger. After dilution by more than a factor 300, I_r has a power law q -dependence over the whole accessible q -range. Curves at different dilutions are similar to those shown in figure 3.5a. For each dilution we determined an apparent molar mass (M_a) and radius of gyration (R_{ga}) using $KC/I_r = (1 + (qR_{ga})^2/3)/M_a$. M_a is proportional to the osmotic compressibility of the system and R_{ga} is proportional to the correlation length of the concentration fluctuations. Again a master curve can be formed by plotting $(I_r/KC)/M_a$ as a function of qR_{ga} . The master curve which represents the structure factor of the progressively diluted systems is compared in figure 3.5b with the structure factor of the highly diluted aggregates formed at different concentrations.

Naturally, the limiting power law q -dependence at $qR_{ga} \gg 1$ is the same for both structure factors and depends on the fractal dimension of the aggregates. The crossover to this limiting power law behaviour is different, however, because in the case of progressive dilution one measures the cut-off of the fractal structure at the correlation length of the system, whereas in the case of highly diluted aggregates one measures the cut-off of the fractal structure at the radius of gyration.

In figure 3.7 we compare the dependence of M_a on R_{ga} for progressively diluted solutions with that of M_w on R_{gz} of highly diluted aggregates. Again we observe a power law dependence: $M_a \propto R_{gz}^{-1.65}$. Within the experimental error the power law exponent is the

same as for highly diluted samples, but the prefactor is smaller in the case of progressively diluted solutions. The smaller prefactor is consistent with the more gradual transition of $S(q)$ to its limiting power law q -dependence at large qR_{gz} . The concentration dependence of M_a is shown in figure 3.15. For semi-dilute solutions of flexible polymers in good solvents $\pi \propto C^{2.3}$ is expected theoretically²⁶ and observed experimentally³⁰. Utilizing eq.3.1 one expects for such systems $M_a \propto C^{-1.3}$ which may be compared to $M_a \propto C^{-1.5}$ obtained here, see solid line in figure 3.15.

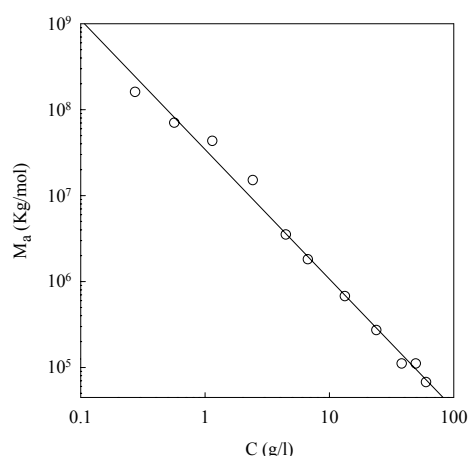


Figure 3.15. Dependence of the apparent molar mass on the concentration for progressive dilutions of a solution containing very large ovalbumin aggregates ($>1\mu\text{m}$) formed at $\mu=3\text{ mM}$ and pH 7.

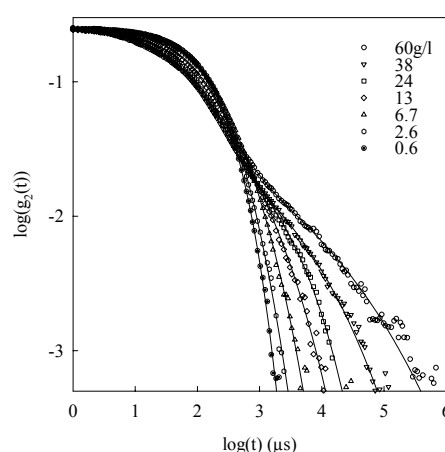


Figure 3.16. Double logarithmic representation of autocorrelation functions of different dilutions of an ovalbumin solution at $C=60\text{ g/l}$ that was heated at 78°C for 20 hours (pH 7 and 3 mM). The solid lines represent non-linear least squares fits.

As discussed above for undiluted samples close to the gel point the correlograms are characterized by three relaxational modes: 1) the diffusion of inactive ovalbumin, 2) the cooperative diffusion of the aggregates, and 3) a broad slow mode often observed in gelling systems which could be due to self diffusion of branched aggregates. Figure 3.16 shows the correlograms at different dilutions. One clearly observes the contribution of the three relaxation modes at the higher concentrations. The relaxation time of mode 1 is not modified much by dilution, but the relative amplitude decreases when the system is diluted and becomes negligible for $C < 10\text{ g/l}$. The relaxation time of mode 3 decreases rapidly with increasing dilution, while that of mode 2 increases weakly. For $C < 2\text{ g/l}$ the two modes have merged and the correlation functions are well described by a monomodal relaxation time distribution.

The static and dynamic light scattering results may be understood if we assume that the system consists of mainly linear interpenetrated aggregates with a small fraction of branched clusters. When the system is diluted the correlation length increases which leads to decrease of the cooperative diffusion coefficient. Dilution also leads to a decrease of the viscosity and thus to faster diffusion of the branched clusters. Again there is a resemblance with cross-linked PMMA.²⁹ Progressive dilution of cross-linked PMMA close to the gel point also leads to a rapid decrease of the relaxation time of mode 3 until it merges with mode 2. However, the concentration dependence of the scattering intensity is much stronger for cross-linked PMMA ($M_a \propto C^{-3}$) and is consistent with theoretical predictions for the dilution of percolating clusters. The results reported here for ovalbumin are closer to that expected for the dilution of linear chains. Another difference is that the maximum of the size distribution of cross-linked PMMA remains situated at the position of linear PMMA formed in the absence of EGDMA and simply broadens with increasing reaction time. This result is again consistent with the prediction of percolating clusters. For ovalbumin the maximum shifts with increasing reaction time. We conclude that branching of the linear ovalbumin aggregates formed at low ionic strength is not very important unless the system is very close to the gel point. A few measurements of progressive dilution of β -lactoglobulin aggregates at pH 2 showed qualitatively the same effects as for ovalbumin.³¹

3.4 CONCLUSIONS

Heated ovalbumin at pH7 forms linear aggregates of monomeric ovalbumin, with very little branching at low ionic strength, but with strong branching at 0.1 M NaCl. The aggregates are semi-flexible and have a self similar structure characterized by a fractal dimension of 1.7 at low ionic strength and 2.0 at 0.1M NaCl.

At low ionic strength heated ovalbumin solutions remain transparent and can be studied with light scattering techniques. The scattering intensity increases with heating time until the linear aggregates start to overlap after which the intensity decreases. The correlation length of the solutions at low ionic strength remains small due electrostatic interactions, which explains why they remain transparent. The degree of branching increases when the aggregates overlap and leads to gel formation for concentrations above 60 g/L. Progressive

dilution shows that the system close to the gel point is similar to a semi-dilute solution of flexible polymers.

The concentration fluctuations fully relax by cooperative diffusion for concentrations below the gel point. At concentrations approaching the gel point an additional slow relaxation process is observed possibly caused by self-diffusion of aggregates and restructuration. The terminal relaxation time becomes very long when the gel is formed, which leads to slow fluctuations of the scattering intensity.

ACKNOWLEDGEMENTS

We thank Martien Cohen Stuart for stimulating discussions.

REFERENCES

1. Clark, A.H. In *Functional properties in food macromolecules*; Mitchell, J. R., Ed.; London 1998: Elsevier applied science, (77-142).
2. Creamer, L.K.; Jimenez-Flores, R.; Richardon, T. (1988). *Trends biotechnology*, 6, 163-169.
3. Mine, Y. Recent advances in the understanding of egg white protein functionality. (1995). *Trends in Food Science and Technology*, 6, 225.
4. Croguennec, T., Nau, F., Pezennec, S., Brule, G. (2002) *Journal of Agricultural and Food Chemistry*, 48 (10), 4883-4889
5. Nisbet, A.D.; Saundry, R.H.; Moir, A.J.G.; Fothergill, L.A.; Fothergill, J.E. (1981) *Eur. J. Biochem.*, 115, 335.
6. Perlmann, G.E. (1952). *J. Den. Physiol.* 35, 711-726.
7. Linderstrøm-Lang, K.; Ottesen, M. (1949). *Compt. rend. trav. Lab. Carlsberg Ser. Chim.* 26, 403-442.
8. Hatta, H.; Kitabatake, N.; Doi, E. (1986). *Agric. Biol. Chem.*, 50, 2083.
9. Nemoto, N.; Koike, A.; Osaki, K.; Koseki, T.; Doi, E. (1993). *Biopolymers*, 33, 551.
10. Mine, Y. *J. Agric.* (1996). *Food Chem*, 44, 2086.
11. Koseki, T.; Kitabatake, N.; Doi, E. (1989). *Food Hydrocolloids*, 3, 123.
12. Gimel, J.C.; Durand, D.; Nicolai, T. (1994). *Macromolecules*, 27(2), 583.
13. Le Bon, C.; Nicolai, T.; Kuil M. E.; Hollander, J.G. (1999). *J.Phys Chem B*, 103, 10294
14. Hagiwara, T.; Kumagai, H.; Nakamura K.(1996). *Biosci. Biotech. Biochem.*, 60, 1757
15. Barbano, D.M.; Clark, J.L.; Dunham, C.E.; Flemming, J.R. (1990). *J. Assoc. Off. Anal. Chem.*, 73, 849.
16. Verhoef, J.C.; Barendrecht, E.(1977). *Anal. Chim. Acta*, 94, 395.
17. Brown W., Ed. *Light Scattering. Principles and Developments*, Clarendon Press, Oxford, 1996.
18. Higgins, J.S.; Benoit, K.C. *Polymers and Neutron Scattering*, Clarendon Press, Oxford, 1994.

19. Berne, B.; Pecora, R. *Dynamic light scattering*, Wiley, New York, 1976.
20. Stepanek, P. In *Dynamic Light Scattering*, Brown, W., Ed.; Oxford University Press, Oxford, 1993.
21. Le Bon, C.; Nicolai, T.; Durand, D. (1999). *Int. J. Food Sci. and Tech.*, 34(5/6), 451.
22. Smith, M.B.; Back, J.F. (1962). *Nature*, 193, 878
23. Schäfer, A.; Drewes, W.; Schwägele, F. (1999). *Nahrung*, 43, 86.
24. Nicolai, T; Durand, D; Gimel, J.C. In *Light Scattering. Principles and Developments* (chapter 6), Brown W., Ed.; Clarendon Press, Oxford, 1996.
25. Nicolai, T; Durand, D; Gimel, J.C. In *Light Scattering. Principles and Developments*, Brown W., Ed.; Clarendon Press, Oxford, 1996, (201-231).
26. de Gennes, P.G. *Scaling Concepts in Polymer Physics*. London, Cornell University Press, 1979.
27. Durand, D.; Gimel, J.C.; and Nicolai, T. (2002). *Physica A*, 304, 253-265
28. Lesturgeon, V.; Nicolai, T.; and Durand, D. (1999). *Eur. Phys. J. B*, 9, 71.
29. Takata, S.; Norisuye, T.; Tanaka, N., Shibayama, M. (2000). *Macromolecules*, 33, 5470.
30. Lesturgeon, V., Nicolai, T., and Durand, D., (1999). *Eur. Phys. J. B*, 9, 83.
31. Noda, I.; Kato, N.; Kitano, T.; Ngasawa, M. (1981). *Macromolecules*, 14, 668.
32. Aymard, P.; Nicolai, T.; Durand, D.; Clark A. (1999). *Macromolecules*, 32, 2542.



CHAPTER 4

X-RAY AND LIGHT SCATTERING STUDY OF THE STRUCTURE OF LARGE PROTEIN AGGREGATES AT DIFFERENT IONIC STRENGTH

Pouzot, M., Nicolai, T., Visschers, R. W., and Weijers, M.

Food Hydrocolloids 2005, 19, 231-238

Food Hydrocolloids 2005, 19, 231-238

ABSTRACT

The structure of large ovalbumin and β -lactoglobulin aggregates formed after heat-denaturation at neutral pH was studied using a combination of light and small-angle X-ray scattering. The effect of the electrostatic interactions was investigated by varying the ionic strength. The results were compared with images obtained using cryo-TEM. The structure of ovalbumin aggregates is compatible with that of semi-flexible strings of monomers that are more flexible and increasingly branched with increasing ionic strength. The persistence length increases with decreasing ionic strength. β -lactoglobulin aggregates consist of clusters of primary aggregates that are formed in the first step of the aggregation process. At low ionic strength the association of primary aggregates is mostly head to tail, while with increasing ionic strength denser clustering of the primary aggregates is observed.

4.1 INTRODUCTION

Generally, heat-induced denaturation of globular proteins leads to aggregation. Aggregates grow during heating, leading to gelation at sufficiently high protein concentrations. This phenomenon is important for applications in the food industry. The use of different globular food proteins, such as ovalbumin and β -lactoglobulin, may result in the formation of different structures on a mesoscopic level. Therefore different functionalities of food products on a macroscopic level can be obtained.

In general, if a protein solution is heated below a critical protein concentration, the aggregation process stops and a polydisperse distribution of aggregates is formed. Generally, this critical gelation concentration (C_g) increases with decreasing ionic strength. For one globular protein, β -lactoglobulin, it has been found that the arrest of the growth occurs when almost all ($> 90\%$) the native proteins have aggregated.¹ The rate of aggregation is highly temperature dependent, but the structure of the aggregates does not depend on the heating temperature.^{1,2} However, the structure of the aggregates, and therefore that of the gels, depends on the type of globular protein, the pH and the ionic strength. Characterisation of the aggregate structure is necessary for a full understanding of the gelation process and the structure and mechanical properties of the gel.

The structure of the aggregates can be investigated using electron microscopy and scattering techniques. Light scattering has been used to characterize the structure of aggregates formed by heating β -lactoglobulin,^{2,3} ovalbumin,⁴ and bovine serum albumin⁵ on length scales between about 20 nm and 1 μ m. For these proteins, it was found that the structure is self-similar on length scales much larger than that of the individual proteins. Small-angle X-ray (SAXS) and neutron (SANS) scattering techniques have been used to characterize the structure on smaller length scales.⁶⁻⁹ Ideally, one would like to combine different scattering techniques in order to cover a large range of length scales for the same system, which has rarely been done.

Electron microscopy has also been used to study the structure of globular protein aggregates.^{4,9-15} In most cases, it was found that the aggregates are thin strands under conditions of strong electrostatic repulsion, and more dense and globular closer to the isoelectric point or when the interactions are screened by adding salt. Unfortunately, the sample treatment needed for standard electron microscopy is potentially seriously perturbing. So far only few studies have been reported using the cryo-TEM technique, in

which the sample is rapidly frozen, preventing extensive formation of observable ice crystals, and no further sample treatment is needed to observe the system with a transmission electron microscope.

Here we present a study of the influence of the ionic strength on the structure of very large ovalbumin (OA) and β -lactoglobulin (β -lg) aggregates using light scattering and SAXS. The results are compared with cryo-TEM images of the aggregates. In this work the pH was kept constant at 7, but is also compared with results for β -lg at pH 2.

OA is the main protein component in egg-white with molar mass 45 Kg mol^{-1} and a radius of about 3 nm.^{4,16,17} Upon heating, OA aggregates in the form of strings of monomers that crosslink and depending on the ionic strength, form branched clusters or at sufficiently high protein concentrations form a gel.^{4,10} β -lg is the main protein component in whey, with molar mass 18 Kg mol^{-1} and a radius of about 2 nm.^{18,19} At low pH (\sim pH 2), β -lg also forms strings of monomers that are more or less rigid and more or less branched depending on the ionic strength.^{9,11,20} However, at pH 7 the aggregation of β -lg is a two-step process.²¹ It forms first so-called primary aggregates containing about 100 monomers and with a hydrodynamic radius of about 15 nm. Cryo-TEM images of these primary aggregates show that they have an elongated shape with diameter of about 10 nm and a length of about 50 nm.¹⁰ There are indications that the molar mass of these primary aggregates increases weakly with increasing ionic strength.²² At low protein concentrations and low ionic strength the primary aggregates are stable, but with increasing concentration and ionic strength they associate to form the larger clusters that we study here.²²

4.2 MATERIALS AND METHODS

4.2.1 SAMPLE PREPARATION

The ovalbumin (OA) used for this study was purified from egg white of freshly laid hens' eggs (less than 2 h old) based on the procedure of Vachier et al.,²³ and contained a small fraction (6%) of heat-stable ovalbumin. The β -lactoglobulin (β -lg) used in this study was a gift from Lactalis (Laval, France) and contained about equal fractions of the variants A and B. We showed elsewhere that the aggregation rate is the same for the two variants in the mixture.²⁴ The proteins were dissolved in Millipore water with 3 mM NaN_3 added to prevent bacterial growth. Solutions were extensively dialysed against salt-free Milli-Q water at pH 7. After dialysis the ionic strength was set by adding small amounts of a

concentrated NaCl solution. Subsequently, the samples were filtered through 0.2 μm pore size Anotop filters. Protein concentrations were measured after filtration by UV absorption at 278 nm using $\epsilon=0.698 \text{ Lg}^{-1}\text{cm}^{-1}$ for OA and $\epsilon=0.96 \text{ Lg}^{-1}\text{cm}^{-1}$ for $\beta\text{-lg}$. The solutions were heated for up to 24 h in air-tight vials in a thermostat bath at 78°C or 80°C and subsequently rapidly cooled to 20°C. For these heating conditions almost all proteins have aggregated.

4.2.2 SCATTERING EXPERIMENTS

Static light scattering measurements were made using an ALV-5000 multi-bit multi-tau correlator and a Spectra Physics solid-state laser operating with vertically polarized light with wavelength $\lambda=532 \text{ nm}$. The range of scattering wave vectors covered was $3.0 \times 10^{-3} < q < 3.5 \times 10^{-2} \text{ nm}^{-1}$. The temperature was controlled by a thermostat bath and set at 20°C.

Synchrotron small-angle X-ray scattering measurements were performed at the Dutch-Flemish bending magnet BM26B “DUBBLE” beam line at the European Synchrotron Radiation Facility (ESRF) in Grenoble (France). The beamline optics provides an X-ray photon energy range of 6-35 keV (in these experiments energies used were 12.2 and 8 keV, which correspond to the wavelengths of 0.1015 and 0.155 nm, respectively). The beam size at the sample was about 0.35 mm \times 0.5 mm (horizontal \times vertical). The scattering patterns were registered at $\sim 8.5 \text{ m}$ distance from the sample by a two-dimensional (2D) gas-filled multi-wire proportional counter (image size of 512 \times 512 pixels). The range of scattering wave vectors covered was calibrated with the rat-tail collagen standard sample, and this range was $0.08 < q < 1.13 \text{ nm}^{-1}$. The collected 2D data were reduced to the intensity profiles (radial averaging) and normalized for transmission. The temperature was controlled by a thermostat bath and set at 20°C.

The excess scattering over that of the solvent, I_r , is related to the weight average molar mass (M_w) and the structure factor ($S(q)$) of the solute:^{25,26}

$$I_r = KCM_w S(q) \quad (4.1)$$

where C is the concentration and K is an optical constant. For light scattering the optical constant can be obtained using a toluene standard. For SAXS we obtained the optical constant by comparing light and X-ray scattering from native OA.

4.2.3 CRYO-TRANSMISSION ELECTRON MICROSCOPY

Cryo-transmission electron microscopy (cryo-TEM) was done at the Unilever Research Center (Vlaardingen, the Netherlands) using a Philips CM12 transmission electron microscope operating at 120 kV. The formed aggregates were diluted to a concentration of 1 gL^{-1} , in order to study the aggregates separately. A drop of the liquid sample was placed on a perforated carbon film, supported by a 200-mesh copper grid, and most of the liquid was removed by blotting with a filter paper. The thin liquid films formed across the holes were subsequently vitrified by plunging the grid into liquid propane at a temperature below -170°C . The specimens were stored in liquid nitrogen until they were transferred to the cryo-holder. The cryo-holder (Oxford) was cooled by liquid nitrogen to a temperature lower than -170°C . Images were recorded digitally by a Gatan 791 CCD camera using the Digital Micrograph software package.

4.3 RESULTS AND DISCUSSION

We prepared large aggregates of OA and β -lg by heating protein solutions at pH 7 and various concentrations of NaCl for a long time (about 24 h) at elevated temperatures (75 - 80°C). As mentioned in the introduction it has already been established that the structure of the aggregates does not depend on the heating temperature and the protein concentration, although the rate of aggregation for β -lg does depend on these parameters. Since OA shows first-order kinetics (Weijers, Barneveld, Cohen Stuart & Visschers, 2003), its rate of aggregation is not dependent on protein concentration, but only on the temperature. The protein concentrations were chosen such that very large aggregates were obtained after heating, but that yet no gel was formed, i.e. slightly below the critical gelation concentration (C_g). The values of C_g are tabulated in Table 4.1. The structure factor of the aggregates was determined over a wide q -range by combining the results from light and X-ray scattering.

For each system the samples were progressively diluted until we no longer observed the effect of interactions on the q -dependence of I_r/C . The effect of progressive dilution is best observed at very low ionic strength, for which electrostatic interactions are strong and the critical gelation concentration is relatively high. As an example, we have plotted in figure 4.1 the effect of progressive dilution for large β -lg aggregates formed at an ionic strength of 3 mM. Electrostatic interactions induce ordering of the aggregates, which leads to a

Table 4.1. Characteristics of OA and β -lg aggregates formed at pH7.

C_s (mM)	<i>Ovalbumin</i>		<i>β-lactoglobulin</i>	
	C_g (g/L)	l_p (nm)	C_g (g/L)	l_p (nm)
3	60	130	100	90
10	40	-	85	63
20	37	-	60	63
30	15	100	-	-
50	10	60	35	63
100	4	60	15	29

(C_s : salt concentration; C_g : gelation concentration; l_p : persistence length)

so-called interaction peak in the spectrum. With progressive dilution the peak shifts to smaller q values because the average distance between the aggregates increases. The strength of the interactions decreases with dilution so that the peak becomes less pronounced. Similar concentration effects were observed for OA which will be described in more detail elsewhere (publication in preparation).

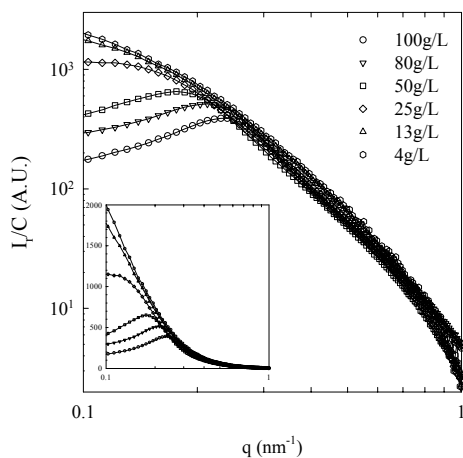


Figure 4.1. Influence of dilution on the q -dependence of the X-ray scattering intensity for β -lactoglobulin aggregates formed by heated at $C=100\text{g/L}^{-1}$ and 3 mM salt. The insert shows the same data in a semi-logarithmic representation.

In this paper we concentrate on the structure of the aggregates determined at sufficiently low concentrations so that interactions are negligible. Figure 4.2 shows the results for OA at a range of ionic strengths and figure 4.3 shows the results for β -lg. If we focus first on the small-scale structure observed with SAXS ($q > 0.1\text{nm}^{-1}$) we find that OA aggregates can be well described as rods:²⁸

$$\frac{I_r}{KC} = \frac{m \cdot \pi}{q} \exp\left(-\frac{q^2 \cdot R_c^2}{2}\right) \quad (4.2)$$

where R_c is the radius of gyration of the cross-section and m is the molar mass per unit length. Good agreement with the experimental results at all ionic strengths investigated is obtained using $R_c=3.35$ nm and $m=26$ Kg mol⁻¹ nm⁻¹, see solid line in figure 4.2 (at $q>0.08$ nm⁻¹).

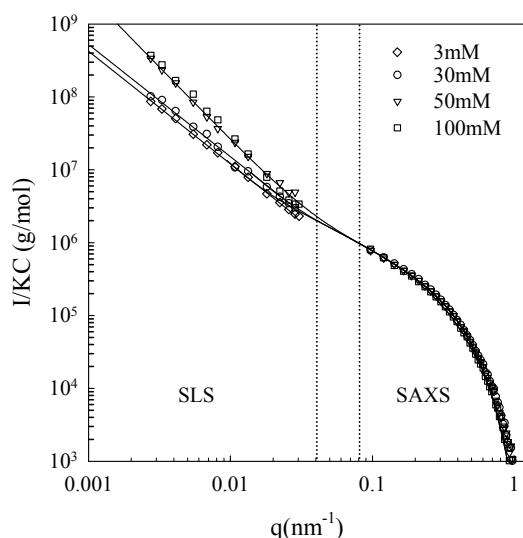


Figure 4.2. q -dependence of I_r/KC of highly diluted large ovalbumin aggregates formed by heating at different ionic strengths (indicated in the figure). SAXS data (q range $0.08 - 1$ nm⁻¹) and LS data (q range $0.002 - 0.03$ nm⁻¹) are combined. The solid lines represent fits to the data; see text.

The results for β -lg aggregates are quite different; see fig.4.3. Here the description in terms of rods works only over a very small q -range at lower ionic strengths and not at all for $C_s \geq 100$ mM. The solid line in figure 4.3 (at $q>0.08$ nm⁻¹) was obtained using $R_c=4.7$ nm and $m=38$ Kg mol⁻¹ nm⁻¹. The effect of the ionic strength on the local structure of β -lg aggregates is seen more clearly in figure 4.3b, in which an enlargement of the SAXS data is shown. The values of I_r/KC decrease more steeply for aggregates formed at higher ionic strengths, indicating a denser local structure. The densification is just visible at 100 mM NaCl, and becomes significant at 200 mM NaCl. At the largest q -values the structure factor becomes independent of the ionic strength within the experimental error. This could imply that the structure on length scales close to that of the individual proteins is independent of

the ionic strength, but one should be prudent because the signal to noise ratio is quite high at the largest q -values.

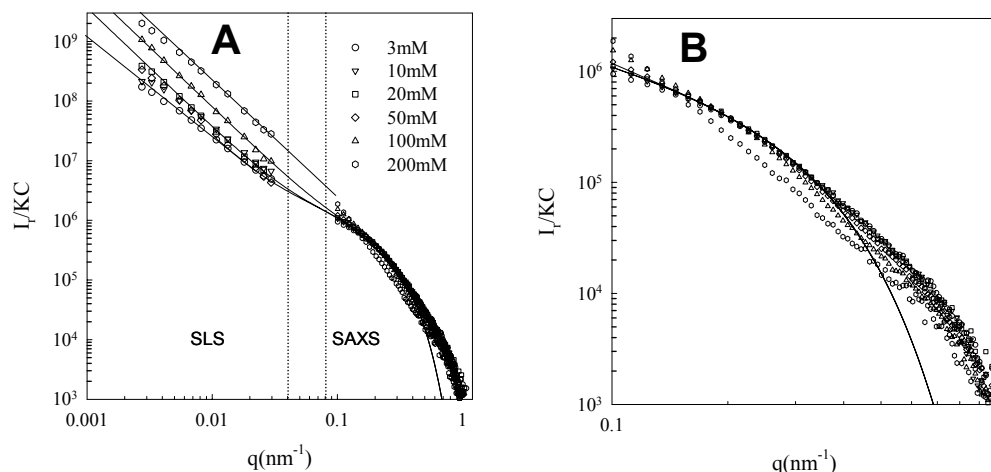


Figure 4.3. (A) q -dependence of I_r/KC of highly diluted large β -lactoglobulin aggregates formed by heating at different ionic strengths (indicated in the figure). SAXS data (q range $0.08 - 1 \text{ nm}^{-1}$) and LS data (q range $0.002 - 0.03 \text{ nm}^{-1}$) are combined. The solid lines represent fits to the data; see text. (B) q -dependence of I_r/KC of highly diluted large β -lactoglobulin aggregates formed by heating at different ionic strengths. Enlargement of SAXS data from figure 4.3A.

As was discussed in detail in Aymard et al.,⁹ eq. 4.2 describes the local structure ($q > 0.1 \text{ nm}^{-1}$) over a slightly larger q -range for β -lg aggregates formed at pH 2 than we find here at pH 7, but the description is not as good as for OA. For β -lg at pH 2, values between 2.3 and 2.6 nm were found for R_c and between 5.4 and 6.1 $\text{Kg mol}^{-1} \text{ nm}^{-1}$ for m .

The values of R_c and m of the OA aggregates at pH 7 and β -lg aggregates at pH 2 are compatible with that of a string of monomers or possibly dimers if we consider that the proteins are not fully spherical and may even be further deformed after. Clearly, such an interpretation is not possible for β -lg aggregates formed at pH 7 even at low ionic strength. The diameter and the mass per unit length of the aggregates is much too large. In fact, cryo-TEM images discussed below show that these aggregates can not be viewed as strands.

The large-scale structure observed with light scattering (fig. 4.2 and 4.3a) is consistent with more extensive studies reported elsewhere.²² On large length scales the structure factor has a power law q -dependence $S(q) \propto q^{d_f}$, where d_f is the so-called fractal dimension.

At higher ionic strengths the fractal dimension is 2 ($C_s \geq 50$ mM for OA and $C_s \geq 10$ mM β -lg) while at lower ionic strengths it is about 1.6 ($C_s \leq 30$ mM for OA and $C_s = 3$ mM β -lg).

To describe the transition between the local rod-like structure (SAXS) and the overall fractal structure (SLS), the data may be compared to the structure factor of an infinitely long and infinitely thin semi-flexible chain in the range $R_g^{-1} \ll q \ll R_c^{-1}$. A simple model of semi-flexible chains, so-called Kratky-Porod chains, describes the chains as ideal random coils for which the orientational correlation between the segment directions decreases exponentially with the distance between the segments along the chain (Δl). If α_{12} is the angle between segments 1 and 2, then $\cos(\alpha_{12}) = \exp(-\Delta l/l_p)$, where l_p is the persistence length. Des Cloiseaux²⁹ derived an analytical expression for the structure factor of this model chain in terms of a recursive expression. This expression leads to $S(q) \propto q^{-2}$ for $q \ll l_p^{-1}$, because excluded volume interactions are ignored. Therefore we have added a line with slope -1.6 to describe the data at low q -values for the results obtained at low ionic strengths.

As mentioned above, this recursive expression gives a fractal dimension of 2 on length scales larger than l_p . This indeed describes the observed q -dependence of OA rods at ionic strength above 30 mM. The data below ionic strength of 30 mM are well described with a fractal dimension of 1.6. The added a line with slope -1.6 describes the data at low q -values for the results obtained at low ionic strengths. The results of the fits are shown in figures 4.2 and 4.3a and the values of the persistence length obtained from the fits are given in Table 4.1. For OA this approach is quite useful and shows that the persistence length decreases with increasing ionic strength. Koseki et al.¹¹ reported $l_p = 23$ nm, $R_c = 6$ nm and $m = 16$ Kg mol⁻¹ nm⁻¹ for OA aggregates formed at pH 7 and 20 mM salt. These data were not determined directly, but deduced from the relation between the molar mass and the radius of gyration or the viscosity, which involved a correction for polydispersity. From electron microscopy they found a much smaller radius of about 2.5 nm.

The same analysis for β -lg aggregates at pH 2 showed a much stronger effect of the ionic strength on the persistence length.⁹ For β -lg aggregates at pH 7 the interpretation in terms of semi-flexible chains is doubtful. However, the analysis shows that the transition between a more extended local structure and the fractal overall structure depends little on the ionic strength for $C_s < 100$ mM and that for $C_s = 200$ mM such a distinction cannot be made.

An earlier SANS study of β -lg aggregates at pH 7 and 100 mM NH_3COOH gave results that are intermediate between those obtained at 100 mM and 200 mM NaCl.^{7,10} The critical gelation concentration for this system was also found to be intermediate.¹ This comparison suggests that NH_3COOH screens electrostatic interactions somewhat more efficiently than NaCl.

Cryo-Tem images of large OA and β -lg aggregates formed at different ionic strengths are shown in figs.4.4 and 4.5, respectively. For OA the aggregates are semi-flexible thin strands at all ionic strengths with a diameter that is compatible with the SAXS results. The main effect of increasing the ionic strength is that the extent of branching becomes more important, which can be clearly observed at $C_s = 20$ and 30 mM. Also it seems that the persistence length and contour length of the flexible linear aggregates decreases with increasing ionic strength. Cryo-TEM images of β -lg aggregates at pH 2 show strands with a diameter close to that of monomers.¹⁰

At all ionic strengths, at neutral pH, the β -lg aggregates are formed by association of short curved strands with a length of about 50 nm and a diameter of about 10 nm (figure 4.5). These short strands are the primary aggregates that are formed in the first step of the aggregation of β -lg at pH 7. At low ionic strength and low protein concentrations only these primary aggregates are formed.¹⁰ The diameter of the primary aggregates at low ionic strength is about 10 nm. At low ionic strength the large aggregates are mainly constructed by head to tail association of the primary aggregates. Increasing the salt concentration up to 50 mM NaCl, did not result in the formation of significant different structures, which was also observed with SAXS. Increasing the salt concentration up to 100 mM resulted in a slightly denser clustering of the primary aggregates, whereas at 200 mM NaCl significantly denser clusters are observed. It seems that these clusters are denser than the structures at low ionic strength, which is in good agreement with results obtained from small-angle X-ray experiments.

4.5 CONCLUSIONS

Ovalbumin aggregates formed by heating solutions at pH 7 can be well described in terms of semi-flexible strings of monomers. The persistence length of the strings varies from about 130 nm at very low ionic strength to 60 nm at 100 mM NaCl. Cryo-TEM images show that the strings are weakly branched at low ionic strength, but that the degree

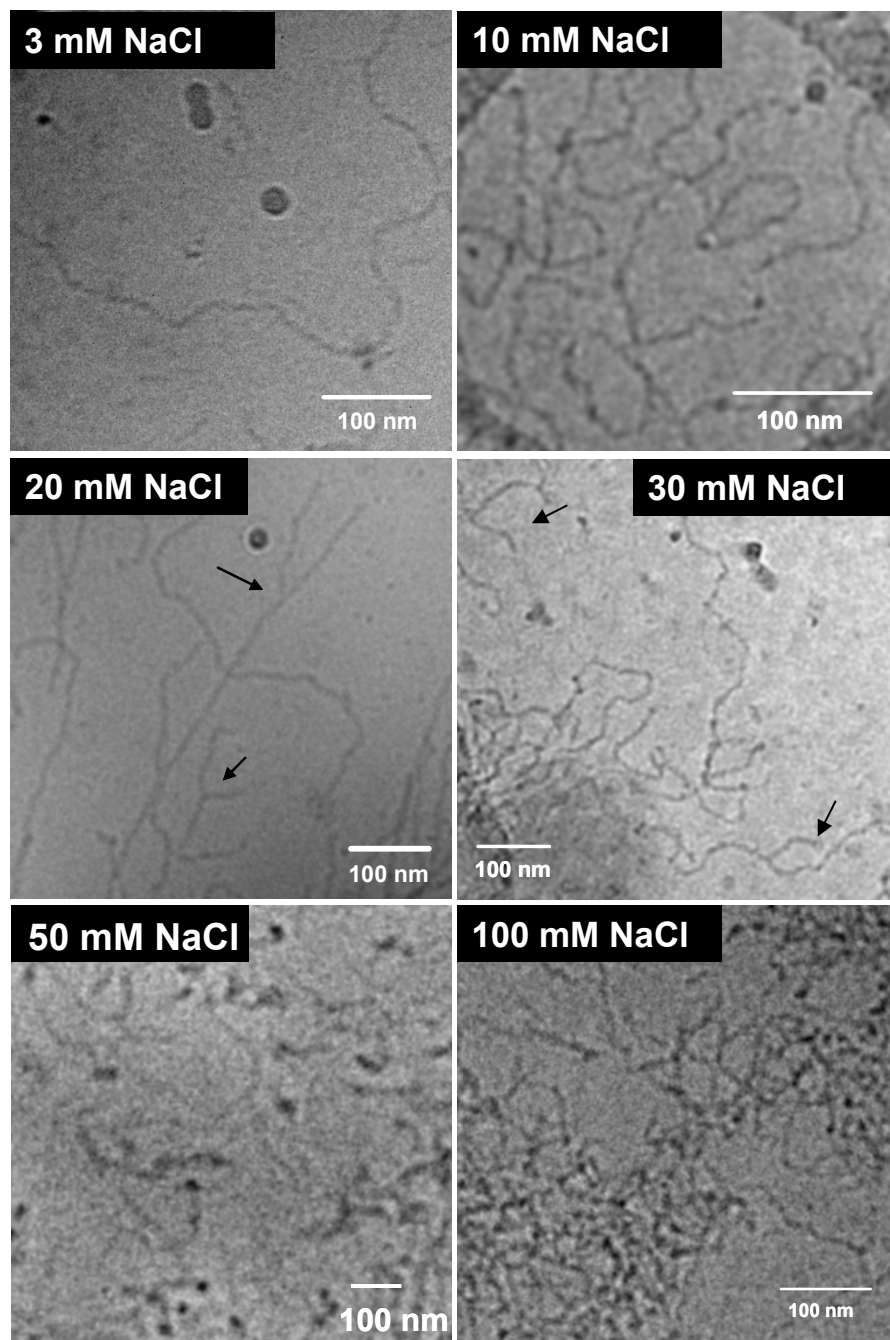


Figure 4.4. Cryo-TEM images of large ovalbumin aggregates formed after heating for 22 h at 78°C at different ionic strengths Heating conditions: $C_s=3$ mM, $C_p=55$ gL⁻¹; $C_s=10$ mM, $C_p=35$ gL⁻¹; $C_s=20$ mM, $C_p=37$ gL⁻¹; $C_s=30$ mM, $C_p=12$ gL⁻¹; $C_s=50$ mM, $C_p=5$ gL⁻¹; $C_s=100$ mM, $C_p=4$ gL⁻¹.

of branching increases with increasing ionic strength. The local structure of the aggregates is independent of the salt concentration up to at least 100 mM NaCl.

β -Lactoglobulin aggregates formed at pH 7 are not strings of monomers (in contrast to aggregates formed at pH 2), but consist of clusters of primary aggregates. The primary

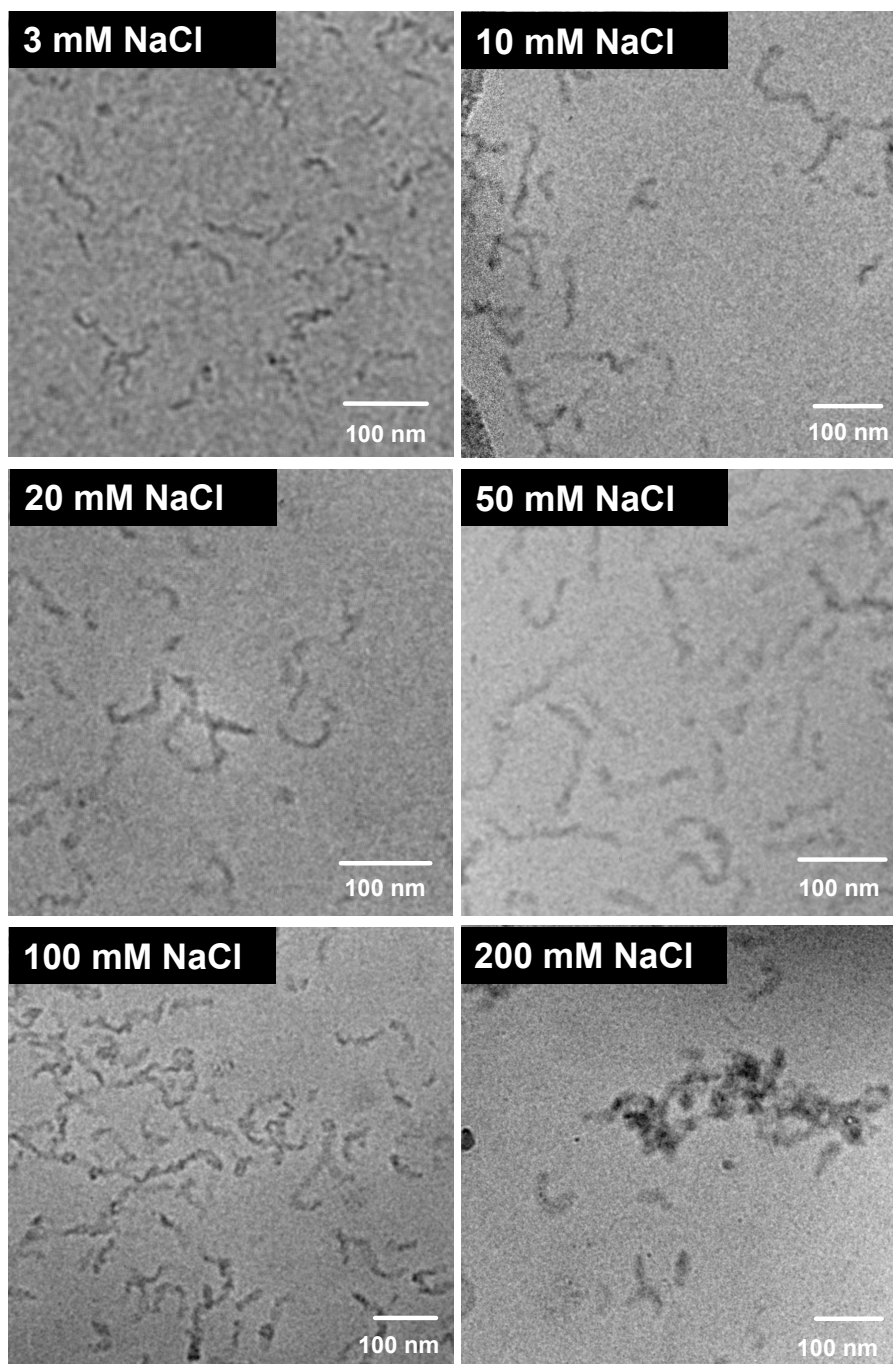


Figure 4.5. Cryo-TEM images of large β -lactoglobulin aggregates formed after heating for 24 h at 80°C at different ionic strengths Heating conditions: $C_s = 3$ mM, $C_p = 100$ gL⁻¹; $C_s = 10$ mM, $C_p = 85$ gL⁻¹; $C_s = 20$ mM, $C_p = 60$ gL⁻¹; $C_s = 50$ mM, $C_p = 35$ gL⁻¹; $C_s = 100$ mM, $C_p = 15$ gL⁻¹; $C_s = 200$ mM, $C_p = 7$ gL⁻¹.

aggregates are formed in a first step of the aggregation process and are relatively well-defined particles containing about 100 monomers. They are curved strands with a length of about 50nm and a diameter of about 10 nm. At low ionic strength the association of the

primary aggregates is mainly head to tail. The local structure of the aggregates becomes denser at NaCl concentrations above 100 mM.

ACKNOWLEDGEMENTS

Johan Hazekamp is thanked for his contribution to the Cryo-TEM measurements at Unilever Research (Vlaardingen). The Netherlands organization for advancement of research (NWO) is acknowledged for providing the possibility and financial support for performing SAXS measurements at the DUBBLE (experiment nr: 26-02-143 and 26-02-207). Igor Dolbnya and Wim Bras are gratefully acknowledged for their technical assistance at the DUBBLE (Grenoble). The authors gratefully acknowledge stimulating discussions with Martien Cohen Stuart and Dominique Durand on the aggregation behaviour of globular proteins. The Wageningen Centre for Food Sciences is acknowledged for financial support on performing cryo-TEM experiments.

REFERENCES

1. Le Bon, C., Nicolai, T., & Durand, D. (1999a). *Macromolecules*, 32, 6120.
2. Le Bon, C., Nicolai, T., & Durand, D. (1999b). *Int. J. Food Sci. Technol.*, 34, 451.
3. Vreeker, R., Hoekstra, L.L., den Boer, D.C., & Agterof, W.G.M. (1992). *Food Hydrocolloids*, 6, 423.
4. Weijers, M., Visschers, R.W., Nicolai, T. (2002). *Macromolecules*, 35, 4753.
5. Hagiwara, T., Kumagai, H., & Nakamura, K. (1996). *Biosci Biotech Biochem*, 60, 1757.
6. Clark, A.H., & Lee-Tuffnell, C.D. (1980). *Int.J.Peptide Res.*, 16, 339.
7. Gimel, J.C., Durand, D., & Nicolai, T. (1994). *Macromolecules*, 27, 583.
8. Renard, D., Axelos, M., & Lefebvre, J. (1995) In *Food Macromolecules and Colloids*, Dickinson, E., & Lorient, D. eds.; Royal Society of Chemistry, Cambridge, p 390.
9. Aymard, P., Nicolai, T., & Durand, D. (1999). *Clark A Macromolecules*, 32, 2542.
10. Durand, D., Gimel, J.C., & Nicolai, T. (2002). *Physica A*, 304, 253.
11. Koseki, T., Kitabatake, N., & Doi, E. (1989). *Food Hydrocolloids*, 3, 123-135.
12. Gosal, W.S., Clark, A.H., Pudney, P.D.A., & Ross-Murphy, S.B. (2002). *Langmuir*, 18, 7174.
13. Weijers, M., Sagis, L.M.C., Veerman, C. Sperber, B. & van der Linden, E. (2002). *Food Hydrocolloids* 16, 269.
14. Veerman, C., Sagis, L.M.C., Heck, J., van der Linden, E. (2003). *Int. J. Biol. Macromol.*, 31, 139.
15. Veerman, C., de Schiffart, G., Sagis, L.M.C., van der Linden, E. (2003). *Int. J. Biol. Macromol.* 33, 121.
16. Stein, P.E., Leslie, A.G.W., Finch, J.T., & Carrell, R.W. (1991). *J. Mol. Biol.*, 221, 941.
17. Nemoto, N., Koike, A., Osaki, K., Koseki, T., & Doi, E. (1993). *Biopolymers*, 33, 551.

18. Papiz, M.Z., Sawyer, L., Eliopoulos, E.E., North, A.C.T., Findlay, J.B.C., Sivaprasadarao, R., Jones, T.A., Newcomer, M.E., & Kraulis, P.J. (1986). *Nature*, 324, 383.
19. Pessen, H., Kumosinski, T.F., & Farrell, H.M.J. (1988). *J. Ind Microbiol.*, 3, 89.
20. Veerman, C., Ruis, H., Sagis, L.M.C., & van der Linden, E. (2002). *Biomacromolecules*, 3, 869.
21. Aymard, P., Gimel, J. C., Nicolai, T., & Durand, D. (1996). *J. Chim. Phys.*, 93, 987.
22. Baussay, K., Le Bon, C., Durand, D., & Nicolai, T. (2003). *Int. J. Biol. Macromol.*, 34, 21.
23. Vachier, M.C., Piot, M., & Awedé, A.C. (1995). *J. Chromatogr. B*, 66, 201.
24. Le Bon, C., Durand, D., & Nicolai, T. (2002). *Inter. Dairy J.*, 12, 671.
25. Higgins, J.S., & Benoit, K.C. (1994). In *Polymers and Neutron Scattering*, Clarendon Press, Oxford.
26. Brown W, editor (1996). *Light Scattering Principles and Developments*. Oxford: Clarendon Press.
27. Weijers, M., Barneveld, P.A., Cohen Stuart, M.A., & Visschers, R.W. (2003). *Protein Sci.*, 12, 2693.
28. Porod, G. (1996). In *Small Angle X-Ray Scattering*, Glatter, O., Kratky, O., Eds., Academic Press, Oxford.
29. Des Cloizeaux, J. (1973). *Macromolecules*, 6, 403.

CHAPTER 5

HEAT-INDUCED FORMATION OF “ORDERED” STRUCTURES OF OVALBUMIN AT LOW IONIC STRENGTH STUDIED BY SMALL ANGLE X-RAY SCATTERING

Weijers, M., Visschers R. W., Cohen Stuart, M.A. and Barneveld, P.A.
2004, submitted

ABSTRACT

Small Angle X-ray Scattering (SAXS) has been performed on native ovalbumin solutions and heated ovalbumin systems at neutral pH and low ionic strength. In native ovalbumin solutions there is a partial ordering, where the interparticle distance (d_{\max}) scales with the protein concentration (C) as $d_{\max} \sim C^{0.28}$. This exponent indicates that the ovalbumin monomers behave as a uniform distribution of charged spheres in solution. The q -dependent scattering intensity of ovalbumin aggregates can be well described by a form factor of rods. The dependence of d_{\max} for aggregates on the protein concentration was found to be $d_{\max} \sim C^{0.51}$, this scaling behavior is in good agreement with that theoretically derived for the distribution of spaces in a random network of straight fibers. The existence of a well-defined interparticle distance between aggregates is confirmed by cryo-TEM. The scattering profiles of native and aggregated ovalbumin were successfully fitted including both form factor and structure factor, using the preferred distance (L), a measure of disorder (σ/L), and the radius (R or a) as fitting parameters.

5.1 INTRODUCTION

Proteins in solution are generally charged, except when the pH of the solution is close to their iso-electric point. The repulsive character of proteins in solution is a general phenomenon and has also been observed for (ellipsoidal) globular proteins, like ovalbumin^{1,2}, β -lactoglobulin^{3,4,5} and lysozyme.^{6,7} The electrostatic interactions between these monomers are purely repulsive as characterized by an interaction peak usually observed with Small Angle X-ray Scattering (SAXS) or Small Angle Neutron Scattering (SANS).

Upon heating above 55°C, the native structure of a protein molecule is partly altered in terms of secondary and tertiary structure. This denaturation process results in the exposure of free thiol groups, when available, and hydrophobic patches at the surface of the molecule. These hydrophobic patches interact, and as a result intermolecular aggregation of the protein molecules occur. Heating an ovalbumin solution at low ionic strength and protein concentrations below the critical gelation concentration results in the formation of fibrillar aggregates.^{8,9,10} Above a critical protein concentration a space-filling network may be formed. The micro-, meso-, and macrostructure of these aggregates and gels, and their mechanical properties will vary depending on protein concentration, ionic strength, pH and heating conditions.

Ovalbumin is a globular egg white protein, with a molar mass of 46000 g/mol and a radius of about 3 nm.^{1,2,3} The shape, size and surface properties of ovalbumin monomers in aqueous solutions have been studied by Matsumoto *et al.*^{1,2} From these studies, the overall structure of an ovalbumin molecule can be approximated by a slightly elongated ellipsoid with dimensions of $7.0 \times 4.5 \times 5.0$ nm. The radius of gyration obtained from the angle dependence for X-ray is about 2.7 nm and does not depend on ionic strength.

Inoue and Matsumoto also studied the structure of ovalbumin monomers at high protein concentrations ($C = 93 - 560$ g/L) with SAXS.¹¹ They found that the wave vector corresponding to the peak maxima scaled as $C^{-0.33}$ for the concentration regime between 93 and 373 g/L and as C^{-1} for the concentration regime between 373 and 560 g/L. No detailed investigations were made at lower protein concentrations (< 100 g/L). The effects of ionic strength and heating on the mesoscopic structure were investigated roughly with SANS.¹² So far, no detailed investigations have been reported on the scaling of interparticle distance (d_{\max}) on the protein concentration for native ovalbumin solutions at low protein

concentrations or of aggregates in solutions (so-called “scaling behavior”). However, a few papers have described the experimental scattering peaks of native lysozyme and BSA under specific conditions using form factor and structure factor.^{3,7,13} In this study, we systematically investigated the following:

- (1) The scaling behavior for native ovalbumin solutions at pH 7 and low ionic strength;
- (2) The influence of dilution on the scattering of long fibrillar aggregates in order to determine the scaling behavior. The concentration dependence for uniform random suspensions of fibrils has been derived theoretically by Ogston¹⁴;
- (3) Influence of the initial protein concentration on d_{\max} , for ordered fibrillar structures in solution and gels. The presence of regular structures in ovalbumin systems is discussed and was confirmed with cryo-TEM micrographs.
- (4) Interpretation of the q -dependent scattering patterns of ovalbumin monomers and aggregates as presented in (1) and (2), using the model of Farsaci for the structure factor.

5.2 MATERIALS AND METHODS

5.2.1 MATERIALS

Ovalbumin was purified from egg white of freshly laid hens' eggs (less than 2 h old) based on the procedure of Vachier *et al.*¹⁵ Ovalbumin was dissolved in double-distilled water with 3 mM NaN_3 to prevent bacterial growth. The solutions were subsequently stirred for at least 2 h at ambient temperature to allow the protein to dissolve. The pH of the solution was adjusted to 7.0 and the solution was subsequently centrifuged and filtered (0.45 μm ; Millex-SV, Millipore Corp., Bedford, MA) to remove a small fraction of insoluble material. The protein solutions were heated for 22 hours in screw-cap vials containing about 5 ml of ovalbumin solution in a water bath at a temperature of 78°C. After heating, the solutions were rapidly cooled by placing the tubes in ice-water. For time-resolved measurements the samples were heated using a Peltier element. Protein concentrations were measured by UV absorbance at 280 nm and using an absorption coefficient $\epsilon=0.698 \text{ L g}^{-1}\text{cm}^{-1}$.

5.2.2 METHODS

Small Angle X-ray Scattering (SAXS) measurements were performed on the BM 26 DUBBLE beam line of the European Synchrotron Radiation Facility (ESRF) in Grenoble (France). The beam line optics provides an X-ray energy range of 6-35 keV (in these experiments energies were used of 12.2 and 8 keV, which correspond to wavelengths of 0.1015 and 0.155 nm, respectively). The beam size at the sample was about 0.35 mm × 0.5 mm. Measurements were made under vacuum using a Philips PW 1730 constant potential generator (Cu-K α X-rays). A two-dimensional gas-filled detector with CCD-camera (Photonic Science Xios-II, 1024*1024, resolution $\sim 23\mu\text{m}$) was used, located at the maximum distance of ~ 8.5 m from the sample. The q-range was calibrated with rat-tail collagen and the range of scattering wave vectors covered was $0.08 < q < 1.13 \text{ nm}^{-1}$. The collected data were converted to a 1-D intensity profile and normalized for transmission. The data were subsequently corrected for the background scattering.

Cryo-transmission electron micrographs were obtained at the Unilever Research Center (Vlaardingen, the Netherlands) using a Philips CM12 transmission electron microscope operating at 120 kV. A drop of the liquid sample was placed on a perforated carbon film, supported by a 200-mesh copper grid, and most of the liquid was removed by blotting with a filter paper. The thin liquid films formed across the holes were subsequently vitrified by plunging the grid into liquid propane at a temperature below -170°C . The specimens were stored under liquid nitrogen until they were transferred to the cryo-holder. The cryo-holder (Oxford) was cooled by liquid nitrogen to a temperature lower than -170°C . Images were recorded digitally by a Gatan 791 CCD camera using the Digital Micrograph software package.

5.3 RESULTS

5.3.1 NATIVE OVALBUMIN IN AQUEOUS SOLUTION

5.3.1.1 SIZE OF NATIVE OVALBUMIN MOLECULES

The scattering caused by a solution of native ovalbumin molecules at neutral pH is adequately described by that of a dispersion of (negatively) charged spheres, as reported by several authors.^{1,2} The radius of gyration (R_g) of the spheres can be determined in very dilute systems, for which the inter-particle interaction is negligible. This condition is usually at low volume fractions ($\phi \leq 1\%$) for colloidal systems of globular particles. For

monodisperse, dilute systems of particles, experimental data at low q can be described by the well known Guinier approximation:

$$I(q) \approx \phi V(\Delta\rho)^2 e^{\frac{-q^2 R_g^2}{3}} \quad (5.1)$$

where $\Delta\rho$ is the difference in scattering length density between the globules and the solvent and V the volume of a globule. Plotting $\ln I(q)$ versus q^2 results in the well known Guinier plot. From the initial slope of the Guinier plot, the radius of gyration of the ovalbumin molecule can be calculated. Figure 5.1 shows a Guinier plot, in which the scattering intensity of a native ovalbumin solution (10 g/L, 100 mM NaCl) is plotted versus q^2 .

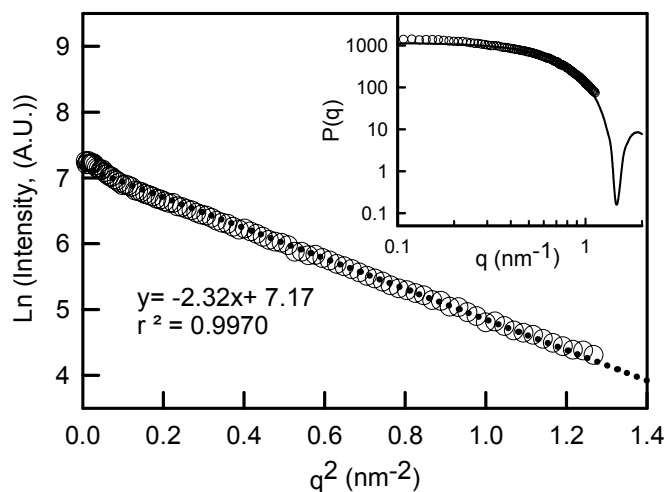


Figure 5.1. Guinier plot, $\ln I$ vs q^2 for spheres. Circles represents data obtained from SAXS measurements on native ovalbumin solutions (10 g/L, 100 mM NaCl, and pH 7). Inset: A fit of the scaled data to the theoretical form factor $P(q)$ for homogeneous spheres as a function of q (given $R_p = 3.05 \text{ nm}$) in a double-log plot (solid line), circles represent same experimental data.

The R_g obtained from the slope equals 2.6 nm, which agrees with values found in literature (2.37 – 2.81). Assuming spheres, the radius of an ovalbumin monomer can also be obtained from a direct fit to $I(q)$ using the form factor of spheres (eq. 5.2).

$$I(q) \approx (\Delta\rho)^2 \phi V \left(3 \frac{\sin qR_p - qr_p \cos qR_p}{(qR_p)^3} \right)^2 \quad (5.2)$$

where R_p is the radius of a hard sphere. For the same system, we obtained $R_p = 3.05$, as is shown in the inset of Figure 5.1. For clarity the theoretical form factor is shown for a

somewhat larger q -range than for the experimental data. For a homogeneous scattering sphere, the radius of gyration is related to its geometrical radius R_p as:

$$R_g = R_p (3/5)^{1/2} \quad (5.3)$$

The R_g calculated from eq.5.3 (here $R_p = 3.05$) equals 2.4 nm, which is slightly less than the 2.6 nm obtained from the Guinier approximation. This deviation might be due to the ellipsoidal character of an ovalbumin molecule.

5.3.1.2 SCALING BEHAVIOR OF NATIVE OVALBUMIN IN AQUEOUS SOLUTIONS

Figure 5.2 shows the reduced scattering intensity, I/C , plotted versus wave vector q (nm^{-1}) for different concentrations (C) of native ovalbumin at pH 7. A single peak was observed with a clear maximum (q_{max}), which shifted to higher q -values (i.e. smaller distances) with increasing protein concentration.

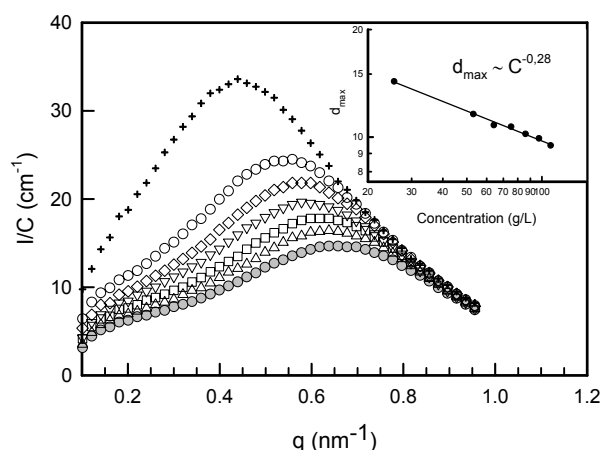


Figure 5.2. Scattered intensity normalized by the protein concentration as a function of q for native ovalbumin solutions (200 ppm NaN_3 , pH 7) at different protein concentrations. Inset: scaling between d_{max} and ovalbumin concentration on a double logarithmic scale. (+) 25.5; (o) 53.1; (\diamond) 64.2; (∇) 75.3; (\square) 86.0; (Δ) 97.4; (\bullet) 109 g/L.

The shift to higher q -values is due to the presence of more particles in the medium. Since q_{max} is related to a dominant distance in the protein system (d_{max}) by $d_{\text{max}} = 2\pi/q_{\text{max}}$, the interparticle distance in the system can be calculated (Table 5.1). The inset of Figure 5.2 shows the concentration dependence of the interparticle distance. A power law is observed: d_{max} scales with the concentration as $C^{-0.28}$.

Table 5.1. Peak position values as a function of protein concentration for native ovalbumin solutions, aggregates/gels and dilutions of long fibrils at pH 7 and 200 ppm NaN₃.

<i>Native</i>		<i>Aggregates/gels</i>		<i>Dilution series*</i>	
C (g/L)	q _{max}	C (g/L)	q _{max}	C (g/L)	q _{max}
25.51	0.439	25.51	0.199	53.10	0.252
53.10	0.542	32.89	0.215	45.00	0.234
64.20	0.582	43.96	0.232	42.00	0.223
75.30	0.588	53.10	0.252	37.00	0.210
85.95	0.616			31.90	0.195
97.40	0.634			27.60	0.181
108.50	0.664			22.30	0.161

* Aggregates prepared at 53.1 g/L and subsequently diluted

A similar dependence is found for β -lactoglobulin monomers at pH 9 and low ionic strength⁵. From theoretical calculations of charged spheres, the same exponent was found (0.28).^{5,16} Calculations based on a uniform distribution of spheres, as is used in a paracrystalline model ($q_{\max} \sim C^{0.33}$), describes our data less correctly. Matsumoto and Chiba¹ found an experimental relation of $q_{\max} \sim C^{0.22}$ for native ovalbumin in solution, but this relation was only founded on three data points.

5.3.1.3 FITTING EXPERIMENTAL INTERACTION PEAK OF OVALBUMIN MONOMERS IN AQUEOUS SOLUTION

As shown in the previous section, charged ovalbumin monomers form partially ordered structures in solution, which results in a scattering peak. If one considers ovalbumin monomers as spheres, the spectra as shown in Figure 5.2 can be fitted if a suitable model for the structure factor is chosen. Farsaci *et al.*¹³ developed a solvable model for the structure factor, in which single scatterers are partially ordered due to the competition between a restoring force that tends to keep the nearest neighbors at a preferred distance, L , and the stochastic character of the scattering elements in ordered solutions (thermal stochastic motion). Giordano *et al.*⁷ applied this model successfully in order to describe the spectrum of native lysozyme at pH 5. We used the structure factor given by Farsaci *et al.*¹³

$$S(q) = \frac{\text{Sinh}\left[\frac{q\sigma}{2}\right]^2}{\text{Cosh}\left[\frac{q\sigma}{2}\right]^2 - \text{Cos}qL} \quad (5.4)$$

where σ is the rms of the deviation of the actual distance from that preferred, and thus σ is a measure of the stochastic character of the scattering elements. If $\sigma \rightarrow 0$, this means a perfectly ordered structure. On the contrary, for large values of σ , the structure factor tends to unity, which means unstructured fluid.

The experimental data shown in Figure 5.3 are fitted to a model which includes both form factor and structure factor (eq. 5.2 and eq. 5.4.). From these fits, values of L , σ/L and R_p are obtained. These values are shown in table 2. An additional scaling parameter was used to scale the experimental data.

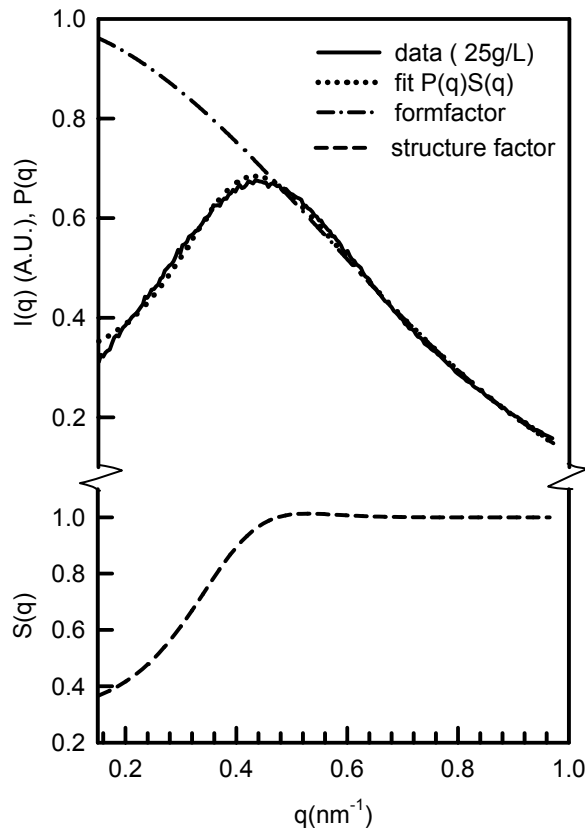


Figure 5.3. q -Dependence of the scattering intensity of a 25.5 g/L native ovalbumin solution (200 ppm NaN_3 , pH 7). The data were fitted using a form factor of spheres and the static structure factor from eq.5.4.

Several interesting observations can be made:

1. The preferred distance, L , decreases with increasing protein concentration. This is in agreement with the observations from the previous section.
2. The measure of disorder, σ/L , decreases with increasing protein concentration, which is obviously due to stronger electrostatic repulsion as the concentration increases. Therefore σ decreases also because the monomers have less freedom to move from their actual distance, and σ decreases from 8 nm to 4.7 nm as the protein concentration increases from 26 to 109 g/L. The values of σ are in line with the observations by Giordano⁷, who obtained values of σ between 5.6 and 4.9 in a similar concentration range.
3. The radius of a sphere (R_p) decreased slightly with increasing protein concentration. The average value of R_p is in reasonable agreement with the values obtained in dilute systems. However, we cannot offer an explanation for this observation.

We conclude from fitting the q -dependent scattering intensity over a wide range of native ovalbumin solutions, that the scattering peaks can be quantitatively described by the model of Farsaci *et al.*,¹³ using L , σ/L , R_p as fitting parameters.

Table 5.2. Values of the parameters obtained from fitting the experimental data. C is the concentration native ovalbumin; L is the preferential distance; σ/L is a measure of disorder, where σ is the rms displacement from L ; and R_p is the radius of an ovalbumin molecule.

C (g/L)	L (nm)	σ/L (-)	R_p (nm)
25.51	9.98	0.80	2.96
53.10	8.44	0.70	2.80
64.20	8.04	0.68	2.72
75.30	7.80	0.68	2.69
85.95	7.44	0.67	2.62
97.40	7.26	0.67	2.56
108.50	7.04	0.66	2.50

5.3.2 LONG FIBRILLAR AGGREGATES IN AQUEOUS SOLUTION

It has been previously demonstrated^{8,10} that ovalbumin forms long linear aggregates ($L_c \sim 1 \mu\text{m}$) when a solution is heated at low ionic strength and at protein concentrations slightly below the critical gelation concentration ($C_g \approx 60 \text{ g/L}$, depending on the batch used). From light scattering experiments and cryo-TEM, the radius of gyration, molecular weight and contour length (L_c) of the aggregates have been determined. Here, we describe how the diameter of these strands can be accurately measured, as well as the structure of the system, i.e. interparticle distance between aggregates using SAXS. A combination of light scattering data and SAXS data gives information about the persistence length (L_p) of the aggregates; a value of $L_p \approx 130 \text{ nm}$ has been reported recently.¹⁰ All these results provide detailed information on the aggregate characteristics and aggregation behavior of heated ovalbumin systems.

5.3.2.1 SCALING BEHAVIOR OF FIBRILLAR AGGREGATES UPON DILUTION IN AQUEOUS SOLUTIONS

Long linear aggregates of ovalbumin were prepared by heating an ovalbumin solution at 53.1 g/L . These aggregates were subsequently diluted to various concentrations and the q -dependence of the scattering intensity was determined.

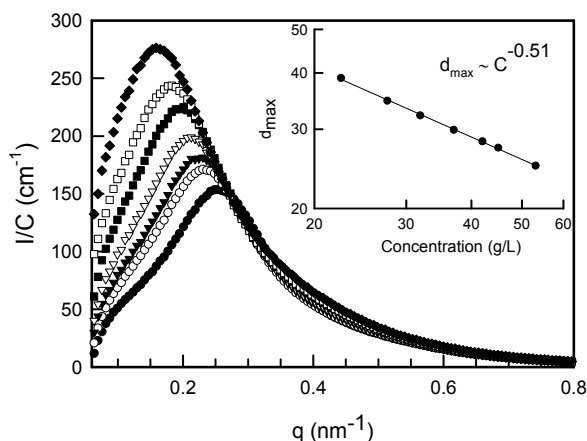


Figure 5.4. Scattered intensity normalized by the protein concentration as a function of q for aggregated ovalbumin solutions (heated at 53 g/L , 200 ppm NaN_3 , $\text{pH } 7$), diluted to different protein concentrations. Inset: scaling between d_{max} and ovalbumin concentrations on a double logarithmic scale. (●) 53.1 ; (○) 45.0 ; (▼) 42.0 ; (▽) 37.0 ; (■) 31.9 ; (□) 27.6 ; (◆) 22.5 g/L .

These scattering curves were normalized for the protein concentration and plotted versus wave vector q . These results are presented in Figure 5.4. In the concentration range

between 53 and 20 g/L, we observed a single peak due to (inter)molecular ordering. The formation of ordered structures seems to be a generally observed phenomenon for charged solutes.^{4,5,6} The position of the scattering peak shifted towards lower q , and at concentrations below 20 g/L the peak position could not be measured due to limitations of the beamstop (Table 5.1). The inset of Figure 5.4 shows the concentration dependence of the interparticle distance. In contrast to the results of monomers, the power law observed here is $d_{\max} \sim C^{-0.51}$. This scaling behavior is in good agreement with that derived by Ogston¹⁴, who considered an expression for the distribution of spaces in a random network of straight fibers and derived the concentration dependence of d_{\max} of $d_{\max} \sim C^{-0.5}$. In this particular model, the fibrils were considered to be straight, of infinite length and of negligible thickness ($D \ll L$).

5.3.2.2 CROSS-SECTION OF LONG OVALBUMIN AGGREGATES

In order to determine the radius of the fibrils, one can fit the experimental data using the classical expression for the form factor for long cylinders:

$$I(q) = \frac{\pi^2}{q} \phi a^2 (\Delta\rho)^2 \left(2 \frac{J_1(qa)}{qa} \right)^2 \quad (5.5)$$

where $\Delta\rho$ is the difference in scattering length density between the aggregates and the solvent, ϕ the volume fraction, J_1 the first-order Bessel function, and a the radius of the cross-section of the cylinder (Fig. 5.5). L is the preferred distance between cylinders.

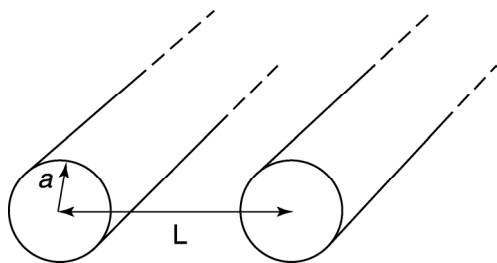


Figure 5.5. Schematic representation of two infinite long cylinders with: a the radius of the cross-section of the cylinder; L the preferred distance between the cylinders.

The cross-section can also be estimated by a so-called cross-section Guinier plot:

$$q \cdot I(q) \approx \pi^2 \phi a^2 (\Delta\rho)^2 e^{\frac{-q^2 R_c^2}{2}} \quad (5.6)$$

where $R_c = a/\sqrt{2}$ is the radius of gyration of the cross-section. Here, plotting $\ln(q \cdot I(q))$ versus q^2 results in a straight line. The radius of gyration of the cross-section can be calculated from the slope of the straight line.

Figure 5.6 shows the cross-section Guinier plot. In this experiment, long flexible fibrils were formed at an ovalbumin concentration of 53.1 g/L and subsequently diluted to 1 g/L, so that interaction can be neglected. From the slope a radius of gyration of the cross-section of 3.2 nm is found. The inset of Figure 5.6 shows the theoretical scattering function of infinitely long cylinders with a radius of the cross section (a) of 4.2 nm (i.e. $R_c = 3.0$ nm). Circles represent data obtained from SAXS experiments. Since the intensity is not on an absolute scale, a prefactor is used, but this does not influence the value of a and R_c . The values of R_c found here are compatible with aggregates consisting of a string of monomers or possibly dimers, particularly if we take into account that the proteins are not fully spherical and may even be further deformed after aggregation. It seems very unlikely that more than 2 monomers can be accommodated within the observed radius.

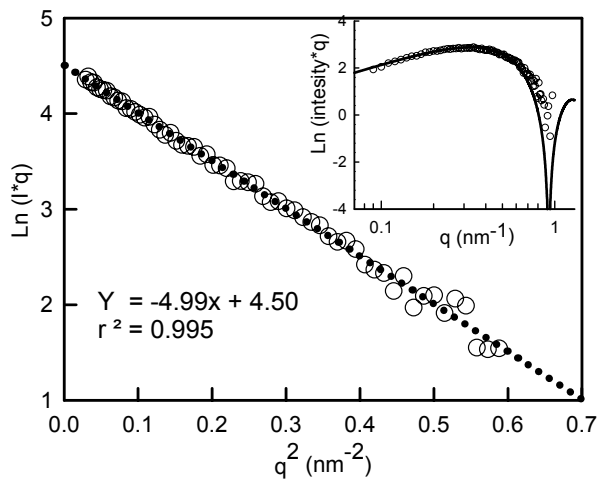


Figure 5.6. Cross-section Guinier plot, $\ln(I \cdot q)$ vs q^2 for long flexible rods. Circles represent data obtained from SAXS measurements on aggregated ovalbumin fibrils (prepared at 53 g/L, diluted with 200 ppm NaN₃ to 1 g/L). Inset: Theoretical form factor $P(q)$ as a function of q for long flexible rods with $R_p = 4.15$ nm in a semi-log plot (solid line), circles represent same experimental data.

If we assume that the ovalbumin aggregates behave as long cylinders, it is tempting to fit the spectra as shown in Figure 5.4 using the structure factor as presented in equation 5.4. Indeed, Figure 5.7 shows a typical fit of the experimental data, including both a form factor of long cylinders (eq. 5.5.) and the structure factor (eq. 5.4.). The same procedure is used as for ovalbumin monomers with the exception that in this case the form factor for long flexible aggregates is used. From the fit, values of L , σ/L and R are obtained (data not shown). Although the fits appear to be quite satisfactory, the dependence of L on the protein concentration does not follow the experimental trend. We believe that the model of Farsaci *et al.*¹³ is not applicable in this case because the structure factor is too much influenced by the orientation of the fibrils.

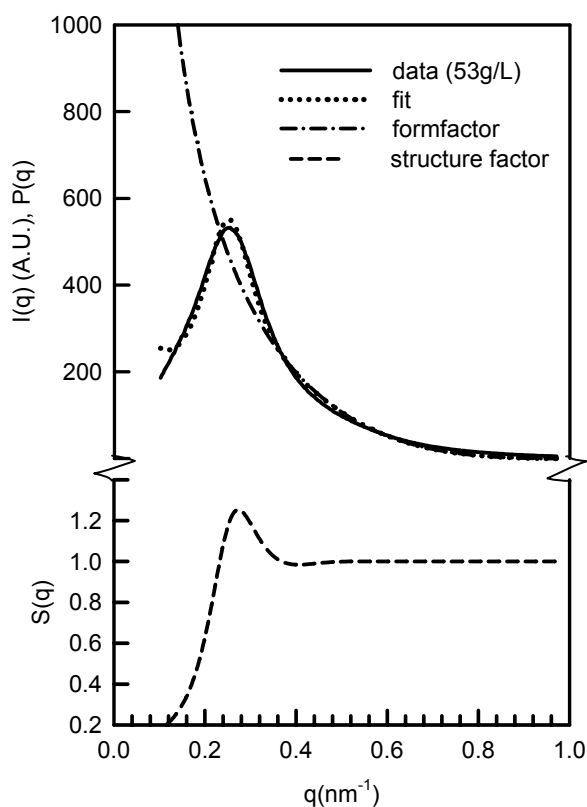


Figure 5.7. q -Dependence of the scattering intensity of a 53.1 g/L aggregated ovalbumin solution. The data were fitted using a form factor of aggregates and the static structure factor from eq. 5.4.

5.3.3 SCALING BEHAVIOR OF OVALBUMIN AGGREGATES HEATED AT DIFFERENT PROTEIN CONCENTRATIONS

Heating ovalbumin solutions at low protein concentrations (far below C_g), and at low ionic strength results in the formation of short linear aggregates. Increasing the initial

protein concentration in heating experiments resulted in an increase in aggregate length.^{8,17} All these aggregate solutions and gels are transparent. Figure 5.8 shows the scattering intensity of transparent systems, which were heated at various protein concentrations.

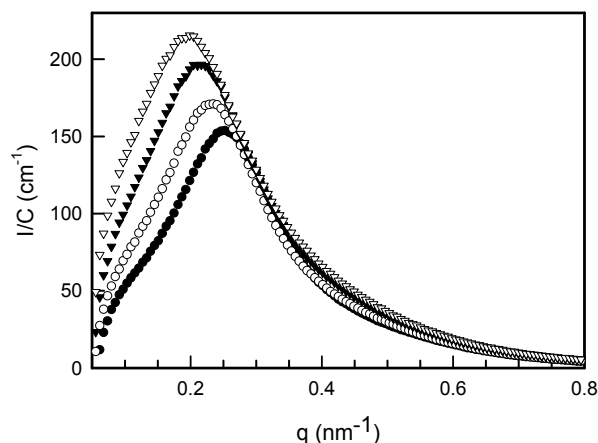


Figure 5.8. Scattered intensity normalized by the protein concentration as a function of q for aggregated ovalbumin solutions initially heated at various protein concentrations (200 ppm NaN_3 , pH 7): (∇) 25.51; (\blacktriangledown) 32.89; (\circ) 43.96; (\bullet) 53.1 g/L.

Increasing the protein concentration results in a shift of q_{max} towards higher q , indicating smaller distances. The clear peak is due to long-range interaction between the aggregates and this is supported by cryo-transmission electron micrographs (next section). From the cross-section Guinier plots, the radius of the cylinder, R_c , is calculated as a function of protein concentration. As expected, the radius of the fibrils did not depend on the protein concentration at heating, as can be observed from Figure 5.8; for $q > 0.3$ all data overlap. The dependence of d_{max} on the protein concentration scaled as $C^{-0.32}$, which resembles more the behavior of monomeric ovalbumin (Fig. 5.8). Apparently, when heated at concentrations below 50 g/L, the formed fibrils are not yet long enough to reach the infinite rod limiting behavior with $d_{\text{max}} \sim C^{-0.5}$.

5.3.4 CRYO-TRANSMISSION ELECTRON MICROSCOPY

At 50 g/L, the SAXS profile (Figure 5.8) shows a single interaction (or scattering) peak at $q = 0.24 \text{ nm}^{-1}$. This corresponds to a preferential distance of 26 nm in the aggregated system. We assumed that these distances are long-range correlations between long linear aggregates. This assumption is in good agreement with the cryo-transmission electron micrograph shown in Figure 5.9.

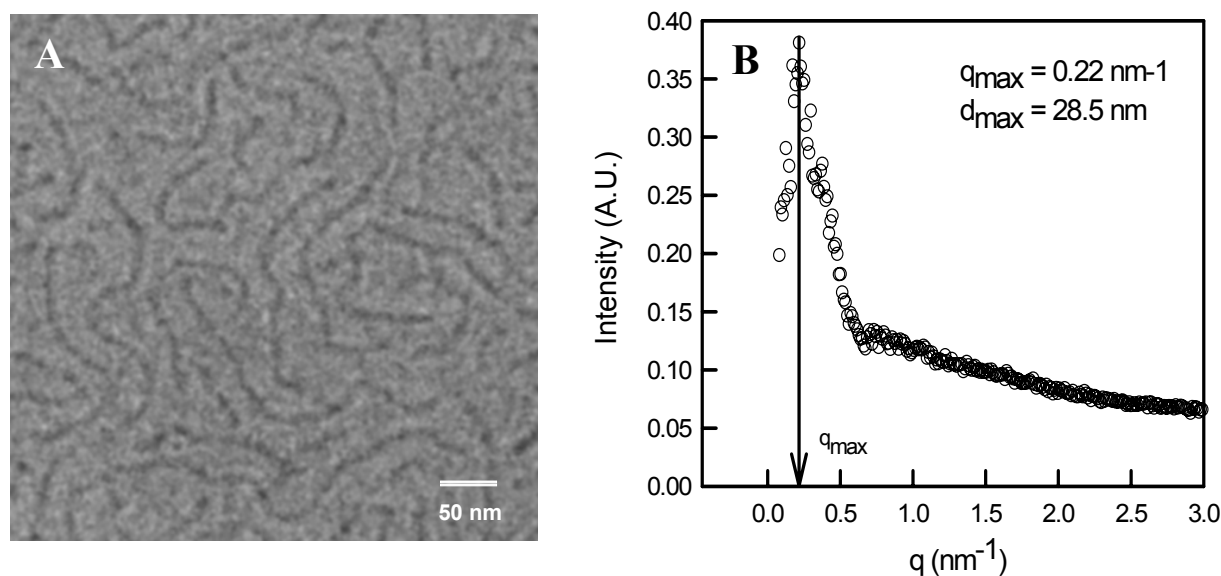


Figure 5.9. (A) Cryo-TEM of a 50 g/L ovalbumin solution heated for 22 hr at 78°C. (B) Radial averaged Fourier transform (in 1D-representation) of figure A.

In this experiment, a drop of the 50 g/L solution with soluble linear aggregates was put on a grid and instantaneously vitrified in liquid propane, to prevent formation of ice-crystals. From the micrograph in figure 5.9, a radial averaged Fourier transform is determined and a q_{\max} of 0.22 nm^{-1} is observed, corresponding to a preferential distance in the system of 28 nm, and is in good agreement with values found from X-ray scattering. Hence, q_{\max} indeed corresponds to interparticle distances between long linear fibrils in the system.

5.4 DISCUSSION

In this study, the influence of the protein concentration (C) on the scaling behavior of native ovalbumin solutions, aggregated ovalbumin solution and gels, and diluted solutions of long fibrils were investigated.

For native ovalbumin solutions, the q_{\max} position increases from 0.44 nm^{-1} up to 0.66 nm^{-1} for protein concentrations between 25.5 – 109 g/L respectively. This corresponds to distances between monomers of 14 – 9.5 nm. The decrease in interparticle distance with increasing protein concentration can obviously ascribe to the concentration effect. For native ovalbumin solutions, the power law behavior of d_{\max} scales with an exponent of -0.28. This agrees well with experimental SANS data on β -lactoglobulin at low ionic strength described by Renard *et al.*⁵ At these conditions, both proteins are globular and have a comparable charge per surface area. In the same concentration range Renard *et al.*⁵

found an exponent with value -0.27 , which was in good agreement with the theoretical value of -0.28 calculated from Belloni’s model on charged hard spheres. The exponent of -0.28 that we obtained suggest that protein-protein interactions between native ovalbumin monomers are accurately described by that of hard spheres with an electric double layer.

For non-diluted aggregate solutions and gels, the interparticle distance is larger than for monomers. Here, the correlation length in the whole system is measured, which is obviously larger than in the case of monomers. The exponential relation between d_{\max} and the protein concentration at heating was -0.32 . Renard obtained an exponent of -0.5 in the same concentration range for β -lactoglobulin, which is significantly larger than the value for ovalbumin determined by us. The difference might be explained by the fact that our fibrils formed at low protein concentration were not yet long enough to reach the infinite rod limiting behavior of $d_{\max} \sim C^{-0.5}$. The differences between ovalbumin and β -lactoglobulin may be due to significant differences in structure of the aggregates upon heating.

For a dilution series of long fibrils, we found the limiting behavior, typical of long rods, for which one expects a dependence of $d_{\max} \sim C^{-0.5}$. This scattering behavior has not previously been reported in the literature for ovalbumin systems. Our experimental results are in good agreement with theoretical predictions of the scaling of d_{\max} for this case; form factor for infinite rods describes long ovalbumin aggregates ($\sim 1 \mu\text{m}$) diluted to 1 g/L very well in the range measured. As far as we know, this has not been demonstrated for β -lactoglobulin. Systematic investigations on experimental data from SLS and SAXS data will result in additional information on the persistence length of fibrils under different conditions.^{10,18}

5.5 CONCLUSIONS

For ovalbumin solutions at neutral pH and low ionic strength, the protein is net negatively charged. Therefore, the electrostatic repulsion results in the presence of a correlation (or interaction) peak for native, aggregated and gelled systems, observed by SAXS. For native ovalbumin the form factor can be well described by a sphere. The dependence of the protein concentration on the interparticle distance (d_{\max}) for monomers was found to be $d_{\max} \sim C^{-0.28}$, which implied that the system behaved as a uniform distribution of charged spheres. The interaction peak of these native ovalbumin systems

could be well described using both a form factor of spheres, and a structure factor based on a solvable model, from which relevant interparticle distances were obtained.

The total scattering intensity of ovalbumin aggregates formed at neutral pH could be well described with the form factor of long cylinders (rods). The dependence of the protein concentration on the interparticle distance (d_{\max}) for aggregates was found to be $d_{\max} \sim C^{-0.51}$, this scaling behavior is in good agreement with that theoretically derived for the distribution of spaces in a random network of straight fibers. The interaction peak corresponds to a dominant length scale in the system and cryo-TEM showed that this reflects the interparticle distances between long linear fibrils in the system. The cross-sectional radius of gyration of the fibril was approximately 3 nm, which is compatible with aggregates consisting of a string of monomers (or possibly dimers), particularly if we take into account that the proteins are not fully spherical and may be further deformed after aggregation.

ACKNOWLEDGMENTS

We acknowledge Igor Dolbnya and Wim Bras for their technical assistance at DUBBLE in Grenoble. Jasper van der Gucht and Stefan van der Burgh are gratefully acknowledged for discussions and technical assistance at DUBBLE. The Netherlands Organization for the Advancement of Research (NWO) is acknowledged for providing facilities and financial support for performing measurements at DUBBLE.

REFERENCES

1. Matsumoto, T.; Chiba, J. (1990). *J. Chem. Soc. Faraday Trans.*, 86, 2877.
2. Matsumoto, T.; Inoue, H. (1993). *Journal of colloid and Interface Science*, 160, 105.
3. Clark, A.H.; Tuffnell, C.D. (1980). *Int. J. Peptide Protein Res.*, 16, 339.
4. Bendedouch, D.; Chen, S. (1983). *J. Phys. Chem.*, 87, 1473.
5. Renard, D.; Axelos, M.A.V.; Boué, F.; Lefebvre, (1996). *J. Biopolymers*, 39, 149.
6. Matsuoka, H.; Ise, N.; Okubo, T.; Kunugi, S.; Tomiyama, H.; Yoshikawa, Y. (1985). *J. Chem. Phys.*, 83, 378.
7. Giordano, R.; Grasso, A.; Teixeira, J. (1991). *Physical Review A*, 43, 6894.
8. Weijers, M.; Visschers, R.W.; Nicolai, T. (2002). *Macromolecules*, 35, 4753.
9. Koseki, T.; Kitabatake, N.; Doi, E. (1989). *Food Hydrocolloids*, 3, 123.
10. Pouzot, M.; Nicolai, T.; Visschers, R. W.; Weijers, M. (2004). *Food Hydrocolloids* (accepted).
11. Inoue, H.; Matsumoto, T. (1994). *J. Rheol.*, 38, 973.

12. Sugiyama, M.; Nakamura, A.; Hiramatsu, N.; Annaka, M.; Kuwajima, S.; Hara, K. (2001). *Biomacromolecules*, 2, 1071.
13. Farsaci, F.; Fontanella, E.; Salvato, G.; Wanderlingh, F.; Giordano, R.; Wanderlingh, U. (1989). *Phys. Chem. Liq.*, 20, 205.
14. Ogston, A.G. (1958). *Trans. Faraday Soc.*, 54, 1754.
15. Vachier, M.C.; Piot, M.; Awedé, A.C. (1995). *J. Chromatogr. B*, 66, 201.
16. Belloni, L. (1986). *J. Chem. Phys.*, 85, 519.
17. Weijers, M., Barneveld, P.A., Cohen Stuart, M.A.; Visschers, R.W. (2003). *Protein Science*, 12, 2693.
18. Aymard, P.; Nicolai, T.; Durand, D.; Clark A. (1999). *Macromolecules*, 32, 2542.

CHAPTER 6

INFLUENCE OF THE IONIC STRENGTH ON THE STRUCTURE OF
HEAT-SET GELS OF OVALBUMIN

Weijers, M., Nicolai, T. and Visschers, R.W.

Macromolecules 2004, accepted

Macromolecules 2004, accepted

ABSTRACT

The effect of the NaCl concentration (C_s) on the structure factor and the turbidity of heated ovalbumin solutions was investigated using cross-correlation dynamic light scattering. The heated systems are characterized by a correlation length, which depends on protein and salt concentration, beyond which they are homogeneous. At length scales below this correlation length, the systems have a self-similar, fractal, structure. For $C_s \geq 100$ mM, very turbid systems are formed with correlation lengths that show strong concentration dependence, and the correlation length rapidly rises above $1\ \mu\text{m}$ at protein concentrations above 4 g/L. For $C_s \leq 30$ mM NaCl the systems remain transparent with relatively small correlation lengths (< 20 nm). At 50 mM NaCl the correlation length first increases strongly with increasing protein concentration followed by a decrease above 8 g/L. At both 30 mM and 50 mM, an unexpected increase in the correlation length and turbidity is observed at high protein concentrations (above 40 g/L and 30 g/L, respectively). From the present work we conclude that the structure of heated globular protein solutions and gels is generally determined by the interplay between the growth of the aggregates and the electrostatic interaction between the aggregates.

6.1 INTRODUCTION

Heat-induced denaturation of globular proteins in aqueous solution generally leads to aggregation of the proteins. Above a given critical protein concentration, C_g , which depends on pH, temperature, ionic strength and type of protein, a gel is formed.^{1,2} The structure of these gels depends on the strength of electrostatic interactions during heating. In the presence of strong interactions, i.e. far from the isoelectric point (pI) of the protein and at low ionic strength, the gels are transparent and consist of (thin) strands of aggregated proteins. When interactions are weak, i.e. near pI of the protein and at high ionic strength, the gels become turbid and the aggregates are more branched and clustered. Under these conditions micro phase separation may possibly occur, which renders the gels heterogeneous at large length scales.

In part I of this series³ the effect of varying the NaCl concentration on the structure and the turbidity was reported for β -lactoglobulin solutions and gels after prolonged heating. It was shown that the length scale of the heterogeneity of the gels increases strongly from less than 20 nm below 50 mM NaCl to more than 1 μ m above 200 mM. At intermediate salt concentrations (100 mM and 150 mM) the scattering wave vector (q) dependent structure factor ($S(q)$) could be well described by the following simple equation:

$$S(q)=(1+q^2R_a^2/3)^{-1} \quad (6.1)$$

Where R_a is an apparent radius of gyration in undiluted systems that characterizes the length scale beyond which the system is homogeneous. At intermediate salt concentrations, R_a increases with increasing protein concentration as the size of the aggregate increases, but is smaller than the z-average radius of gyration of the aggregates, R_{gz} , because the aggregates interpenetrate. R_a reaches a maximum close to C_g after which it decreases as the system becomes denser. The maximum value of R_a is about 300 nm at 100 mM and almost 2 μ m at 150 mM for β -lactoglobulin gels.

In the present paper we study the influence of adding NaCl on the structure of heated ovalbumin solutions, which we will compare with the results obtained for β -lactoglobulin. Ovalbumin is the main protein component in egg-white, with a molar mass of 45 Kg/mol and a radius of about 3 nm.^{4,5,6} At pH 7 ovalbumin associates in the form of linear chains with a degree of branching that depends on the ionic strength.^{4,7,8} In the absence of added

salt, gels are formed only at relatively high protein concentrations ($C_g \approx 60$ g/L). These gels are clear and the structure factor measured by X-ray scattering ($0.1 < q < 4$ nm⁻¹) is characterized by a so-called interaction peak at small scattering wave vectors.⁹ In the q -range covered by light scattering ($0.002 < q < 0.025$ nm⁻¹), the scattered light intensity is independent of q , implying that the gels are homogeneous at length scales larger than about 15 nm. With increasing salt concentrations C_g decreases and the gels become increasingly turbid for $C_s > 30$ mM.

6.2 MATERIALS AND METHODS

6.2.1 MATERIALS

The ovalbumin used for this study was purified from egg white of freshly laid hens' eggs (less than 2 h old) based on the procedure of Vachier et al.,¹⁰ and contained a small fraction (6%) of heat-stable ovalbumin. The ovalbumin was dissolved in Millipore water with 3 mM NaN₃ added to prevent bacterial growth. The pH was set at 7 using a NaOH solution. NaCl solutions were used to set the ionic strength. The solutions were filtered through 0.45 μ m pore size filters (Millex-SV, Millipore Corp., Bedford, MA). Protein concentrations were measured using refractive index measurements and UV absorbance at 280 nm. Consistent results were obtained using refractive index increment $dn/dC = 0.181$ and absorption coefficient $\epsilon = 0.698$ Lg⁻¹cm⁻¹.

6.2.2 METHODS

The experimental methods are described in part I. Light scattering measurements were carried out at 20°C using a commercial version of the 3D cross-correlation instrument. The small angle X-ray scattering (SAXS) experiments were done on the DUBBLE beamline at the ESRF synchrotron facilities (Grenoble, France).

Confocal scanning laser microscopy (CSLM) images were recorded at NIZO food research (Ede, The Netherlands) on a LEICA TCS SP1 CSLM, equipped with an inverted microscope (model Leica DM IRBE), used in the single photon mode with an Ar/Kr laser. Ovalbumin was labelled with the fluorochrome rhodamine B for which the excitation wavelength and emission maximum are, respectively, 568 nm and 625 nm. Before heat treatment rhodamine B (20 μ L; 0.1% w/w) was added to 1 mL protein solution.

Subsequently the solutions were heated for 1 hr at 78°C in the CSLM sample cell and allowed to cool to room temperature before imaging.

6.3 RESULTS

6.3.1 DILUTED OVALBUMIN AGGREGATES

Ovalbumin solutions at pH 7 and different NaCl concentrations were heated at 78°C for 24 h. After this prolonged heat treatment all proteins had aggregated except a small fraction (6%) of heat-stable ovalbumin. The critical protein concentration, C_g , beyond which the samples gelled or precipitated decreases with increasing salt concentration, see fig. 6.1. For comparison we have included the results for β -lactoglobulin at pH 7 taken from ref.11. For 200 mM or higher NaCl concentrations a precipitation was observed for protein concentrations down to 1g/L.

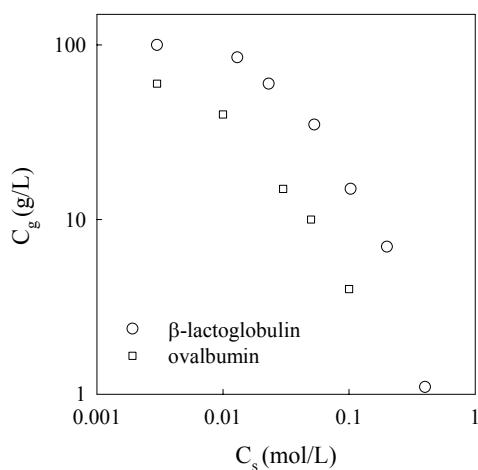


Figure 6.1. Critical gelation concentration (C_g) as a function of the NaCl concentration for ovalbumin and β -lactoglobulin at pH 7.

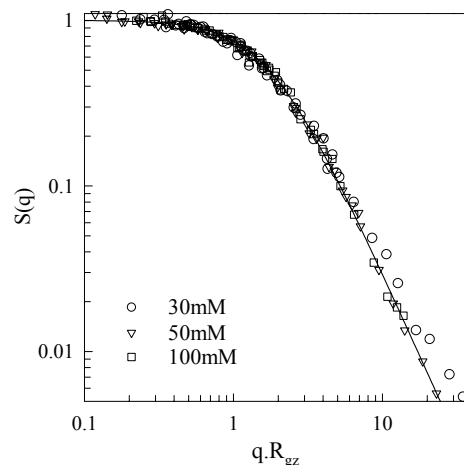


Figure 6.2. Structure factors of highly diluted ovalbumin aggregates formed after prolonged heating at different NaCl concentrations. The solid line represents $S(q) = (1 + q^2 R_{gz}^2 / 3)^{-1}$.

For $C < C_g$, we determined the structure factor ($S(q)$) of the ovalbumin aggregates in dilute solution by measuring the q -dependence of the relative excess scattering (I_r). From these data, the weight average molar mass (M_w) and the z -average radius of gyration (R_{gz}) were determined as described in ref. 4. The size of the aggregates increased with increasing protein concentration, and very close to C_g the aggregates became too large to measure. In ref. 4 it was shown that the structure of ovalbumin aggregates is self-similar and is

characterized by a fractal dimension (d_f), i.e. $S(q) \propto q^{-d_f}$ for $q \cdot R_{gz} \gg 1$.^{12,13} We found that $d_f=2.0$ at 100 mM and $d_f=1.7$ without NaCl.

Figure 6.2 compares the structure factors at 30, 50 and 100 mM NaCl. At 50 and 100 mM the results can be well described by $S(q)=(1+q^2 R_{gz}^2/3)^{-1}$ over the whole q -range, but at 30 mM the data deviate upward from this equation at large q -values, an effect similar to that reported in ref. 4 for systems without NaCl. Cryo-TEM images of the aggregates show that the aggregates consist of linear strands that are increasingly branched with increasing ionic strength.⁸ SAXS measurements show that the thickness (R_g) of the strands is independent of the ionic strength, but that the persistence length varies.⁸

6.3.2 UNDILUTED OVALBUMIN SYSTEMS

In the absence of NaCl, heated ovalbumin solutions at pH 7 were clear over the whole concentration range up to at least 100 g/L. Fig. 6.3 shows the concentration dependence of the turbidity of the heated protein systems at 30, 50 and 100 mM NaCl. At 30 mM, the gels were transparent except for $C > 80$ g/L where we observed, unexpectedly, a dramatic increase of the turbidity. At 50 mM, the turbidity increases to a maximum at $C \approx 20$ g/L after which it decreases a little, but again there was a strong increase in turbidity at high protein concentrations. At 100 mM, the turbidity increased strongly already at low protein concentrations. We did not anticipate the increase at high protein concentrations at 30 mM and 50 mM NaCl since it was not observed for heated β -lactoglobulin systems, see part I.¹⁵

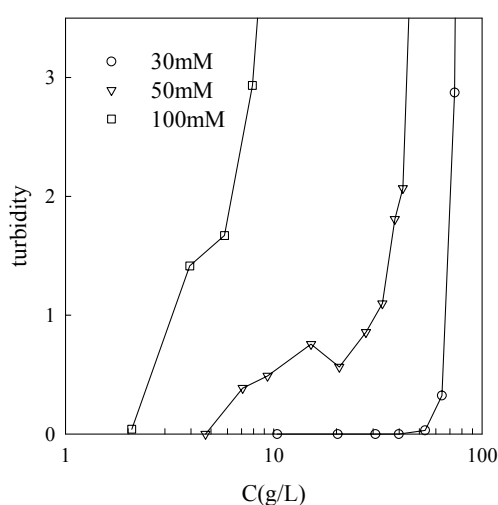


Figure 6.3. Concentration dependence of the turbidity of heated ovalbumin solutions at different NaCl concentrations.

This phenomenon will be discussed in the discussion section.

The q -dependence of I_r/H_C was determined for a range of protein concentrations at different NaCl concentrations, where H is an optical constant (or contrast factor).⁴ Extrapolation of I_r/H_C to $q=0$ yields an apparent molar mass, M_a , which is inversely proportional to the osmotic compressibility. The structure factor is determined by plotting $S(q)=I_r/(H C M_a)$ as a function of $q R_a$. R_a was obtained by fitting the initial q -dependence to eq. 6.1. The results obtained at 100 mM, 50 mM and 30 mM NaCl are shown in figs 6.4, 6.6 and 6.5, respectively. In the absence of NaCl, I_r is independent of q over the whole concentration range investigated.

At 100 mM NaCl, the q -dependence of I_r/H_C becomes more important with increasing concentration and for $C=4$ g/L and 7.9 g/L we observe within the experimental error the same power law behaviour over the whole accessible q -range, see fig. 6.4a. This implies that the correlation length of the gels is larger than 1 μm for $C \geq 4$ g/L, which explains the high turbidity of these systems. The structure factor can only be determined over a limited concentration range because the turbidity becomes too high for $C > 8$ g/L. Fig. 6.4b shows that within the experimental error the structure factor is independent of the concentration and can be described by the same simple equation (eq. 6.1) used in part I for β -lactoglobulin.

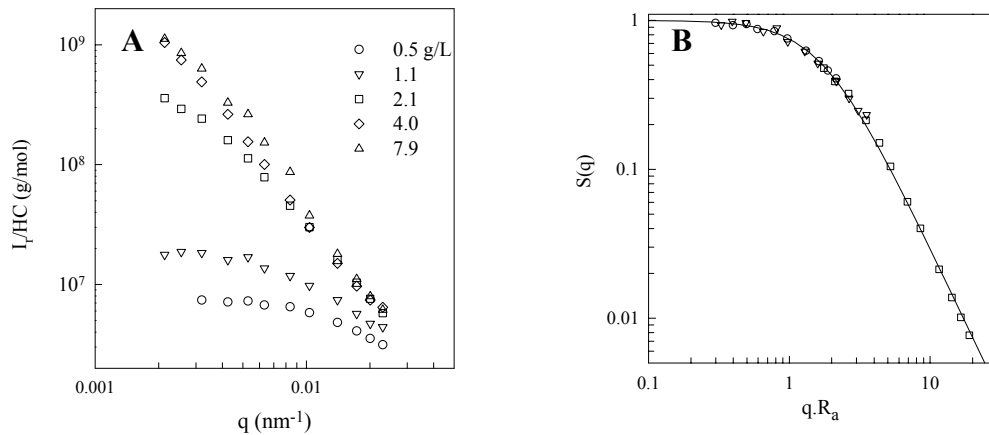


Figure 6.4. (A) q -dependence of I_r/H_C of ovalbumin solutions in 100 mM NaCl at different protein concentration after prolonged heating. (B) Structure factor obtained by normalisation of the data shown in fig. 6.4A. The solid line represents eq. 6.1.

At 30 mM NaCl, and protein concentrations up to 50 g/L, I_r/H_C showed no q -dependence in the range covered by light scattering and is only weakly dependent on the

protein concentration, see fig. 6.5a. At higher concentrations ($C > 50$ g/L), we observe a significant increase of I_r/HC which also becomes q -dependent, see figure 6.5a. Figure 6.5b shows that the structure factors at these higher protein concentrations are not independent of the concentration and cannot be well described by eq. 6.1. The q -dependence of $S(q)$ is stronger than predicted by eq. 6.1 and appears to increase with increasing protein concentration, indicating a denser structure.

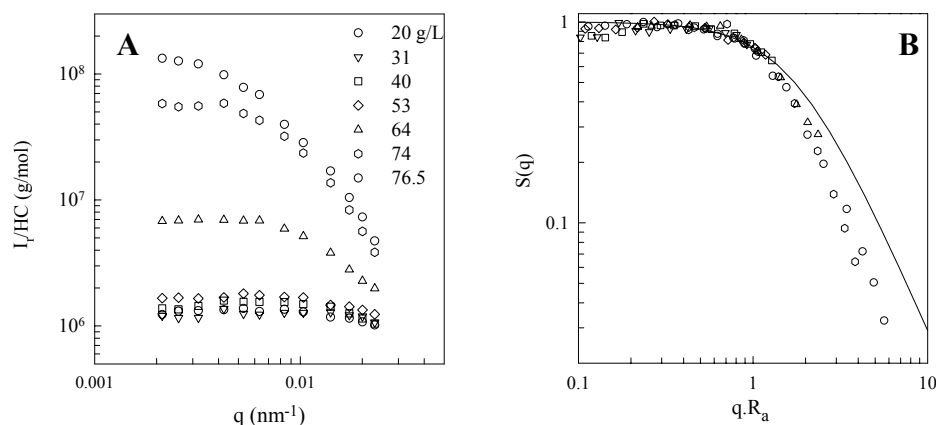


Figure 6.5. (A) q -Dependence of I_r/HC of ovalbumin solutions in 30 mM NaCl at different protein concentration after prolonged heating. (B) Structure factor obtained by normalisation of the data shown in fig. 6.5A. The solid line represents eq. 6.1.

At 50 mM NaCl the concentration dependence of I_r/HC is more complex. For clarity we show the low and high concentration data in separate figures (figs 6.6a and 6.6b). Figure 6a shows that when increasing the protein concentration up to about $C_{\max} \approx 7$ g/L the q -dependence of I_r/HC increases similarly to that at 100 mM NaCl as shown in fig. 6.4a. However, between 7 and 28 g/L, I_r/HC decreases with increasing protein concentration and its q -dependence becomes weaker (fig. 6.6b). So far, this behaviour is similar to that observed for heated β -lactoglobulin solutions at 100 mM NaCl. However, when we increase the protein concentration even further I_r/HC increases again and its q -dependence becomes stronger. The increase of the correlation length takes place simultaneously with the increase in turbidity for $C > 20$ g/L. Below 7 g/L the structure factor can be described by eq. 6.1, but at higher concentrations we observe a clear deviation, see fig. 6.6c. The q -dependence becomes stronger with increasing protein concentration, again indicating a denser structure. In fact, the results for $C > 30$ g/L (50 mM NaCl) resemble those obtained at 30 mM NaCl for $C > 50$ g/L.

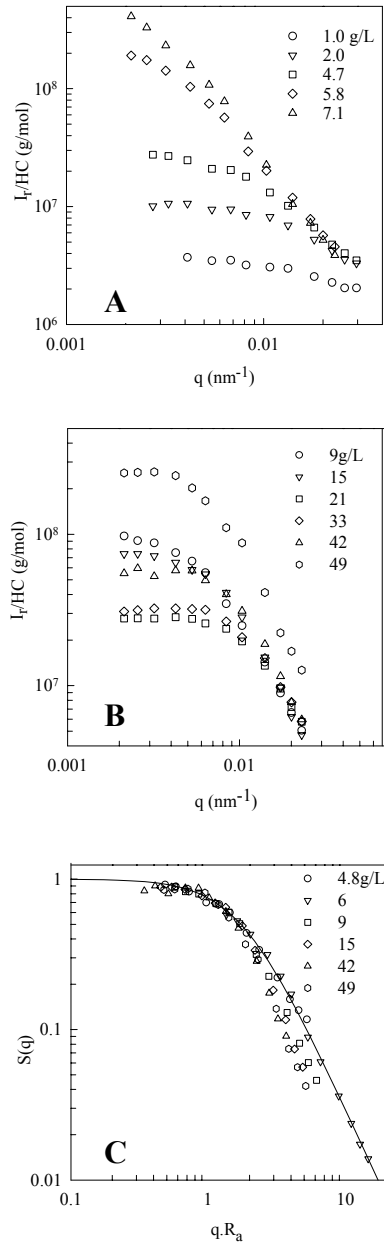


Figure 6.6. (A) and (B) q -dependence of I_r/H_C of ovalbumin solutions in 50 mM NaCl at different protein concentration after prolonged heating. (C) Structure factor obtained by normalisation of the data shown in fig. 6.5A and 6.5B. The solid line represents eq. 6.1.

From the initial q -dependence of I_r/H_C shown in figures 6.4, 6.5 and 6.6, we can still determine M_a and R_a using eq. 6.1 even if the full q -dependence is not described by this equation. The concentration dependence of R_a at different NaCl concentrations is plotted in fig. 6.7 and is compared with that of R_{gz} of the diluted aggregates. The latter diverges at C_g , where a gel is formed. At very low concentrations, interaction between the aggregates is small and $R_a \approx R_{gz}$. With increasing concentration interaction increases and the aggregates start to interpenetrate. As a consequence R_a becomes smaller than R_{gz} .

At 100 mM NaCl, R_a increases strongly with increasing protein concentration and becomes larger than 1 μ m for $C > 2$ g/L. The gels are heterogeneous on the micron length

scales at least up to a protein concentration of 8 g/L, beyond which the gels are too turbid to allow accurate measurements. At 50 mM NaCl, R_a also increases strongly with increasing protein concentration and becomes larger than 1 μm at $C_{\text{max}} \approx 7$ g/L, but then R_a decreases with increasing concentration to $C \approx 30$ g/L, where R_a is reduced to about 80 nm. At higher concentrations R_a increases again. At 30 mM NaCl, a maximum is observed at $C_{\text{max}} \approx 2$ g/L, where $R_a \approx 80$ nm. From 2 g/L (fig. 6.7) to about 30 g/L R_a decreases to about 35 nm, and above that concentration it increases again. We note that the maximum occurs close to the gel point at 50 mM NaCl and well below the gel point at 30 mM.

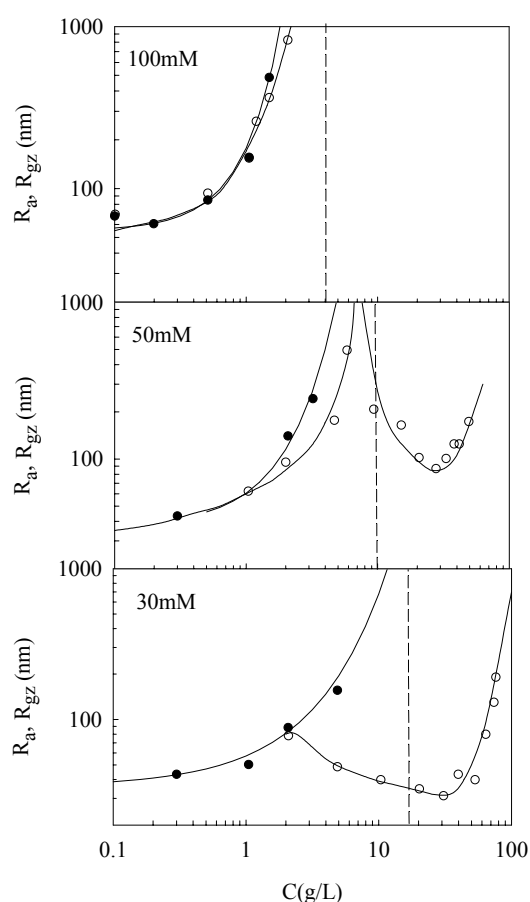


Figure 6.7. Concentration dependence of R_{gz} for diluted aggregates (filled symbols) and of R_a for undiluted heated ovalbumin systems (open symbols), at different NaCl concentrations. Dashed vertical lines indicate C_g and the solid lines are guides to the eye.

In fig. 6.8 we have plotted M_w as a function of R_{gz} for the diluted aggregates and M_a as a function of R_a for the undiluted systems. For self-similar aggregates one expects to find $M_w \propto R_{gz}^{df}$, where the prefactor depends on the elementary unit of the fractal structure. Within the experimental error the results at different salt concentrations have the same power law dependence with exponent 2, but the results at 30 mM are not incompatible with an exponent 1.7. The dependence of M_a on R_a as presented in figure 6.8 shows two different behaviours. The data obtained at lower protein concentrations fall on top of those

of the diluted aggregates (R_a , $R_g \leq 100$ nm). For these systems the structure factor is the same as that of the diluted aggregates. At higher protein concentrations M_a is systematically larger for a given value of R_a ($R_a > 100$ nm), implying that these systems are denser, which is consistent with the structure factors of these systems (see figs. 6.4, 6.5 and 6.6). Nevertheless, M_a apparently has the same scaling dependence on R_a over the limited range of experimental data.

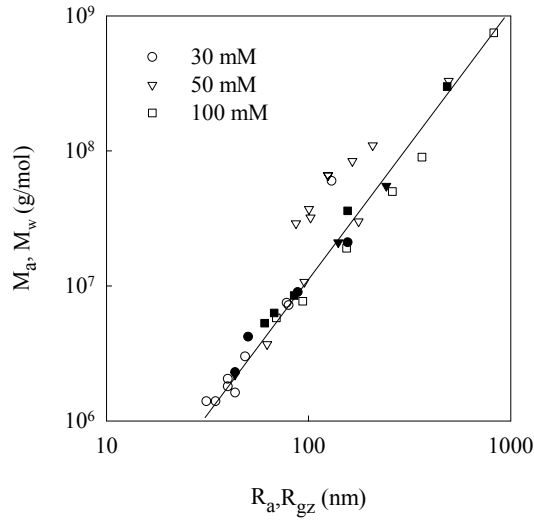


Figure 6.8. Dependence of R_{gz} of diluted aggregates (filled symbols) and of R_a of undiluted heated ovalbumin solutions (open symbols) on M_w and M_a , respectively, at different NaCl concentrations. The line has slope 2.

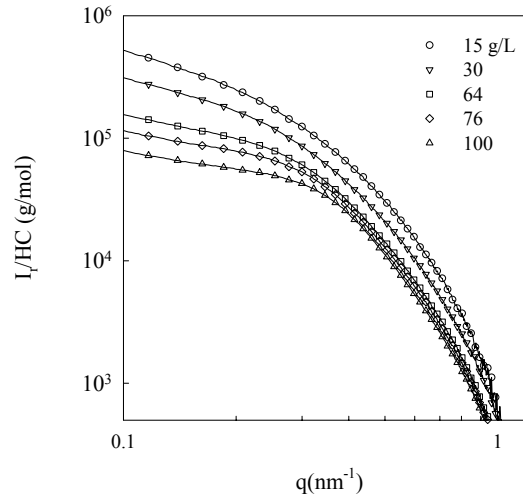


Figure 6.9. Wave vector dependence of I_r/HC of heated ovalbumin solutions in 30 mM NaCl at different protein concentrations obtained from SAXS measurements.

6.4 DISCUSSION AND CONCLUSIONS

In this study, the effect of salt concentration on the structure and turbidity of heated ovalbumin solutions was investigated and compared with that of β -lactoglobulin. Apart from the strong upturn of the turbidity and R_a at high protein concentrations, results obtained for ovalbumin were similar to those obtained for β -lactoglobulin as presented in part I.¹⁵

The effect of the protein concentration on the turbidity and R_a , shown in figs 6.3 and 6.7, can be explained as follows. When the proteins are heated they denature, which leads to aggregation. The aggregates grow in number and size until all native proteins are consumed. The heat treatment of the samples studied here (and also in part I)¹⁵ was such

that almost all native proteins were aggregated. As shown in figure 6.7, the number and the size of the aggregates after heat treatment increase with increasing protein concentration, which causes R_a to increase. At low concentrations interaction between the relatively small aggregates is negligible and R_a is approximately equal to the z-average radius of gyration of the aggregates. However, with increasing concentration repulsive interaction becomes more important, and the aggregates also interpenetrate, so that $R_a < R_{gz}$. Beyond a certain protein concentration the effect of increasing interaction starts to dominate over the effect of increasing size and number of the aggregates. As a consequence R_a passes through a maximum and decreases with increasing protein concentration at higher concentrations. It is obvious that the value and position of the maximum, R_{max} and C_{max} respectively, depend on the strength of the interaction and thus on salt concentration, type of protein and pH.

Qualitatively, the effect of varying the salt concentration may be understood in terms of varying electrostatic interaction. Using cross-correlation dynamic light scattering in undiluted protein systems, one measures the combined effects of growth of the aggregates and increasing repulsive interaction between the aggregates. On the one hand, stronger electrostatic repulsion, i.e. lower salt concentrations, causes the protein to aggregate less easily, so that the aggregate size increases more weakly with increasing protein concentration. This is why the critical gelation concentration (C_g) increases with decreasing ionic strength. On the other hand, interaction between the aggregates increases with decreasing ionic strength. As a consequence, the decrease of the scattering intensity caused by repulsive interaction dominates over the increase caused by aggregate growth at lower protein concentrations if the salt concentration is lower. Therefore, one expects that the value of R_{max} (R_{max} at 50 mM $\approx 1 \mu\text{m}$; R_{max} at 30 mM $\approx 80 \text{ nm}$) will decrease with decreasing ionic strength. A shift of C_{max} (C_{max} at 50 mM $\approx 7 \text{ g/L}$; C_{max} at 30 mM $\approx 2 \text{ g/L}$) was observed. In summary, the value of C_{max} is determined by the interplay between the concentration dependence of the aggregate size, the strength of the interaction and the structure of the aggregates. There is no direct correlation between C_{max} and C_g ; at 30 mM $C_{max} < C_g$ and at 50 mM NaCl $C_{max} \approx C_g$. The stronger the interaction is, the smaller is C_{max} compared to C_g .

Comparing ovalbumin and β -lactoglobulin we find that the critical concentration for gelation is smaller for ovalbumin over whole range of NaCl concentrations investigated, see fig. 6.1. Furthermore, the transition from transparent (homogeneous) to turbid

(heterogeneous) gels occurs at lower NaCl concentrations for ovalbumin (between 30 and 100 mM NaCl) than for β -lactoglobulin (between 50 and 200 mM NaCl). Nevertheless, the protein concentration dependence of R_a for ovalbumin at 50 mM is remarkably similar to that for β -lactoglobulin at 150 mM. It appears that the effect of NaCl on the general features of heated ovalbumin solutions is the same as for β -lactoglobulin but shifted to lower NaCl concentrations. The origin of the different sensitivity to added salt may be due to different aggregation mechanisms of the two proteins. As discussed in part I, the aggregation of β -lactoglobulin at pH 7 occurs in two steps; in the first step well-defined primary aggregates containing about 100 monomers are formed, which associate in a second step to form large fractal aggregates or a gel. Ovalbumin forms a linear string of monomers or dimers with a degree of branching that increases with increasing salt concentration.

Apart from the higher sensitivity of ovalbumin to NaCl, the main difference between β -lactoglobulin and ovalbumin is the unexpected upturn of the turbidity and R_a at high protein concentrations for the latter. The upturn starts at higher protein concentrations if we decrease the NaCl concentration (30 g/L and 40 g/L at 50 mM and 30 mM NaCl, respectively). We have observed an increase of M_a even in salt-free water for $C > 80$ g/L although the solution remains clear up to at least 110 g/L. The light scattering results inform us that the gels formed at high concentrations are increasingly heterogeneous with increasing protein concentration.

The appearance of large scale heterogeneity at high protein concentrations can be observed with CSLM as is shown in fig.6.10 at 30 mM and 50 mM NaCl. At low concentrations the gels that are formed after heat treatment are fully transparent and homogeneous, but at high concentrations the gels are heterogeneous even on the micron scale. The heterogeneity appears at lower concentrations at 50 mM than at 30 mM NaCl. At salt concentrations of 100 mM NaCl or higher, CSLM shows that the gels are heterogeneous on the micron scale even at low protein concentrations.

In order to establish whether there is a local rearrangement of the aggregates at high protein concentrations, we used SAXS to determine the structure of the heated systems at 30 mM NaCl at small length scales. The q -dependence of I_r/HC is shown in fig. 6.9 for different protein concentrations. At low protein concentrations the structure factor is

characteristic for that of dilute semi-flexible chains.⁸ With increasing concentration the scattering intensity at low q values decreases due to increasing repulsive interactions, but

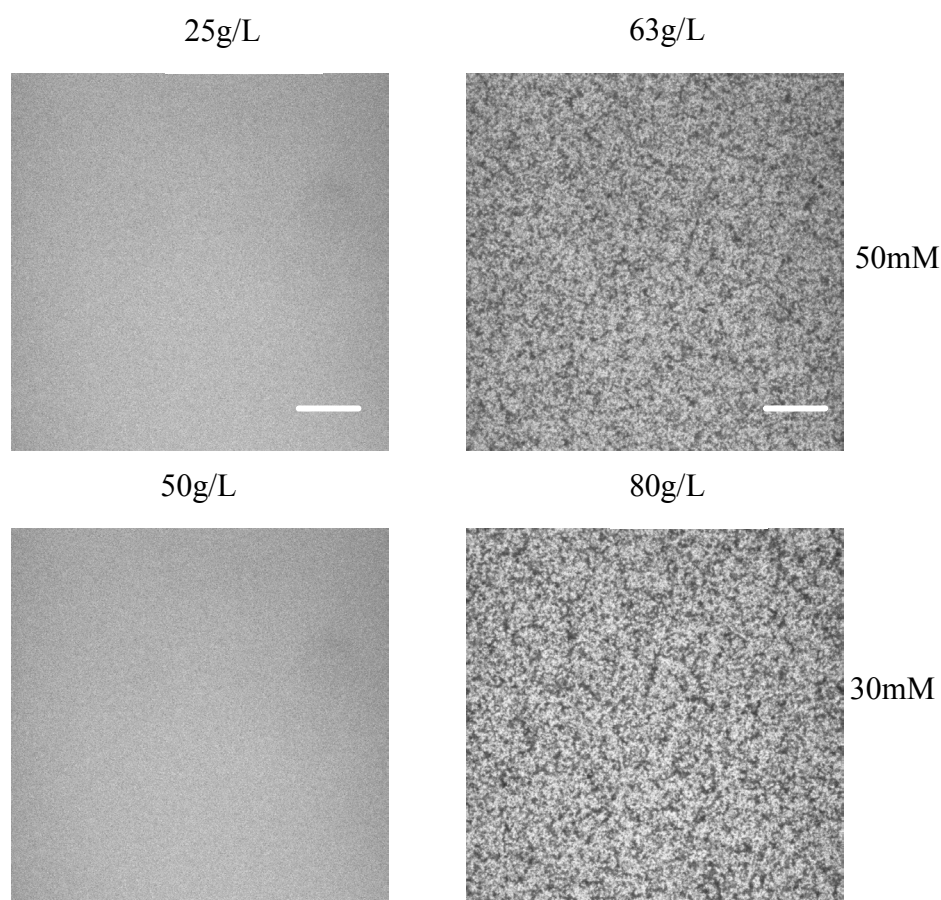


Figure 6.10. CSLM photos of ovalbumin gels formed by heating at 78 during 1h at the different concentrations and NaCl concentrations indicated in the figure. The bar represents 25μm.

we do not observe the dramatic increase of the scattering intensity for $C > 50\text{g/L}$ in the q -range covered by SAXS as was observed with light scattering. This implies that the local structure is still controlled by the strong electrostatic repulsion between the aggregates even if at large length scales the systems become heterogeneous. Preliminary results on another globular protein (bovine serum albumin) also show an increase at very high protein concentrations.¹⁴ Clearly, more research is needed to understand the origin of the large scale heterogeneity that appears at high concentrations of ovalbumin and bovine serum albumin, but that is not observed for β -lactoglobulin.

The main conclusion from the present work and that reported in part I (ref. 15) is that the structure of heated globular protein solutions and gels is generally determined by the interplay between the growth of the aggregates and the electrostatic interaction between the

aggregates. This interplay leads to a maximum in the turbidity at a certain protein concentration where the heterogeneity is maximum. The degree of heterogeneity and thus the value of the turbidity at the maximum, increases with decreasing electrostatic interaction. The unexpected upturn of the turbidity at high protein concentrations has not been observed for β -lactoglobulin systems and is not a universal feature for globular protein gels.

ACKNOWLEDGEMENTS

Igor Dolbnya and Wim Bras are thanked for their technical assistance at the DUBBLE (Grenoble, France). The Netherlands Organization for the Advancement of Research (NWO) is acknowledged for providing the possibility and financial support for performing measurements at the DUBBLE.

REFERENCES

1. Clark, A.H. In *Functional properties of food macromolecules*, Mitchell, J.R., ed.; Elsevier Applied Science, London and New-York, 1998, p 77.
2. Gosal, W., Murphy, S.B. (2000). *Curr. Opin Coll. Int. Sc.*, 5, 188.
3. Pouzot, M.; Nicolai, T.; Durand, D. (2004). part I. *Macromolecules*, accepted.
4. Weijers, M.; Visschers, R.W.; Nicolai, T. (2002). *Macromolecules*, 35, 4753-4762.
5. Stein, P.E.; Leslie, A.G.W.; Finch, J.T.; Carrell, R.W. (1991). *J. Mol. Biol.*, 221, 941.
6. Nemoto, N.; Koike, A.; Osaki, K.; Koseki, T.; Doi, E. (1993). *Biopolymers*, 33, 551.
7. Koseki, T.; Kitabatake, N.; Doi, E. (1989). *Food Hydrocolloids*, 3, 123, *ibid* p.135.
8. Pouzot M.; Visschers, R. W. , Nicolai T., Weijers, M. (2005). *Food Hydrocolloids*, 19, 231.
9. Weijers, M.; Visschers, R. W. unpublished results.
10. Vachier, M.C.; Piot M.; Awedé, A.C. (1995). *J. Chromatogr. B*, 66, 201-210.
11. Baussay, K., Le Bon, C., Durand, D., & Nicolai, T. (2003). *Int. J. Biol. Macromol.*, 34, 21.
12. Brown W., Ed. *Light Scattering. Principles and Developments*, Clarendon Press, Oxford, 1996.
13. Higgins, J.S.; Benoit, K.C. *Polymers and Neutron Scattering*, Clarendon Press, Oxford, 1994.
14. Donato. L.; Garnier C.; Nicolai, T. unpublished results.
15. Pouzot, M., Durand, D., and Nicolai, T. (2004). *Macromolecules*. Accepted.

CHAPTER 7

ELECTROSTATICS CONTROLS FIBRIL FORMATION

PART II: ELUCIDATION OF THE MOLECULAR MECHANISM OF AGGREGATION

Weijers, M., Broersen, K., Barneveld, P.A., Cohen Stuart, M.A., Jongh de, H.H.J.,
Hamer, R.J., and Visschers R.W. 2004, submitted

ABSTRACT

The effect of surface charge on the heat-induced denaturation kinetics, aggregation and gelation properties of ovalbumin (OVA) at pH 7 was studied by chromatography, differential scanning calorimetry, electrophoresis, and cryo-transmission electron microscopy and turbidity measurements. The denaturation kinetics of differently charged OVA variants appeared to be independent of protein concentration and was successfully described with irreversible first-order kinetics, as was previously shown for unmodified OVA. Increasing the net charge on OVA molecules promoted the formation of stiff fibrillar aggregates upon heating. Also, these highly charged proteins showed a significant decrease in the rate of disulfide bond formation during heating compared to less charged variants. More branched and clustered aggregates were formed from OVA molecules with a lower surface charge. Gels from these aggregates appeared to be more turbid, whereas the highly charged aggregates appeared to form gels which were transparent over a much larger range of ionic strength (up to 500 mM.)

These results demonstrate that the charge density on the protein molecule plays a major role in the formation of fibrillar structures and therefore in the formation of transparent gels. By controlling the charge density on the protein molecules, the magnitude of electrostatic repulsion can be changed, which allows us to control fibril formation and therefore the turbidity and rheological properties of OVA networks.

7.1 INTRODUCTION

Fibril formation is becoming one of the major topics in biology, medicine and food industry.¹⁻⁵ An important requisite for fibril formation that has been recently identified by the research groups of Serrano⁶ and Dobson⁷ is the electrostatic contribution.

In this study we used a chicken egg white protein, ovalbumin, for studying the effect of electrostatic interactions on the thermal stability and fibril formation. The effect of electrostatic interactions on the thermal stability is discussed in the paper of Broersen et al.⁸, whereas denaturation kinetics, self-assembly into fibrillar aggregates and network formation are presented here. In order to study the effect of electrostatic repulsion, OVA was chemically engineered, leading to different OVA variants with varying net charge. Four OVA variants (OVA-1, OVA-5, OVA-12 and OVA-26) were selected with calculated net charge, ranging from -1 to -26 at neutral pH. In the preceding paper, it was demonstrated that these variants showed no changes in the overall topology, i.e., in protein conformation, surface-exposed hydrophobicity, disulfide interaction potential or energy content. Therefore we consider this ovalbumin series as an excellent model system to study the effect of electrostatic interactions on the denaturation kinetics, aggregation and gelation properties.

In biological systems, the first event leading to aggregation is normally enzymatic cleavage or misfolding, whereas in food systems it is usually heat-induced denaturation. The fact that many proteins show irreversible heat-induced denaturation⁹⁻¹¹ is mostly due to the occurrence of subsequent aggregation processes.¹² We have previously shown that the denaturation of OVA-12 can be well described with irreversible first-order kinetics.¹³ The denaturation is followed by protein-protein interactions that may lead to aggregation, in which electrostatic interactions can play an important role.^{7,14}

Protein aggregation is governed by the balance between hydrophobic interaction and electrostatic repulsion between denatured proteins. Electrostatic repulsion can be altered by chemical engineering of the charged residues. A few papers show that heat-induced aggregation of OVA and egg white protein was retarded if the charge on the protein was increased.¹⁵⁻¹⁸ Mine showed that increasing the net charge affects under specific the transparency and elasticity of OVA gels, but the mechanism for this is not clear.¹⁸ Also, none of these papers study the effect of modification on the overall topology of the protein, which is essential in the discussion of the effect of charge on aggregate and gel properties.

To unambiguously understand the impact of protein net charge on fibril formation, it is evident that the two steps involved require a full investigation. The first step, namely the denaturation process is described in detail in the preceding paper,⁸ showing the similarity of the various particles at the starting point of aggregation. The present work follows up by investigating the effect of protein net charge on the overall aggregation process and on subsequent gel properties in terms of turbidity. The results demonstrate that understanding and controlling fibril formation is of great importance for controlling gel properties and is of relevance to biotechnological applications and life sciences.

7.2 MATERIALS AND METHODS

Reagents and Chemicals

Ovalbumin was purified from fresh hen eggs according to a previously described purification protocol of Kusters et al.¹⁹ The method to chemical engineer the OVA variants (OVA-26, OVA-5, and OVA-1) are described in the preceding paper.⁸

DSC

The experimental method has been described elsewhere.⁸ Samples were prepared at protein concentrations of 10 g/L, pH 7.0, without added salt. The same solution without the protein was used in the reference cell. The temperature was scanned from 25 to 120°C at a scanning rate of 1.00°C min⁻¹. To obtain C_p^{eff} curves, reference-reference baselines were obtained at the same scan rate and subtracted from the sample curves. Subsequently, a baseline correction was applied assuming $\Delta C_p = 0$. The fits have been performed, using the theory described by Sanchez-Ruiz for a practical two-state model.¹⁰

HPSEC

For the determination of the fraction non-denatured native OVA (OVA-12, OVA-26, OVA-5, and OVA-1) upon heating, different series of screw-cap vials containing ca. 5 ml of OVA solution with different initial protein concentrations were heated for various times up to 24 h at 72.0, 66.8, 72.0, and 69.4°C respectively (corresponding to 7°C below their actual peak temperature, determined with DSC). Next, the vials were cooled in ice-water and the protein solutions were diluted to a final concentration of non-denatured protein

between 0.1 to 5 g/L, to be within the calibration range. Then, the pH was adjusted to the iso-electric point (± 0.1) of the OVA variant (Table 7.1) with 0.1M HCl, causing the denatured and aggregated OVA to precipitate. After centrifugation at 20,000g for 5 minutes at room temperature, the concentration of non-denatured OVA in the supernatant was determined by HPSEC (Phenomenex BioSep-SEC-S2000 column, 300×7.5 mm) with UV detection at 280 nm.

SDS-PAGE

SDS-PAGE was performed to follow the formation of disulfide cross-linked aggregates during heating. The experimental method is described elsewhere.⁸ Samples were prepared at protein concentrations of 5 and 10 g/L, pH 7.0, without added salt.

Agarose Gel Electrophoresis

SDS-agarose continuous gel electrophoresis (1 % (w/w) agarose) was performed to determine the differences in molecular weight of the different variants of OVA aggregates prepared just below their critical gelation concentration. The experimental method is described elsewhere.²⁰ Samples were prepared at protein concentrations (C^*) as mentioned in table 7.4, pH 7.0, without added salt.

SEC-MALLS

SEC-MALLS experiments were performed as described before to determine the total amount of monomeric protein as well as the amount of aggregates.¹³ Samples were prepared at protein concentrations of 5 and 10 g/L, pH 7.0, without added salt.

Cryo-TEM

Cryo-transmission electron microscopy was carried out as described elsewhere²¹, using a Philips CM12 transmission electron microscope operating at 120 kV. Images were recorded digitally by a Gatan 791 CCD camera using the Digital Micrograph software package. Samples were prepared at protein concentrations (C^*) as mentioned in table 7.4, pH 7.0, without added salt.

Turbidity measurements

Turbidity measurements were performed at 78°C on a Cary 1E UV-vis spectrophotometer (Varian Nederland B.V.) equipped with a temperature controller. OVA samples were prepared at different protein concentrations (5- 100 g/L) and ionic strength (3 – 500 mM). The turbidities of the OVA solutions and gels were calculated from steady-state absorbance at 500 nm (typically after 1 h heating). Samples were measured in quartz cuvettes with a path length (l) of 0.2 cm.

The diagram of states (Figure 7.8) was divided into three regimes: transparent, translucent and turbid. These samples were defined transparent when the turbidity was lower than 0.4 cm^{-1} , i.e. more than 92% of the light passes through the sample in a 0.2 cm sample cell. Translucent sample have turbidities between 0.4 and 18 cm^{-1} , i.e more than 2.5% and less than 92% of the light passes the sample. Samples with turbidity higher than 18 cm^{-1} were defined as turbid, i.e. less than 2.5% of the light passes through the sample.

7.3 RESULTS

7.3.1 DENATURATION AND AGGREGATION KINETICS

Series of a single protein, ovalbumin, with different net charges have been prepared by chemical engineering of the folded protein (succinylation of lysine groups and methylation of carboxyl groups). Four differently charged OVA variants were studied: OVA-1, OVA-5, OVA-12 and OVA-26, in which -1 to -26 are the calculated net negative charges on the surface of the protein molecules at pH 7.0. Changing the net charge on the protein molecules caused a shift in the isoelectric point (Table 7.1, and ref. 8). The preceding paper demonstrated no significant changes in the size, hydrophobicity, sulfhydryl-disulphide exchange index (SEI), and molecular structure between these differently charged proteins.

Table 7.1. Iso-electric point, net charge at pH 7 and degree of modification for ovalbumin variants after chemical processing.

<i>Ovalbumin variant</i>	<i>pI (-)</i>	<i>Net charge</i>	<i>Degree of modification (%)</i>
OVA-26	3.5	-26	33
OVA-12	4.7	-12	0
OVA-5	5.0	-5	15
OVA-1	5-7	-1	23

*Data taken from part I.³¹

Since there are no changes on a molecular level, it can therefore be concluded, in this work, what the impact is of electrostatic interactions on the mechanism of fibril formation and on the gelation properties.

7.3.1.1 CONVERSION OF MONOMERS INTO AGGREGATES INDUCED BY HEATING

The kinetics of heat-induced conversion of OVA monomers to aggregates at pH 7.0 was determined using high-performance size-exclusion chromatography (HPSEC). To allow a proper comparison of the denaturation kinetics, the protein solutions were incubated at a temperature which was shifted by a fixed amount (in this case -7°C) with respect to their denaturation peak temperature as determined for each variant with DSC (Table 7.2). The fraction monomers as a function of heating time is shown in Figure 7.1 for the OVA variants at different protein concentrations. Two interesting observations can be made. Firstly, for the different OVA variants no significant difference in rate constant for denaturation is observed.

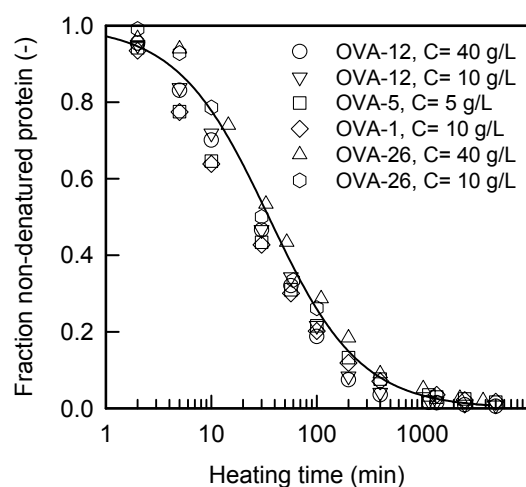


Figure 7.1. Heating time dependence of the fraction non-denatured OVA for different OVA variants measured with HPSEC. The OVA solutions were heated 7°C below their peak temperature (T_p). T_p is tabulated in table 7.1. Solid line is a guide to the eye.

Secondly, the half-time of the reaction (half of protein denatured and aggregated) was independent of the initial protein concentration for all variants. This suggests that denaturation is the rate-limiting step for all OVA variants. Moreover, first-order behavior has been shown previously for OVA-12,¹³ and also applies for the charged OVA variants used in this study.

7.3.1.2 FITTING DSC THERMOGRAMS OF OVALBUMIN VARIANTS WITH IRREVERSIBLE FIRST-ORDER KINETICS

It was previously shown that the DSC thermograms of the differently charged OVA variants decreased in peak temperature for OVA-26, OVA-5 and OVA-1 compared to OVA-12.⁸ It can be concluded that all calorimetric transitions were irreversible, since in the reheating runs no transitions could be detected. The calorimetric behavior of OVA-12 can be well described by a two-state irreversible denaturation model ($N \rightarrow D$) (for details see ref. 13).

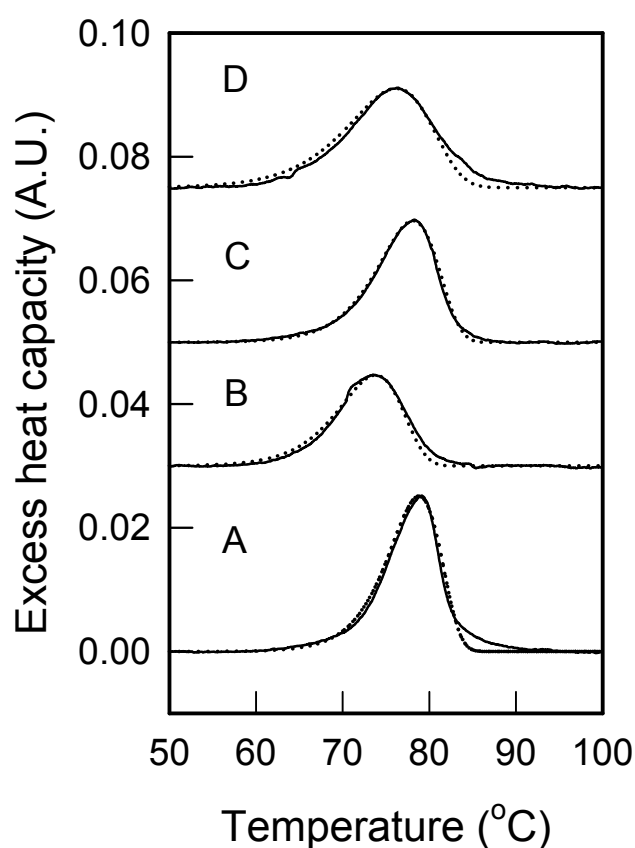


Figure 7.2. Differential scanning calorimetry thermograms and the best fit of the two-state irreversible denaturation model for the OVA variants in solution at a scan rate of 1.0 °C/min (solid lines), pH 7 and protein concentrations of 10 g/L. (A) OVA-12; (B) OVA-26; (C) OVA-5 and (D) OVA-1. Dashed lines represent irreversible first-order fits.

Figure 7.2 shows the fits of the experimental DSC profiles for the OVA variants at 1.0°C/min, using this two-state model. It can be concluded that the two-state irreversible model successfully reproduces the experimental data in the whole temperature range for

OVA-26, OVA-12 and OVA-5. The model describes the experimental data of OVA-1 less well, suggesting that OVA-1 denatures via an intermediate state. In the preceding paper it has been shown that neutralization of surface charge leads to a significant increase in thermodynamically stable intermediate upon denaturant-unfolding. However, figure 7.1 already showed that such unfolding in an intermediate does not affect the observed kinetics. From the fits, the energy of activation (E_a) and the frequency factor of the Arrhenius equation (A) can be obtained (Table 7.2).

Table 7.2. Values of the parameters obtained from fitting the experimental DSC data. T_p is the peak temperature at a scan rate of 1°C/min; E_a the energy of activation; and A the frequency factor of the Arrhenius equation.

<i>Ovalbumin variant</i>	T_p (°C)	E_a (kJ/mole)	$\ln(A \text{ (min}^{-1}\text{)})$
OVA-26	73.8	269	92
OVA-12	78.8	338	114
OVA-5	78.1	293	99
OVA-1	76.2	208	70

From these data, the rate constant (k) of the rate-limiting step can be calculated using the Arrhenius equation. Figure 7.3 shows the rate constants calculated at different temperatures for the four OVA variants using Table 7.2. The symbols represent the experimental values of k at which the OVA solutions were heated (i.e. 7°C below T_p , figure 7.1).

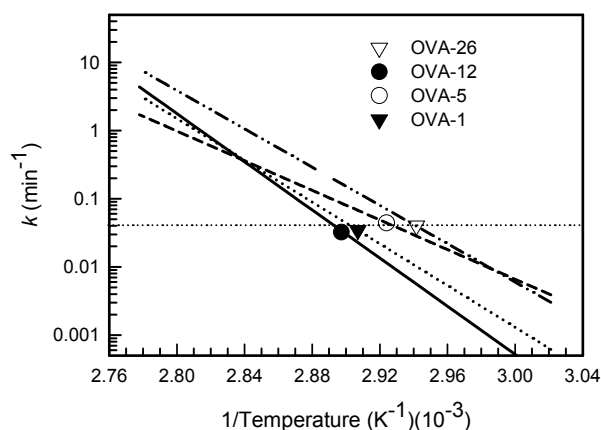


Figure 7.3. Rate constant (k) for different OVA variants as a function of temperature. First-order rate constant changes with temperature as described in the Arrhenius equation; frequency factor and energy of activation are obtained from table 7.2. The symbols give the rate constants at which the solutions of OVA variants were heated (7°C below T_p) as presented in figure 7.1.

As a function of temperature, the value of k , for the OVA variants, calculated from the Arrhenius equation (Fig. 7.3) should be in line with the rate constants obtained from the data in Figure 7.1 (see ref. 13 for calculations). Indeed, the rate constants calculated from DSC values are approximately the same for the OVA variants and are in agreement with values obtained from the results of HPSEC presented in Figure 7.1. We therefore conclude that the aggregation of the OVA variants follows irreversible first-order kinetics.

7.3.2 CHARACTERIZATION OF THE PHYSICOCHEMICAL PROPERTIES OF PROTEIN AGGREGATES

When testing the reactivity of thiol groups in the OVA variants, at ambient (25°C) and elevated (58°C) temperatures, the thiol content and sulphydryl-disulfide (SH-SS) exchange index of the proteins were not substantially changed (Table 7.3). This validates the assumption that the potential for chemical cross-linking of the reactive particles generated by heating the OVA variants was comparable. The surface hydrophobicity of the charged OVA variants was also shown to remain unaffected.⁸ We therefore assume that differences found in aggregate properties are primarily due to changes in net charge on the surface of the protein molecule.

Table 7.3. Second-order rate constant for sulphydryl-disulphide exchange and the sulphydryl-disulphide exchange index (SEI), for ovalbumin variants measured at 25°C and 58°C.

Ovalbumin variant	<i>Rate constant ($M^{-1} s^{-1}$)</i>		<i>SEI*</i>	
	$k_{25^{\circ}C}$	$k_{58^{\circ}C}^*$	SEI _{25°C}	SEI _{58°C} [*]
OVA-26	0.67	2.61	3.14	3.28
OVA-12	0.34	3.09	3.43	3.21
OVA-5	0.41	3.59	3.35	3.14
OVA-1	0.66	7.65	3.15	2.81
Glutathione	922	4990	0	0

* SUC and LMET variants were heated at 54°C and 56°C, respectively

7.3.2.1 SDS-PAGE AND AGAROSE ELECTROPHORESIS

To obtain information on dominating forces in aggregate formation we also studied whether the aggregates formed from the OVA variants contained disulphide cross-linked proteins using SDS-PAGE (for small aggregates) and agarose electrophoresis (for large aggregates). Protein aggregates of OVA variants were prepared by heating 5 g/L native

protein solutions at pH 7.0 and low ionic strength. From Figure 7.4, two interesting observations can be made.

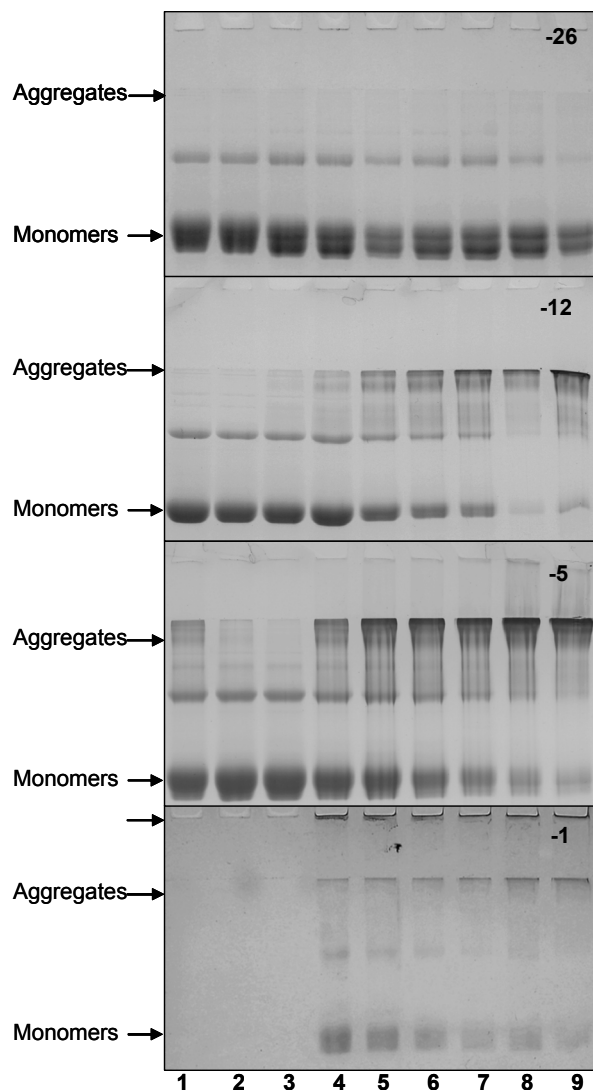


Figure 7.4. SDS PAGE of unheated and heated solutions of the OVA variants (5 g/L, 200 ppm NaN₃, pH 7, 72°C). Lane 1, unheated OVA; lane 2-9, OVA heated for 2, 5, 10, 30, 60, 100, 500 and 1000 minutes. Note that the additional protein band in the native OVA sample is due to impurities of ovotransferrin.

Firstly, upon heating solutions OVA-12, OVA-5, and OVA-1 showed that the monomeric protein band decreased in time due to the formation of disulphide bonds. The variant with a net charge of -26 showed almost no decrease of the monomeric protein band during heating, indicating that under these conditions no or a very few disulfide cross-linked monomers are formed. Analysis of the data, i.e. the fraction non-disulphide cross-linked monomers versus heating time, from Figure 7.4 is presented in Figure 7.5. The second observation is that with decreasing net charge the formed aggregates becomes

significantly larger since the migration velocity decreases. In case of the OVA-1 variant the aggregates became so large that they were not able to enter the gel matrix. Aggregate formation was studied in detail by SEC-MALLS.

The formation of disulphide cross-linked aggregates prepared by heating solutions of OVA variants slightly below their critical gelation concentration was determined with agarose electrophoresis. Obviously larger aggregates were formed compared to the aggregates prepared at low protein concentrations. Similar effects of disulphide bonding kinetics were obtained as presented for SDS PAGE (data not shown). Although, aggregates prepared from OVA-26 formed in the end disulphide cross-linked aggregates, the rate of disulphide bonding was significantly lower than for the lower charged variants.

We conclude from gel electrophoresis experiments that increasing the net charge on the native protein molecule results in a significant decrease of disulfide bond formation during aggregation.

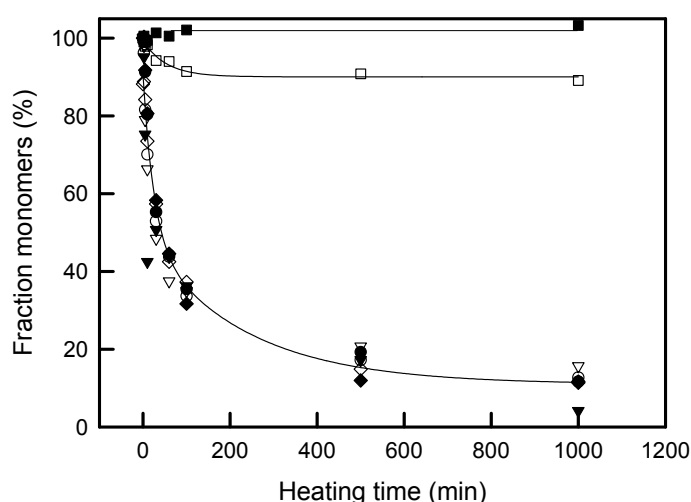


Figure 7.5. SDS PAGE analysis of data as shown in Figure 7.4. Filled and open symbols represent OVA variants heated at a protein concentration of 5 g/L and 10 g/L, respectively. OVA variants: OVA-26 (■, □); OVA-12 (◆, ◇); OVA-5 (●, ○); OVA-1 (▼, ▽). Solid lines are guides to the eye.

7.3.2.2 SEC-MALLS

Size-exclusion chromatography was used to study the effect of net charge on the aggregate size and its polydispersity. Therefore, OVA solutions were heated at 72°C, samples were taken at various heating times ranging from 0 to 5000 minutes. After heat treatment the samples, containing monomeric fractions as well as aggregated fractions,

were cooled to room temperature and injected onto the SEC MALLS column without further treatment.

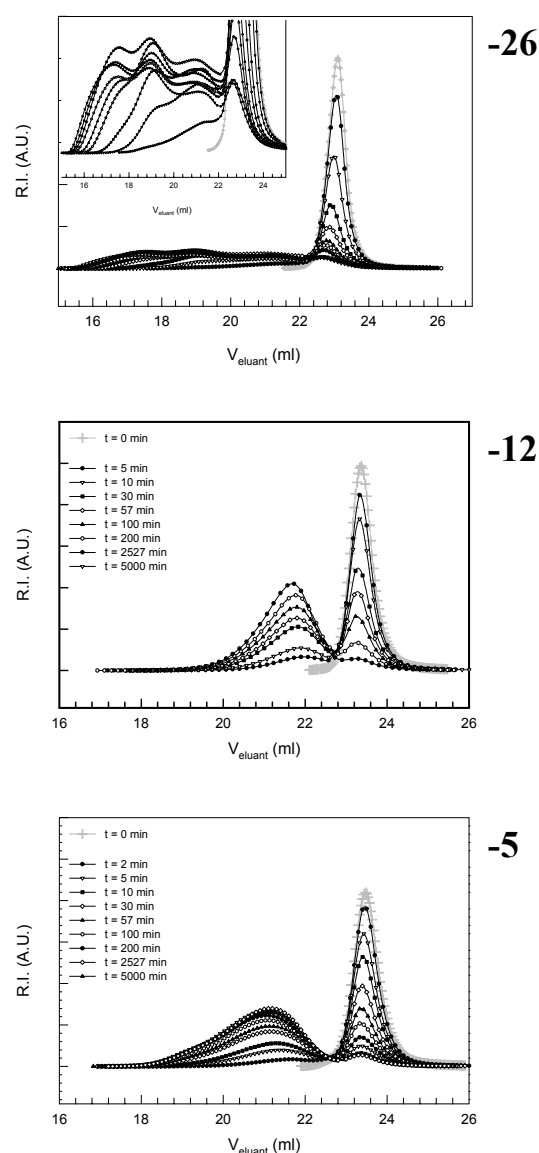


Figure 7.6. Chromatograms of heated solutions of OVA variants. PH 7.0, C = 10 g/L, 200 ppm NaN₃ at different heating times at 72°C. OVA-26 was heated at a protein concentration of 40 g/L. The inset in the upper panel is an enlargement of the SEC-MALLS data from the same graph.

Figure 7.6 shows elution profiles of heated solutions of OVA variants (OVA-26, OVA-12, and OVA-5). The peak at volumes between 22.5 and 24.5 ml corresponds to non-aggregated monomers. With increasing heating time, the fraction of monomers decreases. The size distribution of the monomeric fraction was narrow; the polydispersity was about 1.0 (indicating a monodisperse fraction) and did not increase upon heating. OVA aggregates elute at volumes between 16 and 22.5 ml. With increasing heating time, the relatively broad aggregate peak shifts to smaller elution volumes and the scattered intensity of the aggregate peak increases. This indicates that the size and number of the aggregates

formed as a function of heating time increases. In the upper panel, chromatograms of OVA-26 solutions heated at 40 g/L instead of 10 g/L are shown. The inset demonstrates that no clear distinction can be made between monomers and aggregates. The lower two panels show that the aggregates were always large enough to be clearly distinguished from the non-aggregated proteins. This indicates that under these conditions no or very few stable oligomers (dimers, trimers etc.) are formed. The aggregates formed by OVA-5 elute at smaller volumes, implying that these aggregates are larger than those formed from OVA-12 at a protein concentration of 10 g/L.

The results indicate that increasing the net charge on OVA molecules causes the formation of smaller (i.e. lower molecular weight) aggregates with a larger molecular size distribution ($M_w/M_n \sim 3$).

7.3.2.3 CRYO-TEM

Figure 7.7 shows cryo-TEM images of the aggregates obtained from heating the OVA variants. The effect of net charge on fibril formation, branching and cluster formation is clearly shown. The characteristics of these aggregates are summarized in Table 7.4. The hydrodynamic radius (R_h), the contour length (l_c) and the shape of the aggregates are clearly influenced by the net charge. Decreasing net charge resulted in an increase of the R_h of the protein aggregates as well as the degree of branching. The flexibility, i.e. the persistence length increased with increasing net charge. The aggregates prepared from OVA-26 were much smaller and appeared less flexible than the lower charged variants. Qualitatively, more oligomers were present in these samples (observed from additional images), which is in good agreement with the results from SEC-MALLS. The l_c of the aggregates seems to show an optimum between a net charge of -12 and -5. At higher net charge the aggregates were significantly shorter and at lower net charge the aggregates became clustered and therefore it was unreliable to determine a l_c .

7.3.2.4 CRITICAL GELATION CONCENTRATION

The critical gelation concentration (C^*) is defined as the minimum protein concentration to form a percolating three-dimensional protein network capable of retaining water molecules within the structure. C^* was determined by heating concentration series of the differently charged OVA variants. The C^* appeared to show an optimum for the OVA-12 variant (Table 7.4) at a protein concentration of 55 g/L. For OVA-26, the C^* was found

to be significantly lower, 42 g/L, which might be explained by the increased rigidity of the rods (see discussion section). For OVA-5, C^* appeared to be 52 g/L and the C^* for OVA-1 was reduced by a half (25 g/L) compared to the optimum.

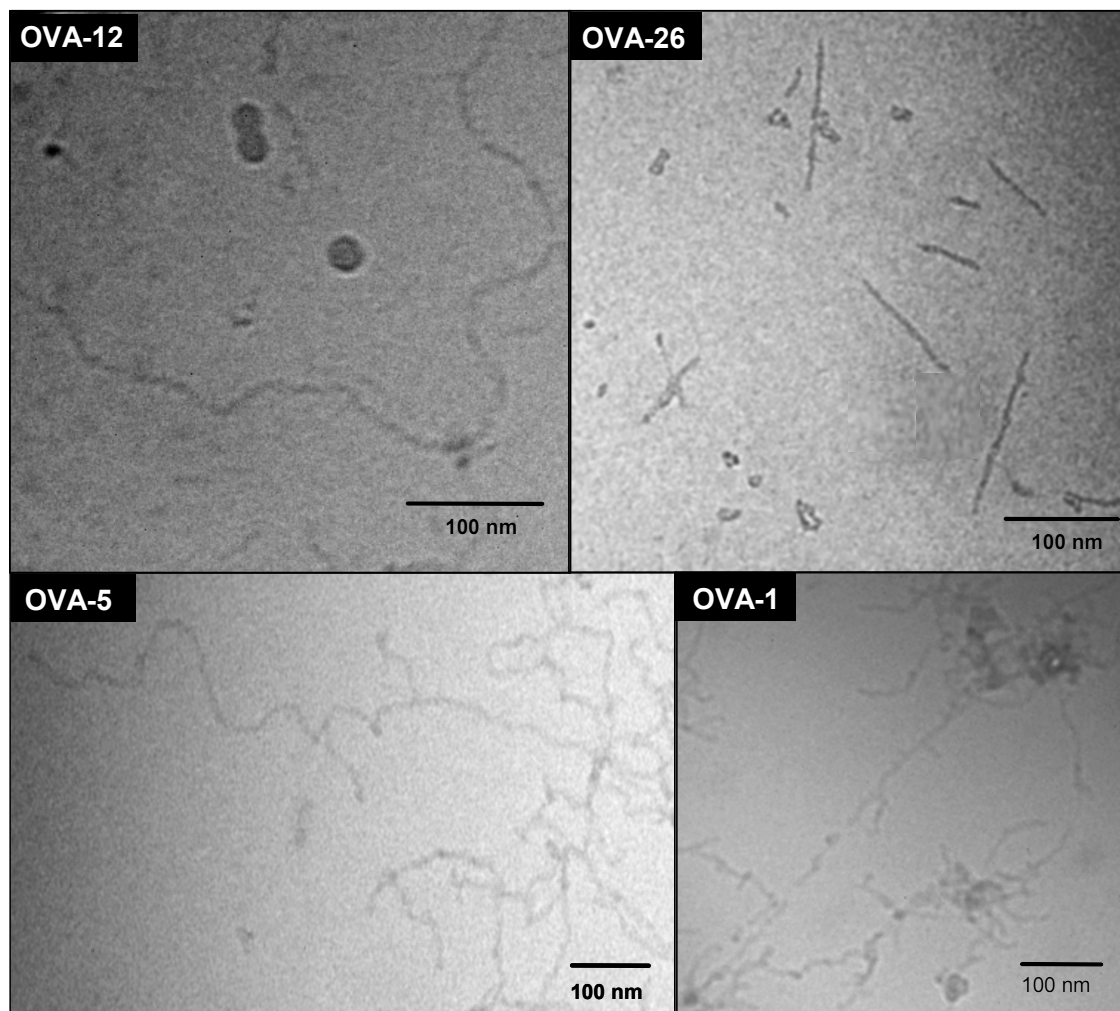


Figure 7.7. Cryo-TEM images of large OVA aggregates formed after heating for 24 h at 72°C at pH 7, 200 ppm NaN_3 . OVA variants were initially heated at: $C=55$ g/L (OVA-12); $C=42$ g/L (OVA-26); $C=52$ g/L (OVA-5); and $C=25$ g/L (OVA-1), and diluted to 1 g/L before cryo-TEM images were recorded.

We may conclude from the aggregate characterization that decreasing electrostatic repulsion leads to an increase in the degree of branching. Increasing the net charge on OVA aggregates results in the formation of smaller and more rigid aggregates with a more polydisperse size distribution.

Table 7.4. Aggregate characteristics: intermolecular disulfide bonding (S-S), hydrodynamic radius obtained from dynamic light scattering (R_h), contour length (L_c), shape, and critical gelation concentration (C^*) of OVA variants.

<i>Ovalbumin variant</i>	<i>S-S</i>	R_h (nm)	L_c (nm)	<i>shape</i>	C^* (g/L)
OVA-26	+/-	72-85	20 - 200	rigid rods	42
OVA-12	+	85	400 - 1100	lin-flex chains ^a	55
OVA-5	+	105	400 - 1000	lin-flex chains ^a ; branched	52
OVA-1	+	581	~ 400	clusters of branched aggregates	25

^a Linear flexible chains

7.3.3 FUNCTIONAL PROPERTIES OF HEAT-INDUCED OVALBUMIN GELS

The turbidity (τ) of OVA gels (pH 7.0) as a function of protein concentration at various ionic strengths was determined after heating at 78°C for 1 h. Figure 7.8A shows the diagram of states of OVA-12. We classified τ in three regimes: transparent, translucent and turbid (see materials & methods section). The transitions from transparent to translucent and from translucent to turbid are indicated in the figures by dotted lines. The individual measurements are presented by various symbols as explained in the figure legend.

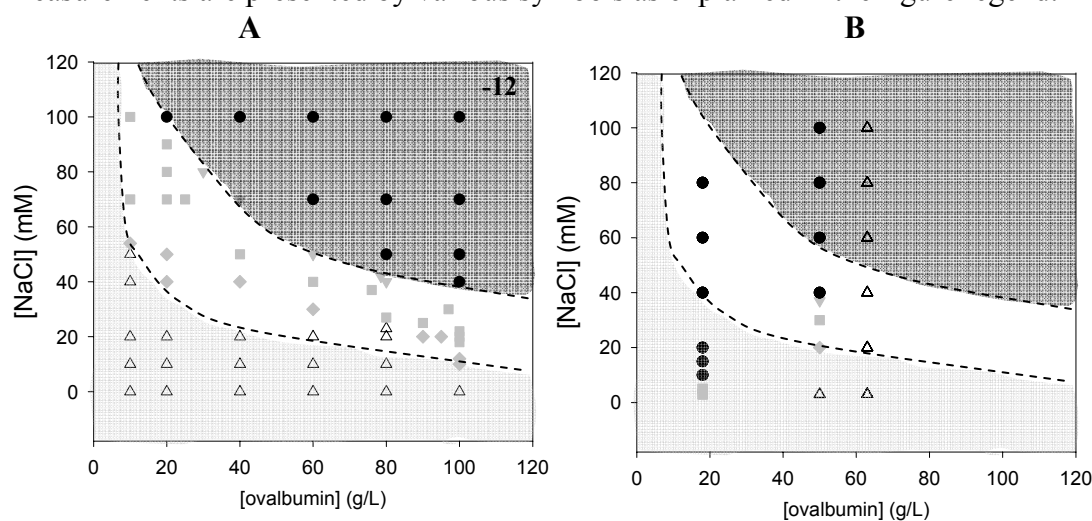


Figure 7.8. Phase diagram of heat-induced systems of OVA variants. Native OVA solutions were heated at different protein concentrations and ionic strength. The turbidity (τ) was measured in a spectrophotometer at 500 nm. Solutions were heated for 1 h at 78°C. Symbols: (Δ) transparent solution or gel, $\tau < 0.4 \text{ cm}^{-1}$; (\diamond) “low” translucent system, $0.4 \leq \tau \leq 1.04$; (\blacksquare) “medium” translucent system, $1.05 \leq \tau \leq 11.4$; (\blacktriangledown) “heavy” translucent system, $11.5 \leq \tau \leq 18.4$; (\bullet) turbid system, $\tau > 18.4$ (A) Phase diagram of OVA-12; (B) Turbidity of OVA-26, OVA-5 and OVA-1 gels are incorporated in the phase diagram of OVA-12. Note that for OVA-26, OVA-5 and OVA-1 the turbidity is measured at different ionic strength, at one protein concentration.

The results in Figure 7.8A show that increasing the ionic strength at all protein concentrations initially resulted in the formation of translucent gels, whereas increasing the ionic strength further led to more turbid gels. The turbidity of OVA-26, OVA-5 and OVA-1 gels was determined as a function of ionic strength at a single protein concentration of 62, 50, and 18 g/L respectively (Figure 7.8B). The same heating conditions were used as for OVA-12. Gels obtained from heating OVA-26 solutions at 62 g/L and ionic strength up to 500 mM appeared transparent whereas OVA-12 showed turbid gels at these high salt concentrations. Gels obtained from heating solutions of OVA-5 and OVA-1 resulted in turbid systems at much lower ionic strength, than for OVA-12 systems.

It is concluded from the TEM images, and from the diagram of states that controlling the charge density on the protein molecules controls fibrillar properties and thereby the turbidity of protein networks.

7.4 DISCUSSION

DENATURATION AND AGGREGATION KINETICS

In order to obtain a better understanding of the mechanism of fibril formation in general, to control the formation of these structures and to use them in for instance biotechnological applications, the effect of electrostatics on the mechanism of denaturation, fibril formation, and their resulting networks was studied. OVA variants were produced with different net charges at pH 7.0. Looking at the denaturation and aggregation kinetics of these OVA variants, it was shown that it followed first-order kinetics. For all these variants irreversible denaturation was observed, that could be well described with the “two-state” model for irreversible denaturation. Changing the charge on the surface of the OVA molecules resulted in a destabilization, i.e. both E_a , and T_p decreased. So, any disruption of the ionic network on the native protein resulted in a destabilization of the protein. No correlation was found between the net charge on the protein and the activation barrier and T_p of unfolding. Apparently, the altered kinetics of denaturation has no effect on the aggregation kinetics (Figure 7.1). All variants appeared to have similar denaturation kinetics 7°C below their T_p and it can be concluded that mechanistically the denaturation process follow a comparable first-order mechanism, since the Arrhenius parameters E_a , T_p , and A are related such that under these conditions always the same rate constants were obtained. However, the DSC thermograms for OVA-1 appeared to fit less well, which has

been explained by the formation of an unfolding intermediate as observed with fluorescence spectroscopy.⁸ Nevertheless, we have no indication (Table 7.2) that this affects the generation of reactive particles. Therefore, the effects on aggregate formation and characteristics discussed here cannot be attributed to the occurrence of the intermediate state.

CHARACTERIZATION OF THE PHYSICOCHEMICAL PROPERTIES OF PROTEIN AGGREGATES

The effect of charge on disulphide bonding kinetics, size (R_h , L_c), shape, persistence length (L_p), and rigidity (L_p) of OVA fibrils was investigated with SDS-PAGE, SEC-MALLS and cryo-TEM, and will be discussed below.

We concluded from the results section that increasing net charge on the native protein molecule resulted in a significant decrease in the rate of disulphide bond formation during heat-induced aggregation. This was clearly shown for the OVA-26 variant. The slow rate at which disulfide bonds were formed might be due to an unfavorable combination of the location of the free thiol groups and the disulphide bond, and the distribution of charges on the heavily charged denatured protein molecules (Figures 7.4 and 7.5). The formation of S-S bonds may require a close proximity of the reactants (S-S and SH), which could be influenced by these two factors. This thiol-disulphide exchange mechanism is generally accepted and described in literature.²²⁻²⁵ The absence of intermolecular disulphide bonds in nanotubes of α -lactalbumin²⁶ and also might be expected for β -lactoglobulin at pH 2, because at this pH the NH_3 and COO^- residues will be protonated. The formation of rigid rods has also been observed for β -lactoglobulin at pH 2, where the net charge was $\sim +20$,²⁷ however we did not find any information on the formation of intermolecular disulphide bonds in this system. Clearly the occurrence of disulphide bridging is not a dominant property of fibril formation in these cases.

Results on SEC-MALLS analysis showed that increasing the net charge on OVA molecules caused the formation of smaller aggregates (R_h and L_c decreases) with a larger molecular size distribution. This was confirmed by cryo-TEM images. These images showed that shape of the aggregates was significantly influenced by the net charge. Aggregates formed from heating an OVA-26 solution resulted in the formation of a mixture of small and large rigid rods varying in size (L_c) between 20 and 200 nm. The formation of a heterogeneous dispersion of these aggregates might be due to an increase in

electrostatic repulsion on the protein molecule. By increasing the net charge on a protein molecule, the rigidity, i.e. the persistence length increased. Stiff fibrils ($L_p \gg$) were formed, whereas by decreasing the net charge more branched and clustered fibrils are formed ($L_p <$). The formation of such stiff rods could be explained by the very high net negative charge on the protein molecules. For these types of molecules it is energetically unfavorable to form long semi-flexible fibrils compared to rigid rods. Since OVA-1 still forms linear aggregates, we believe that the charge distribution on an unfolded protein molecule also plays a crucial role in fibril formation.

The importance of electrostatic repulsion in fibril formation is further supported by the observation that increasing the negative charge on OVA-12 fibrils, after their formation (post-succinylation) resulted in a breaking up from 1 μm to fragments of about 50-100 nm (data not shown). This suggests that the fibrils were broken up by electrostatic forces. This is only possible for those links in the chain which are not covalent. It can be concluded that by changing the net charge on the protein molecule, the formation of fibrillar structures can be controlled. The formation of these structures has a direct impact on the properties of protein gels.

FUNCTIONAL PROPERTIES OF OVA GELS

The formation of transparent gels of OVA depends on the ability of the protein to form fibrillar structures. The characteristic dimension of the structure of these gels is smaller than the wavelength of visible light. Gels prepared of the OVA-26 variant remain transparent over a wide range of ionic strength (Figure 7.8), suggesting that the formation of fibrils remained even at high ionic strength. Transparent gels prepared of the OVA-12 variant could be formed at low ionic strength. In this regime it has been previously reported that fibrillar structures are formed.²⁸ It was not possible to form transparent gels from the OVA variant with lower net charges in the presence of NaCl, indicating that the characteristic dimension of the structure of these gels is in the order of the wavelength of visible light. Thus the ability to form transparent gels depend on the properties of the fibrils, such as: contour length (L_c), rigidity (L_p), degree of branching and spatial organization. The same parameters are of interest in understanding critical gelation concentration. The C^* (ionic strength 3 mM) appeared to show an optimum at a concentration of 55 g/L for the OVA-12 variant. For OVA-26, the C^* was reduced to 42 g/L.

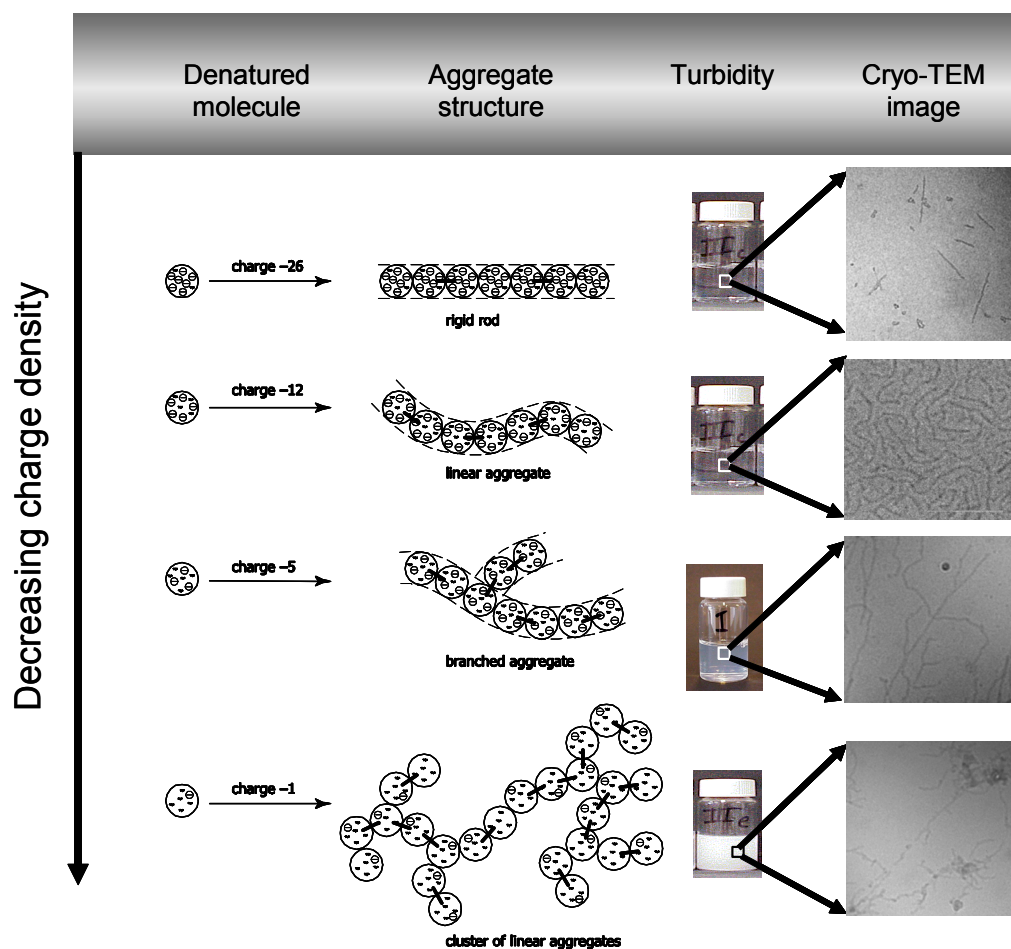


Figure 7.9. A proposed model for the thermal denaturation and aggregate formation of OVA with various charge densities on the surface of the protein molecule. Shadows (ϵ) indicate hydrophobic areas exposed by thermal denaturation, minus signs (\ominus) and dashed symbols ($-$) indicate the calculated net charge at pH 7 and disulphide bonding respectively. Turbidity and cryo-TEM images are illustrations of experimental results.

The L_c of OVA-26 aggregates has been reduced by a factor of 4 compared to the L_c of OVA-12 fibrils, which should result in the C^* to increase. However, the rigidity was increased as well, resulting in a decrease in C^* . Since C^* generally depends on an ensemble of different properties of the fibrils, such as: contour length (L_c), rigidity (L_p), degree of branching and spatial organization, the stiffer aggregates may be more effective in forming a network because of larger excluded volume and more constrained packing effects. For OVA-1, at an ionic strength of 3 mM, the C^* was reduced by a half. Because the electrostatic interactions are decreased, branched linear aggregates are formed. As a result, a percolated network is formed at lower protein concentrations. A similar effect has been observed for heat-induced OVA systems at high ionic strength; here the C^* is also reduced significantly.²⁹

In conclusion, the charge density on the protein molecule has a major effect: higher charge density leads to fibrillar structures and transparent gels. High net charge densities on protein molecules generally leads to the formation of transparent gels over a wide range of ionic strength, whereas decreasing net charge results in the formation of turbid gels already at low ionic strength compared to OVA-12. To account for the formation of rigid rods, the existing scheme of Koseki has been extended.³⁰ These results are summarized in the scheme presented in Figure 7.9. The addition of negative charge on the surface of the protein molecule results in the formation of heat-induced rigid rods, which are visualized by cryo-TEM images. The other extreme is when almost all charge is eliminated from the surface of the protein molecule; here the heat-induced aggregates are branched and clustered due to decreased electrostatic repulsion. This consequently leads to the formation of turbid gels at low ionic strength and protein concentrations above C^* . Finally, we conclude that controlling the charge density on the protein molecules, i.e. the electrostatic repulsion, allows us to control the extent of fibril formation and therefore the turbidity of OVA networks.

7.5 CONCLUSIONS

While in the preceding paper⁸ it was demonstrated that the denaturation process provided comparable reactive particles, this work showed that they follow similar kinetics. The differences in the formed aggregate structures could be attributed solely to differences in colloidal stability, while the chemical interaction only played a minor role. This knowledge may provide an important tool for the understanding of fibril formation in other (biological) fields, i.e. amyloid formation, as well as knowledge on the manipulation of biotechnological processing techniques.

ACKNOWLEDGEMENTS

The authors gratefully acknowledge Anne van de Pijpekamp for performing the turbidity measurements and Hans Kusters for determining the sulfhydryl-disulphide exchange rate.

REFERENCES

1. Gosal, W. S., Clark, A.H., Pudney, P.D.A., and Ross-Murphy, S.B. (2002). *Langmuir*, 18, 7174.
2. Koo, E.H., Lansbury, P.T., Jr., and Kelly, J.W. (1999). *Proc. Natl. Acad. Sci.*, 96, 9989.

3. Kallberg, Y., Gustafsson, M., Persson, B., Thyberg, J., and Johansson, J. (2001) *J. Biol. Chem.*, 16, 12945.
4. Shah, J.V., and Janmey, P.A. (1997). *Rheol. Acta*, 36, 262.
5. Ellis, R.J., and Pinheiro, T.J.T. (2002). *Nature*, 416, 483.
6. Lopez De La Paz, M., Goldie, K., Zurdo, J., Lacroix, E., Dobson, C.M., Hoenger, A., and Serrano, L. (2002). *Proc. Natl. Acad. Sci., USA* 99, 16052.
7. Zurdo, J., Guijarro, J.I., Jiménez, J.L., Saibil, H.R., and Dobson, C.M. (2001). *J. Mol. Biol.*, 311, 325.
8. Broersen, K., Weijers, M., Groot de, J., Jongh de, H.H.J., and Hamer, R.J. (2004). (submitted)
9. Donovan, J.W., and Beardslee, R.A. (1975). *J. Biol. Chem.*, 250, 1966.
10. Sanchez-Ruiz, J.M., Lopez-Lacomba, J.L., Cortijo, M., and Mateo, P.L. (1988). *Biochemistry*, 27, 1648.
11. La Rosa, C., Milardi, D., Grasso, D.M., Verbeet, M.P., Canters, G.W., Sportelli, and L., Guzzi, R. (2002). *Eur. Biophys. J.*, 30, 229.
12. Klibanov, A.M., and Ahern, T.J. (1987). In *Protein Engineering*. D.L. Oxender and C.F. Fox, editors. Alan R. Liss, New York, pp. 213.
13. Weijers, M., Barneveld, P.A., Cohen Stuart, M.A., and Visschers, R.W. (2003). *Protein Sci.*, 12, 2693.
14. Sheinerman, F.B., Norel, R., and Honig, B. (2000). *Curr. Opin. Struct. Biol.*, 10, 153.
15. Nakamura, R., Sugiyama, H., and Sato, Y. (1978). *Agric. Biol. Chem.*, 42, 819.
16. Ma, C.-Y., and Holme, J. (1982). *J. Food Sci.*, 47, 1454.
17. Ma, C.-Y., Poste, L.M., and Holme, J. (1986). *Can. Inst. Food Sci. Technol. J.*, 19, 17.
18. Mine, Y. 1996. *J. Agric. Food Chem.*, 44, 2086.
19. Kosters, H., Broersen, K., Groot de, J., Simons, J.-W., F.A., Wierenga, P., and Jongh de, H.H.J. (2003). *Biotechn. Bioengineering*, 84, 61.
20. Alting, A.C., Hamer, R.J., de Kruif, C.G., and Visschers R.W. (2000). *J. Agric. Food Chem.*, 48, 5001.
21. Weijers, M., Visschers, R.W., and Nicolai, T. (2002). *Macromolecules*, 35, 4753.
22. Saxena, V.P., & Wetlaufer, D.B. (1970). *Biochem.*, 9, 5015.
23. Watanabe, K., & Klostermeyer, H. (1976). *J. Dairy Res.*, 43, 411.
24. Creighton, T.E. (1978). *Prog. Biophys. Mol. Biol.*, 33, 231.
25. Alting A.C., Weijers, M., Hoog de, E.H.A., van de Pijpekamp, A.M., Cohen Stuart, M.A., Hamer, R.J., Kruif de, C.G., and Visschers, R.W. (2004). *J. Agric. Food Chem.*, 52, 623.
26. Graveland-Bikker, J.F., Ipsen, R., Otte, J., and de Kruif, C.G. J. (2004). *Langmuir*, 20, 6841.
27. Aymard, P., Nicolai, T., Durand, D., and Clark A. (1999). *Macromolecules*, 32, 2542.
28. Pouzot, M., Nicolai, T., Visschers, R. W., and Weijers, M. (2005). *Food Hydrocolloids*, 19, 231.
29. Weijers, M., Visschers, R.W., and Nicolai, T. (2004). Accepted for publication in *Macromolecules*.
30. Koseki, T., Kitabatake, N. and Doi, E. (1989). *Food Hydrocolloids*, 3, 123.

PART II

NETWORK FORMATION UNDER COLD-SETTING CONDITIONS

CHAPTER 8

ACID-INDUCED COLD GELATION OF GLOBULAR PROTEINS: EFFECTS OF PROTEIN AGGREGATE CHARACTERISTICS AND DISULFIDE BONDING ON RHEOLOGICAL PROPERTIES

Alting A.C.& Weijers, M., de Hoog, E.H.A., van de Pijpekamp, A.M., Cohen Stuart, M.A.,
Hamer, R.J., de Kruif, C.G., and Visschers, R.W.
J. Agric. Food Chem. 2004, 52, 623-631

J. Agric. Food Chem. 2004, 52, 623-631

ABSTRACT

The process of cold gelation of ovalbumin and the properties of the resulting cold-set gels were compared to those of whey protein isolate. Under the chosen heating conditions most protein was organized in aggregates. For both protein preparations, the aggregates consisted of covalently-linked monomers. Both types of protein aggregates had comparable numbers of thiol groups exposed at their surfaces, but had clearly different shapes. During acid-induced gelation, the characteristic ordering caused by the repulsive character disappeared and was replaced by a random distribution. This process did not depend on aggregate characteristics and probably applies to any type of protein aggregate.

Covalent bonds are the main determinants of the gel hardness. The formation of additional disulfide bonds during gelation depended on the number and accessibility of thiol groups and disulfide bonds in the molecule and was found to clearly differ between the proteins studied. However, upon blocking of the thiol groups long fibrillar structures of ovalbumin contribute significantly to gel hardness, demonstrating the importance of aggregate shape.

8.1 INTRODUCTION

The ability to gel is an important function of proteins in food systems. Proteins from different sources can produce gels which vary in textural properties.¹ Most food protein gels are formed during heating and are therefore referred to as heat-induced gels. For a relatively small number of proteins, gelation at ambient temperature is reported.² One process to achieve this is the so-called cold-gelation process. In the first step, a solution of native proteins is heated and soluble aggregates are formed by heating at a pH distant from the iso-electric point and at low ionic strength. Upon cooling, the aggregates remain soluble and no gelation occurs. In the second step, gelation is induced at ambient temperature by reduction of the electrostatic repulsion,³ either by adding salt or by changing the pH towards the iso-electric point of the proteins. Gelation caused by lowering pH is called acid-induced gelation.

In the literature, several studies have reported cold gelation of whey protein isolate (WPI).^{1,3,4-19} Most of these concerned the salt-induced type of cold gelation of WPI and only a few studies dealt with the acid-induced type.^{3,14,15,17-19} Previously,^{3,17-19} we demonstrated that in the acid-induced cold gelation process, first a protein network is formed by physical interactions, which is subsequently stabilized by the formation of disulfide bonds. The formation of disulfide bonds took place in spite of the acidified conditions and will likely also occur under more favorable conditions in the salt-induced type of cold gelation of WPI. The formation of disulfide bonds was shown to be of great importance for the mechanical properties of cold-set WPI gels and for their physical stability (syneresis).^{3,17-19}

Whereas the cold gelation of commercially available WPI was intensively investigated, far less is known about the cold gelation of globular proteins in general. Therefore, in this study the cold gelation process of ovalbumin was compared with that of WPI. In contrast to WPI or β -lactoglobulin (β -lg) that both form aggregates with a curved strand-like morphology,^{18,20} ovalbumin can form soluble fibrillar aggregates²¹ under the conditions applied in the cold gelation process. β -Lg is the most abundant protein in WPI (>75%) and determines to a large extent the behavior of WPI during heat treatment. Since the different proteins in WPI may have different denaturation kinetics, the use of protein mixtures instead of pure protein fractions may have an impact on the final properties of the gels when heat-set gels are prepared. However, here cold gelation was used, in which

aggregation and gelation takes place sequentially, which makes it possible to study the direct relation between aggregate properties and final gel properties. In addition to the shape, other aggregate characteristics, such as size and number of thiol groups do not differ between aggregates of WPI or β -lg prepared under the same conditions.^{3,18,20}

Both β -lg and ovalbumin are globular proteins with a net negative charge at neutral pH (iso-electric points around 5). The molecular masses are 18 and 46 kDa for β -lg and ovalbumin, respectively. β -Lg contains two cystines and one cysteine residue and ovalbumin contains six cysteine residues, two of which form a cystine. For both proteins, the thiol groups are buried in the three-dimensional structure of the native protein, but are exposed upon denaturation of the protein molecule. The thiol groups and cystines both play an important role in the heat-induced aggregation of these proteins.^{22,23}

In contrast to heat-induced gelation, in which aggregation and gelation occur at the same time, in cold gelation these two processes occur separately. Here we took advantage of the fact that in the first step stable soluble aggregates were formed, of which the properties could be controlled before gelation was induced. Covalently-linked aggregates of ovalbumin and WPI were prepared, which were comparable in terms of their hydrodynamic diameter, electrophoretic mobility, and number of thiol groups, but were clearly differently shaped. Results on the cold gelation of ovalbumin are discussed and compared to the cold-gelation of WPI.

8.2 MATERIALS AND METHODS

8.2.1 MATERIALS

Glucono- δ -lactone (GDL), 5,5'-dithiobis-(2-nitrobenzoic acid) (DTNB), sodium dodecylsulphate (SDS), Rhodamine B and N-ethylmaleimide (NEM) were obtained from Sigma Chemicals (St. Louis, MO, USA). Electrophoresis-grade agarose was obtained from Life Technologies (Paisley, Scotland). Phastgel Blue R tablets were from Pharmacia Biotech (Uppsala, Sweden). The whey protein isolate (WPI) BiPro was a kind gift from Davisco Foods International Inc. (Le Sueur, MN, USA). The WPI consisted (based on dry weight) of β -lg (74%), α -lactalbumin (α -lac)(12.5%), bovine serum albumin (5.5%) and immunoglobulins (5.5%). The total amount of proteins in the powder was 97.5% and it further contained lactose (0.5%) and ash (2%) (24). Ovalbumin was purified from fresh

chicken egg white based on the procedure of Vachier et al.²⁵ Both protein sources were essentially salt free and no added salt was used in these experiments.

8.2.2 METHODS

Preparation of aggregates

WPI aggregates were prepared at protein concentrations of 3 and 9% (w/w) as described elsewhere.¹⁸ Ovalbumin was dissolved in double-distilled water at ambient temperature at a protein concentration of 2 and 5% (w/w). Ovalbumin aggregates were prepared by heating the ovalbumin solutions in a water bath for 22 h at 78°C.²⁶

After heating, the dispersions of aggregates were rapidly cooled to ambient temperature in running tap water. The amount of native proteins after the heat treatment was determined with a standard assay involving acid precipitation and gel-permeation chromatography.²⁷ The dispersions of aggregates were stored at 4°C until use (typically, within a few days) and diluted to 2% (w/w) with double-distilled water just before the start of the gelation experiments.

Blocking and determination of reactive thiol groups

The number of accessible thiol groups at the surface of the aggregates before and after chemical blocking was determined using DTNB, also known as Ellman's reagent²⁸ as described elsewhere.¹⁷ The assay was performed in the absence of urea and SDS, to avoid measurement of non-surface thiols. NEM was added to a final concentration of 2 mM to block the remaining surface thiol groups.¹⁷ The effectiveness of this treatment was also checked for ovalbumin by the use of the Ellman's reagents.

SDS-agarose electrophoresis

SDS-agarose gel electrophoresis (0.4 % (w/w) agarose) was performed as described before¹⁷ to determine the differences in molecular size of the differently treated protein aggregates. Aggregates (in solution or gel) were dissolved in an SDS-containing buffer (5% SDS, pH 7.0) to a final protein concentration of 0.5% (w/w). Staining was done with Phastgel Blue R.

Viscosity and voluminosity

The voluminosity (Φ) of ovalbumin and WPI-aggregates in very dilute solutions was determined using the Einstein's expression $\eta_r = 1 + 2.5\Phi$. In this expression η_r stands for the relative viscosity η/η_s , where η is the solution viscosity and η_s the viscosity of the continuous phase. The concentration dependent viscosity of dilute solutions of ovalbumin and WPI-aggregates (0-6 g/L) (heated at 78 and 68.5°C respectively at different protein concentrations) were measured with an Ubbelohde capillary viscometer placed in a water bath of 20°C. The voluminosity was determined from the initial slope of the concentration dependence of η_r using Einstein's expression ($\Phi = \text{slope}/2.5$).

The intrinsic viscosity was determined using the Huggins equation: $\eta_{sp}/c = [\eta] + k[\eta]^2c$. Extrapolation of the plot of η_{sp}/c versus c to zero protein concentration gives the intrinsic viscosity. In this equation c stands for the concentration of protein (g/mL). The specific viscosity, η_{sp} , was calculated from $\eta_{sp} = (t-t_0)/t_0 (= \eta_r - 1)$, where t_0 = the efflux of water and t = the efflux of protein solution in the viscosity measurement using an Ubbelohde capillary viscometer (20°C).

The calculations of both the intrinsic viscosity and the voluminosity are based on at least 10 measurements of the efflux times of the different protein solutions and dilutions.

GDL-induced gelation

GDL was added as a powder to the dispersions of aggregates (concentration of protein 2% (w/w)) to induce cold gelation at ambient temperature. To observe gelation of the aggregates around their iso-electric points, it was required to add 0.15% (w/w) and 0.16% (w/w) of GDL to WPI and ovalbumin solutions, respectively. The pH was monitored simultaneously in samples placed in a water bath kept at 25°C or determined after 21 h of incubation at ambient temperature. The final pH value of both WPI and ovalbumin gels was around 5. The gelation point was determined by means of small deformation measurements (see rheological section).

Turbidity measurements

Turbidity measurements were made at 25°C and at a protein concentration of 2% (w/w) on a Cary 1E UV-Vis spectrophotometer (Varian) equipped with a temperature controller. The turbidity was measured at 500 nm with time using cuvettes with a path length of 1 mm.

Scattering techniques

Small angle X-ray scattering (SAXS) measurements were made at the Dutch-Belgian beam-line (DUBBLE) at the European Synchrotron Radiation Facility at Grenoble (France). The energy of the beam was 12.2 keV (wavelength $\lambda = 1.015 \text{ \AA}$) and 8 keV (wavelength $\lambda = 1.55 \text{ \AA}$), the detector was a two-dimensional (512 x 512 pixels) gas-filled detector placed at 8 m distance. The scattering wave vector was between 0.1 and 1.0 nm⁻¹ (corresponding to a length scale between 6.3 and 62.8 nm in real space). The temperature of the samples was kept constant at 25°C.

Small angle neutron scattering was performed as described by Tuinier et al.²⁴ The scattering wave vector was between 0.015 and 0.75 nm⁻¹ (corresponding to a length scale between 8.4 and 42.4 nm in real space).

Small angle light scattering (SALS) experiments were done on a custom-built set-up.²⁹ The scattering wave vector was detected between 0.7 and 3.0 μm^{-1} (corresponding to a length scale between 2 and 9 μm in real space). The protein concentration of the samples was 2 % (w/w) in all cases; the temperature was kept at 25°C. The scattering pattern of the samples was recorded as a function of time during 20 h after the addition of GDL.

Confocal microscopy

Imaging was performed as described elsewhere.¹⁷ The protein gels were stained by applying 2 μl of an aqueous solution of 0.05% Rhodamine B. Confocal images were made of the cold-set WPI gels acidified for 24 h. Fast Fourier transform (FFT) spectra were made from these images, with a range between 0.81 and 160 μm^{-1} (corresponding to a length scale between 39 nm and 7.78 μm in real space).

Rheological measurements

Small-amplitude oscillatory measurements were made with a Carri-Med CLS² 500 rheometer (TA Instruments, Leatherhead, UK) using a sand-blasted (roughened) conical concentric cylinder measuring unit (inner radius 8.60 mm, outer radius 9.33 mm). Immediately after the addition of GDL, samples were brought into the concentric cylinder and covered with a thin layer of paraffin oil to prevent evaporation. All experiments were done in oscillation mode at a frequency of 1 rad s⁻¹ (0.159 Hz) and an applied strain of 1%, which is within the linear region. The formation of a gel network was monitored by the

development of the storage modulus (G') and loss modulus (G'') during 21 h at 25°C. The initial increase in G' was defined as the gelation point. The maximum linear strain was determined by a strain sweep experiment.

Gel hardness was determined by deformation under a compression force approximately 21 h after the addition of GDL, as described elsewhere¹⁷ by means of a texture analyzer (type TA-XT2, Stable Micro Systems Ltd., Godalming, England) equipped with a wire mesh-device.

Cryo-TEM of dispersions of aggregates

Cryo-transmission electron microscopy was done as described elsewhere,²⁶ using a Philips CM12 transmission electron microscope operating at 80 kV. Images were recorded digitally by a Gatan 791 CCD camera using the Digital Micrograph software package.

TEM of acid-induced cold-set gels

Samples of cold-set gels were fixed in 2.5 % glutaraldehyde for 1 h and stored in 0.25% glutaraldehyde at 4°C for 48 h. The fixed samples were rinsed in distilled water and dehydrated at ambient temperature in a graded series of acetone/water mixtures (70%, 80%, 96%) for 15 min each, followed by 100% acetone (2x30 minutes). An epoxy resin, EMBED 812, was infiltrated using graded mixtures of EMBED 812 and acetone in three steps of 1 h each. Final infiltration was done overnight in 100% epoxy resin. The samples were embedded in BEEM capsules and subsequently polymerized at 60°C for 48 h. After polymerization, thin sections were cut using a Leica Ultracut FCS ultramicrotome and collected on 100 mesh-Formvar-coated copper grids. The proteins on the grids were stained for 1 min with Reynold's lead citrate followed by 15 s of saturated uranyl acetate in distilled water. The grids were imaged using a Philips CM12 transmission electron microscope operating at 80 kV accelerating voltage.

8.3 RESULTS AND DISCUSSION

8.3.1 PREPARATION OF DISULFIDE CROSS-LINKED OVALBUMIN AGGREGATES

Protein aggregates of ovalbumin were prepared by heating solutions of native proteins at pH 7 and at low ionic strength. For WPI this resulted in dispersions of protein aggregates consisting of covalently cross-linked protein monomers.^{17,30} Agarose gel

electrophoresis in the presence of the denaturant SDS was used to demonstrate the formation of aggregates of covalently linked ovalbumin monomers under comparable conditions (Figure 8.1). Figure 8.1A shows that upon prolonged heating of a 3% (w/w) ovalbumin solution at 78°C, aggregates were formed that did not dissociate in the presence of SDS. Similar to WPI,¹⁷ the migration velocity of the protein band caused by the ovalbumin aggregates becomes similar to that of the ovalbumin monomers, after addition of DTT (Figure 8.1B). Since DTT is known to disrupt disulfide bonds, the electrophoresis results strongly indicated that, like the WPI aggregates, ovalbumin aggregates consisted of disulfide-linked ovalbumin monomers.

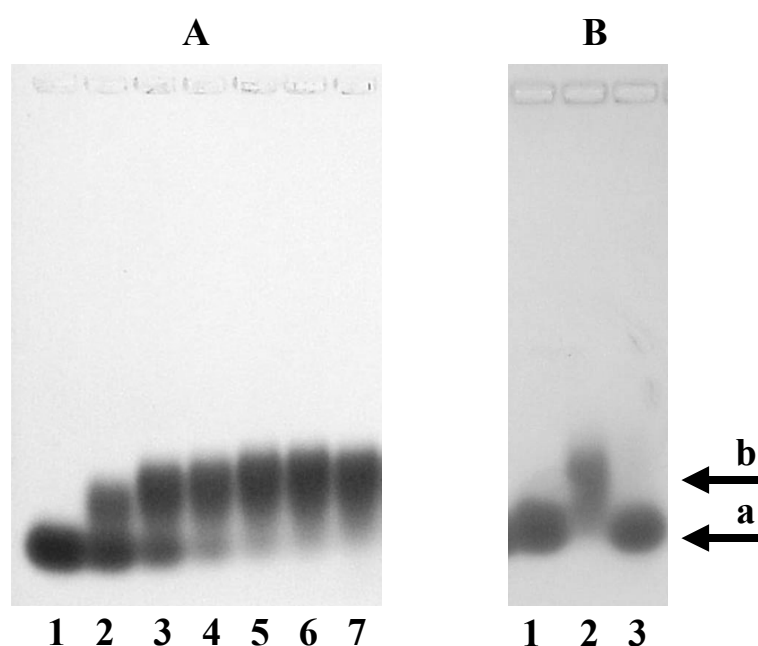


Figure 8.1. (A) SDS agarose gel electrophoresis of heated and unheated ovalbumin solutions (3 %, 78°C). Lane 1, unheated ovalbumin, lanes 2-7 ovalbumin heated for 30, 300 1026, 2683, 5000 min and for 8 days. (B) SDS agarose gel electrophoresis of ovalbumin aggregates with and without the addition of DTT. Lane 1: unheated ovalbumin (monomers), lane 2: ovalbumin aggregates (5 % protein 22 h 78°C) without DTT, lane 3: ovalbumin aggregates with DTT. Arrows a: protein monomers, arrow b protein aggregates.

The kinetics of denaturation and formation of internally disulfide cross-linked aggregates of ovalbumin were clearly different from that of WPI, where denaturation and formation of disulfide cross-linked aggregates under the applied conditions is reported to go hand in hand.³⁰ Figure 8.1A clearly shows that even after heating for 300 min the major part of the denatured ovalbumin has not been converted into aggregates consisting of

disulfide cross-linked monomers, whereas after 180 min of heating at 78°C more than 99% of the native ovalbumin molecules is denatured, insoluble at pH 4.6, and physically aggregated.³¹ Prolonged heating, up to 17 h, was required to form the covalent disulfide bonds in physically aggregated denatured ovalbumin molecules. Kitabatake et al.²² also found that in the early stage of aggregation non-covalent bonding played a major role instead of covalent disulfide bonding. Hence, for denatured ovalbumin, physical aggregation of monomers preceded the formation of internal disulfide bonds within these aggregates. With the aid of SDS-agarose electrophoresis, we determined the time needed at a temperature of 78°C to form aggregates consisting of covalently cross-linked monomers in which more than 90% of the ovalbumin participated. Independent of the protein concentration this time was 22 h (Table 8.1).

8.3.2 CHARACTERIZATION OF PROTEIN AGGREGATES

8.3.2.1 SIZE

In the present study, protein solutions were heated at two concentrations, one far below and one close to the reported gelation concentration.^{9,26,32} As reported elsewhere, the heat treatment of protein solutions at increasing initial protein concentrations resulted in protein aggregates with increasing hydrodynamic radii as determined by dynamic light scattering (Table 8.1).^{15,18,21,26,27} For both proteins the electrophoretic mobility depended on the protein concentration at heating and decreased with increasing protein concentration (not shown). Some caution is justified, because the apparent radii of the aggregates in solution were calculated from a standard cumulant fit of the auto-correlation function of the scattered intensity, assuming that the aggregates have a roughly spherical shape. Hence, these results are only indicative. Indeed, cryo-TEM observations demonstrated that the aggregates prepared did not have a spherical shape (see below).

8.3.2.2 SHAPE

Microstructural analysis by means of cryo-TEM showed (Figure 8.2; Table 8.1) that after heat treatment at low ionic strength, a pH around 7 and dependent on the protein concentration, aggregates were formed differing in shape and size, curved strand-like and long fibrillar aggregates for WPI^{18,20} and ovalbumin,^{21,26} respectively. Under the applied

Table 8.1. Characteristics of WPI and ovalbumin aggregates

<i>Sample^a</i>	<i>Heating conditions</i>	<i>Number of thiol Groups (mM)</i>	<i>Hydrodynamic radius (nm)^b</i>	<i>Contour length determined by cryo-TEM (nm)</i>	<i>Percentage denaturation^d (%)</i>
3% WPI	24 h 68.5°C	0.18	15	20-60	>95
9% WPI	2 h 68.5°C	0.34	38	40-100	>95
2% ova	22 h 78°C	0.26	12	30-150	>99
5% ova	22 h 78°C	0.40	35	400-700	

a Protein concentration given is the concentration at heating (w/w).

b The hydrodynamic radii were determined by means of dynamic light scattering, assuming that the aggregates have a roughly spherical shape.

c According to Alting et al.¹⁸ and Weijers et al.³¹

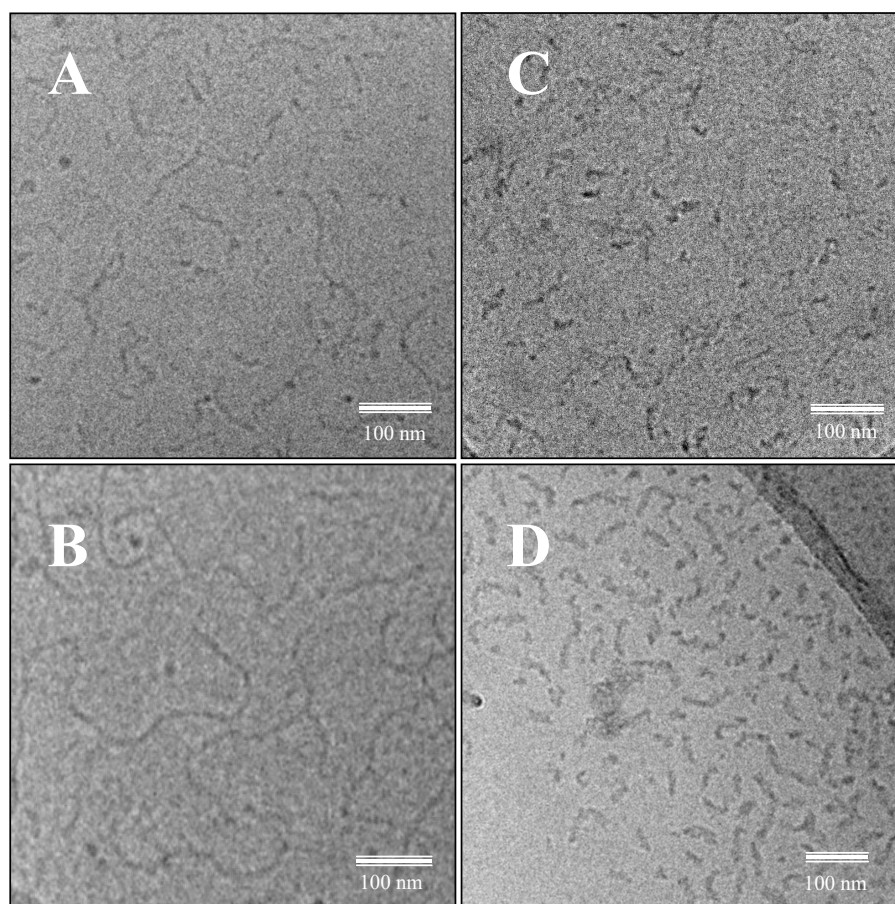


Figure 8.2. Cry-TEM micrographs of dispersions of aggregates heated at different protein concentrations (w/w). (A) 2.5% ovalbumin, 22 h 78°C; (B) 5% ovalbumin, 22 h 78°C; (C) 3% WPI, 24 h 68.5°C and (D) 9% WPI, 2 h 68.5°C.

conditions, both proteins had a net negative surface charge and formation of soluble linear aggregates is therefore promoted.³³

Note that the particle sizes as observed by cryo-TEM appeared to be significantly larger than those observed with dynamic light scattering (DLS), which can probably be explained by the elongated shape of the aggregates.

8.3.2.3 NUMBER OF EXPOSED THIOL GROUPS

Table 8.1 shows that at the point in time that 95-99% of the protein was aggregated into covalently linked monomers, a lower number of thiol groups was detectable for aggregates prepared at a lower initial protein concentration. For WPI this was explained by differences in the occurrence of oxidation or degradation reactions^{18,34,35} caused by a difference in heating time to reach 95% aggregation. The results of ovalbumin heated at different protein concentrations cannot be fully explained in this way, as these were heated for the same period of time. The blocking of the thiol groups by means of a treatment with NEM had no effect on the size as determined with both DLS and agarose electrophoresis for both the WPI and ovalbumin aggregates.

8.3.3 ACID-INDUCED COLD GELATION

Before gelation was induced by the addition of GDL, dispersions of aggregates prepared at various protein concentrations were diluted to a protein concentration of 2% (w/w). In water, GDL slowly hydrolyzes, yielding gluconic acid, which caused a gradual decrease of the pH and induces gelation of the dispersions of aggregates towards their iso-electric points. The resulting properties of the final cold-set ovalbumin gels such as the appearance and the large deformation mechanical properties clearly differed from cold-set WPI gels.

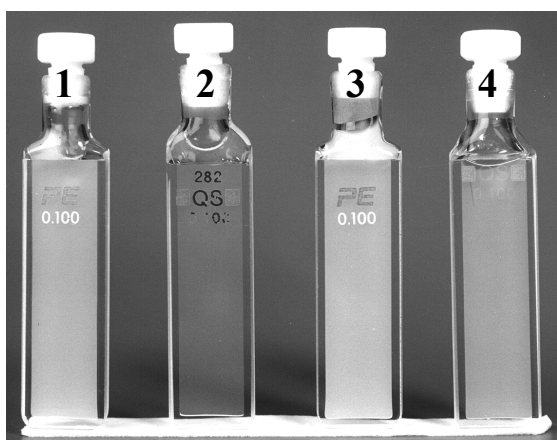


Figure 8.3. Appearance of cold-set gels (2% (w/w) protein) of ovalbumin and WPI.

- 1: WPI, initial protein concentration 9% (w/w).
- 2: Ovalbumin, initial protein concentration 5% (w/w).
- 3: WPI, initial protein concentration 3% (w/w).
- 4: Ovalbumin, initial protein concentration 2% (w/w).

8.3.4 APPEARANCE OF COLD-SET GELS

The ovalbumin gel prepared from a dispersion heated at a protein concentration of 2% is translucent and the gel prepared from a dispersion prepared at 5% (w/w) is transparent (Figure 8.3). On the other hand, both the WPI gels, prepared from dispersions initially heated at protein concentrations of 3% and 9% (w/w), were turbid (see also Table 8.2, $A_{500\text{nm}}$ after 21h). Kitabatake et al.²² also reported the formation of transparent ovalbumin gels using a different gelation method. Visually, treatment with NEM had no influence on the appearance, although small but reproducible differences in turbidity could be determined for WPI (Table 8.2), which is discussed elsewhere.¹⁹

Table 8.2. Rheological and scattering characteristics of acid-induced gelation of ovalbumin and WPI

<i>Sample</i>	<i>G' (21h)</i> (Pa)	<i>A_{500 nm}</i> (21 h)	<i>Initial increase</i> <i>in G' (Gelation</i> <i>point) (min)</i>	<i>Initial</i> <i>increase in</i> <i>A_{500 nm} (min)</i>	<i>pH at</i> <i>gelation</i>	<i>Maximum</i> <i>linear</i> <i>strain (%)</i>
9% WPI	680	0.57	235	200	5.48	55
9% WPI+NEM	663	0.70	240	230	5.57	14
3% WPI	399	0.80	323	263	5.52	11
3% WPI+NEM	435	0.86	300	246	5.59	8
5% ovalbumin	2980	0.045	130	114	5.82	22
5% ovalbumin + NEM	2960	0.044	130	115	5.78	17
2% ovalbumin	1093	0.23	185	169	5.65	11
2% ovalbumin + NEM	1050	0.22	210	195	5.70	11

Values given are average values. Measurements were done at least in duplicate with an experimental error lower than 10% and lower than 5% for WPI and ovalbumin, respectively.

8.3.5 LARGE DEFORMATION PROPERTIES

Figure 8.4 shows the force-distance curves of cold-set gels of both ovalbumin (Figure 8.4A) and WPI (Figure 8.4B) determined by gel penetration measurements. For cold-set gels of ovalbumin, we observed a clear effect of the protein concentration at heating on the gel hardness (Figure 8.4A). More force (approximately 6 times) had to be applied to penetrate gels prepared from dispersions heated at a protein concentration of 5% (w/w) than gels prepared from dispersions heated at 2% (w/w). Surprisingly, no effect of the thiol-blocking agent on gel hardness was observed. This suggests that instead of the ability

to form disulfide bonds, other aggregate characteristics, such as the shape will contribute to these differences.

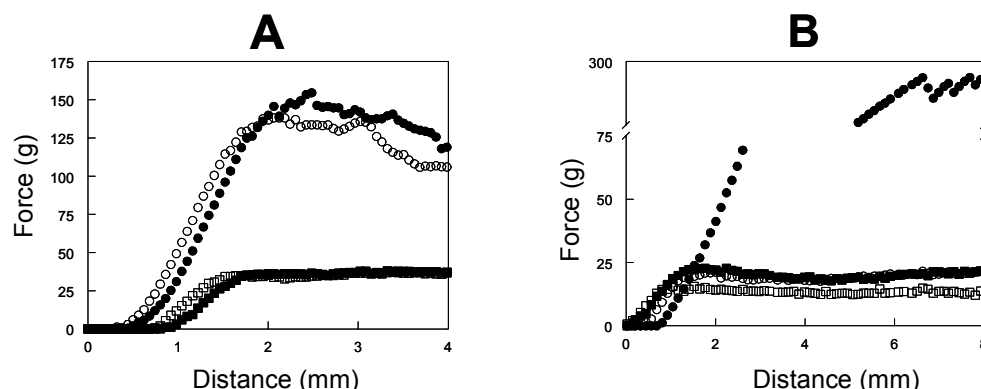


Figure 8.4. Effect of thiol-blocking on the large deformation properties of acid-induced cold-set gels of ovalbumin (A) and of WPI (B) at a protein concentration of 2% (w/w) after 24 h of acidification. The circles represent the higher initial protein concentrations at heating, 5% (w/w) and 9% (w/w) for ovalbumin and WPI, respectively. The squares represent the low initial protein concentrations at heating, 2% (w/w) and 3% (w/w), for ovalbumin and WPI, respectively. The closed symbols represent the untreated aggregates, the open symbols the NEM-treated aggregates. Note that there is break in the y-ordinate in Figure 8.4B.

As reported previously,^{17,18} 2% (w/w) cold-set WPI gels of dispersions initially heated at 9% (w/w) protein were approximately 10 times stronger than gels prepared from dispersions initially heated at 3% (w/w) protein (Figure 8.4B). There, we concluded that the hardness of cold-set WPI gels, in contrast to ovalbumin, is determined by the number of thiol groups rather than by the size of the aggregates or other structural features. Figure 8.4B shows that indeed only a minor effect of the difference in hydrodynamic diameter (Table 8.1) on the gel hardness remained, if the thiol groups present on the surface of the WPI aggregates were chemically blocked.

To determine the effect of structural properties (size or shape) of protein aggregates on gel hardness, cold-set gels prepared from aggregates treated with a thiol-blocker were compared. The effect of the initial protein concentration at heating on gel hardness was much larger for ovalbumin (approximately 600%) than for WPI (approximately 20%). This significant difference cannot be merely explained by differences in the number of elastic effective junctions, which directly relate to the value of G' . The effects of the initial protein concentration on small deformation properties were much smaller (see below). The results can possibly be explained by the formation of entanglements in the case of significantly longer fibrils (40-60 versus 500 nm) in the case of ovalbumin.

8.3.6 STRUCTURAL PROPERTIES

In Figure 8.5, the SAXS patterns are shown for the acid-induced cold gelation of ovalbumin. Before acidification, a clear peak was observed, corresponding to an ordering of aggregates with a typical inter-particle distance of approximately 26 nm, that shifted towards lower q -values upon acidification. Simultaneously, broadening of the peak was observed and finally the peak disappeared, which indicated that the dominant length scale (inter-particle distance), present before acidification, disappeared. Comparable results were found on the addition of an increasing amount of sodium chloride (results not shown).

Furthermore, no significant differences between the SAXS patterns of untreated and NEM-treated aggregates were observed during the acidification. For WPI the same results were obtained, but at a significantly higher protein concentration (higher than 6% (w/w)) than for ovalbumin (2% (w/w)), by the use of both SAXS and SANS. At a protein concentration of 9%, typical inter-particle distances of approximately 25 nm and 26 nm were observed for WPI-aggregates by the use of SANS and SAXS, respectively.

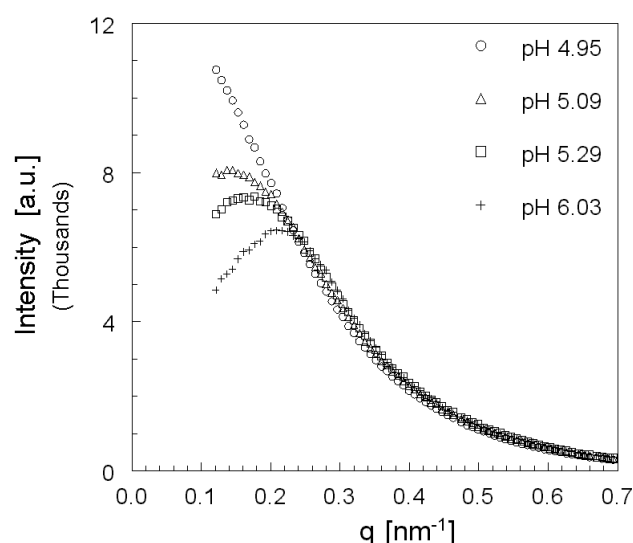


Figure 8.5. Evolution of the SAXS pattern of a 4% (w/w) solution of ovalbumin aggregates during acidification.

The SAXS measurements also showed that after a gel is formed at a certain pH (see also Table 8.2), the structure continued to change upon lowering the pH. This suggests that once a gel was formed, structural rearrangements still took place. These observations were

confirmed by small deformation and turbidity measurements that continued to increase even after the final pH was reached (see below).

SALS measurements of ovalbumin aggregates in solution showed no dominant length scale. During acid-induced gelation an increase in scattering intensity, which was not q -dependent in the wave vector range measured, was observed, but no dominant length scale was observed. Similar results were obtained for WPI, which were consistent with the confocal microscopy results for WPI described below. The protein structures in the transparent ovalbumin gels could not be visualized probably because these structures were smaller than the resolution of the microscope.

Confocal images were made of the cold-set WPI gels 24 h after GDL addition. No difference was observed in the 2D Fourier spectra of confocal images of gels formed from aggregates with or without thiol-blocking treatment. Furthermore, no dominant length scale was observed in this range; therefore we concluded that both the ovalbumin and WPI cold-set gels were homogeneous at the length scales probed (over a range of 6.3 nm to 9 μm in real space).

8.3.7 SMALL DEFORMATION AND SCATTERING PROPERTIES

Figure 8.6 shows representative results of the development with time of the storage modulus (G'), the turbidity (absorbance at 500 nm) and the pH during acidification of dispersions of both ovalbumin (Figure 8.6A) and WPI (Figure 8.6B) aggregates, with and without NEM treatment. In Table 8.2, the results are summarized in six parameters, namely the G' after 21 h, the turbidity after 21 h, point in time of the initial increase in G' (gelation point), point in time of the initial increase in turbidity, the pH at the gelation point and the maximum linear strain.

Since the acidification curves (pH versus time) of the two proteins were almost identical, results were compared on a time scale instead of a pH scale. There seems to be a relation between the length of the protein aggregates and the point of gelation, defined as the initial increase in G' . Long fibrils (ovalbumin, initially heated at 5% (w/w)) showed the earliest point of gelation in time and the shortest linear aggregates (WPI, initially heated at 3% (w/w)) showed the latest point of gelation at the same protein concentration. NEM treatment had no significant effect on the gelation point in all cases.

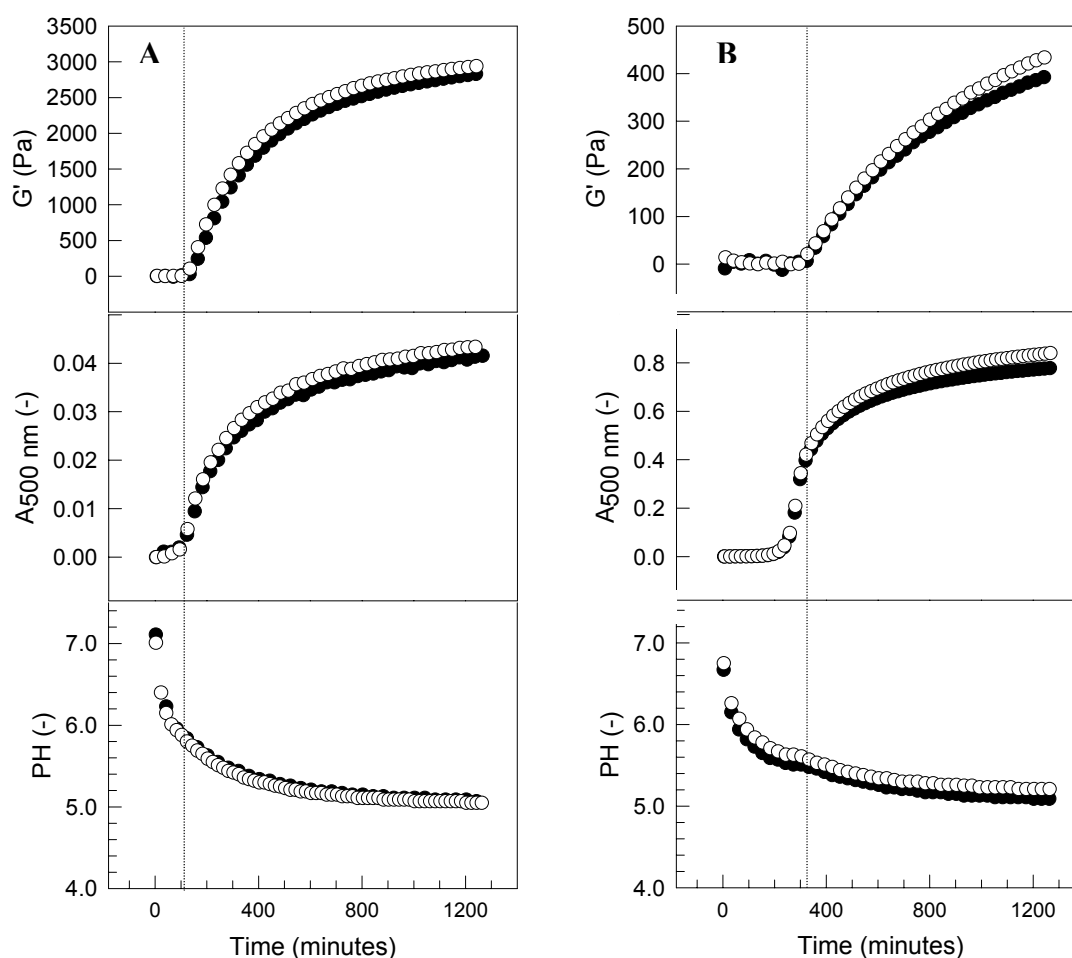


Figure 8.6. Development of the storage modulus (G'), the turbidity (expressed as $A_{500 \text{ nm}}$) and the pH with time for ovalbumin, initially heated at 5% (w/w) (A) and for WPI, initially heated at 3% (w/w) (B) after the addition of GDL. The closed symbols represent the untreated aggregates, the open symbols the NEM-treated aggregates. Note that the y-ordinate values are different for (A) and (B).

The G' value reached 21 h after the addition of GDL increases from about 400 Pa for the shortest linear aggregates to approximately 3000 Pa for the longest linear aggregates. G' and G'' developed concurrently with time, G' being dominant over the whole time scale measured. $\tan \delta$ (G''/G') was the same (0.13-0.15) for all systems. For gel systems, this value indicates that the visco-elastic gel systems still contained a significant viscous part (G''). NEM treatment of the aggregates had only a minor effect on the development of the storage modulus (G').

To explain the formation of disulfide bonds and the effect of that on the large deformation properties of acid-induced cold-set WPI gels, we previously^{3,17-19} postulated that, first a protein network was formed by physical interactions, which was subsequently

stabilized by the formation of disulfide bonds. Here we extended this model (Figure 8.7) and explained the large differences in G' and turbidity of the various protein systems by differences in overlap concentration. Cold gelation was induced by reduction of electrostatic repulsion between aggregates.³ In the case of relatively short linear aggregates (Figure 8.7 upper panels) the aggregates were too small to percolate directly. In this case, the aggregates first became organized in clusters, which were subsequently able to form a space-filling network. This was supported by viscosity measurements (Table 8.3) and by the observation that shorter linear aggregates (WPI 3% (w/w)), showed an increase in turbidity, indicating an increase in aggregate size, before a gel was formed. The number of junctions between the clusters will mainly determine the small deformation properties (in linear region) of the final gels.

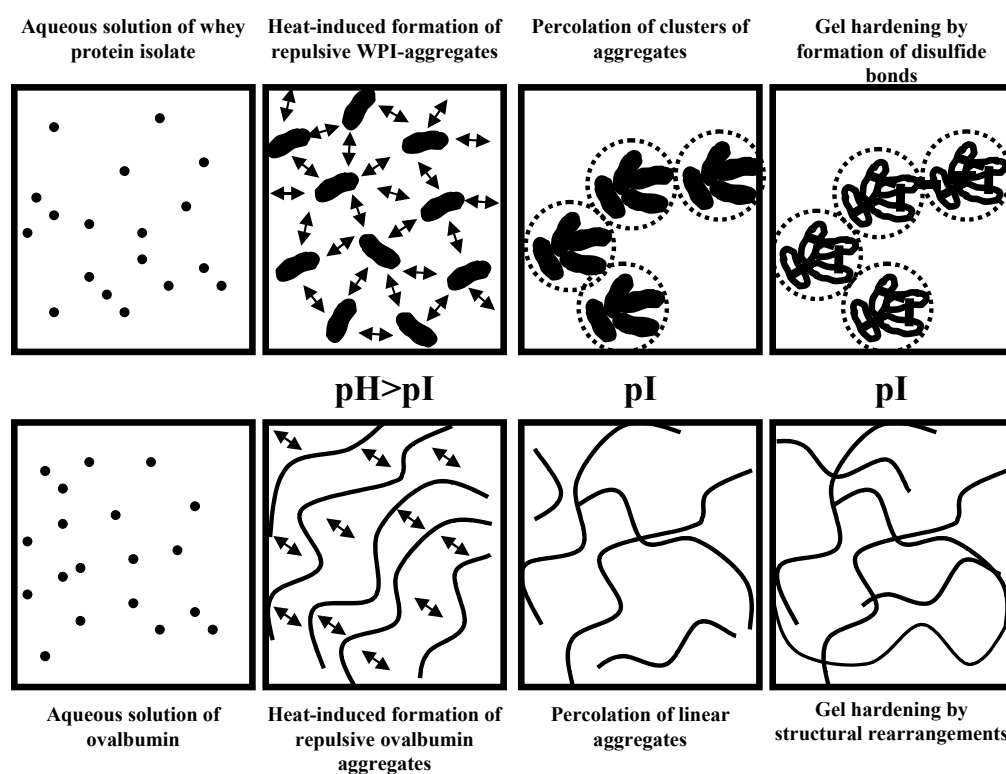


Figure 8.7. Schematic representation of the acid-induced cold gelation of small (upper panels) and long (lower panels) linear protein aggregates.

In the case of relatively long linear aggregates (Figure 8.7 lower panels), formation of a space-filling network occurred immediately after reduction of electrostatic repulsion, resulting in shorter gelation times. In contrast to the short linear WPI aggregates, SAXS measurements showed that the long ovalbumin aggregates maintained a typical inter-

Table 8.3. Intrinsic viscosity and voluminosity of ovalbumin and WPI aggregates by heating at different protein concentrations

<i>Protein concentration at heating (%)</i>	<i>Intrinsic viscosity of the aggregates (ml/g)</i>	<i>Voluminosity of the aggregates(ml/g)</i>
WPI 3%	20	7.3
WPI 9%	47.3	21.5
OVA 2%	23.9	10.2
OVA 5.5%	205	80.8

particle distance at this protein concentration caused by electrostatic repulsion. By the reduction of the repulsion, these aggregates were able to directly form a space-filling network by physical interactions such as hydrophobic interactions and van der Waals attraction. It is known that a protein gel cannot consist of solely entanglements between the structure elements. In addition no nematic liquid crystalline phases were observed and no disulphide bonds were formed. Therefore, we may conclude that most of the junctions between the individual fibrils will contribute to the small deformation properties, which explain the higher G' values found for this homogeneous protein gel. The increase of G' with time, once the final pH is reached, can be explained by the occurrence of structural rearrangements, leading to more junctions. Viscosity measurements on the long fibrillar aggregates (Table 8.3) showed a tremendous increase in intrinsic viscosity and voluminosity of ovalbumin fibrils, initially heated at high ovalbumin concentrations. These results strongly suggest that increased voluminosity (contour length and rigidity) of the fibrillar aggregates leads to shorter gelation times and increased G' .

The maximum linear strain for WPI initially heated at 9% (Table 8.2) was significantly larger than for the other samples. Reduction of the number of thiol groups, either by chemical blocking or by heating at relatively low protein concentration resulted in a clear reduction of the maximum linear strain. For ovalbumin, the effect of NEM was not significant. However, the maximum linear strain did vary with the size of the ovalbumin aggregates. These results are in good agreement with those obtained from the penetration experiments.

8.3.8 TEM OF ACID-INDUCED PROTEIN GELS

Figure 8.8 shows TEM micrographs of cold-set gels prepared from protein solutions initially heated at different concentrations. TEM micrographs confirmed our postulated model (Figure 8.7). WPI gels prepared from an initial protein concentration of 3%

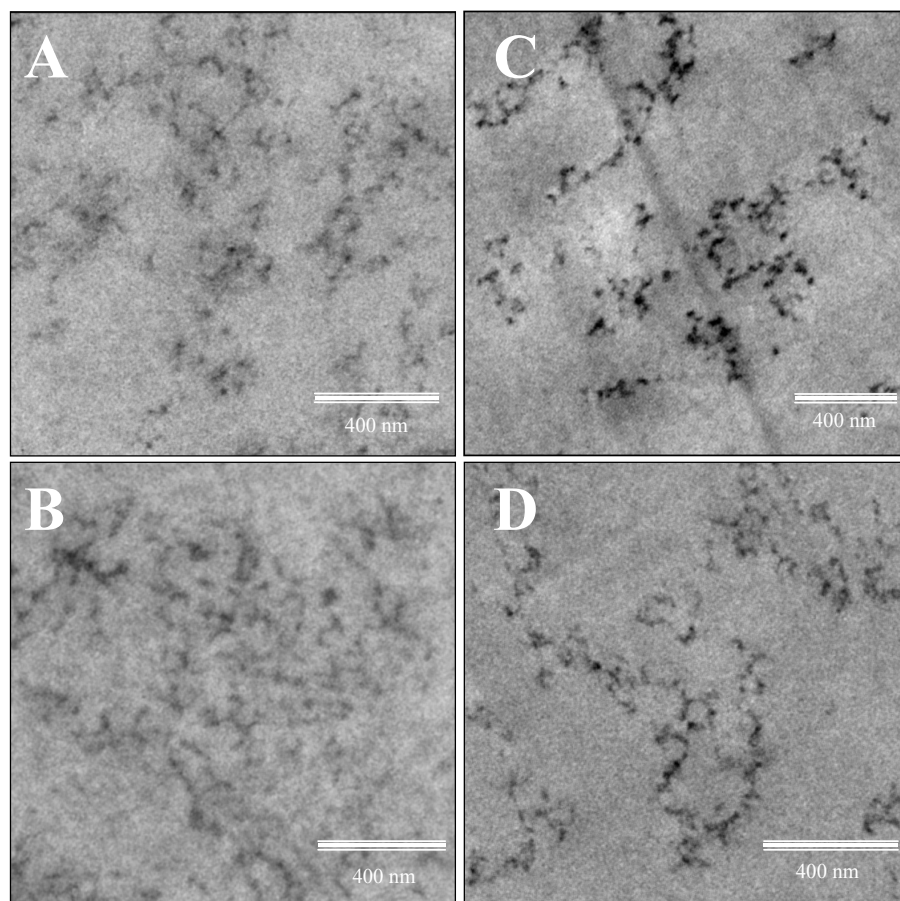


Figure 8.8. TEM micrographs of 2% (w/w) cold-set protein gels of ovalbumin and WPI initially heated at different protein concentrations (w/w). Ovalbumin, 2% (A), ovalbumin, 5% (B), WPI, 3% (C) and WPI, 9% (D).

(Figure 8.8c) clearly shows clusters of small aggregates, this is less pronounced for WPI gels prepared from an initial protein concentration of 9%, which shows less dense structures (Figure 8.8d). As expected, gels prepared from ovalbumin fibrils show a much more homogeneous structure (Figures 8.8b). The effect of NEM on gel structure was determined for WPI gels, and showed no difference with the control. Note that these micrographs were taken from cross-sections through the gel and not from a thin film as in the cryo-TEM measurements, therefore long fibrillar structures as observed in Figure 8.2 cannot be observed.

8.3.9 DETERMINATION OF DISULFIDE CROSS-LINKING IN ACID-INDUCED GELS

Finally, to observe differences in the size of the protein structures before and after acid-induced gelation, SDS-agarose electrophoresis was applied (Figure 8.9). The acid-induced ovalbumin gels dissolved more easily in the SDS-containing electrophoresis buffer than

the WPI gels. Unexpectedly, but in agreement with the rheological results, electrophoresis of cold-set gels of ovalbumin did not reveal changes in electrophoretic mobility after gelation (Figure 8.9; lanes 5-8). The results of the electrophoretic analysis clearly demonstrated that no disulfide cross-linked structures were formed during the cold gelation of ovalbumin aggregates, although these contained reactive thiol groups.

As reported previously for cold-set gels of WPI,^{17,18} disulfide cross-linked protein structures were formed during gelation in the absence of the thiol-blocker NEM. The structures had a clearly decreased electrophoretic mobility (increased size) compared to the electrophoretic mobility of the initial aggregates (before gelation) (Figure 8.9; lanes 1 and 3). The differences in electrophoretic mobility observed between gels prepared from WPI aggregates heated at initial protein concentrations of 3% and 9% were explained by the difference in the number of the thiol groups and therefore in a difference in ability to form disulfide cross-links.¹⁸ In the presence of NEM, no decrease was observed in electrophoretic mobility (lanes 2 and 4), and the mobility was identical to that before gelation.

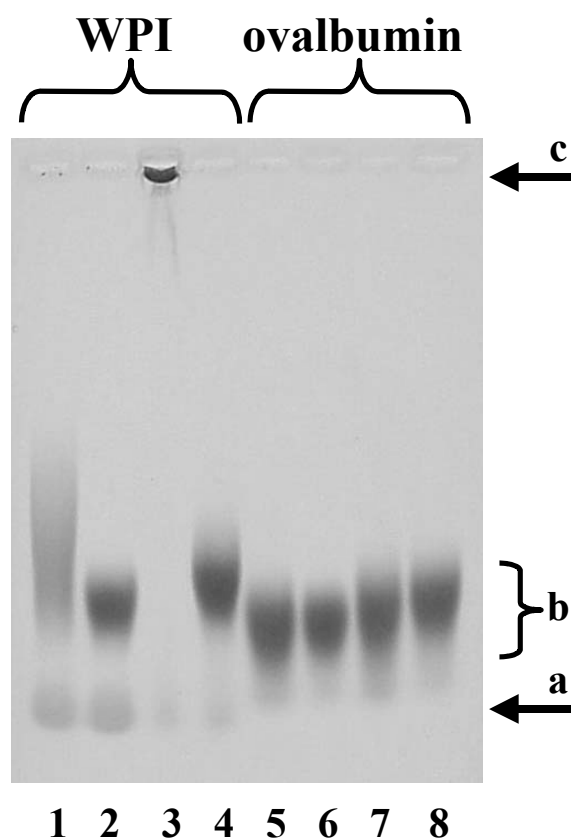


Figure 8.9. SDS agarose gel electrophoresis of, in SDS-containing buffer, redissolved cold-set gels of untreated and NEM-treated WPI (lanes 1-4) and ovalbumin (lanes 5-8).

Lane 1: 3% untreated WPI, lane 2: 3% NEM-treated WPI. Lane 3: 9% untreated WPI, lane 4: 9% NEM-treated WPI, lane 5: 2% untreated ovalbumin, lane 6: 2% NEM-treated ovalbumin, lane 7: 5% untreated ovalbumin and lane 8: 5% NEM-treated ovalbumin.

The protein concentrations given are the concentrations at heating (w/w). Arrow a: protein monomers, arrow b: protein aggregates, arrow c: protein structures that are unable to enter the agarose matrix.

Formation of disulfide bonds during the acid-induced gelation is of crucial importance for the properties of cold-set WPI gels.¹⁷ However, the results of large deformation experiments and the SDS-agarose electrophoresis presented here clearly show that during the acid-induced cold gelation of ovalbumin no additional disulfide bonds were formed, although such bonds did form during the preparation of the ovalbumin aggregates. An explanation might be found in the accessibility of the disulfide bond in ovalbumin. Different ways for the formation or reduction of disulfide bonds are known, but the one that normally takes place in the aggregation of proteins is the thiol-disulfide exchange reaction.^{18, 36, 37, 38, 39} As measured by the use of the Ellman's reagent, the thiol groups of the cysteine-residues were accessible for reaction after the heat-induced preparation of ovalbumin aggregates. In contrast, the accessibility of the disulfide bond can be different at conditions during heating (78°C and pH 7.2) compared to the conditions during gelation (ambient temperature and pH 5), due to (reversible) conformational changes of the ovalbumin molecule. The decreased accessibility of the disulfide bond will prohibit disulfide cross-linking during gelation. Legowo et al.⁴⁰ observed that the addition of α -lac, a protein containing four disulfide bonds, significantly increased the hardness of heat-set ovalbumin gels. This also confirms that the thiol group of ovalbumin is available for reaction and that the disulfide bonds in α -lac are accessible for reaction with the heat-exposed thiol groups of ovalbumin, in contrast to the one in ovalbumin. Indeed, Legowa et al.⁴⁰ demonstrated the contribution of the Cys6-Cys120 disulfide bond of α -lac in the interaction between α -lac and ovalbumin.

Note that WPI is a mixture of proteins. It mainly consists of β -lg, but the second major protein is α -lac. Although formation of disulfide bonds was observed in acid-induced cold-set gels of pure β -lg,³ it was reported that WPI yields stronger gels after induction by high-pressure treatment and that this also caused by the incorporation of α -lac in the protein network.⁴¹ The same effect was observed in heat-induced gels of β -lg.⁴²⁻⁴⁴

8.4 CONCLUSIONS

For both protein preparations, ovalbumin and WPI, repulsive aggregates were made consisting of disulfide cross-linked monomers. Both type of aggregates possessed exposed thiol groups at their surface (Figure 8.7). At pH 7, the aggregates of both WPI and ovalbumin had a net negative charge and typical inter-particle distances in the nm range

were observed using different scattering techniques. This distance scaled with the protein concentration. If the net charge of the aggregates approached neutrality the characteristic length scale observed before gelation disappeared and over a wide range of length scales (nm to μm) no other characteristic length scale could be observed. Cold-set gels were formed by reduction of the electrostatic repulsion.¹⁸ Therefore we concluded that during this process the protein system changed from an ordered into a more randomly organized structure. Since formation of the microstructure, as a result of the reduction of electrostatic repulsion, did not depend on aggregate characteristics, it can be defined as a non-protein-specific mechanism and therefore this mechanism will apply to any type of protein aggregate that is acidified towards its iso-electric point.

Differences in size and shape of the protein aggregates were found to influence small deformation properties of protein gels. Longer aggregates have a lower overlap concentration, which causes gelation to commence earlier and results in more effective junctions, yielding higher G' values.

Covalent bonds are the main determinants of the gel hardness. The formation of additional disulfide bonds after gelation not only depends on the number of thiol groups, but also on the number and accessibility of disulfide bonds in the molecule and may differ significantly from one protein to another. However, in the absence of covalent bonds long fibrillar structures can also contribute significantly to gel hardness.

ACKNOWLEDGEMENTS

Marcel Paques and Johan Hazekamp are thanked for their contribution to the (cryo)-TEM measurements, Igor Dolbnya and Wim Bras for their technical assistance at the DUBBLE in Grenoble and Roland Wientjes for his helpful advice concerning the rheological measurements and Ton van Vliet for fruitful discussions. The Netherlands organization for the advancement of research (NWO) is acknowledged for providing the possibility and financial support for performing measurements at the DUBBLE.

REFERENCES

1. Barbut, S., Foegeding, E.A. (1993). *J. Food Sci.*, 58, 867.
2. Bryant, C.M., McClements, D.J. (1998). *Trends Food Sci. Technol.*, 9, 143.
3. Alting, A.C., de Jongh, H.J.J., Visschers, R.W., Simons, J.F.A. (2002). *J. Agric. Food Chem.*, 50, 4674.

4. Vreeker, R., Hoekstra, L.L. den Boer, D.C., Agterof, W.G.M. (1992). *Food Hydrocolloids*, 5, 423.
5. Sato, K., Nakamura, M., Nishiya, M., Kawanari, M., Nakajima, I. (1995). *Milchwissenschaft*, 50, 389.
6. Roff, C.F., Foegeding, E.A. (1996). *Food Hydrocolloids*, 10, 193.
7. Hongsprabhas, P., Barbut, S. (1996). *Food Res. Int.*, 29, 135.
8. Hongsprabhas, P., Barbut, S. (1997). *Int. Dairy J.*, 7, 827.
9. Hongsprabhas, P., Barbut, S. (1997). *J. Food Sci.*, 62, 382.
10. Hongsprabhas, P., Barbut, S. (1997). *Lebensm.-Wiss. U.-Technol.*, 30, 45.
11. Hongsprabhas, P., Barbut, S. (1997). *Food Res. Int.*, 30, 451.
12. Hongsprabhas, P., Barbut, S., Marangoni A.G. (1999). *Lebensm.-Wiss. U.-Technol.*, 32, 196.
13. Elofsson, C., Dejmek, P., Paulsson, M., Burling, H. (1997). *Int. Dairy J.*, 7, 601.
14. Ju, Z.Y., Kilara, A. (1998). *J. Agric. Food Chem.*, 46, 1830.
15. Ju, Z.Y., Kilara, A. (1998). *J. Agric. Food Chem.*, 46, 3604.
16. Kinekawa, Y-I., Foyuki, T., Kitabatake, N. (1996). *J. Dairy Sci.*, 81, 1532.
17. Alting, A.C., Hamer, R.J., de Kruif, C.G., R.W. Visschers. (2000). *J. Agric. Food Chem.*, 48, 5001.
18. Alting, A.C., Hamer, R.J., de Kruif C.G., Paques, M., Visschers, R.W. (2003). *Food Hydrocolloids*, 17, 469.
19. Alting, A.C., Hamer, R.J., de Kruif, C.G., Visschers, R.W. (2003). *J. Agric. Food Chem.*, 51, 3150.
20. Le Bon, C. (2001). These, Université du Maine, France.
21. Koseki, T., Kitabatake, N., Doi, E. (1989). *Food Hydrocolloids*, 3, 123.
22. Kitabatake, N., Hatta, H., Doi, E. (1987). *Agric. Biol. Chem.*, 51, 771.
23. Mine, Y., Noutomi, T., Haga, N. (1990). *J. Agric. Food Chem.*, 38, 2122.
24. Tuinier, R., Dhont, J. K. G., De Kruif, C. G. (2000). *Langmuir*, 16, 1497.
25. Vachier, M.C., Piot M., Awedé, A.C. (1995). *J. Chromatogr. B*, 66: 201.
26. Weijers, M., Visschers, R.W., Nicolai, T. (2002). *Macromolecules*, 35, 4753.
27. Hoffmann, M.A.M., Van Mil, P.J.J.M (1997). *J. Agric. Food Chem.*, 45, 2942.
28. Ellman, G.L. (1959). *Arch. Biochem. Biophys.*, 82, 70.
29. De Hoog, E. H. A., Tromp, R. H. (2003). *Colloids and Surfaces A. Physiochem. and Eng. Asp.*, 213, 221.
30. Roefs, S.P.F.M., De Kruif, C.G. (1994). *Eur. J. Biochem.*, 226, 883-889.
31. Weijers, M., Barneveld, P.A., Cohen Stuart, M.A.; Visschers, R.W. (2003). *Protein Science*, 12, 2693.
32. Otte, J., Ju, Z.Y.; Skriver, A., Qvist, K.B. (1996). *J. Dairy Sci.*, 79, 782.
33. Doi, E. (1993). *Trends Food Sci. Technol.*, 4, 1.
34. Nashef, A.S., Osuga, D.T., Lee, H.S., Ahmed, A.I., Whitaker, J.R., Feeney, R.E. (1977). *J. Agric. Food Chem.*, 25, 245.
35. Watanabe, K., Klostermeyer, H. (1976). *J. Dairy Res.*, 43, 411.
36. Creighton, T.E. (1978). *Prog. Biophys. Mol. Biol.*, 33, 231.
37. Saxena, V.P., Wetlaufer, D.B. (1970). *Biochem.*, 9, 5015.

38. Shimada, K., Cheftel, J.C. (1989). *J. Agric. Food Chem.*, 37, 161.
39. Monahan, F.J., German, J.B., Kinsella, J.E. (1995). *J. Agric. Food Chem.*, 43, 46.
40. Legowo, A.M., Imade, T., Yasuda, Y., Okazaki, K., Hayakawa, S. (1996). *J. Food Sci.*, 61, 281.
41. Ipsen, R., Olsen, K., Skibsted, L.H., Qvist, K.B. (2002). *Milchwissenschaft*, 11/12, 650.
42. Rojas, S.A., Goff, H.D., Senaratne, V., Dagleish, D.G., Flores, A. (1997). *Int. Dairy J.*, 7, 79.
43. Matsudomi, N., Oshita, T., Sasaki, E., Kobayashi, K.(1992). *Biosci. Biotechnol. Biochem.*, 56, 1697.
44. Legowo, A.M., Imade, T., Hayakawa, S. (1993). *Food Res. Int.*, 26, 103.



CHAPTER 9

STRUCTURE AND RHEOLOGICAL PROPERTIES OF ACID-INDUCED
EGG WHITE PROTEIN GELS

Weijers, M., Velde van de, F., Stijnman, A., Pijpekamp van de, A.M., and Visschers, R.W.
Food Hydrocolloids 2004, accepted

Food Hydrocolloids 2004, accepted

ABSTRACT

This study compares the rheological properties of acid-induced gels prepared of industrial spray-dried egg white proteins (EWP) with the acid-induced gels prepared of ovalbumin (OA) and whey protein isolate (WPI). Also we aimed to form transparent gels of EWP by means of the cold-gelation process. We showed that it was not possible to prepare cold-set gels because ovotransferrin (OT) was found to interfere with fibril formation. Therefore, we developed a new purification method in which first OT was selectively denatured by a heating step, subsequently precipitated by acidification and removed by centrifugation. Finally, the supernatant was desalted by ultra filtration. This resulted in a preheated EWP preparation which mainly contains OA (>80%). By removing OT using this new preheat procedure transparent gels were obtained after acid-induced gelation. Fracture properties of various EWP preparations were determined and compared with the fracture properties of acid-induced gels of OA and WPI. Gels formed from different EWP preparations were weak (fracture stress 1-15 kPa, fracture strain 0.3-0.7), and the networks were consisted of thin strands with hardly any additional disulphide bonds formed during the gelation step. In conclusion, the microstructure of the aggregates formed in the first step of the cold-gelation process and the additional disulphide bonds formed during the second step appeared to be the determining factors contributing to the hardness and deformability of acid-induced gels of egg white proteins.

9.1 INTRODUCTION

Consumers continuously demand more tasty, natural, healthy, convenient and new (e.g. transparent) food products. Fracture properties are important because the perception of texture is in part an evaluation of fracture properties when a gel-type food is consumed.¹ Texture is a quality parameter and generated in several foods by protein structures. Therefore, improving protein structures can provide an answer on constant requests for innovation. Typical food proteins of interest include proteins derived from milk, soy, fish and egg, and are used in a number of foods including beverages, confectionary, desserts, dairy products and meat and fish products.

In traditional food applications, protein solutions are heated at relatively high temperatures ($>60^{\circ}\text{C}$) to induce denaturation. Heating above a critical gelation concentration or percolation threshold, C^* , results in the formation of gelled systems, whereas heating below C^* thickens solutions but does not cause gelation. The application of heat-induced gelation has limitations or is not always desired.² For instance, heat gelation is relatively simple and fast, but not 100% efficient, cold gelation is more complex but the gelation process is easier to control, more efficient and an advantage might be that heat-labile or volatile compounds can be added (in the gelation step) without any losses or off-flavor occurring.

The formation of acid-induced cold-set gels involves two stages. In the first stage, the preparation of a heat-denatured protein solution of soluble aggregates occurs at neutral pH and low ionic strength. In the second step, at ambient temperature, gelation is induced by changing the pH towards the iso-electric point of the protein, because this reduces the electrostatic repulsion between the aggregates and therefore promotes the formation of a percolation network.^{3,4} Dependent on the type of aggregates produced in the first stage, different gel network structures and rheological properties can be obtained. Bryant et al. (1998) published a clearly described and complete overview on cold-set gels derived from heat-denatured whey proteins. We previously reported the formation of transparent cold-set gels of ovalbumin (OA), whereas whey protein isolate (WPI) forms turbid gels. Since purified OA is not food grade available, industrial egg white powder was used. These preparations were not able to form cold-set gels, since they already formed turbid gels at low protein concentration, because of the ionic strength in egg white powders is relatively high. Recently, we filled a patent which describes the procedure to prepare transparent gels

Table 9.1. Overview of egg white protein composition and molecular properties. The references of this table are presented in Chapter 1.

<i>Protein</i>	<i>% (w/w)</i>	<i>pI</i>	<i>M_w (kDa)</i>	<i>T_d (°C)</i>	<i>Cysteines</i>	<i>-SH</i>	<i>S-S</i>
<i>Ovalbumin</i>	54	4.5-4.9	45	75-84	6	4	1
<i>Ovotransferrin</i> (<i>conalbumin</i>)	12-13	6.0-6.1	77.7	61-65 (76,5, Al ³⁺)	30	-	15
<i>Ovomucoid</i>	11	4.1	28	77	18	-	9
<i>Ovomucin</i>	1.5-3.5	4.5-5.0	110, 5500-8300, 220-270000		(2)	-	
<i>Lysozyme</i>	3.4-3.5	10.7	14.3-14.6	69-77	6		4
<i>G2 ovoglobulin</i>	1.0	4.9-5.5	47-49				
<i>G3 ovoglobulin</i>	1.0	4.8, 5.8	49-50				
<i>Ovoflavoprotein</i>	0.8	4.0	32-35, 80		5		2
<i>Ovostatin</i>	0.5	4.5-4.7	760-900				
<i>Cystatin</i>	0.05	5.1	12				
<i>Avidin</i>	0.05	10.0	55-68.3		2		1

from industrial egg white powder.⁵ This opens new possibilities for applications in food products. This paper describes the molecular background of the patent and compares the rheological properties of acid-induced gels prepared of industrial spray-dried egg white proteins (EWP) with the acid-induced gels prepared of ovalbumin (OA) and whey protein isolate (WPI).

Similar to WPI, egg white powder consist of a mixture of proteins, of which OA is the most predominant (~54%), followed by ovotransferrin (OT, ~12%) and ovomucoid (OM, ~11%) (Table 9.1). The composition and properties of the egg white have been extensively described in literature.⁶⁻¹¹ Also, interactions between the various purified proteins present in egg white during heating are published.¹²⁻¹⁸ Here aggregate properties are discussed by means of turbidity measurements and SDS-PAGE analysis. However, the influence of OT on the fibril formation of OA has not been described so far and is of major importance to produce transparent gels by means of acid-induced gelation.

Large strain rheological measurements were performed to characterize the fracture properties of acid-induced egg white protein gels and compared with known behaviour of WPI gels. In general, fracture stress reflects hardness and strain reflects deformability or brittleness of gels. Previous publications on WPI gels revealed that gels that fracture at low strain values have networks composed of relatively thin strands and small homogeneous

pores, whereas gels which fracture at high strain values are composed of thicker strands and relatively large homogeneous pores.¹⁹ For WPI gels it was demonstrated that fracture stress and strain can be influenced by the presence of disulphide bonds.^{20,21} However, it is not clear what the effect of microstructure and disulphide bonding is on the turbidity and rheological properties of acid-induced gels of EWP.

The main objective of this study was to investigate the molecular background of the formation of transparent cold-set gels prepared from industrial egg white protein as was filled in a patent.⁵ We investigated the effect of protein composition in egg white proteins on fibril formation and its gelation properties and we provide a new simple procedure to prepare acid-induced cold-set gels from industrial spray-dried egg white proteins. Additionally, we compared network structures, disulphide bonding in acid-induced gels and the fracture properties between egg white protein gels and WPI gels.

9.2 MATERIALS AND METHODS

9.2.1 REAGENTS AND CHEMICALS

Hen egg white powder (high pH, EWP) was obtained from Enthoven (Raalte, The Netherlands). The purified proteins OA (grade III, lot 022K7068), OT (C0755), LZ (L6876) were obtained from Sigma, OM (93621) was purchased from Biochimika, and were used without further purification. Glucono- δ -lactone (GDL, USP), 5,5'-dithiobis-(2-nitrobenzoic acid) (DTNB), sodium dodecylsulphate (SDS), *N*-ethylmaleimide (NEM) and Rhodamine B were obtained from Sigma Chemicals (St. Louis, MO, USA). Electrophoresis-grade agarose was obtained from Life Technologies (Paisley, Scotland). Phastgel Blue R tablets were from Pharmacia Biotech (Uppsala, Sweden). All reagents were of analytical grade.

9.2.2 SAMPLE PREPARATION

In this study, we distinguish five egg white preparations: egg white powder, which is the raw commercial egg white powder; EWP which is the desalted egg white powder; EWP_{preheat}, which is the preheated egg white powder that was subsequently desalted; purified OA, and a mixture of OA and OT. The proteins were dissolved in Millipore water and stirred for 2 h; the pH was adjusted afterwards to 7 by adding 1 M HCL. OA was also mixed with in a ratio of 80:7, in order to study the effect of OT on fibril formation of OA.

9.2.3 PREPARATION OF EWP AND EWP_{PREHEAT}

In order to produce EWP, egg white powder was desalted and concentrated by ultra filtration using the Labscale TFF system from Millipore equipped with three Biomax 30 polyethersulfone membranes (cut off 30 kDa). Figure 9.1 (left panel) shows a schematic representation of the purification and desalting steps of EWP and the subsequent gel formation process.

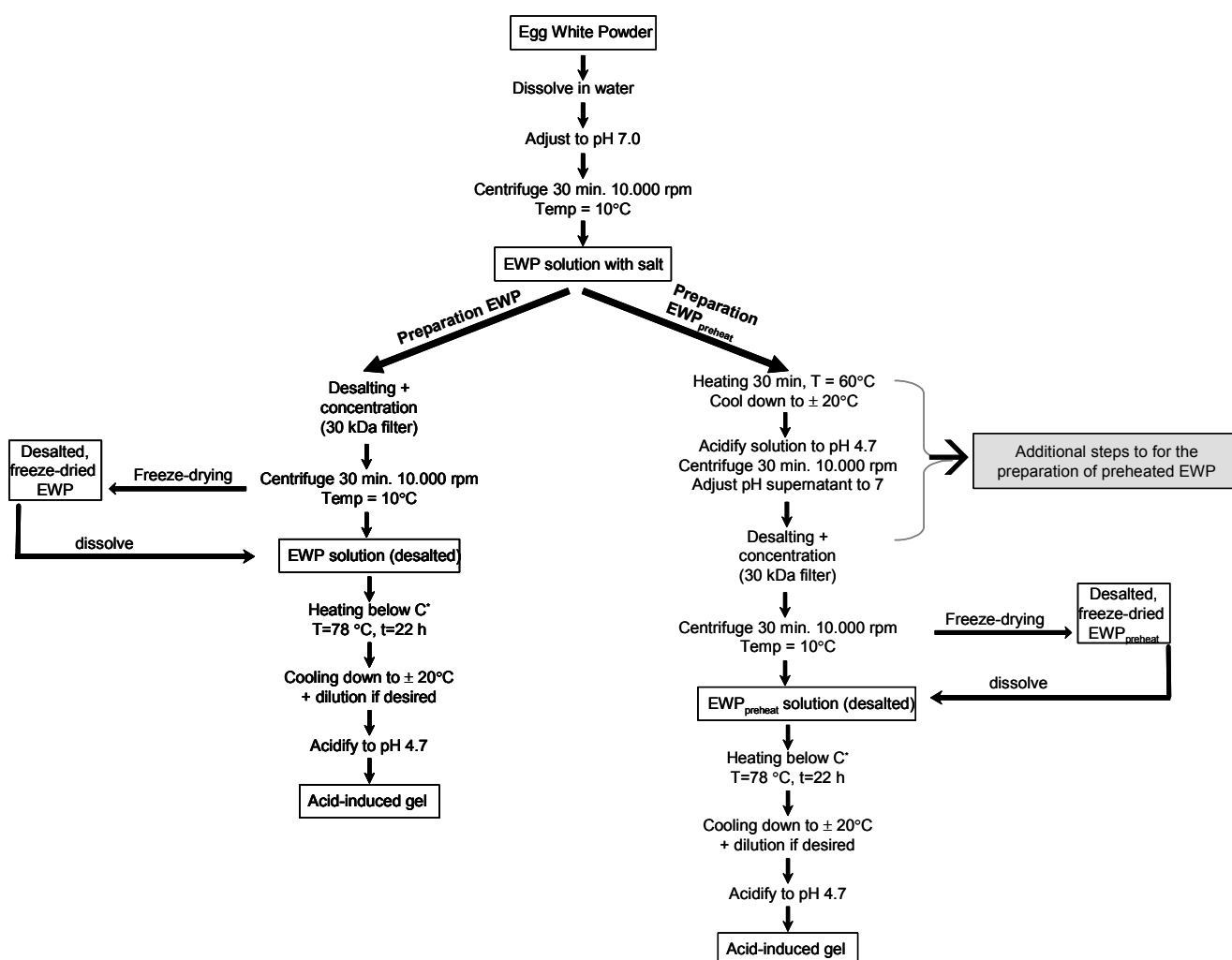


Figure 9.1. Schematic representation of the purification and desalting procedure to prepare EWP and EWP_{preheat}. Also the subsequent acid-induced gelation process is presented.

To remove OT, 30 g/L egg white powder was dissolved and heated for 30 minutes in a water bath at 60°C. Subsequently, the pH was adjusted to 4.7±0.1 with 1M HCl. After centrifugation at 10.000 rpm for 30 minutes at 10°C, the supernatant was moved into the ultra filtration system (Figure 9.1, right panel). This preparation is entitled EWP_{preheat}.

Protein concentrations were determined by UV absorption at 278 nm using $\epsilon=0.698 \text{ Lg}^{-1} \text{ cm}^{-1}$.

9.2.4 PREPARATION OF AGGREGATES

The critical gelation concentration (C^*) was determined by heating concentration series of egg white preparations in a water bath for 22 h at 78°C, unless reported otherwise.

9.2.5 DIFFERENTIAL SCANNING CALORIMETRY

DSC scans were carried out with a SETARAM (Caluire, France) micro DSC III with stainless steel 1 ml sample cells. Calibration was done with naphthalene. Samples were prepared at protein concentrations of approximately 10 g/L, pH 7.0, without added salt. The same solution without the protein was used in the reference cell. The temperature was scanned from 25 to 120°C at a scanning rate of $1.0^\circ\text{C min}^{-1}$.

9.2.6 REVERSED PHASE CHROMATOGRAPHY

Two types of experiments were performed: (1) Determination of the amount of non-denatured protein after heating a 30 g/L EWP for 30 minutes at 25, 45, 50, 55, 60, 70, and 80°C. (2) Determination of the rate of decrease in concentration of non-denatured protein, upon heating (78°C) the egg white preparations at 40 g/L. For both experiments the vials were cooled in ice-water after the heating period, and the protein solutions were diluted to a final concentration of non-denatured protein of 20 g/L. Then, the pH was adjusted to 4.7 ± 0.1 with 0.1M HCl, which causes the denatured and aggregated ovalbumin to precipitate. After centrifugation at 20,000g for 5 minutes at ambient temperature, the concentration of non-denatured protein in the supernatant was determined by RP-HPLC (Du Pont, Zorbax Protein Plus column, 250×4.6 mm). For reversed-phase HPLC, the column was equilibrated with 10% acetonitrile in water containing 0.05% TFA, at a temperature of 40°C. Aliquots of 10-20 μL egg white preparations were loaded onto the column, and elution was carried out by increasing the acetonitrile concentration using a linear gradient. The eluents used were: eluent A: 0.05% TFA in water; eluent B: 0.05% TFA in 100 % acetonitrile. Gradient profile: started with 10% B, after 50, 60 minutes 80% B, 65, 85 minutes 10% B, at a flow rate of 1 mL/min. The proteins were separated on their differences in hydrophobicity and detected at 214 nm.

9.2.7 DYNAMIC LIGHT SCATTERING

Prior to dynamic light scattering experiments, the aggregates were highly diluted so that the effect of interactions and multiple scattering could be neglected. Light scattering measurements were made using the ALV Compact Goniometer System with four detector units (ALV/CGS-4) and two ALV-5000/E multiple tau digital correlators. This setup makes it possible to perform simultaneously angular dependent determination of static and dynamic light scattering. A Coherent Verdi V2 diode-pumped laser was used operating with vertically, linear polarized light with wavelength $\lambda = 532$ nm. The range of scattering wave vectors covered was $4.65 \times 10^{-3} < q < 3.09 \times 10^{-2} \text{ nm}^{-1}$ ($q = 4\pi \cdot n_s \cdot \sin(\theta/2)/\lambda$, with n_s the refractive index of the solution and θ the angle of observation). The temperature was controlled by a thermostat bath to within $\pm 0.1^\circ\text{C}$. The intensity autocorrelation function of the different samples was measured with DLS, and analysed in terms of a distribution of relaxation times, using a double exponential fit. Data on OA were taken from a previous publication.²²

9.2.8 CRYO-TRANSMISSION ELECTRON MICROSCOPY

Cryo-transmission electron micrographs were recorded at Unilever Research, Vlaardingen,²² using a Philips CM12 transmission electron microscope operating at 80 kV. Images were recorded digitally by a Gatan 791 CCD camera using the Digital Micrograph software package.

9.2.9 DETERMINATION OF REACTIVE THIOL GROUPS

The number of accessible thiol groups was determined using DTNB, also known as Ellman's reagent²³ as described elsewhere.²¹ The number of thiol groups was determined using $\epsilon_{412\text{nm}} = 13,600 \text{ M}^{-1}\text{cm}^{-1}$ for 2-nitro-5mercaptobenzoic acid.

9.2.10 SDS-AGAROSE ELECTROPHORESIS

SDS-agarose gel electrophoresis (0.4 % (w/w) agarose) was performed as described before²¹ to determine the differences in molecular size of the differently treated protein aggregates. Aggregates (in solution or gel) were dissolved in an SDS-containing buffer

(5% SDS, pH 7.0) to a final protein concentration of 0.5% (w/w). Staining was done with Phastgel Blue R.

9.2.11 GDL-INDUCED GELATION

GDL was added as a powder to the dispersions of aggregates to induce cold gelation at ambient temperature. Dependent the protein concentration during gelation, different amounts of GDL ($\%GDL(w/w) = 0.0065 \times C_{\text{protein}}(g/L) + 0.045$) were added to reach a final pH of 4.7, which is the iso-electric point of OA. The pH was monitored simultaneously in the samples which were placed in a water bath kept at 25°C or determined after 24 h of incubation at ambient temperature.

9.2.12 TURBIDITY MEASUREMENTS.

Turbidity measurements were performed on a Cary 1E UV-Vis spectrophotometer (Varian) equipped with a temperature controller. The measurements were made at 25°C. The reported turbidity of the gels was calculated from steady-state absorbance (A) at 500 nm (after 20 h). Samples were measured in sample cells (quartz) with a path length (l) of 0.2 cm, and subsequently the turbidity (τ) was calculated as follows:

$$A = -\log \frac{I}{I_0} ; \quad \frac{I}{I_0} = e^{-\tau l}.$$

We divided the turbidity values presented in Table 9.4 into three regimes: transparent, translucent and turbid. These cold-set gels were defined transparent when $\tau < 0.4 \text{ cm}^{-1}$, i.e. more than 92% of the light passes through the sample in a 0.2 cm sample cell. Samples are defined as “low” translucent if $0.4 \leq \tau \leq 1.1$, “medium” translucent if $1.2 \leq \tau \leq 11.4$, and “heavy” translucent if $11.5 \leq \tau \leq 18.4$. Samples with $\tau > 18.4$ were defined as turbid, i.e. less than 2.5% of the light passes the sample.

9.2.13 LARGE STRAIN DEFORMATION RHEOLOGY

Large deformation analysis of the acid-induced gels was performed with in Instron universal testing system (model 5543, Instron Int., Ltd.) using two parallel plates (stainless steel, diameter: 150 mm). Gels were prepared in 60 mL plastic syringes (diameter: 26.1 mm; syringe wall was lightly coated with paraffin oil). Gels were cut into pieces of

22 mm height using an adapted egg slicer (guillotine type). Uniaxial compression until fracture was performed at a crosshead velocity of 1.0 mm/s to a strain of 95%. The plates were lubricated with a drop of paraffin oil to prevent friction forces. Force and deformation were recorded during time and recalculated into true stress (σ_T) and true strain (ε_T) values, according to the following equations:²⁴

$$\sigma_T = \frac{F(t)}{A(t)}$$

$$\varepsilon_T = \ln\left(\frac{H_0}{H_0 - \Delta H}\right)$$

in which $F(t)$ and $A(t)$ are the force and area of the sample at time t , H_0 is the initial height of the sample and ΔH the deformation.

Four replicates of each sample were compressed and the average fracture points (true stress and true strain) were used.

9.3 RESULTS

Ovalbumin is known to form long fibrillar aggregates upon heating.²⁵ Acid-induced gelation of these structures results in the formation of transparent gels at protein concentrations between 50-10 g/L.⁴ In the present study, we show that industrial hen egg white protein did not form transparent cold-set gels under similar conditions. Recently, we found that the removal of OT from industrial egg white products allows the formation of transparent gels.⁵ To explain the lack of transparency, we composed four egg white preparations: purified ovalbumin (OA), desalted egg white powder (EWP), preheated and desalted egg white powder, whereby selectively OT was removed by a preheating step (EWP_{preheat}), and a mixture of ovalbumin and ovotransferrin (OA+OT).

9.3.1 PREPARATION OF PREHEATED EGG WHITE PROTEIN

Commercially available egg white powder contains a high amount of salt. When such a protein solution is heated, already at low protein concentrations (~30 g/L) a turbid gel is formed. A desalting step is necessary to reduce the ionic strength to about 3 mM and therefore allows the formation of possibly fibrillar structures. However, the patent showed that it was still not possible to produce transparent cold-set gels of EWP. Table 9.1 and 9.2

Table 9.2. Composition, peak temperature (T_p) of egg white preparations and the purified proteins. Abbreviations Ovalbumin (OA), Ovotransferrin (OT), Lysozyme (LZ), and Ovomuroid (OM).

Protein preparation	Composition (%)				T_p (°C)
	OA	OT	LZ	OM	
Egg white powder	77.6	8.1	0.8	13.5	58.1 / 78.7
EWP	80.4	7.2	0.6	11.8	57.5 / 78.9
EWP _{preheated}	84.6	0.6	0.8	14	78.1
OA + OT	90 ^a	8 ¹	<1	<1	78.5 ^b
OA	>95	<1	<1	<1	78.9
Ovalbumin (OA)	>95	<1	<1	<1	78.9
Ovotransferrin (OT)	<1	>95	<1	<1	56.9
Lysozyme (LZ)	<1	<1	>95	<1	78.1
Ovomucoid (OM)	<1	<1	<1	>95	75.3

^a This corresponds to a ratio OA:OT of 80:7, which was found in EWP.

^b Concentration OT was too low to be clearly detected. In EWP the T_p of OT could be measured, because additional DSC scans were done at a Microcal MC-2 calorimeter, which detects much lower protein concentrations.

shows that OT is the most heat-labile protein containing 15 disulphide bonds. This suggests that OT aggregates quickly and may interfere with the fibril formation of ovalbumin. Additionally, it is shown Matsudomi et al.¹⁸ that OT itself forms turbid systems, already at low protein concentrations. Therefore, it may be clear that removing OT may have a positive effect of the formation of fibrillar structures and therefore on the formation of transparent cold-set gels.

The composition of egg white preparations was determined by RP-HPLC (Table 9.2). By desalting the egg white powder and preheated egg white powder using a 30 kDa membrane, LZ was removed. In order to optimize the removal of OT, solutions of 30 g/L egg white powder were heated for 30 minutes at different temperatures and subsequently cooled to room temperature. After acidifying the protein solution to the iso-electric point of OA, pH 4.7, and removing insoluble protein material by centrifugation, the amount of monomeric protein was determined with RP-HPLC. Figure 9.2 shows the fraction non-denatured protein as a function of heating temperature for the four detected proteins present in EWP (each protein was normalized and set on 1.0). Heating the EWP solution at 60 °C for 30 minutes, removed more than 90% of the OT, whereas approximately 75% OA was still in its native state. This preheating process did not significantly alter the relative amounts of OM and LZ. After dialyses, the EWP_{preheat} sample finally consisted of about 85% OA and 14% OM (Table 9.2). Since OM is regarded as a heat-stable protein under the

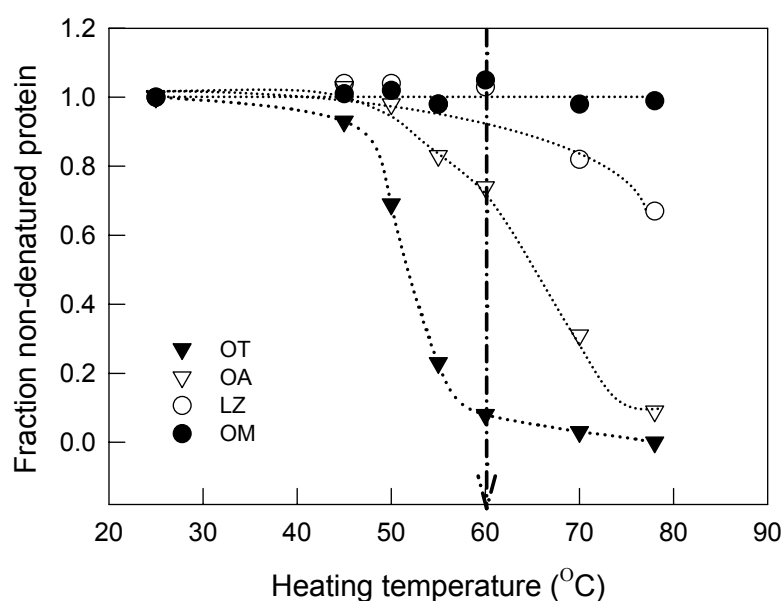


Figure 9.2. Fraction non-denatured protein in EWP as a function of heating temperature after 30 minutes heating. Proteins: OA (∇); OT (\blacktriangledown); LZ (\circ); OM (\bullet).

conditions used in this study, we assume OM not to affect aggregate formation.¹³ Consequently we prepared a food grade egg white protein preparation, which behaves in many aspects as purified OA.⁵ This preparation is further described as EWP_{preheat}.

9.3.2 AGGREGATE FORMATION

Table 9.2 shows the peak temperatures (T_p), determined from DSC, of egg white preparations and purified proteins. The T_p of OT, which is the most heat-labile protein, was found to be 56.9°, and is in good agreement with values found in literature (Table 9.1). The other proteins have their T_p around 78°C. Therefore, only T_p of OA and OT could be clearly distinguished in egg white powder and EWP. In figure 9.3, the fraction non-denatured protein is shown as a function of heating time for the four different egg white preparations. In EWP, and also in the case of the mixture of OA and OT, the rate at which the fraction non-denatured protein decreased was larger for OT than for OA. This was to be expected since the T_p of OT is lower than for OA. Surprisingly, the denaturation rate of OA was not influenced by the presence of OT, i.e. the decrease of non-denatured OA in the purified OA sample, and in the mixture of OA and OT, showed the same time dependence. Unfortunately, Matsudomi et al.¹⁸ only showed results of OA/OT mixtures by means of turbidity and electrophoresis measurements. The aggregate characteristics of OA

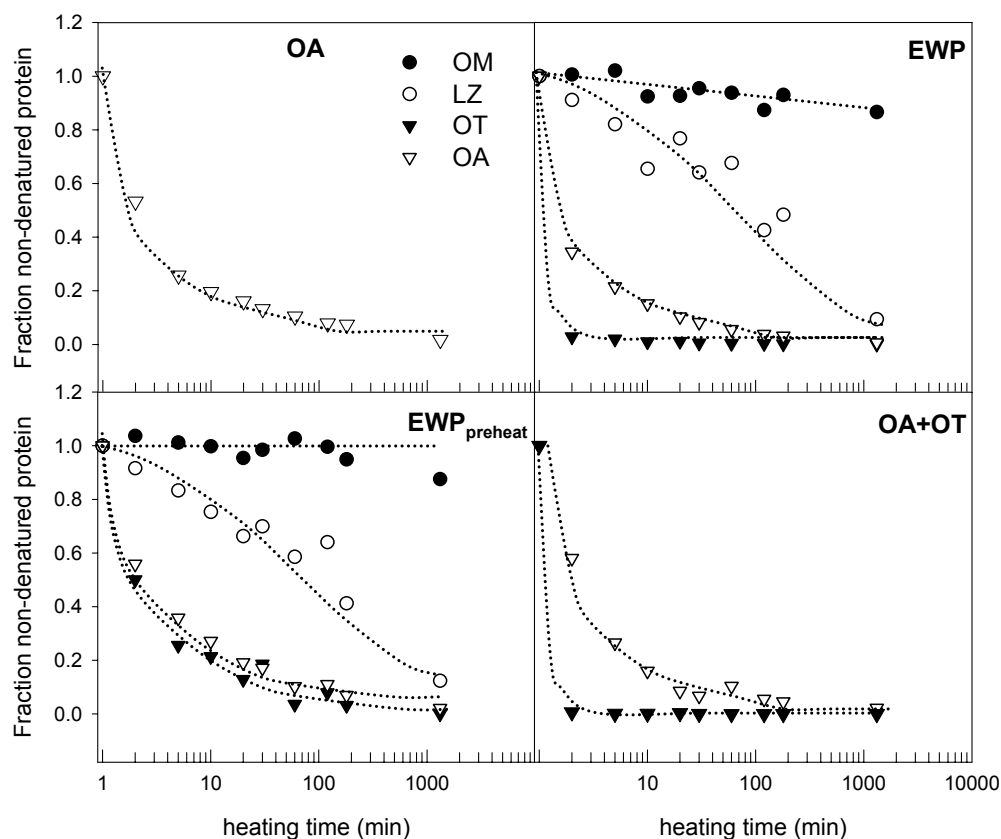


Figure 9.3. Heating time dependence of the fraction non-denatured protein for different egg white preparations. Proteins: OA (∇); OT (\blacktriangledown); LZ (\circ); OM (\bullet). Note that the concentration LZ in EWP and $\text{EWP}_{\text{preheat}}$ is very low ($\sim 0.7\%$), the concentration OT in $\text{EWP}_{\text{preheat}}$ is very low as well ($\sim 0.6\%$).

were drastically changed by the addition of OT, which will be described in the next paragraph. The fraction OM in EWP and $\text{EWP}_{\text{preheat}}$ was not significantly decreased as a result of heating. It is known from literature that the fraction OM is not significantly changed upon heating to $100\text{ }^{\circ}\text{C}$.¹³

9.3.3 CHARACTERIZATION OF PROTEIN AGGREGATES

9.3.3.1 HYDRODYNAMIC RADIUS

The effect of the initial protein concentration at heating on the size of the aggregates was studied by DLS. In general, increasing the protein concentration at heating results in an increase in the hydrodynamic radius of the aggregates.^{22,26} Figure 9.4 shows indeed that the size of the aggregates increases with increasing protein concentration. The protein concentration at which r_h diverges is defined as the critical gelation concentration, C^* (see

Table 9.3. Characteristics of ovalbumin and egg white aggregates: critical gelation concentration (C^*), number of free accessible thiol, contour length (L_c) and ‘shape’. The latter two were determined by cryo-transmission electron microscopy.

<i>Protein preparation</i>	<i>C^* (g/L)</i>	<i>No. of thiol groups (mM)^a</i>		<i>L_c determined by cryo-TEM</i>	<i>‘Shape’</i>
		C^*	$C=20\text{g/L}^b$		
EWP	73	0.31	0.04	20-150 nm	Short linear aggregates
EWP _{preheated}	68	0.43	0.10	50-350 nm	Linear aggregates
OA + OT	68	0.74	0.21	20-300 nm	Linear aggregates, branched fibrils, clusters
OA	57	0.34	0.26	300-1000 nm	Semi-flexible fibrils

^a Determined at pH 7 with Ellman’s assay. The number of thiol groups is expressed as the concentration of thiol groups (mM) in a 20 g/L (w/w) dispersion of protein aggregates. Measurements were done in duplicate with an experimental error lower than 10%.

^b Abbreviations: C^* : aggregates prepared at C^* ; $C=20\text{g/L}$ aggregates prepared at $C=20\text{g/L}$.

table 9.3). For OA, the size of the aggregates increases monotonically from a value close to that of native OA. For EWP_{preheat} similar results are obtained, whereas EWP aggregates are already several times larger than that of native OA, even at low protein concentrations.

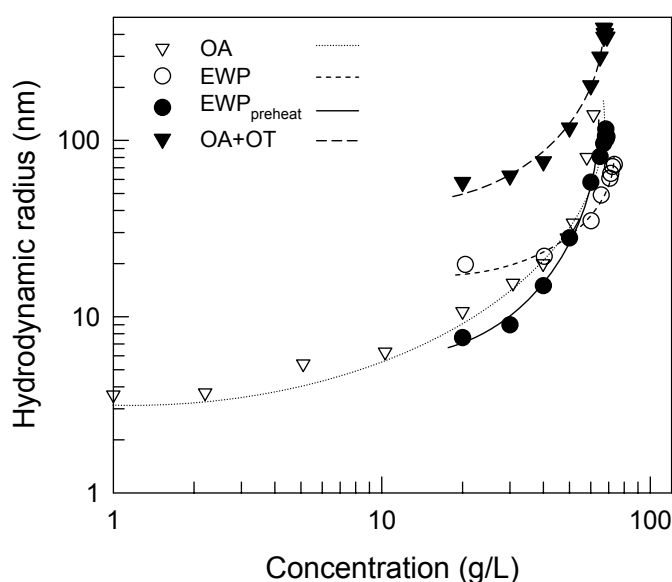


Figure 9.4. Concentration dependence of the hydrodynamic radius of various egg white preparations after heating at 78°C at pH 7. Data on OA are taken from a previous publication.²² Solid and dashed lines are guides to the eye.

Mixtures of OA and OT clearly show that already at low protein concentrations aggregates were obtained with a hydrodynamic radius of about 60 nm. The turbid appearance of these samples, in combination with the large value of r_h indicates that large structures, such as clusters, must be present.

9.3.3.2 CRYO-TRANSMISSION ELECTRON MICROSCOPY

For TEM, aggregates were obtained by heating protein solutions slightly below their C^* (Table 9.3). Microscopy images of OA, EWP, EWP_{preheat}, and OA+OT aggregates are presented in Figure 9.5. OA forms semi-flexible aggregates, which are not branched, have a L_c up to 1 μm , and a diameter of about 4 nm.^{25,27} EWP showed relatively small linear aggregates, which may be a little branched and having approximately the same diameter as for OA. Mixtures of OA with OT formed small, branched aggregates and large protein clusters. The ratio OA to OT was 80:7, which is similar to that present in industrial egg white samples. From these images various types of aggregate structures were observed. This figure show that small linear aggregates ($L_c \sim 50$ nm) and large dense protein clusters were present. From these observations we conclude that OT indeed interferes with the formation of long fibrillar structures of OA.

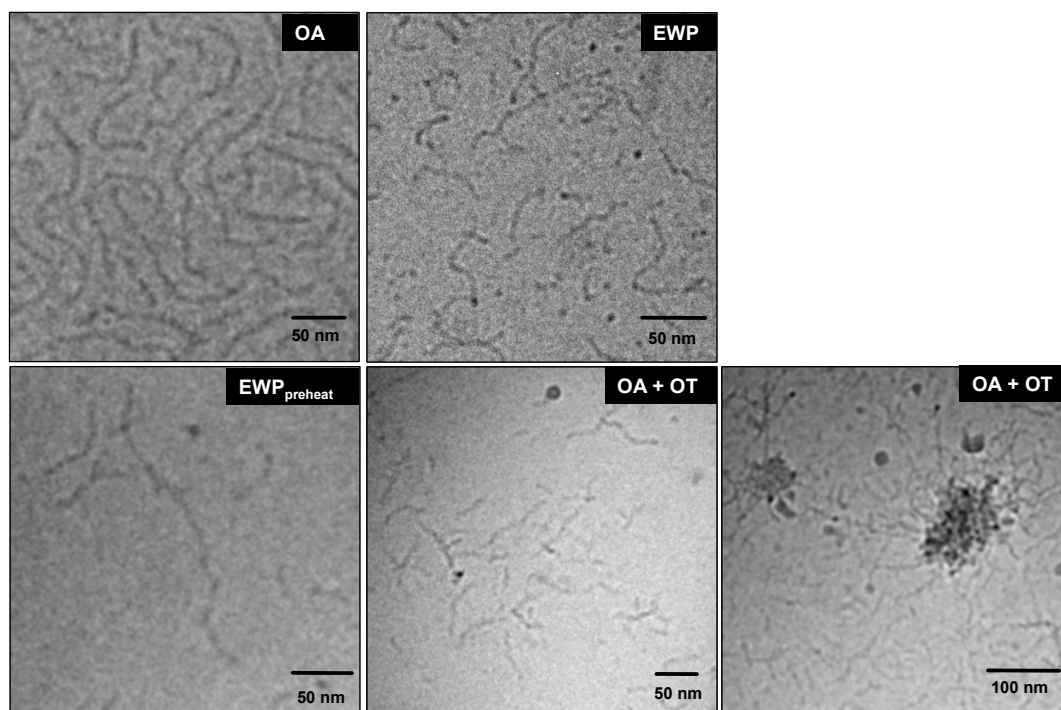


Figure 9.5. Cryo-TEM images aggregates prepared from egg white preparations heated at C^* . Egg white preparations were initially heated at: $C=57$ g/L (OA); $C=73$ g/L (EWP); $C=68$ g/L (EWP_{preheat}); and $C=68$ g/L (OA+OT), and diluted to 1 g/L before cryo-TEM images were recorded.

9.3.3.3 ELECTROPHORETIC MOBILITY

Whether soluble aggregates of egg white preparations were composed of covalent cross-linked aggregates was determined with continuous agarose gel electrophoresis in the presence of SDS. SDS is known to break hydrophobic bonds, but does not break covalent bonds. We previously demonstrated⁴ that these covalent bonds were disulphide bonds, because the addition of DTT to OA aggregates showed the same electrophoretic mobility as for OA monomers. This technique was shown to be very suitable to separate proteins (aggregates) with a diameter of between 3 nm (monomeric protein) and 250 nm.²¹ Since no stacking gel was used, protein bands were rather diffuse. Also, the band caused by aggregates was broadened because of the polydispersity of the aggregates.

The electrophoretic mobility of OA and EWP_{preheat} clearly decreases with increasing heating time, reflecting an increase in aggregate size, in which the aggregates are composed of disulphide cross-linked monomers (Fig. 9.6).

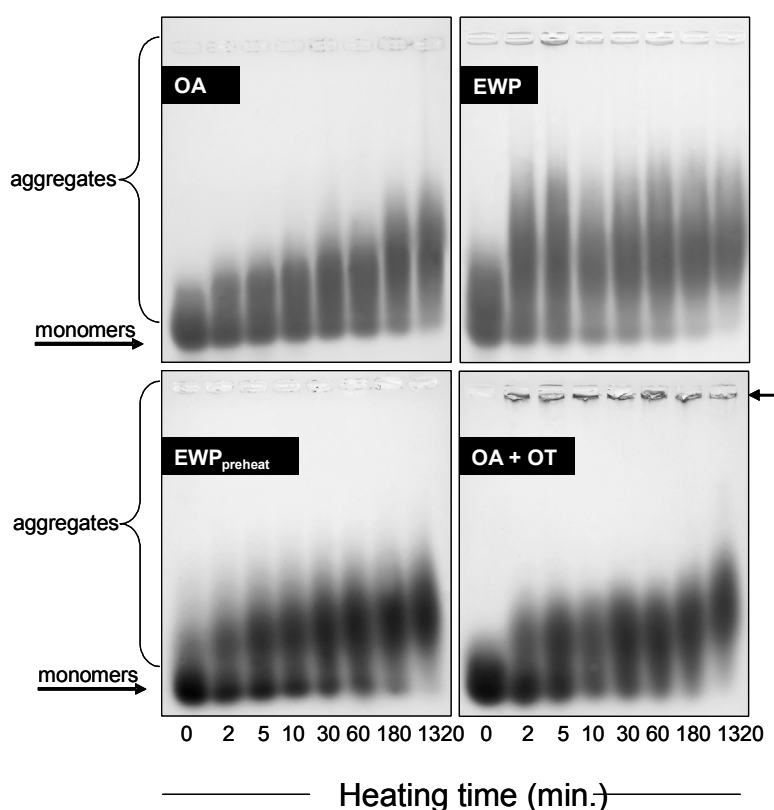


Figure 9.6. SDS agarose gel electrophoresis of heated and unheated solutions of OA, EWP, EWP_{preheat}, and OA+OT at C* (given in Table 9.3). Lane 1, unheated protein preparation; lane 2-8, heated protein preparation for 2, 5, 10, 30, 60, 180, and 1320 minutes. Note that structures formed from OA+OT were partly unable to enter the agarose matrix.

EWP_{preheat} shows similar aggregation behaviour as OA. EWP and the mixture of OA and OT showed already at low heating times the formation of large aggregates, whereas in the OA+OT mixture a fraction of the aggregates was too large to enter the gel matrix (arrow), indicating a large variety of aggregates structures present in this sample.

9.3.4 ACID-INDUCED GELATION

9.3.4.1 TURBIDITY OF COLD-SET GELS

Three types of acid-induced gels were made: aggregates prepared at C^* , and gelation occurs also at C^* , indicated as C^* ; aggregates prepared at C^* , these aggregates were diluted to 20 g/L, and thus gelation occurs also at $C=20\text{g/L}$, indicated as $C^* \rightarrow 20\text{ g/L}$; and aggregates prepared at $C=20\text{g/L}$, and gelation occurs also at $C=20\text{g/L}$, indicated as $C=20\text{g/L}$. Gelation was induced by the addition of GDL. In the aqueous protein solution, GDL slowly hydrolyzes, yielding gluconic acid, which caused a gradual decrease of the pH and thereby induces gelation of the dispersions of aggregates towards the iso-electric point. The turbidity of the cold-set gels of OA, EWP and EWP_{preheat} were followed during acidification (Figure 9.7). Figure 9.7A shows the development of the turbidity (τ) as a function of time for dispersions of aggregates prepared at C^* and acidified at C^* . Two interesting observations are made. Firstly, OA started with an initial $\tau \sim 0\text{ cm}^{-1}$, which means that the dispersion of aggregates were completely transparent at $t=0\text{ min}$. For EWP, the aggregates prepared at C^* already showed some scattering, due to inhomogeneities. This effect was reduced for EWP_{preheat} compared to EWP. Secondly, the final τ appeared to be transparent, light translucent and translucent for OA, EWP, and EWP_{preheat} respectively. We can conclude from these results that EWP_{preheat} resembles more the characteristics of OA than of EWP.

In case were the aggregates were prepared at C^* and acidified at 20 g/L (fig. B) or prepared and acidified at 20 g/L (Fig. C), a significant effect of preheating EWP is shown. Removing OT by preheating resulted in a significant lowering of the turbidity towards that of OA gels. Removing OT, resulted in the formation of longer fibrillar protein structures, as was clear from TEM. On the basis of turbidity measurements, we conclude that more transparent gels upon acidification are formed from EWP_{preheat} compared to EWP gels, which formed more turbid gels. The difference between EWP and EWP_{preheat} becomes

more pronounced at lower protein concentrations because the molecular properties of the aggregates become more important (see discussion section).

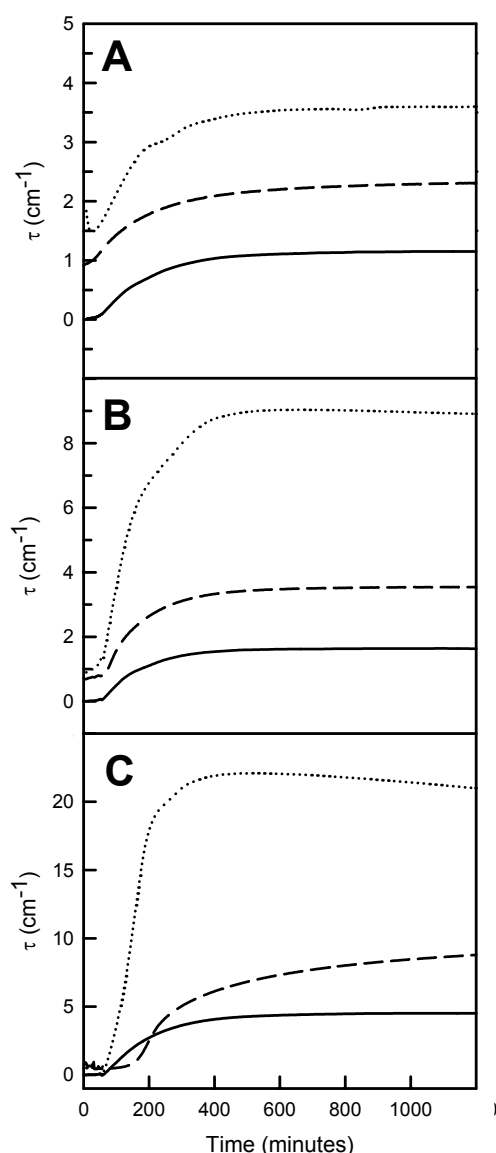


Figure 9.7. Development of the turbidity (τ) during acid-induced gelation of EWP, EWP_{preheat}, and OA under different conditions: (A) C^* ; (B) $C^* \rightarrow 20$ g/L; (C) $C = 20$ g/L. Note that the y-ordinate values are different for graphs A, B and C. Solid lines, long-dashed, and short-dashed represent OA, EWP_{preheat}, and EWP respectively.

9.3.4.2 FRACTURE PROPERTIES OF ACID-INDUCED GELS

Figure 9.8 shows the fracture points of the acid-induced gels of the four egg white preparations. Gels were prepared at C^* (as indicated in Table 9.4), from aggregates prepared at C^* and diluted to a final concentration of 60 to 20 g/L in the gel and heated and acidified at a concentration ranging from 20 to 60 g/L. For comparison, acid-induced gels of WPI-aggregates (heated at 90 g/L) and diluted to a final protein concentration of 90 to 30 g/L were included in Figure 9.8.

Table 9.4. Scattering characteristics, fracture properties, and formation of disulfide bonds in acid-induced cold-set gels of egg white preparations.

<i>Protein preparation</i>	<i>Turbidity: τ (cm⁻¹)^b</i>			<i>Fracture at C*</i>		<i>S-S bridges</i>
	C*	C*→20g/L	20g/L	True stress ^c (kPa)	True strain ^c (-)	
OA ^a	1.1	1.6	4.5	10.5	0.53	-
EWP	3.6	8.9	20.6	15.5	0.70	+
EWP _{preheated}	1.4	2.8	8.4	10.9	0.56	-
OA + OT	17.7	9.9	16.2	10.2	0.57	+

^aThese values slightly differ from those obtained in a previous publication,⁴ because here a less purified ovalbumin sample was used.

^b The turbidity (τ) was measured in a spectrophotometer at 500 nm, values of τ are given after 20 hours.

^c Vales given are average values. Measurements were done at least four times with an experimental error lower than 10%.

The fracture properties of the acid-induced gels of the four egg white preparations were almost identical, e.g. the fracture points overlap with each other. An increasing protein concentration in the gel resulted in an increase in fracture stress and strain. This implies that both a higher force and a large deformation are required to fracture the gel. Thus, at higher protein concentration the gels become more though. Compared to the WPI gels, the egg white protein gels are more brittle, e.g. at a comparable fracture stress the egg white protein gels fracture at a smaller deformation. Studies on cold-set WPI gels reported that there is a relationship between the structural properties of the gels and their rheology.³ Gels that fracture at low strain values, as we observed for all egg white gels, have networks composed of relatively thin strands and small, homogeneous pores, whereas gels which fracture at high strain values (WPI gels) have thicker strands and relatively large, inhomogeneous pores.¹⁹ Our results on egg white gels are consistent with these experimental studies on whey protein gels.

9.3.4.3 DISULPHIDE CROSS-LINKING

To study the formation of covalent disulphide bonds in the gelation process, acid-induced gels were dissolved in a buffer containing SDS to break physical interactions while the covalent bonds remained intact. By way of comparison, gels were prepared from which the aggregates were initially treated with the thiol-blocker NEM, preventing the formation of disulphide bond during acidification and gelation.

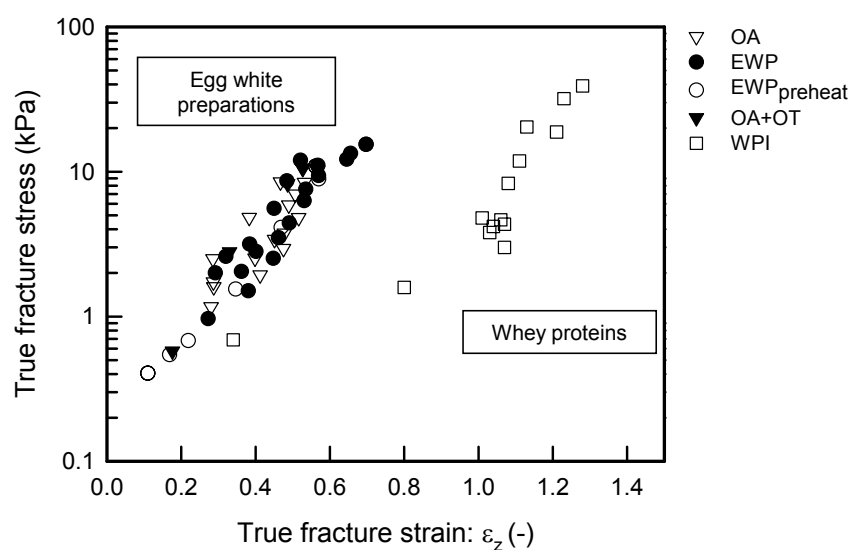


Figure 9.8. Fracture points of egg white preparations and WPI acid-induced cold-set gels. Different data points represent the different gel compositions prepared at C^* , $C^* \rightarrow x$ g/L, and $C=x$ g/L. Different symbols represent different egg white preparations.

Gel electrophoresis on the acid-induced gels of OA and $EWP_{preheat}$ showed no differences between untreated and NEM treated aggregates, which implies that none or very few disulphide bonds are formed during acidification (Fig. 9.9). For OA, the absence of formation of additional disulphide bonds in the gelation stage was previously explained by the inaccessibility of the disulphide bond. The disulphide bond is located in the interior of the OA molecule and therefore hardly a thiol-disulphide exchange reaction occurs.⁴ EWP and OA+OT clearly showed a decreased electrophoretic mobility after acid-induced gelation, compared to the electrophoretic mobility of the gels from which the free thiol groups exposed on the surface of the aggregates were blocked (lanes E and H compared to F and G). These results indicate that after the acid-induced gelation additional disulphide bonds are formed.

9.4 DISCUSSION

Industrial available egg white powder contains high amount of salts, which is known to disturb fibril formation of several food proteins, like OA and β -lactoglobulin.^{25,29} For instance, the structure of ovalbumin was found to be compatible with that of semi-flexible strings of monomers that become more flexible and increasingly branched with increasing ionic strength.²⁵ Heating proteins solutions containing salt concentration of about 100 mM

NaCl, results in the formation of very turbid systems at protein concentrations above 4 g/L.²⁹ This behaviour is generally explained by the fact that at low ionic strength electrostatic repulsion dominates over attractive interactions, and therefore allows the formation of fibrillar structures.

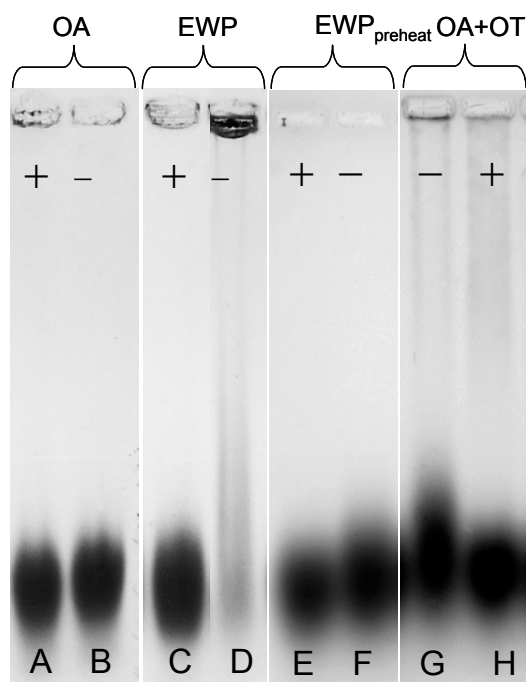


Figure 9.9. SDS agarose gel electrophoresis of cold-set gels redissolved in SDS-buffer. Cold-set gels of: OA (A,B), EWP (C,D), EWP_{preheat} (E,F), and OA+OT (H, G) of untreated (B,D,F,G) and NEM treated (A,C,E,H) protein aggregates.

To obtain salt-free EWP, solutions of commercial egg white powder were dialysed. However, aggregates obtained from heating solutions of desalted egg white powder did not result in the formation of long fibrillar structures as was observed for OA using cryo-TEM (Fig. 9.6). Since salt is not the reason, the insufficient formation of fibrils can be explained by the composition and molecular properties of the proteins present in egg white powder. From Table 9.2 it is clear that OA is the predominant protein in EWP, but OT and OM are also present for about 12%. Both proteins have respectively 15 and 9 disulphide bridges within their native structure. The influence of disulphide bonding is suggested to play a major role on fibril formation and will be discussed below.

The kinetics of the formation of internally disulphide cross-linked aggregates of OA and EWP_{preheat} (no additional source of S-S) was clearly different from that of EWP and

OA+OT (Fig. 9.6). These electrophoresis results showed that the major part of denatured OA and EWP_{preheat} has not been converted into aggregates consisting of disulphide cross-linked monomers, whereas after 180 min. heating at 78°C, more than 90% of the native OA molecules were denatured, insoluble at pH 4.7, and physically aggregated (Fig. 9.3). Prolonged heating up to 22 h was required to form the covalent disulphide bonds in physically denatured molecules. We showed in previous publications that OA forms under these conditions long fibrils up to 1 µm in length.^{4,22,25} This means that in the early stage of aggregation non-covalent bonding played a major role instead of covalent disulfide bonding and here fibrillar structures are formed. On the other hand, studies on WPI and β-lactoglobulin, which contains 2 disulphide bridges and 1 free thiol group in its native state, showed that denaturation and formation of internally disulphide cross-linked aggregates at neutral pH goes hand in hand, and no fibrillar structures were formed. This suggests that there is a strong correlation between the slow kinetics of disulphide bonding and the formation of fibrillar structures. Therefore, a logical argumentation to obtain fibrils of EWP is by removing OT and OM, which are known to have a reasonable amount of disulphide bonds in the molecule. Since OM has been regarded as a heat-stable protein in egg white (Fig. 9.3, and ref 13), OT was removed from the preparation.

We have chosen to compare four different egg white preparations: OA is known to form fibrils and therefore transparent acid-induced gels; EWP was found to form much shorter linear aggregates, therefore EWP_{preheat} was prepared, which is actually EWP without OT; and as a comparison, a mixture of OA+OT was studied to show the negative effect of OT on fibril formation of OA. EWP_{preheat} was prepared by heating a 30 g/L solution of commercial egg white powder for 30 minutes at 60°C. The relatively low peak temperature of OT (Table 9.2) makes that OT was denatured and aggregated for more than 90%, whereas OA remains practically unchanged (Fig. 9.2). Kinetic experiments presented in Fig. 9.3 showed again that OT was the most reactive molecule.

Cryo-TEM images were made to visualize whether OT interferes with OA in the formation of fibrils (Fig. 9.5). Cryo-TEM images of mixtures of aggregated OA+OT (Fig. 9.5) showed different types of structures. On the one hand large clusters of protein aggregates, on the other hand small linear aggregates were observed. This result corresponds very well with electrophoresis results (Fig. 9.6) where part of the protein was not able to enter the gel matrix, whereas the other part showed protein bands with large

electrophoretic mobility, indicating small protein aggregates. The formation of large aggregate structures in the initial aggregate formation is obviously due to the availability of disulphide bonds within OT, which can promote intermolecular disulphide bonding by a thiol-disulphide exchange reaction. The thiol-disulphide exchange mechanism is generally accepted and described in literature.^{4,30-33}

Also, cryo-TEM was used to visualize the effect of removing OT from the egg white powder on fibril formation. The contour length of the EWP_{preheat} aggregates was significantly increased compared to aggregates prepared from EWP (respectively ± 300 nm and ± 50 nm, Table 9.3). However, the size of the EWP_{preheat} aggregates did unfortunately not reach that of OA fibrils (± 500 nm). This might be due to various reasons. Firstly, it was not possible to remove all OT from the EWP_{preheat} sample. The remaining 0.6% OT might influence the formation of fibrils. Secondly, it can be that spray-dried EWP is partly denatured in which the soluble native OA might be less active in fibril formation.

From the results reviewed here, it strongly indicates that OT interferes with fibril formation. The reason for this effect may be that the large amount of disulphide bonds present in OT interacts with OA to form stable branched and/or clustered aggregates, where it is almost impossible for the protein molecule to rearrange. Thus removing OT from egg white powder, and subsequent desalting results in the formation of larger fibrillar structures, which greatly improves the formation of transparent gels in the second step of the acid-induced gelation process (Fig. 9.7). The gelation occurs due to a reduction of electrostatic repulsion, induced by lowering the pH; the aggregates directly form a percolation network. However, this is not the case for short linear aggregates. In the case of short linear aggregates, the aggregates will be first organized in clusters, which are subsequently able to form a space-filling network resulting in a turbid gel. The gel strength and deformability depend on the number and the type of (chemical) bonds within the gel network. This can be adequately described by fracture measurements.

We showed that the aggregates and gels of egg white preparations were made of thin strands, these gels fracture at much lower strain values than for WPI gels. One should expect that an increase in the number of intermolecular disulphide bonds will increase the value of the strain at fracture, i.e., changing the structure from brittle (low strain at fracture) to rubbery (high strain at fracture). Unexpectedly, almost no effect of additional disulphide bonds (fig. 9.9) on the fracture properties (Fig. 9.8) could be observed from the

gels prepared of aggregates of heated OA+OT. This is probably due to the number and availability of disulphide bonds in OT in the sample. Likely all cystines have already interacted during the aggregation process, thus having no further disulphide bonds available for the next gelation process. Legowo *et al.*³⁴ observed that the addition of α -lactalbumin, a protein containing four disulphide bonds, significantly increased the hardness of heat-induced ovalbumin gels.³⁴ Obviously, more research is needed on studying the effect of introducing additional disulphide bonds in the gelation process of egg white preparations on gel hardness and deformability.

The dependence of the strength and brittleness of cold-set gels on a variety of globular food proteins allows manufacturers to create products with a variety of different textural characteristics by controlling the aggregate structure and the amount of disulphide bonds involved in the acid-induced gelation process.^{4,20}

9.5 CONCLUSIONS

OT is the most heat-labile protein with many disulphide bonds. These characteristics resulted in increased aggregation kinetics compared to ovalbumin. OT was found to interfere with OA in the process of fibril formation; disulphide cross-linked aggregates were formed. Therefore we conclude that OT present in egg white powder interferes with fibril formation of OA, and consequently the formation of transparent cold-set gels. Selective removal of OT from egg white powder by means of a simple preheating step, results in increased length of OA fibrils and in gels with almost the same turbidity as obtained from acid-induced gels prepared from purified OA. This procedure is filled in a patent.⁵ Acid-induced gels prepared from egg white preparations appeared to be weak and brittle, most probably due to the fine-stranded microstructure and low degree of disulphide bonding in the acid-induced gelation. Although we showed that disulphide bonding occurs in the gelation step, most probably by a disulphide-thiol exchange reaction, no significant effect on gel hardness could be determined. The deformability was characterized by strain values ranging from 0.3-0.7, whereas WPI gels covered another part of the stress-strain texture map with strain values ranging from 0.5-1.5. Whey protein isolate gel texture was observed as rubbery due to the formation of additional disulphide bonds.

ACKNOWLEDGEMENTS

The authors would like to acknowledge the contribution of Mrs. S. de Jong (WCFS and NIZO food research) for measuring the fracture properties of the acid-induced WPI gels.

REFERENCES

1. Li, H., Errington, A.D., & Foegeding, E.A. (1999). *J. Food Sci.*, 64, 893.
2. Barbut, S., & Foegeding, E.A. (1993). *J. Food Sci.*, 58, 867.
3. Bryant, C.M., & McClements, D.J. (1998). *Trends Food Sci. Technol.*, 9, 143.
4. Alting, A.C., Weijers, M., de Hoog, E.H.A., van de Pijpekamp, A.M. Cohen Stuart, M.A., Hamer, R.J., de Kruif, C.G., & Visschers, R.W. (2004). *J. Agric. Food Chem.*, 52, 623.
5. Visschers, R.W., Velde van de, F., and Weijers, M. Patent application filled on 19th August 2004.
6. Nakamura, R., Umemura, O., & Takemoto, H. (1979). *Agric. Biol. Chem.*, 43, 325.
7. Powrie, W.D. & Nakai, S. (1986). In *Egg Science and Technology*, 3rd ed. (eds. W.J. Stadelman and O.J. Cotterill), p97. Westport, Connecticut.
8. Li-Chan, E., & Nakai, S. (1989). *CRC Crit. Rev. Poultry Biol.*, 2, 21.
9. Mine, Y. (1995). *Trends Food Sci. Technol.*, 6, 225.
10. Handa, A., Takahashi, K., Kuroda, N., & Froning, G.W. (1998). *J. Food Sci.*, 63, 403.
11. Hammershøj, M., Larsen, L.B., Ipsen, R.H., & Qvist, K.B. (2001). *J. Text. Stud.*, 32, 105.
12. Cunningham, F.E., & Lineweaver, H. (1967). Inactivation. *Poultry Sci.*, 46, 1471.
13. Matsuda, T., Watanabe, K., & Sato, Y. (1981). *J. Food Sci.*, 46, 1829.
14. Matsuda, T., Watanabe, K., & Sato, Y. (1982). *J. Food Sci.*, 47, 637.
15. Matsudomi, N., Yamamura, Y., & Kobayashi, K. (1986). *Agric. Biol. Chem.*, 50, 1389.
16. Matsudomi, N., Takasaki, M., & Kobayashi, K. (1991). *Agric. Biol. Chem.*, 55, 1651.
17. Yamashita, H., Ishibashi, J., Hong, Y-H., & Hirose, M. (1998). *Biosci. Biotechnol. Biochem.*, 62, 593
18. Matsudomi, N., Oka, H., & Sonoda, M. (2002). *Food Res. Int.* 35, 821.
19. Roff, C.F., & Foegeding, E.A. (1996). *Food Hydrocolloids* 10, 193.
20. Errington, A.D., & Foegeding, E.A. (1998). *J. Agric. Food Chem.*, 46, 2963.
21. Alting, A.C., Hamer, R.J., de Kruif, C.G. & Visschers R.W. (2000). *J. Agric. Food Chem.*, 48, 5001.
22. Weijers, M., Visschers, R.W., & Nicolai, T. (2002). *Macromolecules*, 35, 4753.
23. Ellman, G.L. (1959). *Arch. Biochem. Biophys.*, 82, 70.
24. Van Vliet, T., & Luyten, H. (1995). In *New Physico-Chemical Techniques for the Characterisation of Complex Food Systems*, (ed. E. Dickinson), p157. Chapman & Hall, Cambridge.
25. Pouzot, M., Nicolai, T., Visschers, R.W., & Weijers, M. (2004). *Food Hydrocolloids* (in press).
26. Baussay, K., Le Bon, C., Durand, D., & Nicolai, T. (2003). *Int. J. Biol. Macromolecules.*, 34, 21.
27. Weijers, M., Visschers R.W., Cohen Stuart, M.A., and Barneveld, P.A. (2004). Submitted.
28. Veerman, C., Ruis, H., Sagis, L.M.C., & van der Linden, E. (2002). *Biomacromolecules*, 3, 869.
29. Weijers, M., Nicolai, T., & Visschers, R.W. (2004). *Macromolecules* (in press).

30. Saxena, V.P., & Wetlaufer, D.B. (1970). *Biochem.*, 9, 5015.
31. Watanabe, K., & Klostermeyer, H. (1976). *J. Dairy Res.*, 43, 411.
32. Creighton, T.E. (1978). *Prog. Biophys. Mol. Biol.*, 33, 231.
33. Shimada, K., & Cheftel, J.C. (1989). *J. Agric. Food Chem.*, 37, 161.
34. Legowo, A.M., Imade, T., Yasuda, Y., Okazaki, K., & Hayakawa, S. (1996). *J. Food Sci.*, 61, 281.
35. Gossett, P.W, and Rizvi, S.S.H. (1984). *Food Technol.*, 38.
36. [http://www.food-allergens.de/symposium-voll\(1\)/data/egg-white/egg-composition.htm](http://www.food-allergens.de/symposium-voll(1)/data/egg-white/egg-composition.htm)
37. Awadé, A.C., and Efstathiou T. (1999). *J. Chromatogr. B*, 723, 69.
38. Hammershøj, M., Larsen, L.B., Andersen, A.B., and Qvist, K.B. (2002). *Lebensm. Wiss. U.-Technol.*, 35, 62.
39. Donovan, J.W., Mapes, C.J., Davis, J.G.D., and Garibaldi, J.A., (1975). *J. Sci. Fd Agric.*, 26, 73.
40. Kitabatake, M., Ishida, A., and Doi, E. (1988). *Agric. Biol. Chem.*, 52, 967.

SUMMARY

SAMENVATTING

SUMMARY

Functional properties of foods such as texture, perception, appearance, shelf life, quality, flavor release, stability are important to consumers and manufacturers. These functionalities reveal themselves on a macroscopic level. The macroscopic properties depend among others on the structure, interactions, chemical reactivity, and organization of the polymers, which in turn depend on the microscopic and mesoscopic properties of the polymers. In order to enhance and control the functional properties of food products, one needs to know the underlying mechanisms of structure formation of the purified (bio)polymers, before one can subsequently understand these mechanisms in more complex systems.

The objective of the research described in this thesis was to investigate the heat-induced denaturation, fibril formation and network properties of food proteins, with the main focus on engineering and understanding (fibrillar) protein structures at neutral pH. In this thesis ovalbumin was frequently used as a convenient model system to study these mechanisms. Identifying the parameters that are of relevance to the structure development and subsequent network formation allowed us to better understand and control these mechanisms for globular food proteins in general. Additionally, we aimed to link the mesoscopic properties of protein aggregates to the macroscopic properties of heat-induced and acid-induced food gels. For that reason, this thesis is divided into two parts, in which the first part (Chapters 2 – 7) deals with a fundamental understanding of heat-induced denaturation, aggregation and gelation of purified ovalbumin systems, whereas the second part (Chapters 8 – 9) focuses more on applications of industrial relevant proteins.

In Chapter 2, the heat-induced denaturation kinetics of purified ovalbumin at pH 7 was studied by chromatography and differential scanning calorimetry. The kinetics was found to be independent of protein concentration and salt concentration, but was strongly dependent on temperature. For purified ovalbumin, the decrease in non-denatured native protein showed first-order dependence. The activation energy obtained with different techniques was about $450 \text{ kJ}\cdot\text{mol}^{-1}$. First-order behavior was studied in detail using differential scanning calorimetry. The calorimetric traces were irreversible and depended strongly on the scan rate. The shape of the thermograms as well as the scan rate dependence can be explained by assuming that the thermal denaturation takes place according to a simplified kinetic process $N \xrightarrow{k} D$, where N is the native state, D is

denatured (or another final state) and k a first-order kinetic constant that changes with temperature according to the Arrhenius equation. Experimental results for the temperature-induced denaturation and aggregation of ovalbumin could be well explained by this kinetic model.

It is known that if proteins are heated to a temperature where they unfold, they can form various types of aggregate structures depending on experimental conditions such as pH, ionic strength, protein concentration etc. This has been extensively studied for β -lactoglobulin, but not for ovalbumin. In order to do obtain a better understanding of aggregation mechanisms of globular proteins in general, a detailed study has been carried out in Chapter 3 on the effects of protein concentration and ionic strength on the aggregate characteristics. Experimental results on aggregate morphology, studied with Light Scattering (Chapters 3 and 4), X-ray scattering (Chapters 4 and 5) and microscopy (Chapter 4) showed that at low ionic ovalbumin molecules form fibrillar structures with little branching, while at high ionic strength denser branched aggregates are formed with a fractal dimension close to that found for other globular protein aggregates. The structure of these ovalbumin fibrils is compatible with that of semi-flexible strings of monomers that are more flexible and increasingly branched with increasing ionic strength. The persistence length increases with decreasing ionic strength, which was quantitatively determined using a model of semi-flexible chains, the so-called Kratky-Porod chains. The results obtained on ovalbumin are compared with β -lactoglobulin under neutral conditions in Chapter 4. We could clearly demonstrate that β -lactoglobulin aggregates were not formed of semi-flexible strings of monomers. β -Lactoglobulin aggregates consisted of clusters of primary aggregates that were formed in the first step of the aggregation process. At low ionic strength the association of primary aggregates was mostly head to tail, while with increasing ionic strength denser clustering of the primary aggregates was observed.

The formation of transparent aggregate solutions and gels at high protein concentrations and at low ionic strength is obviously due to repulsive interactions in the protein system. In order to obtain an in-depth understanding of the interactions in concentrated protein system, we applied in Chapter 5 some basic scaling theories for (hard) spheres, as well as a theoretical model that described the distribution of spaces in a random network of straight fibers. The experimental dependence of the protein concentration on the interparticle distance (d_{\max}) for monomers was found to be $d_{\max} \sim C^{-0.28}$, which implied that the system behaved as a uniform distribution of charged spheres. The interaction peak of these native

ovalbumin systems could be well described using both a form factor of spheres, and a structure factor based on a solvable model, from which relevant interparticle distances were obtained. The total scattering intensity of ovalbumin aggregates formed at neutral pH could be well described with the form factor of long cylinders (rods). The dependence of the protein concentration on the interparticle distance (d_{max}) for aggregates was found to be $d_{\text{max}} \sim C^{-0.51}$, which is in good agreement with the scaling behavior theoretically derived for the distribution of spaces in a random network of straight fibers. The interaction peak in the x-ray scattering profile coincides to a dominant length scale observed in cryo-TEM images confirming that this dominant length scale reflects the average interparticle distances between long linear fibrils in the system.

In Chapter 6 we focus on the role of the ionic strength in determining the structure and the turbidity of ovalbumin gels using cross-correlation dynamic light scattering technique. With this technique we are able to perform light scattering experiments on turbid systems. Here, we consider that the structure of heated globular protein solutions and gels is generally determined by the interplay between the growth of the aggregates and the electrostatic interaction between the aggregates.

The process of fibril formation, as outlined in Chapters 2-6 and in literature, is not only of interest of food industries; it is currently also one of the major topics in biology and medicine. It is generally accepted that electrostatics plays a role in fibril formation, but the relative importance with respect to other factors and the mechanism for this is not clear. In Chapter 7, we further unravel the mechanism of fibril formation, by studying the effect protein net charge on the fibril characteristics. To do so, we produced four differently charged ovalbumin variants with net charges varying between -26 and -1 by means of chemical engineering. We found that increasing the net charge on ovalbumin molecules promoted the formation of stiff fibrillar aggregates. More branched and clustered aggregates were formed from ovalbumin molecules with a lower surface charge. Gels from these aggregates also appeared to be more turbid compared to the highly charged aggregates. The highly charged variants formed gels that were transparent over a much larger range of ionic strength (up to 500 mM). Moreover, the highly charged proteins showed a significant decrease in the rate of disulfide bond formation during heating compared to unmodified proteins. The results presented in Chapter 7 demonstrate that the charge density on the protein molecule plays a major role in the formation of fibrillar structures and therefore in the formation of transparent gels. However, also slow kinetics

of disulphide bonding and charge distribution on the (unfolded) protein molecule contributes to the possibility to produce fibrils.

In the second part of this thesis, the knowledge acquired from purified systems was extended to aggregate and network formation of industrial relevant proteins under cold-setting conditions. Since purified ovalbumin and β -lactoglobulin are not common used in food applications, industrial egg white protein and whey protein isolate were also studied.

Chapter 8 described the process of aggregation and subsequent cold gelation of ovalbumin and compared the properties of the resulting cold-set gels to those of whey protein isolate (WPI). For both protein preparations: ovalbumin and WPI, repulsive aggregates were made consisting of disulfide cross-linked monomers. Both type of aggregates possessed exposed thiol groups at their surface. At pH 7, the aggregates of both WPI and ovalbumin had a net negative charge and typical inter-particle distances in the nm range were observed using different scattering techniques. When the net charge of the aggregates approached neutrality due to acidification, the characteristic length scale observed before gelation disappeared and over a wide range of length scales (nm to μ m) no other characteristic length scale could be observed. Since formation of the microstructure as a result of the reduction of electrostatic repulsion, did not depend on aggregate characteristics, it can be defined as a non-protein-specific mechanism. It is likely that this mechanism will apply to any type of protein aggregate that is acidified towards its isoelectric point. Differences in size and shape of the protein aggregates were found to influence small deformation properties of protein gels. Longer aggregates have a lower overlap concentration, which causes gelation to commence earlier and results in more effective junctions, yielding higher values of the storage modulus (G'). Covalent bonds were found to be the main determinants of gel hardness. The formation of additional disulfide bonds after gelation not only depends on the number of thiol groups, but also on the number and accessibility of disulfide bonds in the molecule and may differ significantly from one protein to another. However, in the absence of covalent bonds long fibrillar structures can also contribute significantly to gel hardness.

In Chapter 9, we concluded this work with an in-depth look at the molecular background of the formation of transparent cold-set gels prepared from industrial egg white protein (EWP). The effect of protein composition in egg white proteins on fibril formation and its gelation properties were investigated and we provide a new simple procedure to prepare transparent acid-induced cold-set gels from industrial spray-dried egg

white proteins. Additionally, we compared network structures, disulfide bonding in acid-induced gels and the fracture properties between EWP gels and WPI gels. Ovotransferrin, a minor protein fraction present in egg white, appeared to interfere with ovalbumin in the process of fibril formation and consequently no transparent cold-set gels could be formed. Selective removal of ovotransferrin from egg white powder by means of a simple preheating step resulted in increased length of ovalbumin fibrils and in gels with almost the same turbidity as obtained from acid-induced gels prepared from purified ovalbumin. Acid-induced gels prepared from EWP appeared to be weak and brittle, most probably due to the fine-stranded microstructure and low degree of disulphide bonding in the acid-induced gelation. Although we showed that disulphide bonding occurs in the gelation step, no significant effect on gel hardness could be determined. The deformability was characterized by strain values ranging from 0.3-0.7, whereas WPI gels covered another part of the stress-strain regime with strain values ranging from 0.5-1.5. Whey protein gels were observed as rubbery due to the formation of additional disulphide bonds.

This thesis presents a detailed description of the denaturation mechanism, aggregate morphology and network properties of ovalbumin under heat- and cold-setting conditions. A key step to influence the functional properties of a food product is changing the aggregates morphology on a mesoscopic length scale. We demonstrated that by controlling the charge density on the protein molecules (either by changing the pH, adding salt or chemical modification), the amount of electrostatic repulsion can be changed, which allows us to control fibril formation and therefore the turbidity and rheological properties of ovalbumin networks. We extended our knowledge on engineering fibrillar protein structures to industrial relevant protein systems (Patent No. 04077348.3). In a wider perspective, this work enables the food industry to design and manufacture microstructures, which can be responsible for specific mouth-feel performance and stability of soft-solid food products, based on biopolymer networks.

SAMENVATTING

Functionele eigenschappen van voedingsmiddelen zoals textuur, uiterlijk, houdbaarheid, aroma release, stabiliteit zijn belangrijk voor zowel consumenten als fabrikanten. Deze eigenschappen worden waargenomen op een macroscopisch niveau. De macroscopische eigenschappen hangen onder andere af van de structuur, interacties, chemische reactiviteit en organisatie van de polymeren, welke op hun beurt weer afhangen van de microscopische en mesoscopische eigenschappen van de polymeren. Om de functionele eigenschappen van levensmiddelen te verbeteren en onder controle te krijgen, is het nodig om de onderliggende mechanismen van structuurvorming van zuivere (bio)polymeren te kennen. Vervolgens is het van belang de mechanismen te begrijpen in meer complexe systemen.

Het doel van het onderzoek beschreven in dit proefschrift was het onderzoeken van hitte-geïnduceerde denaturatie, vorming van fibrillen en netwerk eigenschappen van voedingseiwitten, waarin we ons specifiek richten op het maken en begrijpen van (fibril-vormige) eiwit structuren bij neutrale pH. In dit proefschrift is ovalbumine meerdere malen gebruikt als een handig modelsysteem om deze mechanismen te bestuderen. Het herkennen van de parameters die van belang zijn voor structuur- en netwerkvorming hebben ons in staat gesteld deze mechanismen voor globulaire voedingseiwitten beter te begrijpen en te beheersen. Tevens hebben wij er ons op gericht om mesoscopische eigenschappen van eiwit aggregaten te koppelen aan de macroscopische eigenschappen in hitte-geïnduceerde en zuur-geïnduceerde gelen. Om die reden is dit proefschrift onderverdeeld in twee delen. Het eerste deel (Hoofdstukken 2-7) beschrijft hitte-geïnduceerde denaturatie, aggregatie en gelling van zuivere systemen vanuit een wetenschappelijk oogpunt, terwijl het tweede deel (Hoofdstukken 8 en 9) zich meer richt op de toepassingen van industrieel relevante eiwitpreparaten.

In Hoofdstuk 2 wordt de hitte- geïnduceerde denaturatie kinetiek van zuiver ovalbumine bestudeerd met chromatografie en calorimetrie. De kinetiek van denaturatie bleek eiwit en zout onafhankelijk te zijn, maar was sterk afhankelijk van de temperatuur. De afname van niet-gedenatureerd natief ovalbumine laat een eerste-orde afhankelijkheid zien. De activeringsenergie gemeten met de bovengenoemde technieken was 450 kJ mol^{-1} . Dit eerste-orde gedrag werd grondig onderzocht met calorimetrie. Het denaturatieproces was onomkeerbaar en sterk afhankelijk van de opgelegde scansnelheid. De vorm van het

thermogram en de afhankelijkheid van de scansnelheid kunnen verklaard worden met behulp van een eenvoudig proces, namelijk $N \xrightarrow{k} D$, waarbij N de natieve staat is, D de gedenameerde en k een reactiesnelheidsconstante die zich gedraagt volgens de Arrhenius vergelijking. Experimentele metingen van de temperatuur geïnduceerde denaturatie en aggregatie van ovalbumine konden goed verklaard worden met dit model.

Het is bekend dat indien eiwitten worden verhit tot een temperatuur waarbij zij ontvouwen, er verschillende typen aggregaten worden gevormd, afhankelijk van de experimentele condities, zoals pH, zoutsterkte, eiwitconcentratie etc. Dit is zeer uitgebreid onderzocht voor het eiwit β -lactoglobuline, maar niet voor ovalbumine. Om een beter begrip te krijgen van aggregatiemechanismen in het algemeen, is er in Hoofdstuk 3 gekeken naar het effect van eiwit -en zout concentratie op de karakteristieken van de aggregaten. Er zijn in Hoofdstuk 3, 4 en 5 verschillende technieken gebruikt, zoals lichtverstrooiing, x-ray verstrooiing en cryo-TEM, om een gedetailleerd beeld te krijgen van deze aggregaat eigenschappen. Experimentele vindingen met betrekking tot de structuur van deze aggregaten laten zien dat ovalbumine bij lage zoutsterkte fibrillen met weinig vertakkingen, terwijl bij hoge zoutsterkte vertakte aggregaten worden gevormd. De structuur van de ovalbumine fibrillen kan beschreven worden met een model voor semi-flexibele ketens. De flexibiliteit van de ketens neemt toe met toenemende zoutsterkte. Door een model te gebruiken voor semi-flexibele ketens, namelijk Kratky-Porod chains, was het mogelijk om de persistentie lengte te berekenen, die blijkt af te nemen bij lagere zoutsterkte, omdat de flexibiliteit toeneemt. De verkregen resultaten van ovalbumine worden in Hoofdstuk 4 vergeleken met die van β -lactoglobuline. We laten duidelijk zien dat β -lactoglobuline aggregaten niet overeenkomen met semi-flexibele ketens. Deze aggregaten bestaan uit clusters van primaire aggregaten die gevormd zijn in de eerste stap van het aggregatieproces. Bij lage zoutsterkte associëren deze primaire aggregaten “kop-staart”, terwijl bij hogere zoutsterkte clusters van primaire aggregaten zijn waargenomen.

Het vormen van transparante oplossingen van oplosbare aggregaten en transparante gelen bij hoge eiwitconcentratie en lage zoutsterkte is te verklaren door repulsieve interacties in het systeem. Om een beter begrip te krijgen van de interacties in geconcentreerde systemen hebben we in Hoofdstuk 5 een theorie gebruikt voor de schaling van (harde)bollen, en ook een theoretisch model wat de schaling van fibrillen beschrijft. Monomeren bleken te schalen met een typische afstand in het systeem (d_{\max}) als $d_{\max} \sim C^{-1}$

^{0.28}, hetgeen impliceert dat het systeem zich gedraagt als een uniforme distributie van geladen bollen. De interactie piek van natief ovalbumine kan goed beschreven worden door gebruik te maken van zowel de formfactor van bollen als een structuurfactor, die gebaseerd is op een oplosbaar model. Deze berekening heeft relevante waarden opgeleverd voor d_{\max} . De totale verstrooide intensiteit, in verdunde systemen, van ovalbumine aggregaten kon goed worden beschreven door gebruik te maken van de vormfactor voor lange staven. De concentratie afhankelijkheid schaalt met d_{\max} als $d_{\max} \sim C^{-0.51}$, hetgeen in goede overeenstemming is met het schalingsgedrag, zoals dat theoretisch is afgeleid voor dit soort systemen. De typische afstand in het systeem zoals gemeten is met x-ray verstrooiing is ook bevestigd door cryo-TEM opnamen. Deze microscopische afbeeldingen bevestigen het beeld de dominante lengteschaal in het systeem de afstand is tussen lange lineaire fibrillen.

In Hoofdstuk 6 richten we ons op het effect van zoutsterkte op de structuur en turbiditeit van ovalbumine gelen met behulp van cross-correlatie dynamische lichtverstrooiing. Door deze techniek wordt het mogelijk gemaakt om lichtverstrooiingsexperimenten te doen aan troebele systemen. In dit hoofdstuk hebben we geconcludeerd dat de structuur van verhitte eiwit oplossingen en gelen bepaald wordt door enerzijds de groei van aggregaten en anderzijds de electrostatische interactie tussen de aggregaten.

Het vormen van fibrillen, zoals staat beschreven in Hoofdstuk 2 t/m 6 en in literatuur, is niet alleen belangrijk voor de voedingsmiddelenindustrie, het is tegenwoordig ook een van de belangrijkste onderwerpen in de biologie en geneeskunde. Het is algemeen geaccepteerd dat elektrostatica een rol speelt bij fibril vorming, echter het mechanisme en de belangrijkheid ten opzichte van andere factoren is nog niet duidelijk. In Hoofdstuk 7 wordt dan ook het mechanisme van de vorming van fibrillen onderzocht door het effect van netto-lading op de aggregatie te bestuderen. In dit onderzoek werden vier ovalbumine varianten gemaakt, door middel van chemische modificatie, met verschillende netto-lading variërend van -26 tot -1. Toenemende netto lading op het natieve eiwit bleek de vorming van stijve fibrillen positief te beïnvloeden. Meer vertakte en geclusterde aggregaten werden gevormd als ovalbumine varianten werden gebruikt met een lagere oppervlakte lading. Gelen van deze aggregaten bleken troebeler te zijn dan gelen gemaakt van de sterk geladen ovalbumine variant. Deze gelen bleken over een veel groter zoutsterkte gebied transparant te blijven (tot 500 mM). Bovendien bleek de snelheid van het vormen van disulfide bindingen tijdens de verhitting, duidelijk vertraagd te zijn bij deze sterk geladen variant.

De resultaten uit Hoofdstuk 7 laten zien dat de lading op het eiwitmolecule een belangrijke rol speelt in de vorming van fibrillen en daarom in de vorming van transparant gelen. Desalniettemin speelt de snelheid waarmee disulfide bindingen worden gemaakt en de ladingsdistributie op het (ontvouwen) eiwitmolecule een rol in de mogelijkheid om fibrillen te vormen.

In het tweede deel van dit proefschrift wordt de opgedane kennis opgedaan tijdens het bestuderen van zuivere systemen gebruikt voor het begrijpen van aggregatie en netwerk vorming van industrieel relevante eiwitpreparaten tijdens het koude-gelatings proces. Omdat ovalbumine en β -lactoglobuline in het algemeen niet gebruikt worden in voedselproducten, hebben wij ook industrieel eiwit en wei-eiwit (WPI) onderzocht.

Hoofdstuk 8 beschrijft de aggregatie van ovalbumine en vervolgens de gelering bij hiervan kamertemperatuur. De eigenschappen worden vergeleken met de aggregatie en gelering van WPI. Voor zowel ovalbumine als WPI zijn de gevormde aggregaten opgebouwd uit monomeren met intermoleculaire disulfide bindingen. Vrije thiolgroepen waren aanwezig op the oppervlak van beide typen aggregaten. Bij pH 7 zijn beide aggregaten negatief geladen en laten een typische afstand (\sim nm) zien in het systeem. Als de netto lading afneemt door verzuring verdwijnt de karakteristieke afstand en kon niet meer waargenomen worden op een nm tot μ m lengteschaal. Omdat de vorming van de microstructuur het resultaat is van de afname van elektrostatistische repulsie, hangt dit niet af van de aggregaat karakteristieken, en kan daarom gedefinieerd worden als een niet-eiwit-specifiek mechanisme. Het is aannemelijk dat dit mechanisme van toepassing is op ieder type eiwit aggregaat dat wordt verzuurd naar zijn isoelektrisch punt. Kleine vervormingseigenschappen bleken beïnvloed te worden door verschillen in aggregaat grootte en vorm. Langere aggregaten hebben een lagere overlapconcentratie, wat betekent dat de gelering eerder inzet en resulteert in meer effectieve knooppunten, dit resulteert in hogere waarden voor de opslag modulus (G'). Covalente bindingen bleken de belangrijkste factor voor de vorming van harde gelen. De vorming van extra disulfide bindingen gedurende het gelatingsproces blijkt niet alleen afhankelijk te zijn van het aantal thiol groepen, maar ook van het aantal en de bereikbaarheid van de disulfidebrug in het eiwit molecuul. Indien er geen covalente bindingen worden gevormd kunnen lange fibrillaire structuren significant bijdragen aan de gelsterkte.

Concluderend beschrijft Hoofdstuk 9 de moleculaire achtergrond van de vorming van transparante gelen van industrieel ei-eiwitpreparaten (EWP) bij kamertemperatuur. Hierin wordt het effect van eiwitsamenstelling op de vorming van fibrillen en de geleringseigenschappen onderzocht wat resulteert in een nieuwe techniek om transparante gelen van industrieel ei-eiwit te maken. Tevens worden netwerkeigenschappen, disulfide bindingen en breukeigenschappen tussen gelen van EWP en WPI vergeleken. Ovotransferrine, een eiwit wat in kleine hoeveelheden voorkomt in ei-eiwit, bleek de vorming van fibrillen te verstoren en daardoor de vorming van transparante gelen. Door middel van een simpele voorverhittingsstap bleek ovotransferrine selectief verwijderd te kunnen worden wat resulteert in de vorming van langere fibrillen. De gevormde koude gelen bleken hierdoor dezelfde turbiditeit te hebben als gelen gevormd van zuivere ovalbumine. Gelen van EWP bereid door middel van zuur-geïnduceerde gelering bleken zwak en breekbaar, waarschijnlijk door het fijne netwerk van fibrillen en de kleine hoeveelheid van disulfide bindingen die tijdens het koude geleringsproces zijn gevormd. De mate waarin een EWP gel vervormt kan worden, wordt gekarakteriseerd met “strain values”. Deze bleken te variëren voor EWP tussen 0.3 en 0.7, voor WPI bleken deze gelen te breken bij hogere strain values, namelijk 0.5-1.5. Dit betekent dat WPI-gelen worden ervaren als elastisch, dit komt zeer waarschijnlijk door de vorming van extra disulfide bindingen tijdens het koude geleringsproces.

Dit proefschrift geeft een gedetailleerde beschrijving van het mechanisme van denaturatie, aggregaat structuur en netwerkeigenschappen van ovalbumine bij zowel hitte- als koudegelering. Een belangrijke factor om de functionele eigenschappen van een product te veranderen is het veranderen van de structuren van aggregaten op een mesoscopische lengteschaal. We hebben laten zien dat de vorming van fibrillen, de turbiditeit van het netwerk en de geleigenschappen beheerst kunnen worden door de lading op de eiwitmoleculen te beheersen. Het inzicht over het vormen van fibrillen is vertaald naar industrieel relevante systemen (Patent No. 04077348.3). In een breder perspectief zou dit werk de industrie in staat kunnen stellen om microstructuren te ontwikkelen, welke kunnen bijdragen aan een specifiek mondgevoel en aan de stabiliteit van zachte voedingsproducten op basis van biopolymeren.

DANKWOORD

Wat een heerlijk gevoel om na vier jaar hard werken te kunnen zeggen “Ik ben zo trots op mijn proefschrift en het was het waard om tot in de late uurtjes en in het weekend door te werken”. De zeer goede faciliteiten op NIZO food research, de uitgebreide begeleiding vanuit de Wageningen Universiteit en de vele mogelijkheden die het WCFS mij heeft geboden voor congresbezoeken en internationale samenwerkingsprojecten, hebben ertoe geleid dat ik dit proefschrift met veel trots presenteer. Bij deze wil ik dan ook iedereen bedanken die mij op welke wijze dan ook heeft geholpen. Er zijn tevens een aantal mensen die ik graag bij naam wil noemen.

In de eerste plaats wil ik mijn promotor Martien Cohen Stuart hartelijk bedanken voor de betrokkenheid, de zinvolle en constructieve aanvullingen op de artikelen die we vooral in de laatste twee jaar bediscussieerden. Tevens heb ik het als zeer prettig ervaren dat ik van jou de vrijheid heb gekregen het onderzoek uit te voeren vanuit mijn eigen visie. Ronald, van jou heb ik geleerd om op eigen benen te staan, jij hebt mij vertrouwen gegeven en zodoende bijgedragen aan mijn persoonlijke ontwikkeling. Peter, bedankt voor het geduld en de hulp met betrekking tot de moeilijke verstrooiingstheorie en denaturatie kinetiek; zonder jou was dit proefschrift zeker niet geworden tot wat het nu is. Taco, jij bent diegene geweest die mij op sleeptouw heeft genomen met lichtverstrooiingsmetingen, zowel op het experimentele als op het theoretische vlak heb ik erg veel van jou geleerd. Dominique, merci de m'avoir donné l'opportunité de travailler quelques mois dans votre groupe (Université du Maine, Chimie et Physique des Matériaux Polymères). Ce fut pour moi une expérience enrichissante. Harmen en Rob bedankt voor het kritisch lezen van een aantal artikelen, ik heb het zeer gewaardeerd dat jullie mijn werk altijd van nuttige opmerkingen konden voorzien (ook al bleek er soms geen einde aan te komen). Tevens wil ik Johan Hazekamp (Unilever Research, Vlaardingen) bedanken voor de voortreffelijke samenwerking bij het maken van die cryo-TEM opnames (zie dit proefschrift).

Mijn collega's van het B004 en B015 project, Anke, Ann, Anne, Arno, Els, Fred, Hans, Heleen, Ladislava (Ladka), Maarten, Marijke, Ronald en Saskia bedank ik voor de gezelligheid, interesse en saamenhorigheid binnen de groep. Anne, jij hebt een zeer grote bijdrage geleverd aan het experimentele deel van dit proefschrift, daarvoor ben ik je enorm dankbaar. Tevens ben jij een steun voor mij geweest in soms moeilijke tijden, maar vooral ook in de goede tijden: muziek op het lab, samen in de auto naar Arnhem en de vondst van het overheerlijke BBQ restaurant. Marijke, wij hebben een aantal jaren lief en leed gedeeld

in de kantoortuin, altijd erg gezellig, soms een beetje druk, maar dat hield jij goed in de hand. Op de een of andere manier hebben de heren in de kantoortuin nooit lang stand gehouden.... Ook wil ik jou bedanken voor de hulp tijdens de laatste fase in de afronding van mijn proefschrift. Fred, bedankt voor jouw waardevolle hulp bij het schrijven van hoofdstuk 9. Zonder Ann, die haar afstudeervak bij mij heeft uitgevoerd, was dit hoofdstuk niet geworden zoals het nu is; bedankt Ann! Els en Arno met jullie heb ik een zeer geslaagde tijd in Grenoble gehad, het was hard werken (met af en toe een goed gepland langdurig experiment, maar dat is zeker beloond, tevens heb ik veel van jullie geleerd als doorgewinterde wetenschappers.

Eigenlijk zijn al die Grenoble “uitstapjes” begonnen met de uitnodiging van Jasper en Stefan van de vakgroep Fysische Chemie en Kolloïdkunde om X-ray metingen te gaan doen. We kwamen er in Grenoble voor de eerste keer achter dat ovalbumine een fantastisch systeem is voor dit soort metingen; eindelijk een goede interactie piek. In die tijd was het radieel middelen en verdere dataverwerking geen pretje, daar hebben jullie mij ontzettend goed mee geholpen, bedankt.

Collega fysko-AIO's, ik heb me altijd erg vermaakt op de werkbesprekingen (ook al was ik er niet al te vaak), maar des te gezelliger was het op de AIO-uitjes. Ik denk niet dat er een andere vakgroep op de Wageningen Universiteit is die kan tippen aan deze “cultureel geïnspireerde” feestjes!! Texture collega's, bedankt voor jullie gezelligheid, de hulp, en de interesse die jullie in mijn werk hebben getoond. Kees, fijn dat ik zo vanzelfsprekend in de afdeling ben opgenomen en dat ik altijd jouw kantoortje kon binnenlopen als ik weer eens een vraag had.

Kerens, met jou heb ik zoveel gedeeld in mijn AIO-tijd dat ik even niet weet waar ik moet beginnen. We hebben een langdurig samenwerkingsproject gedaan. Na een wat lange aanloopperiode zijn we op stoom gekomen en hebben nu twee publicaties samen geschreven, waarvan hoofdstuk 7 van dit proefschrift er één betreft. Tussen het ovalbumine opzuiveren door hebben we nog de tijd gecreëerd om te MTB'en. We hebben ook een fantastisch leuke tijd gehad in Grenoble, dat was de eerste ervaring met echt weinig slapen en meten als een idioot. Maar naast werk delen we ook allerlei andere leuke dingen. Daarom wil ik je bedanken voor deze waardevolle vriendschap die we de afgelopen vier jaar hebben opgebouwd. Tevens ben ik erg blij dat jij mijn paranimf wilt zijn. Suzanne, jou wil ik ook graag bedanken voor je vriendschap en het feit dat je mij wilt bijstaan als paranimf. Wij hebben tijdens de lerarenopleiding Scheikunde aan de Hogeschool Holland

lief en leed gedeeld en ondanks het feit dat we ieder een andere weg zijn ingeslagen is onze vriendschap gebleven.

Gelukkig was er naast dit AIO-bestaan ook nog tijd voor familie en sportieve activiteiten met vrienden. Ik wil dan ook mijn tennismaatjes bedanken voor het ‘enorme’ begrip dat jullie altijd hadden als ik weer naar Frankrijk moest voor metingen. Ik krijg nog ieder jaar tijdens de competitie te horen dat we gedegradeerd zijn omdat ik weer naar Frankrijk moest. Maar nu geen smoesjes meer, we gaan er dit jaar weer tegenaan!! Ook ben ik erg blij met mijn fietsmaatjes Kerensa en Hilke; bij jullie kan ik altijd terecht om samen te sporten, te praten en lekker te eten.

Lieve Siem en Renaat, het voelt zo gewoon maar het is toch zo uniek dat wij als zusjes zo’n sterke en intieme band hebben. Ik kan bij jullie altijd met alles terecht (als het maar geen schei-, wis- of natuurkunde betreft); bedankt voor jullie interesse, vriendschap en liefde. Lieve paps en mams, bedankt voor jullie interesse en enthousiasme. Ik weet dat jullie trots op mij zijn en ik ben blij dat ik dat waar heb kunnen maken. Cora en Peter, bedankt voor jullie gastvrijheid en belangstelling. Verder wil ik nog graag mijn opa en oma bedanken, omdat jullie op deze leeftijd nog altijd zoveel interesse tonen in mijn werk en ons met enthousiasme volgen op de (verre) reizen die Jeroen en ik maken. Ik geniet altijd erg van jullie gezelligheid.

Lieve Jeroen, jou wil ik als laatste bedanken. Jij hebt mij altijd de ruimte en vertrouwen gegeven om mijn drukke programma te volbrengen. Jij bent mij gevolgd naar Arnhem (wat een hele stap is voor een Amsterdammer), en jij bent mij tevens komen opzoeken in Le Mans. Jouw humor, liefde en vriendschap maken mij gelukkig. Ik kijk met veel nieuwsgierigheid en enthousiasme uit naar wat wij in de toekomst samen gaan ondernemen.

Mireille

LIST OF PUBLICATIONS

JOURNALS

Weijers, M., Sagis, L.M.C., Veerman, C., Sperber, B., and Linden van der, E. Rheology and structure of ovalbumin gels at low pH and low ionic strength. *Food Hydrocolloids* (2002), 16, 269-276.

Weijers, M., Nicolai, T., and Visschers, R.W. Light scattering study of heat-induced aggregation and gelation behaviour of ovalbumin. *Macromolecules* (2002), 35, 4753-4762.

Weijers, M., Barneveld, P.A., Cohen Stuart, M.A., and Visschers, R.W. Heat-induced denaturation and aggregation of ovalbumin at neutral pH described by irreversible first-order kinetics. *Protein Science* (2003), 12, 2693-2703.

Alting A.C., **Weijers, M.**, de Hoog, E.H.A., van de Pijpekamp, A.M., Cohen Stuart, M.A., Hamer, R.J., Kruif de, C.G., and Visschers, R.W. Acid-induced cold gelation of globular proteins: Effects of protein aggregates characteristics and disulfide bonding on rheological properties. *J. Agric. Food Chem.* (2004), 52, 623-631.

Pouzot, M., Nicolai, T., Visschers, R.W., and **Weijers, M.** X-ray and light scattering study of the structure of large globular protein aggregates. *Food Hydrocolloids* (2005), 19, 231-238.

Weijers, M., Nicolai, T., and Visschers, R.W. Influence of the ionic strength on the structure of heat-set globular protein gels at pH 7. Part II: Ovalbumin. *Macromolecules* (2004). Accepted.

Weijers, M., Visschers R.W., Cohen Stuart, M.A., and Barneveld, P.A. Heat-induced formation of “ordered” structures of ovalbumin at low ionic strength studied by Small Angle X-ray Scattering. (2004). Submitted.

Broersen, K., **Weijers, M.**, Groot de, J., Jongh de, H.H.J., and Hamer, R.J. Electrostatics controls fibril formation. Part I: Electrostatics controls fibril formation. Part I: stability of charged ovalbumin variants. **(2004)**. Submitted.

Weijers, M., Broersen, K., Barneveld, P.A., Cohen Stuart, M.A., Jongh de, H.H.J., Hamer, R.J., and Visschers R.W. Electrostatics controls fibril formation. Part II: denaturation, aggregation and gelation of charged ovalbumin variants. **(2004)**. Submitted.

Weijers, M., Velde van de, F., Stijnman, A., van de Pijpekamp, A.M., and Visschers, R.W. Structure and rheological properties of acid-induced egg white proteins gels. *Food Hydrocolloids* **(2004)**. Accepted.

Nicolai, T., Visschers, R.W., and **Weijers, M.** Microphase separation during aggregation and gelation of globular proteins. **(2005)**. To be submitted.

Velde van de, F., **Weijers, M.**, and Visschers, R.W. Enhanced functionality of egg white proteins. **(2005)**. To be submitted.

CONFERENCE PROCEEDINGS

Weijers, M., Barneveld, P.A., Cohen Stuart, M.A. and Visschers, R.W. Denaturation, aggregation and gelation kinetics of chicken egg white ovalbumin at neutral pH. *Proceedings of the 3rd International Symposium on Food Rheology and Structure* **(2003)**, Zurich, Switzerland, 615-616.

Weijers, M., Barneveld, P.A., Cohen Stuart, M.A. and Visschers, R.W. Fibril formation of globular proteins. *Proceedings of the 11th International Conference on Surface and Colloid Science* **(2003)**, Foz do Iguaçu, Brazil, 17.

Weijers, M., Velde van de, F., Cohen Stuart, M.A. and Visschers, R.W. Structure and rheological properties of acid-induced gels of industrial egg white protein, ovalbumin and

whey protein isolate. *Proceedings of the 7th International Hydrocolloids Conference (2004), Melbourne, Australia*, 16.

Weijers, M., Visschers, R.W., Cohen Stuart, M.A. and Barneveld, P.A. Fibril formation of globular proteins studied with small angle X-ray scattering. *Proceedings of the 18th Conference of the European Colloid and Interface Society (2004), Almeria, Spain*, 51.

PATENT

Visschers, R.W., Velde van de, F., and **Weijers, M.**, Egg protein compositions, their preparation and their use for cold or heat gelation. Application No./Patent No. 04077348.3.

CURRICULUM VITAE

Mireille Weijers werd geboren op 24 april 1975 te Hoogkarspel. In 1993 behaalde zij haar HAVO diploma aan de Oscar Romero te Hoorn. In datzelfde jaar begon zij aan de lerarenopleiding Scheikunde aan de Hogeschool Holland. Na haar afstuderen in 1997 begon zij in datzelfde jaar de opleiding Laboratorium Techniek aan de Internationale Agrarische Hogeschool Larenstein te Arnhem. Zij volgde de specialisatie levensmiddelenanalyse. Haar stage heeft zij gelopen bij het instituut voor agrotechnologisch onderzoek (ATO) in Wageningen. Haar afstudeerstage heeft zij uitgevoerd bij Wageningen Universiteit, sectie Levensmiddelen natuurkunde. Zij studeerde af in 2000. Vanaf oktober 2000 tot en met oktober 2004 was zij als Assistent in Opleiding in dienst van Wageningen Universiteit bij de leerstoelgroep Fysische Chemie en Kolloïdkunde. Gedurende deze vier jaar was zij gedetacheerd bij het Wageningen Centre for Food Sciences en de resultaten van het promotieonderzoek die staan beschreven in dit proefschrift zijn uitgevoerd bij NIZO food research te Ede.

Photographs on cover/back: Renate Weijers

Printing: Ponsen & Looijen BV, Wageningen